

Biochemical and mass spectrometric analysis of yeast cytochrome c peroxidase *in vitro* and *in vivo* gives insights into its biological functions as a H₂O₂ sensor and heme donor protein

Meena Kathiresan

A Thesis
in
The Department of
Chemistry and Biochemistry

Presented in Partial Fulfillment of the Requirements
For the Degree of
Doctorate of Philosophy (Chemistry option Biochemistry) at
Concordia University
Montreal, Quebec, Canada

September 2015

©Meena Kathiresan, 2015

CONCORDIA UNIVERSITY

School of Graduate Studies

This is to certify that the thesis prepared

By: Meena Kathiresan

Entitled: Biochemical and mass spectrometric analysis of yeast cytochrome c peroxidase *in vitro* and *in vivo* gives insights into its biological functions as a H₂O₂ sensor and heme donor protein

and submitted in partial fulfillment of the requirements for the degree of

Doctor of Philosophy Chemistry (Biochemistry)

complies with the regulations of the University and meets the accepted standards with respect to originality and quality.

Signed by the final Examining Committee:

_____ Chair
Dr. Wayne Brake

_____ External Examiner
Dr. Jeffrey Agar

_____ External to Program
Dr. Alisa Piekny

_____ Examiner
Dr. Paul Joyce

_____ Examiner
Dr. Vladimir Titorenko

_____ Thesis Supervisor
Dr. Ann English

Approved by: _____
Dr. Heidi Muchall, Graduate Program Director

September 2015 _____
Dean of Faculty

Abstract

Biochemical and mass spectrometric analysis of yeast cytochrome c peroxidase *in vitro* and *in vivo* gives insights into its biological functions as a H₂O₂ sensor and heme donor protein

Meena Kathiresan, PhD

Concordia University, 2015

The stress response to exogenous H₂O₂ has provided significant insight into thiol-based cytosolic H₂O₂ sensors such as OxyR in *Escherichia coli* and its eukaryotic counterpart Gpx3/Yap1 in *Saccharomyce cerevisiae*. However, sensing of endogenously generated H₂O₂ in mitochondria, the main sites of H₂O₂ production in respiring yeast, is poorly documented. We have recently demonstrated that cytochrome c peroxidase (Ccp1) acts as a mitochondrial H₂O₂ sensor to balance reactive oxygen species (ROS) levels by regulating catalase A (Cta1) activity and attenuating the H₂O₂ stress response during aging. Since Ccp1 is the first heme-based H₂O₂ sensor to be identified, its mechanism of action at the molecular level is of much interest. This thesis reports on how H₂O₂ signals through Ccp1. Activity assays reveal the accumulation of catalytically inactive and heme-free Ccp1 outside mitochondria in respiring cells, when catalase activity starts to increase. Importantly, the burst in H₂O₂ generation during the switch from fermentation to respiration triggers heme-mediated oxidation by H₂O₂ of the proximal Fe ligand, H175. Formation of oxo-H175 weakens the heme-ligand interaction and labilizes the heme group, which is transferred either directly or via unidentified intermediate(s) to apoCta1. The nascent Cta1 activity detoxifies H₂O₂, and apoCcp1 which has conformational lability, undergoes reverse translocation to the vacuole and nucleus. Mass spectrometric characterization of heme-mediated H₂O₂-induced chemical and post-translational modifications in recombinant Ccp1 and Ccp1 isolated from yeast cells, respectively, has allowed us to identify the residues

oxidized as well as to evaluate radical-transfer pathways in Ccp1 in response to both exogenous and endogenous H_2O_2 . Importantly, the mass spectrometry-based approach described here provides a way to fully evaluate the oxidation profile of a protein. Although Cta1 was not found as a binding partner of GST-Ccp1 in GST pull-down assays, the antioxidant proteins, manganese superoxide dismutase (Sod2), thioredoxin peroxidase (Tsa1), the glycolytic enzyme glyceraldehyde-3-phosphate dehydrogenase (GAPDH), the putative heme transporter Pet9 and heat shock proteins 70 and 90 were reproducibly found as Ccp1 binding partners. Combined, the results presented provide insights into the mechanism of H_2O_2 signaling in cells involving heme-mediated redox changes in contrast to the redox chemistry of thiols.

Acknowledgments

I would first like to acknowledge Dr. Ann English for her support and guidance for the duration of my PhD. The training I received in critical thinking, scientific writing and the numerous conferences I was able to attend has greatly enhanced my communication skills and made me a better scientist. It has been a great pleasure learning from her and I will carry these skills with me in the future. Thanks to my committee members Dr. Paul Joyce and Dr. Vladimir Titorenko for their helpful discussions, guidance and rigorous questions during my committee meetings. To Dr. Piekny and Dr. Jeffrey Agar for agreeing to serve as my external examiners and to Dr. Piekny for her support and advice with my microscopy work. To Dr. Brett for allowing me access to CMAC and for his insightful discussions throughout my PhD.

I had the pleasure of working with many talented faculty, students and staff during my time at Concordia. Notable mentions are extended to my lab colleagues Dr. Dorival Martins, Samaneh Dastypeyman, Vinod Parmer, Dr. Maria Shadrina, and Alan Lopes.

I would also like to express my appreciation for the mass spectrometry training I received from Jean-Pierre Falgueyret, Marcos Difalco and Alain Tessier in the Centre for Biological Applications of Mass Spectrometry (CBAMS). I would like to thank Dr. Alexey Denisov for his help in running and analysis of my dityrosine preparation by NMR. I express my gratitude to Marc Ouellet for his friendship and the early morning coffee breaks that were filled with scientific brainstorming. He has given me a lot of support and encouragement over these last four years and for that I am grateful.

A huge thank you goes out to my parents Paul and Solai Kathiresan and my sisters Unna and Uma Kathiresan for always being there and supporting the decisions I made. This degree

would not have been possible without their love and support. Special thanks to my twin sister Unna Kathiresan who listened to my numerous presentations, even if she did not understand everything I was talking about, and encouraged me to keep moving forward. To Dominique Allaire, Tim O’Flaherty and Shawn O’Flaherty for being an amazing second family and always extending a helping hand whenever I needed it. To my “adopted” dog Saffire, who kept me company while I wrote this thesis, your furry face kept my spirits up while I ran into formatting troubles. To my best friend Shou-yun Yin for welcoming me to Montreal and providing me with fun-filled breaks outside of my research for which I am truly grateful.

Finally, thank you to my husband and true love, Derek O’Flaherty for his unwavering belief in my abilities, patience, and constant encouragement throughout my degree. He has been my biggest cheerleader and inspired me to think about my projects from different perspectives. His intelligence, kindness and love has in large part shaped me into the scientist I am today. He constantly challenged me to push beyond my comfort level, and his passion for science has surrounded me in a wonderfully positive environment for the last 3 years. I am grateful for his support and continued love.

Table of Contents

List of Tables	xii
List of Figures	xiii
List of abbreviations	xvi
Chapter 1: General introduction	1
1.1 Hydrogen peroxide as a signaling molecule and hydrogen peroxide sensors	1
1.1 Heme as a signaling molecule	4
1.3 Structure-function characterization of cytochrome c peroxidase <i>in vitro</i>	6
1.4 Function of cytochrome c peroxidase as a H ₂ O ₂ sensor <i>in vivo</i>	8
1.5 LC-MS/MS approach to identify protein chemical and posttranslational modifications.....	10
1.7 Scope of the thesis	10
1.7 Objective of the thesis.....	12
Chapter 2:Respiration triggers heme transfer from cytochrome c peroxidase to catalase in yeast mitochondria	13
2.1 Preface.....	13
2.2 Abstract of the manuscript	13
2.3 Introduction.....	14
2.4 Materials and methods	17
2.4.1 Materials	17
2.4.2 Antibodies.....	17
2.4.3 Yeast strains	18
2.4.4 Imaging of live yeast cells by wide-field fluorescence microscopy	18
2.4.5 Subcellular fractionation of yeast lysates and isolation of crude nuclei	19
2.4.6 Western blotting of Ccp1 and Ccp1-GFP	20
2.4.7 Linear range for Ccp1 detection and the response of anti-Ccp1 toward different chemical forms of recombinant Ccp1.....	21
2.4.8 Heme blotting of Ccp1 isolated from P10 and S10 fractions.....	21
2.4.9 Expression and purification of recombinant Ccp1	22
2.4.10 <i>In vitro</i> heme transfer	22
2.4.11 Mass spectrometric analysis of Ccp1 hyperoxidation <i>in vitro</i> and <i>in vivo</i>	23
2.4.12 <i>In vitro</i> heme transfer	24
2.5 Results	26
2.5.1 Ccp1-GFP and Ccp1 are exported from mitochondria of respiring cells.....	26
2.5.2 Ccp1 is targeted to the nucleus and possibly the vacuole	29

2.5.3 Extramitochondrial Ccp1 is catalytically inactive	30
2.5.4 Cta1 activity increases as Ccp1 exits mitochondria	30
2.5.5 Ccp1 accumulates in the mitochondria of <i>cta1Δ</i> cells	31
2.5.6 Heme-mediated Ccp1 hyperoxidation by H ₂ O ₂ results in heme labilization	32
2.6 Discussion	35
2.6.1 Evidence for Ccp1 as a heme donor.....	35
2.6.2 Cta1 as a mitochondrial acceptor of Ccp1 heme.....	36
2.6.3 Heme labilization by His175 oxidation.....	37
2.6.4 Why cells produce Ccp1 as a sensor.....	37
2.6.5 The role of extramitochondrial apoCcp1	38
2.7 Conclusion	39
2.8 Supplementary information	40
Chapter 3: Detailed LC-MS/MS analysis of H₂O₂-treated cytochrome c peroxidase offers insight into heme-based H₂O₂ signaling	49
3.1 Preface.....	49
3.2 Abstract of the manuscript.....	49
3.3 Introduction.....	50
3.4 Materials and methods	53
3.4.1 Materials	53
3.4.2 Ccp1 oxidation.....	54
3.4.3 LC-MS analysis of intact apo- and holoCcp1 ± H ₂ O ₂ and of Ccp1 derived heme	54
3.4.4 LC-MS/MS analysis of tryptic digests of oxidized Ccp1.	55
3.4.5 Purification and dityrosine fluorescence of monomeric oxidized Ccp1	56
3.4.6 Quantitation of residue oxidation.....	57
3.4.7 Molecular dynamics simulation of O ₂ diffusion in Ccp1.....	57
3.5 Results	57
3.5.1 Oxidation of Ccp1 by H ₂ O ₂ is heme mediated.....	57
3.5.2 Localization of the oxygen adducts in oxidized Ccp1	58
3.5.3 Tyrosine is oxidized mainly to dityrosine.....	60
3.5.4 Oxidation of the proximal iron ligand H175 and of the catalytic distal H52.....	62
3.6 Discussion	64
3.6.1 Intrinsic radical reactivity	64
3.6.2 RT pathways and electron-donor zones in Ccp1.....	67
3.6.3 Comparison of MS and EPR studies on Ccp1 oxidation	69

3.6.4 Characterization of overoxidized Ccp1 provides new insights into its physiological function	71
3.7 Conclusion	72
3.8 Supplementary information	74
Chapter 4: H₂O₂-induced post-translational modifications convert cytochrome c peroxidase into a H₂O₂ sensor and heme donor in respiring yeast	90
4.1 Preface.....	90
4.2 Abstract of the manuscript	90
4.3 Introduction.....	91
4.4 Materials and methods	95
4.4.1 Materials	95
4.4.2 Yeast strains, media, and growth conditions	96
4.4.3 Subcellular fractionation of lysates.....	96
4.4.4 Enrichment by anion-exchange of Ccp1 from P10 and S10 extracts and immunodot blotting analysis.....	97
4.4.5 SDS-PAGE of anion-exchange fractions and in-gel Ccp1 digestion.....	98
4.4.6 LC-MS/MS of the PTMs in the tryptic peptides of Ccp1	98
4.4.7 Semiquantitation of residue oxidation	99
4.4.8 Stepwise oxidation of recombinant Ccp1 with H ₂ O ₂	99
4.5 Results	100
4.5.1 Ccp1 isolated from 16 h or 30 h cells shows little oxidation	100
4.5.2 Ccp1 from 7 d mitochondria is heavily oxidized	104
4.5.3 H175 is mainly in the HisO form in extramitochondrial Ccp1 from 7 d cells.....	106
4.5.4 Ccp1 is phosphorylated at Y153 and Y229.....	106
4.5.5 Stepwise H ₂ O ₂ addition to recombinant Ccp1 promotes tyrosine hydroxylation vs ditryrosine crosslinking.....	108
4.6 Discussion	111
4.6.1 Observed PTMs in Ccp1 confirm that the protein is overoxidized in cells	111
4.6.2 Ccp1 phosphorylation	112
4.6.3 Residues in zone 1 are oxidized in Ccp1 from 16- and 30 h mitochondria and in CpdI... ..	113
4.6.4 Comparison of the PTMs in Ccp1 from 7 d mitochondria and Ccp1 overoxidation <i>in vitro</i>	114
4.6.5 The signal for heme labilization in Ccp1	115
4.7 Conclusion	116

4.8 Supplementary information	117
Chapter 5: Cytochrome c peroxidase pull-down assays in yeast reveal numerous novel binding partners including Sod2, Pet9, GAPDH and Tsa1	122
5.1 Preface.....	122
5.2 Abstract of the manuscript.....	122
5.3 Introduction.....	123
5.4 Materials and methods	126
5.4.1 Materials	126
5.4.2 Construction, expression and purification of GST-Ccp1 from <i>E. coli</i>	126
5.4.3 Preparation of soluble protein extracts from the subcellular fractions of 1- and 7 d wild-type cells.....	128
5.4.4 Screening for Ccp1 interacting proteins in subcellular fractions from 1- and 7 d yeast ...	129
5.4.5 Screening for Ccp1 as an interacting partner of Sod2 using the overexpressed GST-Sod2 fusion protein from 1 d yeast cells.....	130
5.4.6 1D SDS-PAGE and 2D IEF/SDS-PAGE analysis.....	130
5.4.7 LC-MS/MS analysis of Ccp1's interacting partners	132
5.4.8 Western blotting with anti-Ccp1, anti-GST	133
5.5 Results	133
5.5.1 Characterization of the GST-Ccp1 fusion protein	133
5.5.2 1D SDS-PAGE is sufficient to resolve Ccp1's interacting partners	134
5.5.3 GST-apoCcp1 and GST-holoCcp1 bait Sod2, an antioxidant enzyme, in 1 d yeast.....	138
5.5.4 GST-apoCcp1 baits Sod1, an antioxidant enzyme, in 7 d yeast	140
5.5.5 GST-apoCcp1 baits Tsa1, an antioxidant enzyme, in 7 d yeast.....	140
5.5.6 GST-apoCcp1 baits Pet9, a possible heme transporter, in 1 d yeast.....	141
5.5.7 GST-apoCcp1 and GST-holoCcp1 bait the 3 isoforms of GAPDH (Tdh3/2/1) in 1 and 7 d yeast	142
5.5.8 GST-apoCcp1 and GST-holoCcp1 bait Hsp70 and Hsp90 in 1- and 7 d yeast.....	142
5.6 Discussion	144
5.6.1 Ccp1's peroxidase function.....	144
5.6.2 Possible H ₂ O ₂ channeling from Sod2 to Ccp1 and possible Ccp1-Sod1/2 crosstalk.....	145
5.6.3 Interaction with Tsa1 and Hsp70 may target extramitochondrial Ccp1 to the nucleus and vacuole, respectively.....	146
5.6.4 Does Pet9 play a role in heme insertion into Ccp1?	147
5.6.5 Heme transfer may occur between GAPDH and Ccp1	149

5.6.6 Hsp90 may influence Ccp1's heme status	150
5.7 Conclusion	151
5.8 Supplementary information	152
Chapter 6: General conclusions	162
Chapter 7: Future work	166
References	176
Appendix I First page to published manuscripts.....	192
Appendix II Residue oxidation products	194
Appendix III Preparation and synthesis of dityrosine	195

List of Tables

Table 2.1 <i>S. cerevisiae</i> strains used in this study	18
Table S2.1 Normalized CCP activity of subcellular fractions from wild-type and Ccp1-GFP-expressing yeast	40
Table S2.2 Normalized CCP activity of subcellular fractions from wild-type, <i>cta1Δ</i> and <i>ctt1Δ</i> yeast	40
Table S2.3 Percent heme transfer from Ccp1 or hyperoxidized Ccp1 to apoMb.....	41
Table S2.4 Relative peak areas of the oxidized forms of tryptic peptide EVVALMGAHALGK	41
Table S3.1 list of oxidative modifications considered in database search for this study	75
Table S3.2 Peak areas (PA) of the internal reference peptides in the Ccp1 tryptic digests.....	76
Table S3.3 Monoisotopic masses of the tryptic peptides observed in digests of H ₂ O ₂ -oxidized Ccp1.....	77
Table S3.4 CCP activity of H ₂ O ₂ -oxidized Ccp1	79
Table S3.5 Peptides T21 (M172, H175) and T14+T15 (W126, C128) are oxidized at two residues .	80
Table S3.6 O ₂ and internal water exposure of the oxidizable residues in Ccp1 ^a	89
Table 4.1 LC-MS analysis of Ccp1 peptides from 16 h, 30 h and 7 d P10 and S10 extracts.....	101
Table S4.1 Oxidative modifications considered in database searching.....	117
Table S4.2 Monoisotopic <i>m/z</i> values of the MH ⁺ ions of tryptic peptides observed in the digests of Ccp1 from yeast cells	118
Table S4.3 Peptides T21 (M172, H175) is oxidized at two residues	120
Table 5.1 <i>S. cerevisiae</i> strains used in this work.....	126
Table 5.2 GST-apoCcp1 and GST-holoCcp1 interacting proteins detected in 1 d cells	137
Table 5.3 GST-apoCcp1 interacting proteins detected in 7 d cells	137
Table S5.1 CCP activity of GST-holoCcp1	152
Table S5.2 Proteins in GST-apoCcp1 and GST-holoCcp1 pull downs from 1 d yeast extracts (n=2).....	153
Table S5.3 proteins in GST-apoCcp1 pull downs from 7 d yeast extracts (n=4).....	154
Table S5.4 GST binding partners in 1 d and 7 d cell extracts (n=6)	156
Table S5.5 Reported Ccp1 interactions collated from the yeast genome website.....	157

List of Figures

Figure 1.1 Growth phases of <i>Saccharomyces cerevisiae</i> cultivated in rich medium supplemented with 2% glucose.....	2
Figure 1.2 Chemical structure of Heme a, b and c.....	5
Figure 1.3 Structural similarity of class I peroxidases Ccp1 and APX.....	8
Figure 2.1 Ccp1-GFP is mitochondrial in 1 day and vacuolar in 7 day yeast cells; Ccp1 is present in nuclei from 7 day cells.....	28
Figure 2.2 Ccp1 exits mitochondria as yeast begin respiring and extramitochondrial Ccp1 does not possess CCP activity.....	29
Figure 2.3 Catalase activity in wild-type yeast increases at the expense of mitochondrial Ccp1.....	31
Figure 2.4 Ccp1 accumulates in the mitochondria of <i>cta1</i> Δ yeast.....	33
Figure 2.5 Ccp1 is oxidized at His175.....	35
Figure 2.6 Respiration triggered heme transfer in yeast mitochondria.....	39
Figure S2.1 Ccp1-GFP exits mitochondria as yeast begin respiring and extramitochondrial Ccp1-GFP does not possess CCP activity.....	42
Figure S2.2 Ccp1 hyperoxidation by H ₂ O ₂ increases heme transfer to apoMb.....	43
Figure S2.3 Heme from hyperoxidized Ccp1 is not oxidized.....	44
Figure S2.4 H ₂ O ₂ oxidizes holoCcp1 but not apoCcp1.....	45
Figure S2.5 H ₂ O ₂ oxidizes His175, the proximal Fe ligand, in recombinant Ccp1.....	46
Figure S2.6 LC-MS/MS analysis of extramitochondrial Ccp1 isolated from 7 day cells reveals His175 oxidation.....	47
Figure S2.7 The anti-Ccp1 antibody detects the heme free (apo), heme loaded (holoCcp1) and oxidized forms of Ccp1.....	48
Figure 3.1 Oxidizable residues in Ccp1.....	52
Figure 3.2 Deconvolved mass spectra showing that Ccp1 oxidation by H ₂ O ₂ is mediated by its heme.....	58
Figure 3.3 Methionine and cysteine oxidation.....	59
Figure 3.4 Tryptophan residues undergo extensive hydroxylation.....	60
Figure 3.5 Tyrosine oxidation products include TyrOH and dityrosine.....	61
Figure 3.6 LC-MS/MS analysis of tyrosine oxidation in tryptic peptide T6.....	62
Figure 3.7 H ₂ O ₂ oxidizes the proximal heme ligand H175 and the distal H52.....	63
Figure 3.8 Electron-donor zones in Ccp1.....	68

Figure S3.1 Tryptic peptides T1-T34 predicted for Ccp1	74
Figure S3.2 Characterization of intramolecular dityrosine crosslinks in H ₂ O ₂ -oxidized Ccp1	81
Figure S3.3 LC-MS/MS analysis of tyrosine oxidation in peptides T6 and T26	82
Figure S3.4 LC-MS analysis of hemin released from overoxidized Ccp1	83
Figure S3.5 LC-MS/MS analysis of H175 and H52 oxidation in tryptic peptides T21 and T7	84
Figure S3.6 Standard MD simulation of Ccp1 in water with 100 added O ₂ molecules	87
Figure 4.1 Oxidizable residues in Ccp1 and their location in the protein's tryptic peptides	94
Figure 4.2 Purification of Ccp1 from 16 h yeast cells	102
Figure 4.3 Comparison of residue oxidation in Ccp1 from 16- and 30 h mitochondria with that in CpdI generated in vitro	103
Figure 4.4 Comparison of residue oxidation in Ccp1 isolated from the P10 and S10 extracts from 7 d cells with that in recombinant Ccp1 overoxidized with 10 M eq of H ₂ O ₂	104
Figure 4.5 Ccp1 is phosphorylated at Y153 and Y229	107
Figure 4.6 LC-MS/MS analysis of Y153 and Y229 phosphorylation in tryptic peptides T17+T18 and T26	108
Figure 4.7 Effects of bolus vs stepwise addition of H ₂ O ₂ on the tyrosine oxidation products in recombinant Ccp1	109
Figure 4.8 Effects of bolus vs stepwise addition of H ₂ O ₂ on methionine, tryptophan and histidine oxidation products in recombinant Ccp1	110
Figure S4.1 Representative anti-Ccp1 immunodot blots of anion-exchange fractions from yeast cell extracts	120
Figure S4.2 LC-MS/MS analysis of dityrosine formation in tryptic peptides T5+T6, T8 and T26..	121
Figure 5.1 1D SDS-PAGE and 2D IEF/SDS-PAGE analysis of the proteins in GST-holoCcp1 and GST pull down from the S2 extract from 1 d yeast	135
Figure 5.2 Representative 1D gels for a S2, P10 and S10 extracts from 1 d vs 7 d cells.....	136
Figure 5.3 Identification of Sod2 in a GST-holoCcp1 pull down from the P10 extract from 1 d yeast	138
Figure 5.4 Identification of Ccp1 in a GST-Sod2 pull down from a 1 d S2 denucleated extract	139
Figure 5.5 Identification of Pet9 in a GST-apoCcp1 pull down from P10 extract from 1 d yeast....	141
Figure 5.6 Identification of the Tdh3/2/1 isoforms of GAPDH in a GST-apoCcp1 pull down from a S2 extract from 7 d yeast	143
Figure S5.1 SDS-PAGE analysis of GST-Ccp1 purification.....	159

Figure S5.2 Confirmation of GST-Sod2 overexpression in yeast.....	160
Figure S5.3 Sequence alignment of the TDH3/2/1 isoforms of yeast GAPDH.....	161
Figure 7.1 Chemical structure of 2-oxo-histidine and 2-oxo-imidazole.	168
Figure 7.2 Pymol generated cartoon of Ccp1 active site residues and hydrogen bonding network .	170
Figure 7.3 Fragmentation pattern along the polypeptide backbone and sequence ions generated....	172
Figure A2.1 Residue modifications revealed by LC-MS/MS analysis in this thesis.	194
Figure A3.1 Chemical structure of 2-oxo-histidine and 2-oxo-imidazole.	196
Figure A3.2 Pymol generated cartoon of Ccp1 active site residues and hydrogen bonding network	197
Figure A3.3 Fragmentation pattern along the polypeptide backbone and sequence ions generated.	198

List of abbreviations

ABTS	2,2-azino-bis
Ahp1	alkyl hydroperoxide reductase 1
ANT	adenine nucleotide translocator
Apo	heme-free
APX	ascorbate peroxidase
ATP	adenosine triphosphate
BSA	bovine serum albumin
CCP	cytochrome c peroxidase activity
Ccp1	cytochrome c peroxidase protein
<i>ccp1</i> W191F	yeast strain producing the Ccp1W191F protein variant with the W191F mutation
<i>ccp1</i> Δ	yeast strain deleted for the CCP1 gene
CCS	copper chaperone for superoxide dismutase 1
CFU	colony forming unit
CID	collision induced dissociation
CMA	chaperone-mediated-autophagy
CpdI	compound I, the two-electron oxidized form of Ccp1
CpdII	compound II, the one-electron oxidized form of Ccp1
Cta1	catalase A
Ctt1	catalase T
Cyc1	cytochrome protein
Cyc1 ^{II/III}	ferro/ferricytochrome c
CysSO ₂ H	cysteine sulfinic acid
CysSO ₃ H	cysteine sulfonic acid
DEAE	diethylaminoethanol
DHR	dihydrorhodamine 123
DTPA	diethylene triamine pentaacetic acid
DTT	dithiothreitol
<i>E. Coli</i>	<i>Escherichia coli</i>
ECL	enhanced chemiluminescence
EDTA	ethylenediaminetetraacetic acid
Eno1/2	enolase isoform 1 and 2
EPR	electron paramagnetic resonance
ER	endoplasmic reticulum
FECH	ferrochelatase
FM4-64	N-(3-triethylammoniumpropyl)-4-(6-(4-(diethylamino)phenyl)hexatrienyl)pyridinium dibromide
GFP	green fluorescent protein
Gpx3	yeast glutathione peroxidase 3
GSH	reduced glutathione

GST	glutathione S-transferase
Hap1	heme activator protein 1
HisO	oxo-histidine
Holo	heme-loaded
HPLC	high performance liquid chromatography
HMA	high molecular weight aggregate
HRP	horse radish peroxidase
Hsp	heat shock protein
IMS	intermembrane space
IPG	immobilized pH gradient
IPTG	isopropyl β -D-thiogalactopyranoside
K_d	dissociation constant
KPi	potassium phosphate
LB	luria broth
LC-MS	liquid chromatography–mass spectrometry
Mb	myoglobin
MD	molecular dynamics
MetO	methionine sulfoxide
MNP	2-methyl-2-nitrosopropane
MS	mass spectrometry
MS1	spectrum of ions
MS2/ MS/MS	spectrum of ion fragments / tandem mass spectrometry
m/z	mass over charge ratio
NAD ⁺ /NADH	oxidized and reduced forms of nicotinamide adenine dinucleotide
NanoESI	nano-electrospray ionization
NMR	nuclear magnetic resonance
P10	mitochondria enriched pellet from subcellular fractionation
PA	peak area
PBS	phosphate buffered saline
Pcp1	rhomboid protease
PDB	protein data bank
PerR	peroxide responsive repressor
Pet9	major ADP/ATP carrier of the yeast mitochondrial inner membrane
PMSF	phenylmethylsulfonyl
ppm	parts per million
Prx	peroxiredoxin
PTM	post-translational modification
Pug1	protoporphyrin uptake gene 1
PVDF	polyvinylidene fluoride
QM/MM	quantum mechanics/molecular mechanics
RFU	relative fluorescence units

ROS	reactive oxygen species
<i>S. Cerevisiae</i>	<i>Saccharomyces cerevisiae</i>
SDS-PAGE	sodium dodecyl sulphate-polyacrylamide gel
SFL	synthetic fitness or lethality defect
Sod1	yeast superoxide dismutase 1 or copper-zinc superoxide dismutase
Sod2	yeast superoxide dismutase 2 or manganese superoxide dismutase
Tdh1	glyceraldehyde-3-phosphate dehydrogenase isoform 1
Tdh2	glyceraldehyde-3-phosphate dehydrogenase isoform 2
Tdh3	glyceraldehyde-3-phosphate dehydrogenase isoform 3
TEMPO	2,2,6,6-Tetramethylpiperidinyloxy
Trp(OH) ₂	dihydroxytryptophan
TrpOH	hydroxytryptophan
Tsa1	gene encoding thioredoxin peroxidase 1 (Tsa1)

Chapter 1: General introduction

1.1) Hydrogen peroxide as a signaling molecule and hydrogen peroxide sensors

Reactive oxygen species (ROS) are derived from the incomplete reduction of dioxygen (O_2) during the electron transport processes in aerobic respiration (1). ROS include the reactive superoxide anion radical ($O_2^{\bullet-}$) which is generated from the one-electron reduction of O_2 (1). $O_2^{\bullet-}$ can be dismutated to the diffusible non-radical oxidant, hydrogen peroxide (H_2O_2), and homolytic or reductive cleavage of H_2O_2 generates the highly reactive hydroxyl radical ($\bullet OH$) (1–3). The ROS of interest in this thesis is H_2O_2 . At lower physiological levels, H_2O_2 is viewed as a key signalling molecule since: 1) it is chemically stable and diffuses from its site of production, 2) its levels are enzymatically controlled and 3) it reacts specifically with a subset of amino acids and reversibly or irreversibly modifies specific residues (4).

High levels of ROS production lead to a process that is referred to as 'oxidative stress' since ROS are reactive and can damage cellular components such as lipids, proteins and DNA. (5). The deleterious effects of ROS have been linked with aging, carcinogenesis, diabetes and neurodegenerative disorders (6). However, there is substantial evidence that ROS can have a positive influence on cell growth and survival (7, 8). Currently, it is well established that low ROS levels trigger an oxidative stress response and promote lifespan extension, a phenomenon known as hormesis (9). Mitochondria have their own form of hormesis termed mito-hormesis whereby mild mitochondrial stress, triggered by a variety of insults, results in a diverse cytosolic and nuclear response that results in protective long-lasting metabolic and biochemical changes (9). Thus, the intracellular concentration of ROS must be tightly controlled in order to maintain levels of ROS that are beneficial to the organism.

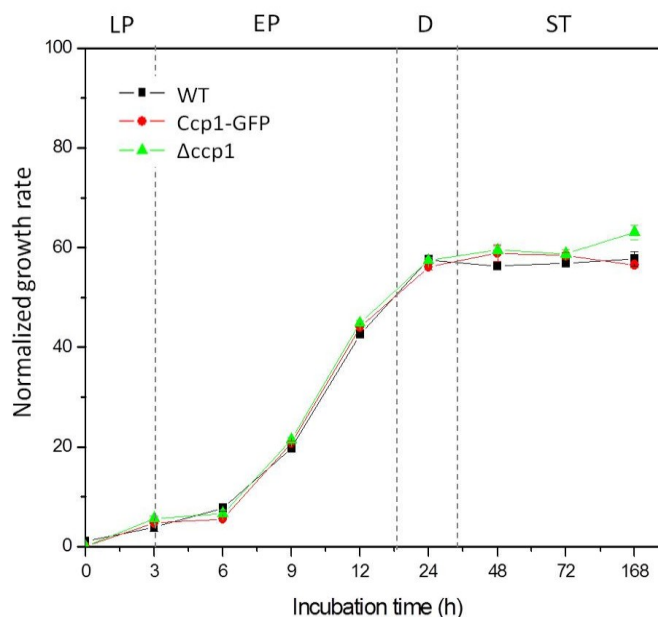


Figure 1.1 Growth phases of *Saccharomyces cerevisiae* cultivated in rich medium supplemented with 2% glucose. Yeast strains were cultured in YPD (1% yeast extract, 2% peptone, 2% glucose) medium under high aeration (medium-to-flask ratio of 1:5) at 30°C. After 72 h of growth, the spent medium was changed to 0.85% aqueous NaCl (saline, wt/v) and cells were grown for a further 7 days. At different time points, 100 μ L aliquots of the cultures were serially diluted in 0.85% saline and plated onto YPD-agar medium. The plates were incubated at 30°C for 2 days and total colony forming units (cfu) were counted after this time. The normalized growth rate corresponds to the total number of cells [$N_t = \log_{10}(N_0)^{GR_t}$]. Here N_t is the total number of cells in the plate at time t , N_0 is the number of cells at time 0, GR_t is the growth rate at time t . LP – lag phase, EP – exponential phase, D- diauxic shift, ST- stationary phase.

Yeast switch from fermentation to respiration when a fermentable carbon source such as glucose becomes limiting (10). Yeast exhibit an initial lag phase when stationary phase cells are inoculated in fresh medium (10). During the subsequent exponential phase, cells proliferate rapidly by fermenting glucose to ethanol. When glucose is largely depleted from the media, cells briefly arrest growth to adjust their metabolism from fermentation to respiration known as the diauxic shift (10). After the switch to respiration, cells start to grow again but at a reduced rate by slowly consuming the ethanol accumulated in the medium (10). When ethanol is exhausted, cells cease dividing and enter into a quiescent state known as stationary phase (10). In this thesis entry into stationary phase was accelerated by switching the cells into 0.85% saline with no carbon

source after three days of growth (11). Since mitochondrial ROS spike during the diauxic shift as shown in Figure 2.5A, yeast cells must be prepared for an imminent spike in mitochondrial ROS.

Oxidant-specific protein sensors regulate ROS by detecting their cellular concentrations and by increasing the expression of antioxidant genes in proportion to these concentrations (12). The major yeast antioxidant enzymes that catalyze the decomposition of H_2O_2 include catalases (two isoforms) (13–15), glutathione peroxidases (three isoforms) (16), cytochrome c peroxidase (one isoform) (17) and thioredoxin peroxidases or peroxiredoxins (peroxiredoxins, five isoforms) (18–20). Catalases decompose H_2O_2 to H_2O and O_2 using H_2O_2 as a reducing substrate (13–15), whereas the peroxidases and the peroxiredoxins reduce H_2O_2 to H_2O using various reducing cofactors (16–20). The multiple cellular locations and synergistic action of these enzymes allow the efficient breakdown of H_2O_2 close to its sites of generation.

Studies on microbial H_2O_2 sensors identify cysteine residues as the dominant targets of H_2O_2 (21, 22). Cysteine residues are reversibly oxidized to sulfenic acids (Cys-SOH) and can be reduced by protein-based or low-mass thiols. However, exposure to excessive ROS leads to irreversible cysteine oxidation to sulfonic acids (Cys-SO₃H), a process that often accompanies cell death (23). To date, the best characterized H_2O_2 sensors are cytosolic peroxiredoxins and glutathione peroxidases, which rely on activated thiols to metabolize H_2O_2 and use thioredoxin and glutathione (GSH) as reducing substrates, respectively (21, 24, 25). Thus, H_2O_2 sensors are rigidly coupled to both cellular H_2O_2 metabolism and to the redox status of the cell, which is controlled by thiols such as GSH oxidation state (21, 24, 25). Interestingly, metal-catalyzed oxo-histidine (HisO) formation in the *Bacillus subtilis* peroxide resistance protein (PerR) transcriptional repressor has recently been defined as a H_2O_2 sensor (26). This report revealed that histidine residues can participate in redox regulation in a thiol-independent fashion. In fact,

in addition to cysteine and histidine, other targets of H₂O₂ include the redox-sensitive residues, tryptophan and tyrosine, as well as largely overlooked sulfur-containing methionine (27). All of these residues have the potential to be involved in cellular H₂O₂ sensing and signalling as explored in this thesis.

1.2) Heme as a signaling molecule

Heme consists of a Fe²⁺ ion in the centre of a porphyrin ring and is ubiquitous among living organisms. Heme, particularly protoporphyrin IX heme (or heme *b*, Figure 1.1), plays a critical role in organisms as a catalytic prosthetic group in proteins that generate energy, sense and consume gasses, and catalyze enzymatic reactions (28, 29). Heme has also been shown to directly control a variety of signal transducers and transcriptional regulators including heme activator protein (Hap1) in the yeast *S. cerevisiae*, iron regulatory protein (IRR) in the bacterium *Bradyrhizobium japonicum*, the mammalian transcriptional repressor Bach1 and the heme-regulated inhibitor (HRI) kinase, to name a few (30).

Heme is synthesized via a highly conserved eight-step biosynthetic pathway which in yeast is regulated by of the oxygen level (31). The last step of this pathway involving Fe²⁺ insertion into protoporphyrin IX is catalyzed by ferrochelatase (FECH) in the mitochondrial inner membrane (31). Although the enzymes for heme biosynthesis and its regulation are relatively well-characterized in eukaryotic cells, trafficking of heme to target proteins residing outside the mitochondrion remains poorly characterized (32, 33). Due to the toxic nature of free heme (34), it is unlikely to diffuse freely within the cell but instead specific pathways, with appropriate heme carriers, must exist to facilitate heme delivery from the mitochondrial matrix to all of its cellular destinations (32, 33). To date, proteins involved in yeast heme trafficking remain largely unknown but putative heme transporters have been identified, including protoporphyrin uptake

gene 1 (*PUG1*), which was detected by microarray analysis of *S. cerevisiae* grown under heme starvation conditions (35) and the major ADP/ATP carrier of the mitochondrial inner membrane (Pet9), which has been reported to bind and import heme intermediates into the mitochondrion (36).

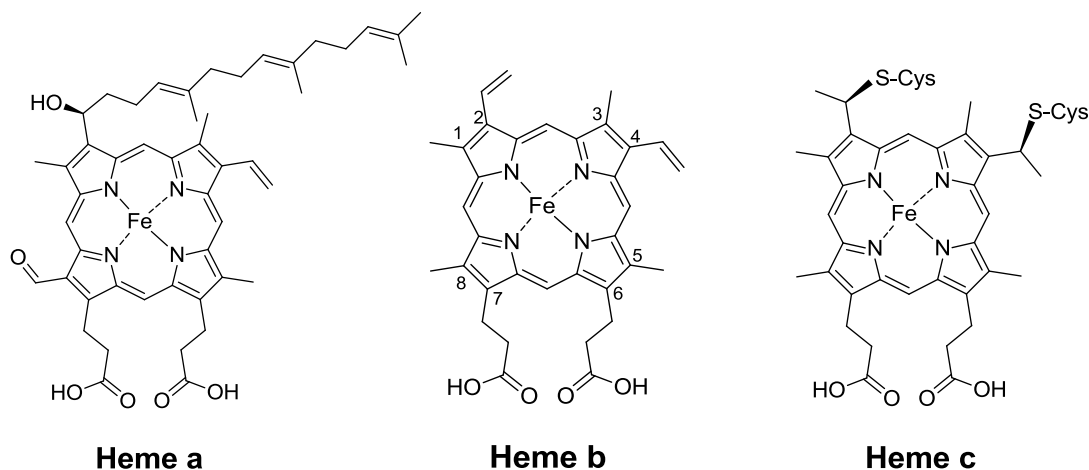


Figure 1.2 Chemical structure of hemes a, b and c. Heme b consists of two vinyl, four methyl and two propionic acid side chains on the conjugated tetrapyrrole ring. In heme c, the two vinyl (C=C) side chains are covalently bonded to cysteine sulfhydryl residues of the apoprotein, while heme a possesses an isoprenoid tail substituted on one of the vinyl groups and a formyl group in place of one methyl groups.

Heme b, found in peroxidases and catalases as well as in hemoglobin, myoglobin and cyclooxygenase enzymes, binds to proteins noncovalently through a single coordination bond between the heme iron and an amino acid side chain (37). Heme c, found in cytochrome c, is synthesized from heme b on the covalent bonding of the heme vinyl groups to two cysteine residues of the protein (Figure 1.1) (37). Heme c is synthesized from heme b, making it a greater energetic investment from the organism from a biosynthetic viewpoint (37). In addition to the variability in the type of heme prosthetic group, the functional versatility of heme proteins is a product of the diverse microenvironment around the heme, which includes the nature of the axial ligands to the iron and the relative solvent/substrate accessibility of the heme (38, 39). Global and

local conformational changes have been compared for the heme-free (apo) and heme-loaded (holo) forms of numerous proteins and for their proximal ligand mutants (38, 39). However, the nature and structural characteristics of the heme-proximal ligand in response to H₂O₂ stress has not been reported for cytochrome c peroxidase, the heme enzyme of interest in this thesis.

1.3) Structure-function characterization of cytochrome c peroxidase *in vitro*

Yeast cytochrome c peroxidase (Ccp1) is a monomeric heme-enzyme localized to the intermembrane space (IMS) of mitochondria (17). Its catalytic cycle couples the two-electron reduction of H₂O₂ to H₂O ($k = 10^9 \text{ M}^{-1} \text{ s}^{-1}$) with two sequential one-electron oxidations of ferrocyclochrome c (Cyc1^{II}), which acts as a reducing substrate for the enzyme (17). Ccp1 was the first heme enzyme to have its crystal structure solved (40) and the complex between Ccp1 and Cyc1 was the first redox-active complex to be crystallized (41). Seven decades of *in vitro* research encompassing genetic engineering of the Ccp1 active site, along with structural, spectroscopic, and kinetic characterization of active-site mutants have provided considerable insight into the mechanism of H₂O₂ activation and the formation of the higher-oxidation state intermediates in Ccp1, namely compound I (CpdI; Fe^{IV},W191⁺) and compound II (CpdII; Fe^{IV}) (17). The Ccp1-Cyc1 interaction remains a paradigm for understanding electron transfer within a protein-protein complex(17).

Ccp1 is mainly α -helical with its *b*-type heme buried in a hydrophobic pocket (Figure 1.2A) (17). H175 in the proximal cavity coordinates to the heme iron and the side-chain of W191 is parallel to, and in Van der Waals contact with, the imidazole ring of H175 (Figure 1.2A) (42). W191 is also in Van der Waals contact with the porphyrin ring. The carboxylate group of D235 is H-bonded to the side chains of H175 and W191 (42). Residues R48, W51 and H52 define the distal heme pocket and overall the active site is highly hydrogen bonded (42). To facilitate H₂O₂

binding, H52 accepts a proton from H_2O_2 and R48 and H52 stabilize the transition state to promote heterolytic cleavage of the oxygen-oxygen bond (42). This results in the formation of an oxyferryl (Fe^{IV}) porphyrin π -cation radical species, which is stabilized by H-bonding with R48 and W51 (42). W191 rapidly reduces the porphyrin π -cation radical to form CpdI (42).

Comparison of the heme active site in Ccp1 with that in ascorbate peroxidase (APX) shows the high structural similarity between these two class I peroxidases (Figure 1.2) (43). Although the proteins share a common catalytic cycle that involves formation of CpdI followed by its reduction by two substrate molecules (43, 44), many differences exist. First, the substrate binding sites are different, which accounts for the low activity of Ccp1 towards ascorbate and of APX towards Cyc^{II} (45). Furthermore, Ccp1 CpdI harbours a protein-based cation radical on W191 while CpdI of APX contains a porphyrin-cation radical even though W179 is in the equivalent position to W191 (43–45). This arises because in APX there is direct coupling of the substrate to the heme so reduction of CpdI occurs through a porphyrin–cation intermediate (43, 44). In contrast, Cyc binds to Ccp1 such that W191 forms part of an electron-transfer pathway between the hemes (17). In the absence of their reducing substrates, W41 in H_2O_2 -treated APX forms a covalent link with the heme (46) while H_2O_2 -treated Ccp1 shows no such crosslink between its heme and the equivalent residue, W51 (47). This further suggests that, although their catalytic sites are highly conserved, Ccp1 and APX are designed to react with different reducing substrates. The structural characterization of Ccp1 and APX also suggests that active site residues are placed strategically in order to prevent heme-protein crosslinks in Ccp1, which suggests that radical transfer pathways in heme peroxidases are driven by different protein functions.

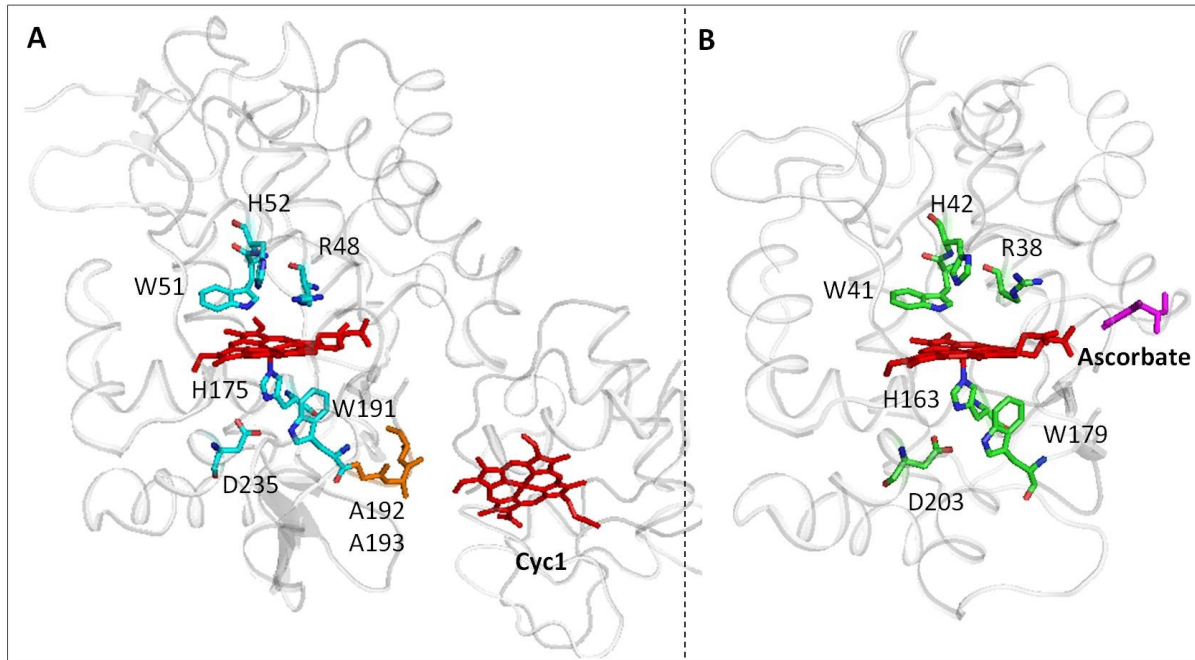


Figure 1.3. Structural similarity of class I peroxidases Ccp1 and APX. PDB cartoon representation of (A) Ccp1 in complex with its reducing partner Cyc1. Residues in orange (A192, A193) define the electron transfer pathway between the Ccp1 and Cyc1 hemes (red sticks). (B) Ascorbate peroxidase (APX) in complex with its reducing substrate, ascorbate (magenta). The key catalytic residues in both proteins are shown as sticks. Figures drawn based on the crystal structure of the Ccp1:Cyc1 complex (PDB:2PCB) and of the APX:ascorbate complex (PDB:10AF).

1.4) Function of cytochrome c peroxidase as a H₂O₂ sensor *in vivo*

The determination of the crystal structures of Ccp1 and of the Ccp1-Cyc1 complex inspired extensive structural and biophysical studies on the mechanism of Ccp1 catalysis (40, 41). After seven decades of *in vitro* research and hundreds of papers written on Ccp1, one might question what is left to discover? However, only a few studies have directly investigated Ccp1's physiological function. Although Ccp1 is not essential for viability and respiration in *S. cerevisiae*, upon H₂O₂ challenge (48, 49), Ccp1 protein levels and activity increase (48, 49), supporting a H₂O₂ detoxifying role for the protein. Furthermore, the *CCP1* deletion mutant yeast strain (*ccp1Δ*) shows increased sensitivity to exogenous H₂O₂ during exponential growth (49).

However, we reported that the response of *ccp1* Δ cells to endogenously generated H₂O₂ is strikingly different than that to exogenous H₂O₂ and points to a signaling role of Ccp1 *in vivo* (50). Although *ccp1* Δ cells accumulate the highest levels of H₂O₂ and exhibit the lowest Cta1 activity, they live longer than wild-type cells (50). This is due to the elevated levels of Sod2 activity induced by H₂O₂ (51–53) which keeps O₂^{•-} levels low. Expression of Ccp1 and Ccp1^{W191F} the catalytically inactive Ccp1 mutant bearing the mutation W191F, increased the activity of the peroxisomal/mitochondrial catalase A (Cta1) (50), which depressed endogenous H₂O₂ levels and lowered the yeast H₂O₂-dependent stress response (7, 53). In turn, significantly depressed mitochondrial superoxide dismutase activity (Sod2), extensive mitochondrial damage and a short-lived phenotype resulted in wild-type and Ccp1^{W191F}-expressing strains relative to the *CCPI*-null mutant. In contrast to its negative effects on mitochondrial fitness, Ccp1 expression increased total catalase and peroxiredoxin activities and provided protection of yeast cells against a bolus addition of H₂O₂ (50). Thus, it was determined that Ccp1 signaling acts as a balance of survival to exogenous stresses and longevity. Furthermore, genetic characterization of Ccp1 and Ccp1^{W191F} shows that in response to exogenous H₂O₂ challenge, both Ccp1 and Ccp1^{W191F} convey an oxidative stress signal to the nuclear transcription factor Skn7 a master regulator of the oxidative stress response in yeast (54). This suggests that the catalytic function of Ccp1 does not drive Ccp1 activation of Skn7 but rather that its signalling function is important.

Heme-based H₂O₂-sensing has not been reported previously and we questioned how H₂O₂ signals through Ccp1 to regulate antioxidant enzyme activities in yeast. Importantly, Ccp1 is capable of responding to exogenous H₂O₂ in the presence of glucose in contrast to the glucose repressed genes involved with cellular respiration (cytochrome c oxidase or Cox1-4 (53)) and antioxidant defense (Cta1(55)) suggesting that Ccp1 is a direct H₂O₂ rather than O₂ sensor, which

contrasts with other heme proteins such as hemoglobin and Hap1 that directly sense O₂. The H₂O₂ sensing function of Ccp1 is the focus of this thesis.

1.5) LC-MS/MS approach to identify protein chemical and post-translational modifications

Mass spectrometric approaches for the analysis of proteins, both native or oxidized, can generally be divided into, “top-down proteomics”, which involves analysis of intact proteins and their fragmentation within the mass spectrometer or “bottom-up proteomics”, which involves prior digestion of the protein(s) and analysis of the peptides are analyzed by mass spectrometry (MS) (56). The peptides frequently are separated by liquid chromatography (LC), and the individual peptides are detected by MS, and tandem MS (MS/MS) is carried out to fragment the peptides into sequence ions (56). The information then is pieced together to reveal the protein identity and/or characteristics (*e.g.*, chemical/post-translational modifications or isoforms) (56). A modified residue is located in a peptide by finding the sequence ions with mass-to-charge (*m/z*) ratios shifted from the expected values (56). The bottom-up approach is used in this thesis and a number of H₂O₂ mediated oxidation products (methionine, cysteine, histidine, tryptophan and tyrosine) were monitored. Selected chemical structures and names can be found in *Appendix II: Residue oxidation products*.

1.6) Outline and scope of this thesis

The key observations of Ccp1 as a H₂O₂ sensor in yeast mitochondria that regulates the activities of other antioxidant enzymes and ROS levels in cells led us to reconsider Ccp1’s physiological roles. Interestingly, Ccp1 shares many features with thiol peroxidases involved in cell signaling. Both rapidly react with H₂O₂ and use low molecular weight proteins as reducing

partners (CycII for Ccp1 and reduced thioredoxin for thiol peroxidases). Differently from thiol peroxidases that rely on oxidation of active-site cysteine(s) to trigger their signaling, Ccp1 senses H₂O₂ by oxidation of its single buried heme. Since Ccp1 is the first heme-based H₂O₂ sensor to be identified, we sought to examine its cellular location, CCP activity, heme status, and its chemical and posttranslational modifications (PTM) to elucidate its sensing and signalling mechanisms.

Here, the role of cytochrome c peroxidase (Ccp1) as a mitochondrial heme donor to Cta1 and its multiple cellular locations in respiring yeast cells are discussed in Chapter 2. Using a mass spectrometric approach we discovered that the H₂O₂ sensing and heme donor roles of Ccp1 are triggered by its overoxidation by H₂O₂ generated from aerobic respiration when the availability of its donor substrate Cyc1 is limited. Ccp1 contains an abundance of oxidizable residues (Tyr, Trp, Met, and His and a single Cys far from its heme), and mapping of heme-mediated oxidation of these residues by up to 10 M eq of H₂O₂ is discussed in Chapter 3. Posttranslational modifications of the protein as a function of cellular location and cell age are presented in Chapter 4. Moreover, a comparison between the *in vitro* and *in vivo* oxidation profiles of Ccp1 confirms that the protein is overoxidized by H₂O₂ in mitochondria, and four radical transfer pathways leading from the heme to its oxidizable residues in the endogenous reduction of H₂O₂ are identified. Using a targeted proteomics approach, interactions of apo- and holoCcp1 with proteins derived from subcellular fractions from 1 d and 7 d cells were probed to gain new insight into Ccp1's relocalization, H₂O₂ signaling and heme-donor functions. The results of this study are reported in Chapter 5.

1.7) Objectives of the thesis

Overall, the key objective of the research presented here can be outlined as follows:

- (a) Characterize Ccp1 as a mitochondrial H₂O₂ sensor and determine how it regulates Cta1 activity.
- (b) Characterize in detail by LC-MS and LC-MS/MS the heme-mediated H₂O₂-induced chemical modifications of Ccp1 using physiologically relevant concentrations of H₂O₂.
- (c) Characterize the post-translational modifications of Ccp1 isolated from fermenting and respiring yeast cells.
- (d) Identify potential binding partners of mitochondrial and extramitochondrial Ccp1 in fermenting and respiring yeast using an N-terminal GST-tagged Ccp1 construct as bait.

Chapter 2: Respiration triggers heme transfer from cytochrome c peroxidase to catalase in yeast mitochondria

2.1) Preface

The work presented in Chapter 2 was published in: Kathiresan M, Martins D and English AM (2014). **Respiration triggers heme transfer from cytochrome c peroxidase to catalase in yeast mitochondria**. Proceedings of the National Academy of Sciences. 111, 17468-17473. Dorival Martins carried out experiments for Figure 2.3B, with helpful discussions and revision of drafts of this paper. The production and interpretation of the other data, writing and revision of the manuscript were performed by me. Dr. English contributed to discussion, data analysis editing and revisions of the paper.

2.2) Abstract of the manuscript

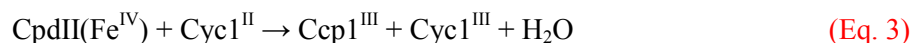
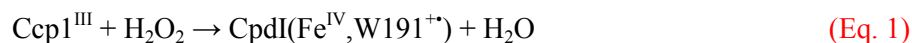
In exponentially growing yeast, the heme enzyme, cytochrome c peroxidase (Ccp1) is targeted to the mitochondrial intermembrane space. When the fermentable source (glucose) is depleted, cells switch to respiration and mitochondrial H₂O₂ levels rise. It has long been assumed that CCP activity detoxifies mitochondrial H₂O₂ because of the efficiency of this activity *in vitro*. However, we find that a large pool of Ccp1 exits the mitochondria of respiring cells. We detect no extramitochondrial CCP activity since Ccp1 crosses the outer mitochondrial membrane as the heme-free protein. In parallel with apoCcp1 export, cells exhibit increased activity of catalase A (Cta1), the mitochondrial and peroxisomal catalase isoform in yeast. This identifies Cta1 as a likely recipient of Ccp1 heme, which is supported by low Cta1 activity in *ccp1Δ* cells and the accumulation of holoCcp1 in *cta1Δ* mitochondria. We hypothesized that Ccp1's heme is labilized by hyperoxidation of the protein during the burst in H₂O₂ production as cells begin to respire. To test this hypothesis, recombinant Ccp1 was hyperoxidized with excess H₂O₂ *in vitro*, which

accelerated heme transfer to apomyoglobin added as a surrogate heme acceptor. Furthermore, the proximal heme Fe ligand, His175, was found to be ~85% oxidized to oxo-histidine in extramitochondrial Ccp1 isolated from 7 day cells, indicating that heme labilization results from oxidation of this ligand. We conclude that Ccp1 responds to respiration-derived H₂O₂ via a novel mechanism involving H₂O₂-activated heme transfer to apoCta1. Subsequently, the catalase activity of Cta1, not CCP activity, contributes to mitochondrial H₂O₂ detoxification.

2.3) Introduction

Cytochrome c peroxidase (Ccp1) is a monomeric nuclear encoded protein with a 68-residue N-terminal mitochondrial targeting sequence (57). This presequence crosses the inner mitochondrial membrane and is cleaved by matrix proteases (58, 59). Mature heme-loaded Ccp1 is found in the mitochondrial intermembrane space (IMS) in exponentially growing yeast (58, 59) but the point of insertion of its single b-type heme is unknown. Under strict anaerobic conditions, Ccp1 is present in mitochondria as the heme-free or apoform (60). Once cells are exposed to O₂ and heme biosynthesis is turned on, apoCcp1 converts rapidly to the mature holoenzyme by noncovalently binding heme (61).

It is well established that mature Ccp1 functions as an efficient H₂O₂ scavenger *in vitro* (17). Its catalytic cycle involves the reaction of ferric Ccp1 with H₂O₂ (Eq. 1) to form compound I (CpdI) with a ferryl (Fe^{IV}) heme and a cationic indole radical localized on Trp191 (W191⁺). CpdI is one-electron reduced by the ferrous heme of cytochrome c (Cyc1) to compound II (CpdII) with ferryl heme (Eq. 2), and electron donation by a second ferrous Cyc1 returns CpdII to the resting Ccp1^{III} form (Eq. 3):



Since Ccp1 production is not under O₂/heme control (60, 61), CCP activity is assumed to be the frontline defense in the mitochondria, a major source of reactive oxygen species (ROS) in respiring cells (62). Contrary to the time-honored assumption that Ccp1 catalytically consumes the H₂O₂ produced during aerobic respiration (48), recent studies in our group reveal that the peroxidase behaves more like a mitochondrial H₂O₂ sensor than a catalytic H₂O₂ detoxifier (49, 50, 63). Notably, Ccp1 competes with complex IV for reducing equivalents from Cyc1, which shuttles electrons from complex III (ubiquinol cytochrome *c* reductase) to complex IV (cytochrome *c* oxidase) in the electron transport chain (64).

Since CCP activity in the IMS siphons electrons from energy production, a H₂O₂ sensor role for Ccp1 should be energetically more favorable for the cell. Key evidence for a noncatalytic role for Ccp1 in H₂O₂ removal is that the isogenic strain producing the catalytically inactive Ccp1^{W191F} protein accumulates *less* H₂O₂ than wild-type cells (50). In fact, this mutant strain exhibits ~3 fold higher Cta1 activity than wild-type cells (50) whereas *CCPI* deletion results in a strain (*ccp1Δ*) with negligible Cta1 activity and high H₂O₂ levels (5). Unlike Cta1, which is the peroxisomal and mitochondrial catalase isoform in yeast (14), the cytosolic catalase Ctt1 (15) exhibits comparable activity in the wild-type, Ccp1^{W191F} and *ccp1Δ* strains (50). Given that both Ccp1 and Cta1 are targeted to mitochondria, we hypothesized that Ccp1 may transfer its heme to apoCta1 in respiring cells.

Cta1 is nuclear encoded with embedded mitochondrial and peroxisomal targeting sequences (65). Like Ccp1, each monomer noncovalently binds a b-type heme and mature Cta1 is active as a homotetramer. Synthesis of the Cta1 monomer is under O₂/heme control such that the

apoenzyme only begins to accumulate during the logarithmic phase of aerobic growth (66). Hence, its O₂/heme independent production (60, 61) allows apoCcp1 to acquire heme while cells are synthesizing apoCta1. This, combined with our observation that Cta1 activity increases in respiring cells producing Ccp1 or Ccp1^{W191F} but not in *ccp1Δ* cells (50), led us to speculate that respiration-derived H₂O₂ triggers heme donation from Ccp1 to apoCta1 within mitochondria.

What experimental evidence would support heme donation by Ccp1? It has been demonstrated that mutation of the proximal heme Fe ligand, His175, to a residue with weak or no Fe-coordinating ability produces Ccp1 variants (H175P, H175L, H175R, H175M) that undergo mitochondrial processing but do not accumulate in isolated yeast mitochondria (67). Presumably, reduced heme affinity allows the Ccp1 variants to unfold and cross the outer mitochondrial membrane (67). Hence, we argued that if wild-type Ccp1 donated its heme, the apoprotein would likewise exit mitochondria. Consequently, we examine here age-dependent Ccp1-GFP localization in live cells chromosomally expressing Ccp1 C-terminally fused to green fluorescent protein (GFP) as well as the distribution of wild-type Ccp1 between subcellular fractions. Since weakening or removal of the proximal Fe ligand on His175 mutation reduces heme affinity (67), His175 oxidation in wild-type Ccp1 should have a similar effect, which we investigate here. We further speculated that in the absence of apoCta1 as an acceptor for its heme, more Ccp1 would remain trapped in the IMS so we compare mitochondrial Ccp1 levels in wild-type and *cta1Δ* cells. Our combined results support triggering of heme donation from Ccp1 to apoCta1 by respiration-derived H₂O₂. Such H₂O₂-activated heme transfer between proteins has not been reported to date and its implications in H₂O₂ signaling are discussed.

2.4) Materials and methods

2.4.1) Materials

The fluorescent dyes (MitoTracker® Red CMXRos, Hoescht and FM4-64) were purchased from Molecular Probes, Invitrogen. Proteins were obtained from the following suppliers: bovine catalase, bovine serum albumin (BSA), horse heart ferrocytochrome c type III, myoglobin (Mb) (Sigma), sequencing grade modified trypsin (Promega), thrombin (Calbiochem) and Zymolase 20T (Amsbio). Other suppliers were as follows: SuperSignal West Pico enhanced chemiluminescence kit, Tween 20 (Thermo Fisher); Ficoll 400, Coomassie (MP Biomedicals); hemin chloride, phenylmethylsulfonyl fluoride (PMSF), Percoll (Sigma); 5 mL HiTrap Q anion-exchange column, Benzamidine Sepharose 4 Fast Flow and DEAE Sepharose resins (GE Healthcare); Ni-NTA resin (Qiagen); pET15b vector (Novagen), and C18 Zip tips (Millipore).

2.4.2) Antibodies

The following antibodies were used for Western blotting: Rabbit anti-Ccp1 serum was kindly provided by Professor David Goodin (University of California, Davis); rabbit anti-GFP antibody (sc-8334 Santa Cruz); mouse anti-porin (ab110326 Abcam); mouse anti-Cyc raised against bovine heart cytochrome c (ab110325 Abcam); mouse anti-homocitrate synthase (MCA-31F5 EnCor Biotechnology); goat anti-rabbit horseradish peroxidase conjugated secondary antibody and goat anti-mouse horseradish peroxidase conjugated secondary antibody (Biorad). Porin, Cyc and homocitrate synthase are used in this study as mitochondrial outer membrane, mitochondrial intermembrane space (IMS) and nuclear markers, respectively.

2.4.3) Yeast strains

Yeast strains used in this study (Table 2.1) are in the BY4741 genetic background. The wild-type strain was purchased from the European *Saccharomyces cerevisiae* Archive for Functional Analysis (EUROSCARF) and the Ccp1-GFP-expressing strain was purchased from Invitrogen Life Sciences. The *cta1Δ* and *ctt1Δ* strains were kind gifts from Christopher Brett (Concordia University), and the DNA template for recombinant His6-Ccp1 expression was generously provided by Yu Li (University of Illinois at Urbana–Champaign, Urbana, IL).

Table 2.1. *S. cerevisiae* strains

Strain	Genotype	Reference
BY4741 Wild-type	<i>MATa his3Δ1 leu2Δ0 met15Δ0 ura3Δ0</i>	Brachmann et al. 1998 (68)
YDR256C	BY4741; <i>cta1Δ::kanMX4</i>	Winzeler et al. 1999 (69)
YGR088W	BY4741; <i>ctt1Δ::kanMX4</i>	Winzeler et al. 1999 (69)
YKR066C	BY4741; CCP1:GFP-HIS3MX6	Huh et al, 2003 (70)

2.4.4) Imaging of live yeast cells by wide-field fluorescence microscopy

Cells expressing Ccp1-GFP were cultured in YPD medium, washed with PBS (10 mM sodium phosphate and 150 mM NaCl, pH 7.4), diluted to 1×10^4 cells/mL in PBS, and co-stained for 30 min at room temperature with probes selective for mitochondria (MitoTracker® at 0.25 μ M) and nuclei (Hoescht at 2.0 μ M). Vacuoles were stained in 7 day cells by incubation with 40 μ M FM4-64 for 60 min on ice and cells were transferred to fresh YPD media for 16 h at 14 °C (71, 72). Following staining, all cells were mounted on a glass slide with a coverslip (Thermo Fisher), and illuminated by a Heliphor LED or halogen light source (for differential interference contrast, DIC) of an inverted epifluorescence microscope (Nikon Eclipse Ti) and examined through an oil-immersed 100x objective using filters selective for GFP (480, 535/25 nm), MitoTracker (555, 630/75 nm), Hoechst (405, 488/75 nm) or FM4-64 (480 nm, 550 long-pass

filter). Digital images were collected with an EMCCD camera (Photometrics Evolve 512) using an exposure time of 100 ms, which was increased to 500 ms for GFP imaging. Image analysis was performed using ImageJ (v. 1.47; NIH), including background subtraction, brightness and contrast adjustment.

2.4.5) Subcellular fractionation of yeast lysates and isolation of crude nuclei

Denucleated (S2), mitochondria-enriched (P10) and mitochondria-depleted (S10) subcellular fractions were isolated from yeast as described previously (63, 73). Western blotting with anti-porin and anti-Cyc confirmed that P10 and S10 were highly enriched and depleted in mitochondria, respectively. Nuclei were isolated following the published protocol (74) with minor modifications. Briefly, yeast grown in YPD medium were harvested at the times indicated, washed twice with 0.85% NaCl and 7 day and older cells were incubated for 15 min at 35 °C in 100 mM EDTA (pH 8.0)/0.5% β -mercaptoethanol to prepare for spheroplasting. This washing step was bypassed for 1- to 4-day cells, which are more susceptible to spheroplasting (74). Cells were pelleted by centrifugation at 2000xg for 5 min at room temperature, resuspended in S buffer (1.2 M sorbitol, 0.5 mM CaCl_2 in 20 mM KPi, pH 6.5) containing 0.5% β -mercaptoethanol, and treated with Zymolase 20T (3 mg/g cell pellet) at 30 °C. Spheroplast formation, monitored by light microscopy, was complete after 1-2 h incubation at 30 °C with gentle agitation. Spheroplasts were pelleted by centrifugation at 2000xg and 4 °C for 10 min, resuspended in FB buffer (18% Ficoll 400, 0.5 mM CaCl_2 , 0.5 mM PMSF in 20 mM KPi, pH 6.5), disrupted with 15 strokes of a Teflon Dounce homogenizer, centrifuged at 1500xg and 4 °C for 10 min to remove cell debris and the supernatant was spun at 24000xg for 15 min at 4 °C in a Beckman SW 41 Ti rotor. The crude nuclear pellet was resuspended at 4 mL/g in FB buffer, homogenized with 10 strokes of the homogenizer, layered onto a 32.5% Percoll gradient and spun at 38700xg for 45

min at 4 °C. Nuclei were recovered as a whitish band in the bottom third of the tube, collected and washed 3x in FB buffer to remove cytoplasmic contaminants. Immunoblotting with anti-homocitrate synthase confirmed the presence of nuclei.

2.4.6) Western blotting of Ccp1 and Ccp1-GFP

The method of equal volumes (75) was used to quantify the relative amounts of Ccp1 in the subcellular fractions by Western blotting. Briefly, the S2 lysate was diluted to 1 mg/mL in homogenization buffer (0.6 M sorbitol, 1 mM EDTA, 1 mM PMSF, 1x protease inhibitor cocktail in 10 mM Tris HCl, pH 7.4), 1 mL was centrifuged at 12000xg at 4 °C for 20 min to obtain ~1 mL of mitochondria-free supernatant (S10) and the mitochondria-enriched pellet (P10) was resuspended in 1 mL of homogenization buffer. Equal volumes (10-20 µL) of the S2, P10 and S10 fractions were loaded onto a 12% resolving (10x6x0.1 cm) SDS-PAGE gel and wet transfer of the electrophoresed proteins to a methanol-activated polyvinylidene fluoride (PVDF, BioRad) membrane was carried out at 100 mA for 2 h. After blocking for 1 h with 5% (w/v) skim milk in TBST (150 mM NaCl, 0.05% v/v Tween 20 in 50 mM Tris, pH 7.6), membranes were incubated with anti-Ccp1 (1:5000 dilution) or anti-GFP (1:1000) for 1 h, washed 3x with TBST, and incubated with the secondary antibody (1:20000) for 1 h. Signals were visualized by ECL using 30 s (Ccp1) and 1 min (Ccp1-GFP) exposure times and digitized in an AlphaImager (Alpha Innotech). After Ccp1 immunodetection, membranes were probed with anti-porin or stained with Coomassie as loading controls. Note that Ccp1 signals are normalized to the porin signal in Figure. 2.4, which compares Ccp1 levels in the P10 fractions from different yeast strains. Figures. 2.2 and S2.1 compare Ccp1 levels in S2, S10 and P10 fractions from wild-type and Ccp1-GFP cells vs age so these Ccp1 signals are normalized to the sum of the Coomassie signals in the same fraction (76) since porin is not present in all subcellular fractions.

2.4.7) Linear range for Ccp1 detection and the response of anti-Ccp1 toward different chemical forms of recombinant Ccp1

A standard curve was generated by loading solutions of recombinant holoCcp1 in the range of 4 fmol-2 nmol onto a 12% resolving SDS-PAGE gel and performing Western blotting with anti-Ccp1 as described in the previous section. The response is found to be linear between 4-120 fmol Ccp1 (Figure. S2.7C). Solutions of 1 μ M recombinant apoCcp1, recombinant holoCcp1 and recombinant holoCcp1 treated with 1 and 10 μ M H₂O₂ in 20 mM KPi/100 μ M DTPA (pH 7.5) for 60 min at room temperature were diluted to 30 nM and 2 μ L of each (60 fmol of Ccp1) was loaded onto a reducing 12% SDS PAGE gel for Western blotting as described above. Anti-Ccp1 detects all chemical forms of the peroxidase equally (Figure. S2.7A,B).

2.4.8) Heme blotting of Ccp1 isolated from P10 and S10 fractions

Mitochondria-enriched P10 and mitochondria-free S10 fractions from 500 mL cultures of 2- and 7 day cells were dialyzed against 20 mM KPi buffer (pH 6.0) overnight and centrifuged at 14000xg for 10 min. The supernatants (1 mL) were applied to the HiTrap Q anion-exchange column equilibrated with the same buffer and attached to a Biotech AKTA Purifier 10 (GE Healthcare). Elution was performed using a linear 0-1 M NaCl gradient over 25 min at a flow rate of 2.0 mL/min, 1 mL fractions were collected and 15 μ L of each was dot blotted onto two PVDF membranes. One membrane was probed with anti-Ccp1 as described above for Western blotting and the second membrane was probed with the ECL reagent (luminol/H₂O₂) for 5 min to detect heme-containing proteins based on their pseudoperoxidase activity (77). BSA and Mb were used as negative (heme-free) and positive (heme-containing) protein controls, respectively. The Ccp1 and heme signals were digitized using the AlphaImager with an exposure time of 2 min.

2.4.9) CCP and catalase activity assays

CCP activity, the catalysis of ferrocyclochrome c oxidation by H₂O₂ (78), was monitored in the subcellular fractions. The assay solution contained 90 μM H₂O₂, 27 μM (~95% dithionite-reduced) horse heart ferrocyclochrome c and 10 mM EDTA in 50 mM KPi (pH 7.0). Following addition of the fractionated lysate (0.1-0.5 mg/mL protein) to 1 mL of assay solution, CCP activity was determined from the initial rates of ferrocyclochrome c oxidation ($\epsilon_{550} = 27.6 \text{ mM}^{-1} \text{ cm}^{-1}$), and 1 unit of specific CCP activity catalyzes the peroxidation of 1 μmol of ferrocyclochrome c/min/mg protein (78). Before assaying for CCP activity, P10 fractions were incubated with 0.02% digitonin in homogenization buffer solution for 10 min at 4 °C to permeabilize the mitochondrial outer membrane (79). Also, the S10 fractions (1 mg) were pre-incubated with 0.1 μM hemin in homogenization buffer for 10 min at 4 °C in attempts to reconstitute extramitochondrial apoCcp1 with heme.

To determine catalase activity, 5.0-20 μL aliquots of soluble protein lysates, prepared as previously described (50), were added to 1.0 mL of 20 mM H₂O₂ in 50 mM KPi (pH 7.0). H₂O₂ decomposition was monitored at 240 nm ($\epsilon_{240}=43.6 \text{ M}^{-1} \text{ cm}^{-1}$) (80), and 1 unit of catalase activity catalyzed the degradation of 1 μmol of H₂O₂ per min. Cta1 and Ctt1 activities were assayed separately following extract fractionation by native PAGE as reported (50).

2.4.10) Expression and purification of recombinant Ccp1

The cDNA for yeast Ccp1 encoding an extra methionine and isoleucine at positions -2 and -1 of the mature protein (9) was subcloned into the NdeI and EcoRI sites of the pET15b vector. *E. coli* BL21(DE3) cells were transformed with pET15b-Ccp1, and grown to an OD₆₀₀ of 0.6 in LB medium with 100 μg mL⁻¹ ampicillin at 37 °C and 250 rpm. IPTG (0.5 mM) was added

to induce Ccp1 overexpression and the culture was further incubated at 37 °C and 250 rpm for 16 h. Cells expressing Ccp1 with an N-terminal His₆-tag were lysed by 3 freeze/thaw cycles in liquid nitrogen/37 °C water bath, and the lysate was added to loading buffer (500 mM NaCl, 10 mM imidazole in 100 mM Hepes, pH 7.5). Following 10 x 10 s sonication cycles, the cell debris was removed by centrifugation at 12000xg for 20 min, 1 mL of Ni-NTA resin was added to 10 mL of supernatant, incubated at 4 °C for 1 h, and the resin was washed with loading buffer containing 10 and then 25 mM imidazole. His₆-Ccp1 was eluted from the resin with 500 mM imidazole in the same buffer, dialyzed against 20 mM KPi (pH 7.5) overnight and the His₆-tag was cleaved by incubation with 5 U of thrombin per mg His₆-Ccp1 for 16 h at 4 °C. Ni-NTA resin was added to remove any uncleaved protein and the free His tag, and the supernatant containing tag-free Ccp1 and thrombin was transferred to an Eppendorf tube with 100 µL of Benzamidine Sepharose 4 Fast Flow resin (pre-equilibrated with 20 mM KPi, pH 7.5) to bind the thrombin. The resultant Ccp1 solution (60 mg/L culture) had a 410/280 nm absorbance ratio of 0.16, indicating that Ccp1 was isolated mainly as the apoform, which was stored in 20 mM KPi (pH 7.5) at -80 °C until use.

2.4.11) *In vitro* heme transfer

Since removal of the buried heme from catalase results in poorly defined products, apoMb, the prototypical heme acceptor (81, 82), was used as a surrogate acceptor of Ccp1 heme *in vitro*. ApoMb was prepared from the horse heart holoprotein by the acid/methyl ethyl ketone method (83). Heme removal was confirmed by the loss of Soret absorbance at 408 nm, and apoMb in 20 mM KPi (pH 7.5) was stored at -20 °C until use. A stock solution of 0.70 mM hemin was prepared in 0.1 M NaOH and its concentration determined by forming the pyridine hemochrome (84). ApoMb or apoCcp1 was incubated with 1.1 molar equivalents of hemin in 20 mM KPi (pH 7.5) for 1 h at 4 °C to reconstitute the holoproteins, unbound hemin was removed

on a 0.8 x 4 cm DEAE Sepharose column equilibrated with the same buffer and the holoproteins were eluted by adding 500 mM NaCl to the buffer. Protein concentrations were determined spectrophotometrically using the following ϵ values ($\text{mM}^{-1} \text{cm}^{-1}$): apoMb ($\epsilon_{280}=59.4$), holoMb ($\epsilon_{408}=188$) (85); apoCcp1 ($\epsilon_{280}=15.8$), holoCcp1 ($\epsilon_{410}=98$) (86).

Heme donation from 20 μM holoCcp1 to 60 μM apoMb was examined in 20 mM KPi (pH 7.5) at 30 °C. Following incubation for 60 min with gentle stirring, the proteins were separated on the DEAE column as described above and the percent heme transfer was estimated from the Soret absorbance of the two proteins (Figure. S2.2A,C). To examine if Ccp1 hyperoxidation by H_2O_2 accelerates heme transfer, 20 μM Ccp1 was pretreated with 200 μM H_2O_2 at 4 °C for 60 min, 0.1 nM catalase was added to remove any unreacted H_2O_2 , and 20 μM hyperoxidized Ccp1 was incubated with 60 μM apoMb. The Soret maximum of the Fe^{III} heme of Ccp1 red shifts from 410 to 419 nm indicative of Fe^{IV} heme formation on H_2O_2 addition (Figure. S2.2A). However, the Fe^{IV} heme decayed to Fe^{III} heme during anion-exchange chromatography so heme loading of Ccp1 was monitored at 410 nm (Figure. S2.2B).

2.4.12) Mass spectrometric analysis of Ccp1 hyperoxidation *in vitro* and *in vivo*

After standing in 20 mM KPi pH (7.5)/100 μM DTPA at 4° C for 60 min, solutions of 5 μM recombinant Ccp1 or apoCcp1 \pm 50 μM H_2O_2 were diluted 5-fold into 2% acetonitrile/0.1% formic acid. Aliquots (2 μL) were loaded onto a reversed-phase Zorbax 300SB-C3 (2.1 x 150 mm, 5 mm) column equilibrated with 5% acetonitrile/0.1% formic and acid attached to an Agilent 1100 HPLC system. The protein was eluted at 0.2 mL/min into the electrospray (ESI) source of a QToF3 Ultima API Mass Spectrometer (Waters) using a 5-95% acetonitrile gradient over 5 min, 95% acetonitrile for 3 min, and 95-5 % acetonitrile over 3 min, all in 0.1% formic acid. The column was re-equilibrated with 5% acetonitrile/0.1% formic acid for 8 min prior to the

next injection. The mass measurements were performed using the following QToF3 parameters: capillary voltage 3.5 kV, cone voltage 35 V, RF lens 50 V, source temperature 80°C and desolvation temperature 300 °C. Protein envelopes were deconvoluted by the MaxEnt1 algorithm to obtain the protein masses given in Figure. S2.4.

The exact mass of protein-derived heme and authentic hemin was recorded on a LTQ Orbitrap Velos mass spectrometer (Thermo Scientific). Hemin or hemoprotein in 5% acetonitrile/0.1% formic acid was injected onto a reversed-phase C4 column (100 µm x 4.0 cm) prepared in-house and attached to an Easy-nLC 1000 (Thermo Fisher). The column was equilibrated with the same solution and samples were eluted at 200 nL/min into the ESI source using a 5–95% acetonitrile gradient and analyzed in full-scan mode (m/z 100–2000) in the Orbitrap high resolution mass analyzer ($R = 60,000$ at m/z 400). Other instrumental parameters were: electrospray voltage 3 kV, CID collision energy 30 V and heated capillary temperature 200 °C.

To identify sites of polypeptide oxidation, 1 µM oxidized Ccp1 was digested overnight with 12.5 ng/µL (1:20) of trypsin in 50 mM Tris (pH 7.4)/100 µM DTPA at 37 °C. The digest was desalted on C18 Zip tips and the tryptic peptides (5 µL/injection) were separated on a reversed-phase C18 column (100 µm x 6.5 cm) prepared in-house and attached to the nanoLC. The column was equilibrated with 2% acetonitrile/0.1% formic acid and peptides were eluted at 200 nL/min into the ESI source using a 2–94% acetonitrile gradient and analyzed in full-scan mode (m/z 350–2000) with the instrumental parameters given above for hemin analysis. Precursor ions of the Ccp1 peptides were selected using a mass exclusion threshold of 10 ppm and subjected to MS/MS in the Velos linear ion trap mass analyzer using a mass tolerance of 0.8 u for the fragment ions. MS/MS fragments with an intensity count of 20 or greater were analyzed

using Proteome Discoverer 1.3.0 (Thermo Scientific) and the Sequest search engine with mass filters for oxidation (+16, +32, +48 u) of Met, Cys, Trp, Tyr and His, and for Cys alkylation by iodoacetamide (+57 u). Sequest correlated the MS/MS spectra with peptide sequences in the Ccp1 Fasta file downloaded from the NCBI website (<ftp://ftp.ncbi.nlm.nih.gov/>). For confident peptide identification, the following Sequest filters were implemented: XCorr ≥ 2 and False Discovery Rate < 0.01 . XCorr is the cross-correlation between the theoretical and experimental MS/MS spectra of the sequenced peptides. The percent oxidation of His175 or Met172 is based on the relative integrated peak areas in the extracted ion chromatograms (XICs) from the primary mass spectra (MS1) (Table S2.4).

Ccp1 was isolated from 2- and 7 day yeast cells as described under *Heme Blotting of Ccp1 Isolated from P10 and S10 Fractions*. The anti-Ccp1 reactive fractions were further subjected to SDS-PAGE on a 12% resolving gel and Coomassie stained. The gel was cut into 1-cm bands and the proteins in each band were reduced with dithiothreitol, alkylated with iodoacetamide, tryptic digested and the peptides were analyzed by LC-MS/MS as described above.

2.5) Results

2.5.1) Ccp1-GFP and Ccp1 are selectively exported from mitochondria of respiring cells.

The cellular location of Ccp1-GFP was tracked in live cells by epifluorescence microscopy. GFP fluorescence and that of MitoTracker, a mitochondrial probe, overlap in 1 day cultures (Figure 2.1A), consistent with previous reports that Ccp1-GFP is localized in the IMS of exponentially growing yeast (58). In contrast, cells from 7 day cultures exhibit distinct regions of GFP and MitoTracker fluorescence, indicating extramitochondrial localization of Ccp1-GFP. GFP fluorescence appears as large circular structures while the mitochondrial morphology

changes from a reticular network in 1 day cells to diffuse spherical organelles in stationary-phase cells as previously reported (87). Notably, GFP fluorescence co-localizes with the vacuolar membrane marker FM4-64 in 7 day cells (Figure 2.1A), suggesting that extramitochondrial Ccp1-GFP may be targeted to the vacuole.

Probing subcellular fractions obtained by differential centrifugation with a polyclonal anti-Ccp1 antibody yields results in agreement with live cell imaging. [We note here that anti-Ccp1 detects all the chemical forms of Ccp1 of interest in our study (apoCcp1, holoCcp1, CpdI, hyperoxidized Ccp1) with the same sensitivity (Figure S2.7A,B). Western blotting reveals a relatively constant amount of Ccp1 or Ccp1-GFP in the denucleated (S2) fractions over 1 to 10 days, but the levels in mitochondria-free (S10) fractions increase dramatically at the expense of those in mitochondria-enriched (P10) fractions (Figures 2.2A,B, S2.1A,B). Notably, Ccp1 is barely detectable in P10 after 10 days but highly abundant in S10, indicating that during this period most of the protein escapes from mitochondria. Furthermore, processing of both Ccp1 and its GFP fusion by the matrix proteases (58) appears to be complete since the immature proteins with their additional 7-kDa mitochondrial targeting sequence would be detectable as anti-Ccp1 and anti-GFP bands above those of the mature proteins (Figures 2.2A, S2.1A).

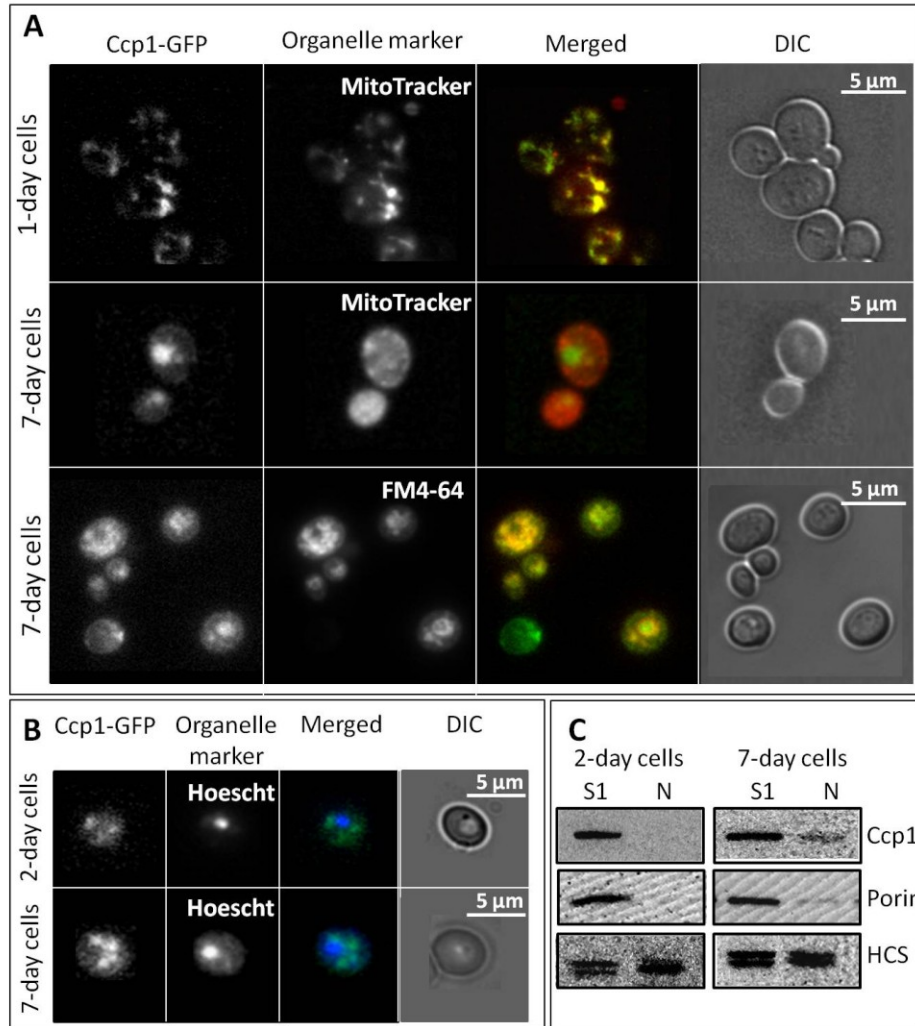


Figure 2.1 Ccp1-GFP is mitochondrial in 1 day and vacuolar in 7 day yeast cells; Ccp1 is present in nuclei from 7 day cells. Live Ccp1-GFP-expressing cells were visualized for (A) GFP (480, 535/25), stained with MitoTracker (555, 630/75) and FM4-64 (480, 550 long-pass filter) to visualize mitochondria and vacuole, respectively, and with (B) Hoescht (405, 488/75) to visualize nuclei. Phase-contrast microscopy (DIC) was used to monitor cell integrity. (C) Immunoblot analysis with anti-Ccp1 of total (S1) and nuclear (N) fractions isolated from 2- and 7 day yeast. Porin and homocitrate synthase citrate (HSC), which exists as 47 and 49 kDa isoforms in yeast (88), were used as nuclear and mitochondrial outer membrane markers, respectively.

To establish whether Ccp1 export is selective or the result of nonspecific mitochondrial membrane damage, the fractions were probed with anti-porin and anti-Cyc1 as mitochondrial outer membrane and IMS markers, respectively. As shown in Figure 2.2A and Figure S2.1A, the

S10 fractions are not immunoreactive with these antibodies, so mitochondria remain intact. Thus, we conclude that apoCcp1 and apoCcp1-GFP selectively exit the mitochondria of respiring cells.

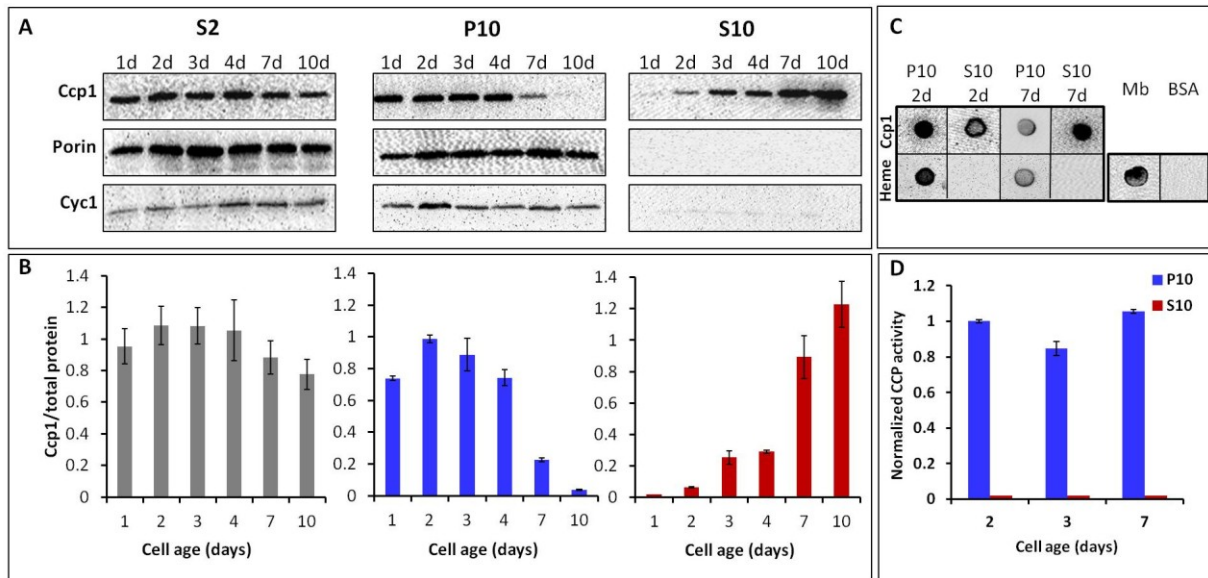


Figure 2.2 Ccp1 exits mitochondria as yeast begin respiring and extramitochondrial Ccp1 does not possess CCP activity. (A) Immunoblot analysis of equal volumes of denucleated (S2), mitochondrial (P10), and cytosolic (S10) fractions vs cell age. Porin and Cyc1 are mitochondrial outer membrane and IMS markers, respectively. (B) The Ccp1 signals in panel A were quantified and normalized to the sum of the Coomassie bands in the same lane (not shown). (C) Dot blot analysis with anti-Ccp1 (top row) and the ECL reagent (luminol/H₂O₂) to detect heme (bottom row) from 2- and 7 day P10 and S10 fractions. Myoglobin and BSA were used as positive and negative heme controls, respectively. (D) Normalized CCP activity in mitochondrial (P10) and cytosolic (S10) fractions. Specific activity was ratioed by the Ccp1 protein levels in panel B, and normalized to the level for 2-day cells (Table S2.1). Results in panels A and C are representative of three independent cultures ($n=3$) and averages \pm SD are plotted in panels B and D.

2.5.2) Ccp1 is targeted to the nucleus and possibly the vacuole.

No overlap between the Hoechst nuclear dye and GFP fluorescence is observed at any cell age (Figure 2.1B), indicating that Ccp1-GFP does not accumulate in the nucleus. Since the fusion protein (62 kDa) is above the size cutoff (60 kDa) for diffusion through the nuclear pore (89), nuclear enriched fractions (N) were probed for native Ccp1 (34 kDa). No Ccp1 was detected in nuclei isolated from 2-day cells but ~10% was reproducibly detected in 7 day nuclei (Figure

2.1C), and may function as a retrograde messenger (90) (See Discussion). Ccp1, like Ccp1-GFP (Figure 2.1A), also may be targeted to the vacuole in 7 day cells. However, this could not be confirmed because vacuoles, which are present in the S10 fraction of young cells, fragment during spheroplasting of 7 day cells.

2.5.3) Extramitochondrial Ccp1 is catalytically inactive.

Staining for the intrinsic peroxidase activity of heme (77) confirmed that Ccp1 purified from 2- and 7 day S10 subcellular fractions is in the apoform (Figure 2.2C). Consistent with this absence of Ccp1 heme, no CCP activity is detected in the S10 fractions at any cell age (Figure 2.2D, Table S2.1) but adding exogenous hemin does not restore activity. Further experiments discussed below reveal that extramitochondrial apoCcp1 is oxidized, which prevents re-formation of catalytically active Ccp1 on hemin addition. In contrast, the purified P10 mitochondrial-enriched fractions stain for heme (Figure 2.2C) and are catalytically active (Figure 2.2D). Ratioing CCP activity against Ccp1 protein level in Figure 2.2B reveals that the activity of mitochondrial Ccp1 is relatively constant with cell age (Figure 2.2D). Interestingly, the fractions containing Ccp1-GFP and Ccp1 exhibit very similar CCP activity (Figure 2.2D, Figure. S2.1C, Table S2.1), suggesting that fusion of Ccp1's C-terminal to GFP does not interfere with CpdI reduction by Cyc1^{II} (Eqs. 2,3).

2.5.4) Cta1 activity increases as Ccp1 exits mitochondria.

As mitochondrial Ccp1 levels drop in wild-type cells, their total catalase activity increases proportionally (Figure 2.3). This led us to postulate that catalase may be an acceptor of Ccp1's heme, which is supported by the depressed catalase activity in *ccp1Δ* cells (Figure 2.3B). We separately monitored the activity of each catalase isoform using an in-gel assay (50), and found

comparable Ctt1 activity in the two strains, but ~5-fold higher Cta1 activity in 7 day wild-type vs *ccp1Δ* cells (Figure 2.3B inset). This identifies apoCta1 as a mitochondrial recipient of Ccp1's heme, which we further examined in catalase-null strains.

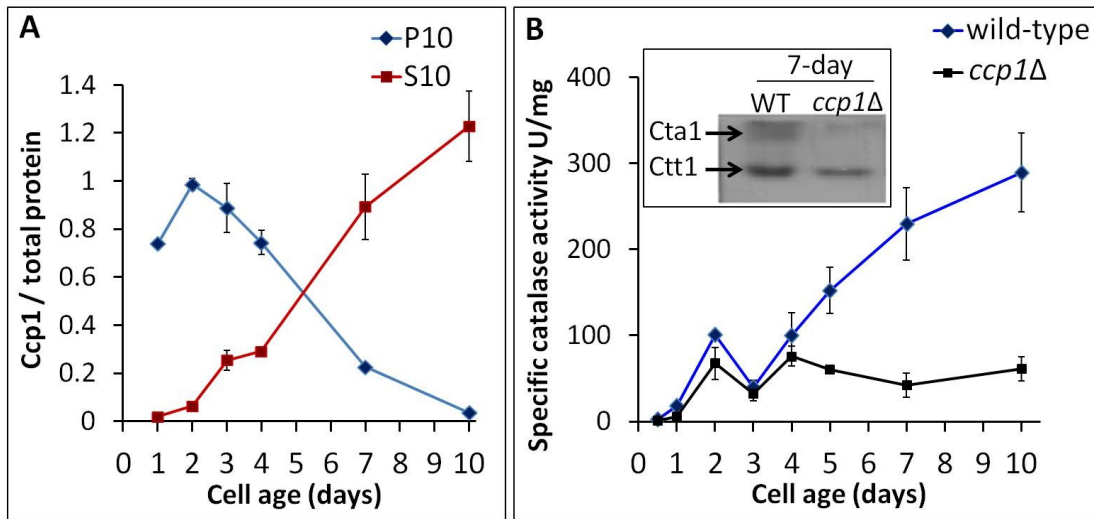


Figure 2.3. Catalase activity in wild-type yeast increases at the expense of mitochondrial Ccp1. (A) Ccp1 protein level vs cell age in the S10 and P10 fractions from Figure. 2.2B. (B) Specific catalase activity in S2 protein extracts from wild-type and *ccp1Δ* cells vs cell age. Results are averages of three independent cultures ($n=3$) \pm SD. Inset: In-gel assay of Cta1 and Ctt1 catalase activities in 7 day S2 protein extracts (2.5 μ g protein/lane).

2.5.5) Ccp1 accumulates in mitochondria of *cta1Δ* cells

If apoCta1 is indeed an acceptor of Ccp1 heme, then holoCcp1 should accumulate in the mitochondria of cells deleted for Cta1. On probing denucleated S2 and mitochondrial-enriched P10 fractions, we detect similar Ccp1 protein levels in 2-day wild-type, *ctt1Δ* and *cta1Δ* strains but 4.5-fold more Ccp1 in 7 day *cta1Δ* mitochondria (Figure 2.4A,B), Hence, more heme-loaded Ccp1 is trapped in mitochondria when apoCta1 is not present as a heme acceptor. Although the total CCP activity of *cta1Δ* cells is double that of wild-type or *ctt1Δ* cells (Table S2.2), ratioing CCP activity against 7 day mitochondrial Ccp1 protein levels (Figure 2.4B) reveals that Ccp1 in *cta1Δ* mitochondria is < 50% active (Figure 2.4C). We attribute this to Ccp1 hyperoxidation by

the elevated H₂O₂ levels found in the *cta1Δ* strain (51), a conclusion supported by the results presented in the next section.

2.5.6) Heme-Mediated Ccp1 hyperoxidation by H₂O₂ results in heme labilization.

Intracellular H₂O₂ levels rise ~10 fold at the diauxic shift around day 2 (Figure. 2.5A) as cells switch to respiratory metabolism (52). Low levels of Cyc1 are likely present in the IMS during these early phases of oxygen adaptation since *CYCI* transcription is induced by oxygen (91) and repressed by glucose (92). Thus, we hypothesize that the burst in respiration-derived H₂O₂ overwhelms the available reducing capacity of Cyc1^{II}, hyperoxidizes Ccp1 and labilizes its heme, which is donated to apoCta1 as the latter accumulates in respiring mitochondria. To test this hypothesis, we compared heme transfer *in vitro* to apoMb from untreated Ccp1 and Ccp1 hyperoxidized by 10 molar equiv of H₂O₂ since the peroxidase is known to consume this quantity of H₂O₂ *in vitro* before heme modification (93). ApoMb, the prototypical heme acceptor (82), was selected because of its high heme affinity ($K_d=3\times 10^{-15}$ M) (94) and high stability (83).

Following incubation with apoMb, ~6 and ~12 μM heme is lost from Ccp1 and hyperoxidized Ccp1, respectively (Table S2.3), based on the decrease in their Soret absorbance (Figure S2.2B). Thus, hyperoxidized Ccp1 donates twice as much heme as the untreated peroxidase. In the absence of an acceptor, the Soret band of hyperoxidized Ccp1 does not decrease (Table S2.3; Figure. S2.2B) so no heme escapes to the solvent. In fact, heme transfer between the proteins is stoichiometric since heme-loaded Mb and apoCcp1 increase by the same concentration (Table S2.3; Figure S2.2B,D).

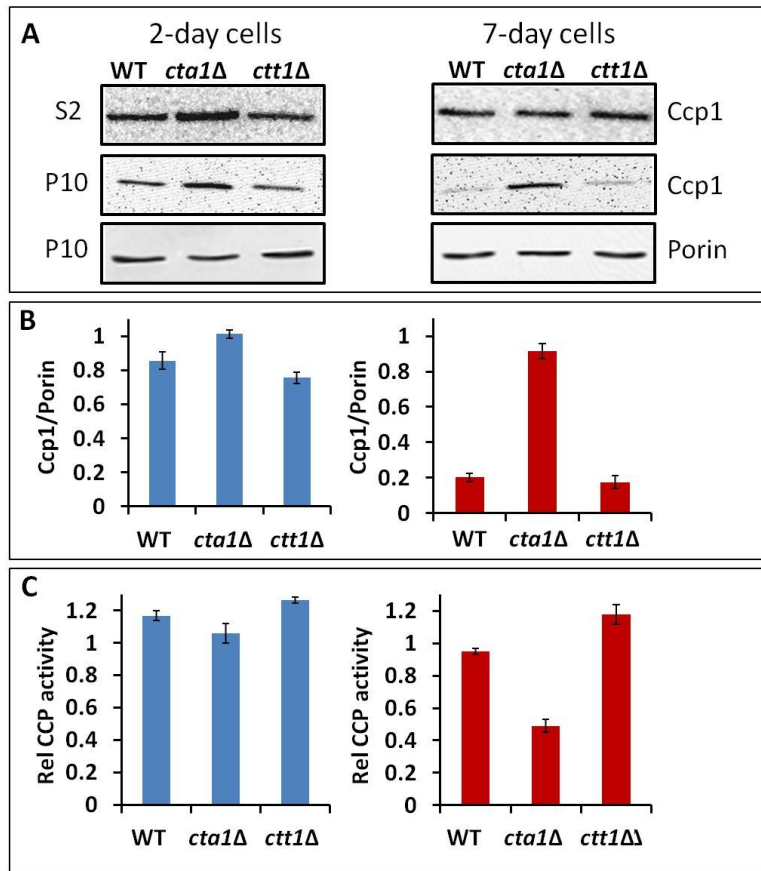


Figure 2.4. Ccp1 accumulates in the mitochondria of *cta1Δ* yeast. (A) Immunoblot analysis of denucleated (S2) and mitochondrial (P10) fractions isolated from wild-type (WT), *cta1Δ* and *ctt1Δ* cells. (B) The Ccp1 signals for the P10 fractions in panel A were quantified and normalized to the porin signal (mitochondrial outer membrane marker) for 2- (blue bars) and 7 day (red bars) cells. (C) Specific CCP activity ($\mu\text{mol}/\text{min}/\text{mg}$ total protein) of the P10 fractions in panel B ratioed by their Ccp1 protein levels to give the relative amount of active CCP remaining in mitochondria. Results in panel A are representative of three independent cultures ($n=3$) and averages \pm SD are plotted in panels B and C.

Ferric heme (hemin) released from reconstituted Mb has an exact mass that differs by < 1 ppm from that of authentic hemin (Figure S2.3). Also, the absorption spectrum of reconstituted Mb is indistinguishable from that of the native protein in Figure S2.2C so we conclude that unmodified heme is transferred from hyperoxidized Ccp1 to apoMb. In contrast, ~ 16 oxygen adducts are detected in the mass spectrum of hyperoxidized Ccp1 (Figure S2.4B), which confirms our previous reports (95, 96) that Ccp1's residues are extensively oxidized by excess

H₂O₂ in the absence of its reducing substrate, Cyc1^{II} (Eqs. 2,3). LC-MS/MS analysis of tryptic peptides from hyperoxidized Ccp1 reveals that 42% of His175 is converted to oxo-histidine (Figure S2.5, Table S2.4). Weakening of the axial ligand on His175 oxidation will labilize Ccp1's heme and we observe a doubling of heme transfer from hyperoxidized Ccp1 to apoMb (Table S2.4).

To establish if Ccp1 is hyperoxidized *in vivo*, we isolated the protein from P10 and S10 subcellular fractions. No oxo-histidine is detected in Ccp1 isolated from 1 day cells but ~85% of His175 is found to be oxidized in the extramitochondrial protein from 7 day respiring cells compared to ~35% His175 oxidation in the mitochondrial protein (Figure 2.5B). The extensive oxidation of His175 in extramitochondrial Ccp1 indicates that the peroxidase is indeed overwhelmed by H₂O₂ *in vivo*. This serves to labilize the heme and we anticipate that heme transfer is more efficient in mitochondria than *in vitro* (Figure S2.2) since apoMb is not a biological partner of Ccp1. The lack of CCP activity on hemin addition to extramitochondrial Ccp1 can also be attributed to decreased heme affinity on His175 oxidation.

Importantly, we note that apoCcp1 is not oxidized by H₂O₂ (Figure S2.4D). Activation of H₂O₂ by heme peroxidases involves binding to the heme Fe^{III} (Eq. 1) and Ccp1 can sequentially bind and reduce multiple molecules of H₂O₂ using its polypeptide as an electron source in the absence of Cyc1^{II} (95, 96). Thus, on activating H₂O₂, Ccp1's heme promotes its own transfer by catalyzing the oxidation of its polypeptide host, including its Fe ligand, His175 (Figure 2.5B,C). We conclude that Ccp1 hyperoxidation by respiration-derived H₂O₂ triggers heme transfer to apoCta1 in mitochondria and that His175 oxidation is critical in this process.

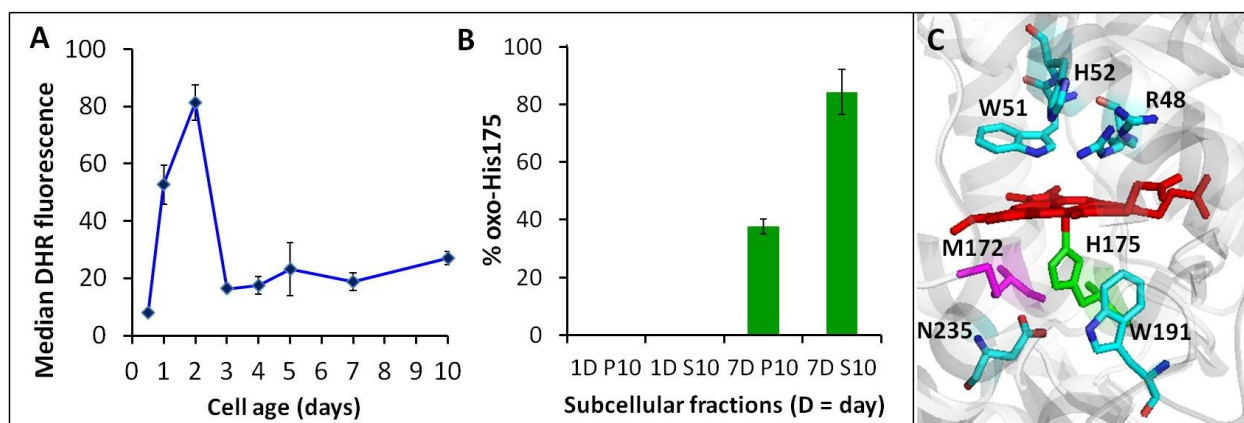


Figure 2.5. Ccp1 is oxidized at His175. (A) FACS measurements of H_2O_2 in wild-type cells stained with dihydrorhodamine 123 (DHR)(50)(50) (50). Data points are the median fluorescence/cell (RFU, relative fluorescence units) measured in 10000 cells per sample. (B) Percentage of oxidized His175 in mitochondrial (P10) and extramitochondrial (S10) Ccp1 from 1 and 7 day yeast cells based on tryptic peptide peak areas in the LC-MS spectra. See Figure. S2.6 and the SI *Materials and Methods* for further experimental details (C) Ribbon diagram of the heme binding site of Ccp1 showing the proximal Fe ligand His175 (green). Residues important in the activation of H_2O_2 following its binding to the vacant sixth coordination site of Fe^{III} are also shown. This figure was generated using Pymol software with the coordinates from PDB1ZBY.

2.6) Discussion

2.6.1) Evidence for Ccp1 as a heme donor

Immature preCcp1 is targeted to yeast mitochondria where it is processed to the heme-loaded mature holoprotein (58, 59, 67). In this state it is trapped in the IMS, hence its classification as an IMS protein in exponentially growing fermenting yeast cells (58, 59, 67). However, using a combination of live cell imaging, immunoanalysis of subcellular fractions and CCP activity assays, we demonstrate that respiration triggers apoCcp1 exit from mitochondria. Reverse translocation of proteins processed by mitochondria depends on the stability of their folded forms (97). Previously, we investigated Ccp1 denaturation and uncovered a conformational stability at the low end of the range reported for globular proteins (98) so it is not

surprising that heme binding is required for Ccp1's retention in the IMS (67). Also, mature holoCcp1 added to isolated mitochondria does not enter these organelles (67), demonstrating that holoCcp1 does not cross the outer mitochondrial membrane. Therefore, escape of Ccp1 from mitochondria is tantamount to its acting as a mitochondrial heme donor. Incidentally, Ccp1's substrate Cyc1 also requires heme for IMS retention (99). Mature Cyc1 possesses a covalently bound heme and deletion of its heme lyase (Cyc3) or mutation of residues that serve as sites of heme attachment (Cys19 and/or Cys22) result in cytoplasmic accumulation of apoCyc1, which adopts an unfolded structure *in vitro* (98).

2.6.2) Cta1 as a mitochondrial acceptor of Ccp1 heme

The synthesis in yeast of both catalase isoforms is heme-regulated. However, Ctt1 activity is detected during the early phases of heme synthesis (55, 66, 101) whereas Cta1 accumulates as the apoprotein in exponentially growing yeast (55, 66, 101). The heme donor to Ctt1 is unknown but Cta1 activity increases in parallel with extramitochondrial apoCcp1 buildup (Figure 2.3A,B), which links holoCta1 formation to H₂O₂-induced labilization of Ccp1's heme. The negligible Cta1 activity found in *ccp1Δ* cells (Figure 2.3B) and the high Ccp1 protein levels in *cta1Δ* mitochondria (Figure 2.4B) further identify apoCta1 as an acceptor of Ccp1 heme.

HoloCcp1 accumulates during heme synthesis (60, 61) so heme-mediated hyperoxidation of the protein occurs when H₂O₂ sharply increases in respiring yeast (Figure 2.5A). Hyperoxidized Ccp1 donates its heme to apoCta1 and Cta1 activity consumes mitochondrial H₂O₂. Hence, H₂O₂ levels are elevated in *cta1Δ* cells (51) despite their two-fold higher CCP activity than wild-type cells (Table S2.2). Trapping more Ccp1 in *cta1Δ* mitochondria does not compensate for the absence of Cta1's H₂O₂ scavenging activity. On the contrary, Ccp1 from

cta1Δ mitochondria is only 50% active (Figure. 2.4C), which we attribute to its hyperoxidation by H₂O₂ due to the limited availability of reducing equivalents from Cyc1^{II} in the IMS.

2.6.3) Heme labilization by His175 oxidation

Irreversible histidine oxidation has been associated with the toxic effects of peroxides in aging and neurodegeneration (102). However in PerR, H₂O₂ binds to the Fe^{II} center of iron-replete PerR, which results in oxidation of the metal's His37 and His91 ligands to 2-oxo-histidine (26, 103). This promotes iron release and apoPerR dissociation from DNA with the induction of target genes including *kat A* (catalase), *ahpCF* (alkyl hydroperoxide reductase) and *hemAXCDBL* (heme biosynthesis operon) (26). Analogous to the non-heme Fe^{II} of PerR, the heme Fe^{III} of Ccp1 binds H₂O₂, which under stress conditions (high H₂O₂, low Cyc1^{II}) oxidizes the proximal His175 ligand to oxo-histidine (Figures 2.5, S2.5) and activates Cta1 catalysis (Figure 2.3). Thus, PerR and mitochondrial Ccp1 sense and mediate a H₂O₂ stress signal by similar iron-dependent mechanisms to regulate key defensive responses at the transcriptional level for PerR and at the posttranslational level for Ccp1. To the best of our knowledge, we provide the first report of heme labilization in a heme protein by ligand oxidation. Binding of nitric oxide to the sixth coordinate position cleaves or weakens the proximal Fe^{II}-His bond in some heme proteins, including soluble guanylate cyclase (104) and nitrophorin isoform 7 (105), but this process has not been associated with heme transfer.

2.6.4) Why cells produce Ccp1 as a sensor

In the absence of a known cellular mechanism for oxo-histidine reduction, it has been speculated that oxidized apoPerR may be degraded (26, 103). Hyperoxidized Ccp1 also may be degraded since Ccp1-GFP is associated with the vacuole in 7 day cells (Figure 2.1A). Why would

yeast use Ccp1 as a sacrificial H₂O₂ sensor instead of producing active Cta1 before cells begin to respire? The H₂O₂ spike around the diauxic shift triggers a beneficial stress response known as mitohormesis (9) that results in increased Sod2 activity and depressed O₂^{•-} levels (50). We reported that the Ccp1^{W191F} strain, which possesses high catalase activity during early exponential growth due to extensive Ccp1^{W191F} hyperoxidation, mounts a weak mitohormesis response and a has short lifespan (50, 63). Thus, it appears that H₂O₂ dismutation by Cta1 activity during the early phases of oxygen adaption abrogate or attenuate the beneficial H₂O₂ stress signal. In contrast, since CCP activity also depends on Cyc1^{II} levels (Eqs. 2, 3), wild-type Ccp1 temporally controls the signal from respiration-derived H₂O₂ to trigger mitohormesis and modulate lifespan (50, 63).

2.6.5) The role of extramitochondrial apoCcp1

A large fraction of apoCcp1-GFP and possibly untagged apoCcp1 translocate to the vacuole (Figure. 2.1A). This may be the cell's mechanism for removing or recycling hyperoxidized apoCcp1 and/or vacuolar apoCcp1 may be involved in signaling analogous to yeast enolase (106). Around 10% of apoCcp1 translocates to the nucleus (Figure 2.1B). There it likely conveys an oxidative stress signal to the nuclear transcription factor Skn7 when yeast are challenged with *exogenous* H₂O₂ (54). We found *ccp1*Δ cells to be considerably more H₂O₂ sensitive than wild-type or *ccp1*^{W191F} cells because of their inability to upregulate catalase and peroxiredoxin activities on H₂O₂ challenge (50). Ccp1 is not present in the deletion mutant to transmit a stress signal to Skn7, which regulates the expression of many antioxidant enzymes, including cytosolic Ctt1 (107, 108). Hence, reverse translocation of apoCcp1 to the nucleus provides a retrograde message (90) vital in the cell's response to exogenous H₂O₂, a process that merits further investigation.

2.7) Conclusions

Figure 2.6 summarizes our model of respiration-triggered heme transfer from Ccp1 to Cta1 in mitochondria. A key step in this model is the heme-mediated oxidation by H_2O_2 of the proximal Fe ligand, His175. Before we identified Ccp1 as a heme-based H_2O_2 sensor (50), *B. subtilis* peroxide resistance protein (PerR) was the only documented non-thiol H_2O_2 sensor (26) since well-characterized H_2O_2 sensor proteins such as Yap1 in yeast and OxyR in bacteria undergo reversible thiol oxidation upon exposure to H_2O_2 (21, 25). Over 70 years of research portrays Ccp1 as an antioxidant enzyme that functions to protect yeast mitochondria by catalytically consuming H_2O_2 (17, 42). Based on our current and previous investigations of its physiological functions (49, 50, 63), Ccp1 may serve in future as a paradigm of heme-based H_2O_2 sensing and heme transfer.

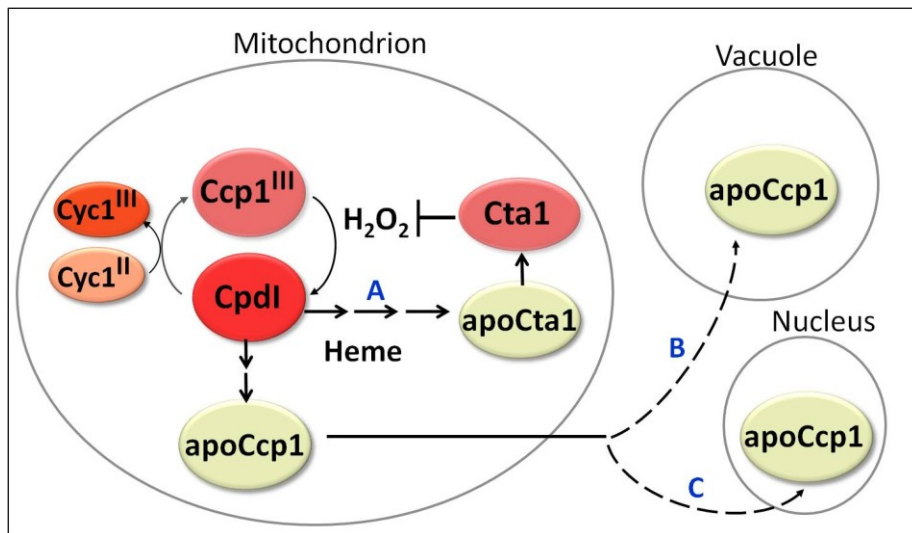


Figure 2.6. Respiration triggered heme transfer in yeast mitochondria. H_2O_2 generated during mitochondrial respiration oxidizes Ccp1 to Compound I (CpdI). The oxidizing equivalents from H_2O_2 can be reduced by $Cyc1^{II}$ or transferred to the peroxidase's residues, including the proximal Fe ligand His175 to yield oxo-histidine. Formation of the latter labilizes the heme group, which is transferred either directly or via unidentified intermediate(s) to Cta1 (path A), and the nascent Cta1 activity detoxifies H_2O_2 . ApoCcp1 has low conformational stability and undergoes reverse translocation to the vacuole (path B) and nucleus (path C).

2.8) Supplementary information

Table S2.1

Normalized CCP activity of subcellular fractions from wild-type and Ccp1-GFP-expressing yeast ^{a-c}

Strain/Cell age	S2 fraction	P10 fraction	S10 fraction ^d
WT 1 day	0.61 ± 0.05	0.84 ± 0.10	ND
Ccp1-GFP 1 day	0.51 ± 0.05	0.80 ± 0.09	ND
WT 2-day	1.00 ± 0.12	1.00 ± 0.03	ND
Ccp1-GFP 2-day	1.00 ± 0.08	1.00 ± 0.09	ND
WT 3-day	1.09 ± 0.07	0.61 ± 0.11	ND
Ccp1-GFP 3-day	1.03 ± 0.22	0.62 ± 0.03	ND
WT 7 day	0.98 ± 0.05	0.34 ± 0.04	ND
Ccp1-GFP 7 day	0.96 ± 0.20	0.38 ± 0.03	ND

^a CCP activity of denucleated (S2), mitochondria-enriched (P10), mitochondria-free (S10) fractions (see *Materials and Methods*).

^b One unit of CCP specific activity catalyzes the peroxidation of 1 μmol of horse heart ferrocyanochrome c per min per mg total protein. The specific activity of each fraction was ratioed by the total amount of protein in that fraction (Fig 2.2B, Fig S1B), and normalized to the specific activity (μmol/min/mg total protein) of 2-day WT S2 (5.71 ± 0.5) and P10 (13.8 ± 1.2) fractions, and Ccp1-GFP S2 (5.90 ± 0.4) and P10 (13.2 ± 1.1) fractions.

^c Results are those from three independent cultures (*n*=3) given as averages ± SD.

^d ND – Not detected

Table S2.2 Normalized CCP activity of subcellular fractions from wild-type, *cta1Δ* and *ctt1Δ* yeast ^{a-c}

Strain/Cell age	S2 fraction	P10 fraction	S10 fraction
WT 2-day	1.00 ± 0.05	1.00 ± 0.10	ND
<i>cta1Δ</i> 2-day	1.08 ± 0.05	1.07 ± 0.09	ND
<i>ctt1Δ</i> 2-day	0.98 ± 0.05	0.95 ± 0.05	ND
WT 7 day	1.07 ± 0.05	0.38 ± 0.01	ND
<i>cta1Δ</i> 7 day	0.88 ± 0.20	0.89 ± 0.03	ND
<i>ctt1Δ</i> 7 day	1.01 ± 0.05	0.40 ± 0.04	ND

^a See footnotes a-d of Table 2.1. Note that CCP activities were ratioed by total protein levels.

Specific activity (μmol/min/mg total protein) is normalized to that of 2-day WT S2 (5.70 ± 0.6) and P10 (13.8 ± 1.4) fractions.

Table S2.3 Percent heme transfer from Ccp1 or hyperoxidized Ccp1* to apoMb

Reagents [#]	Heme content Mb (μM)	Heme content Ccp1 (μM)	% heme transfer
Ccp1	-----	20 ± 0.0	0.0 ± 0.0
Hyperoxidized Ccp1	-----	20 ± 0.0	0.0 ± 0.0
Ccp1 + apoMb	5.7 ± 0.06	14 ± 0.74	32 ± 9.0
hyperoxidized Ccp1 + apoMb	12 ± 0.39	7.9 ± 1.8	64 ± 8.0

*Recombinant Ccp1 (20 μM) was hyperoxidized with 200 μM H₂O₂ for 60 min in 20 mM KPi (pH 7.5) at 4° C.

[#]Ccp1 or hyperoxidized Ccp1 (20 μM) and 60 μM apoMb were incubated in the same buffer at 30 °C for 60 min with gentle stirring. Following their separation by anion exchange, the heme-loading of Mb and Ccp1 was determined spectrophotometrically (Figure. S2.2).

Table S2.4 Relative peak areas of the oxidized forms of tryptic peptide EVVALMGAAHALGK^a

Residue oxidized	Obs mass ^b (u)	Calc mass ^c (u)	Error (ppm) ^c	% peak area 100(P _{ox} /P _{tot}) ^d			
				[Ccp1]:[H ₂ O ₂]			
				1:0	1:1	1:5	1:10
None	1295.7211	1295.7140	5.48	91 ± 0.1	66 ± 10.2	18 ± 1.0	9.2 ± 1.4
Met +16	1311.7108	1311.7089	1.44	8.8 ± 11.1	30 ± 2.9	47 ± 5.7	48 ± 3.1
Met +32	1327.7091	1327.7038	3.99	0.3 ± 0.0	---	---	0.5 ± 0.3
His +16	1311.7050	1311.7089	2.97	---	3.2 ± 2.5	28 ± 2.0	37 ± 3.2
Met +16, His +16	1327.7064	1327.7038	1.95	---	---	6.8 ± 4.0	4.9 ± 0.5

^a Ccp1 (5 μM) was reacted with 1, 5, and 10 molar equiv of H₂O₂ for 1 h at 4 °C in 20 mM KPi (pH 7.5) with 100 μM DTPA prior to tryptic digestion and LC-MS/MS analysis (see SI *Materials and Methods*).

^b The precursor ions selected for MS/MS analysis were filtered using a mass exclusion threshold of 10 ppm.

^c Peptide masses were calculated with Proteome Discoverer and oxidized Met (+16, +32) and His (+16). The error in ppm is given by 10⁶ (Obs mass–Calc mass)/Calc mass.

^d The integrated peak area in the extracted ion chromatogram (XIC) from MS1 of the peptide with the indicated oxidation (P_{ox}) was divided by the sum of the peak areas of all detected forms of the peptide (P_{tot}). The percent oxidation of His175 or Met172 is estimated from 100(P_{ox}/P_{tot}).

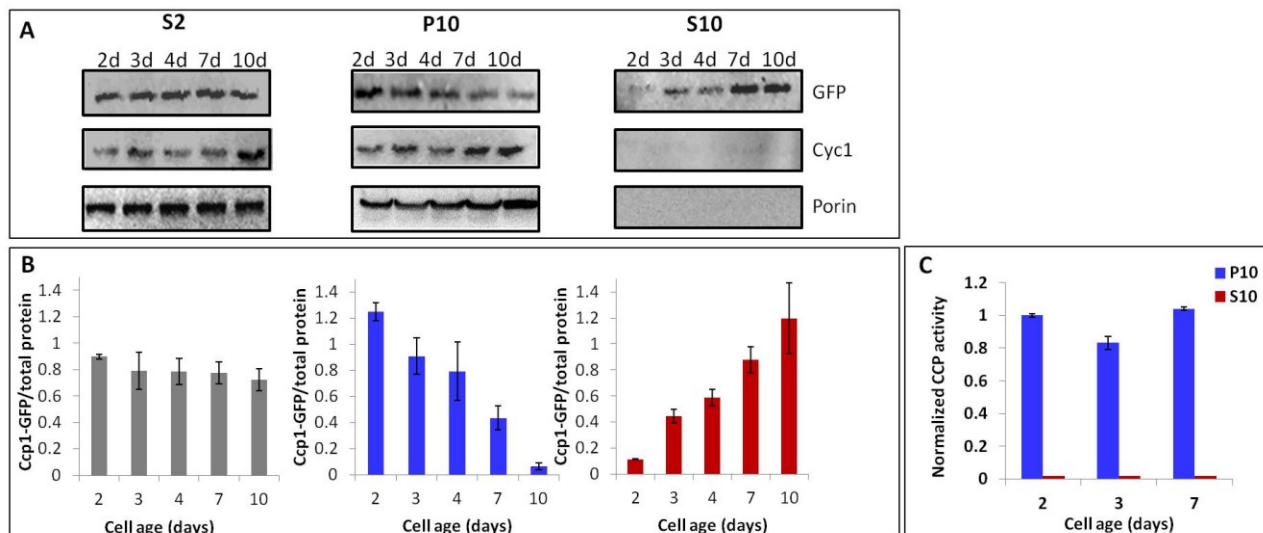


Figure S2.1 Ccp1-GFP exits mitochondria as yeast begin respiring and extramitochondrial Ccp1-GFP does not possess CCP activity. (A) Immunoblot analysis of equal volumes of denucleated (S2), mitochondrial (P10), and cytosolic (S10) fractions vs cell age. Porin and Cyc1 are mitochondrial outer membrane and IMS markers, respectively. (B) The GFP signals in panel A were quantified and normalized to the sum of the integrated intensity of all Coomassie bands in the same lane. (C) Normalized CCP activity in mitochondrial (P10) and cytosolic (S10) fractions. Specific activity was ratioed by the Ccp1 protein levels in panel B, and normalized to the level for 2-day cells (Table S2.1). Results in panel A are representative of three independent cultures ($n = 3$) and averages \pm SD are plotted in panels B and C.

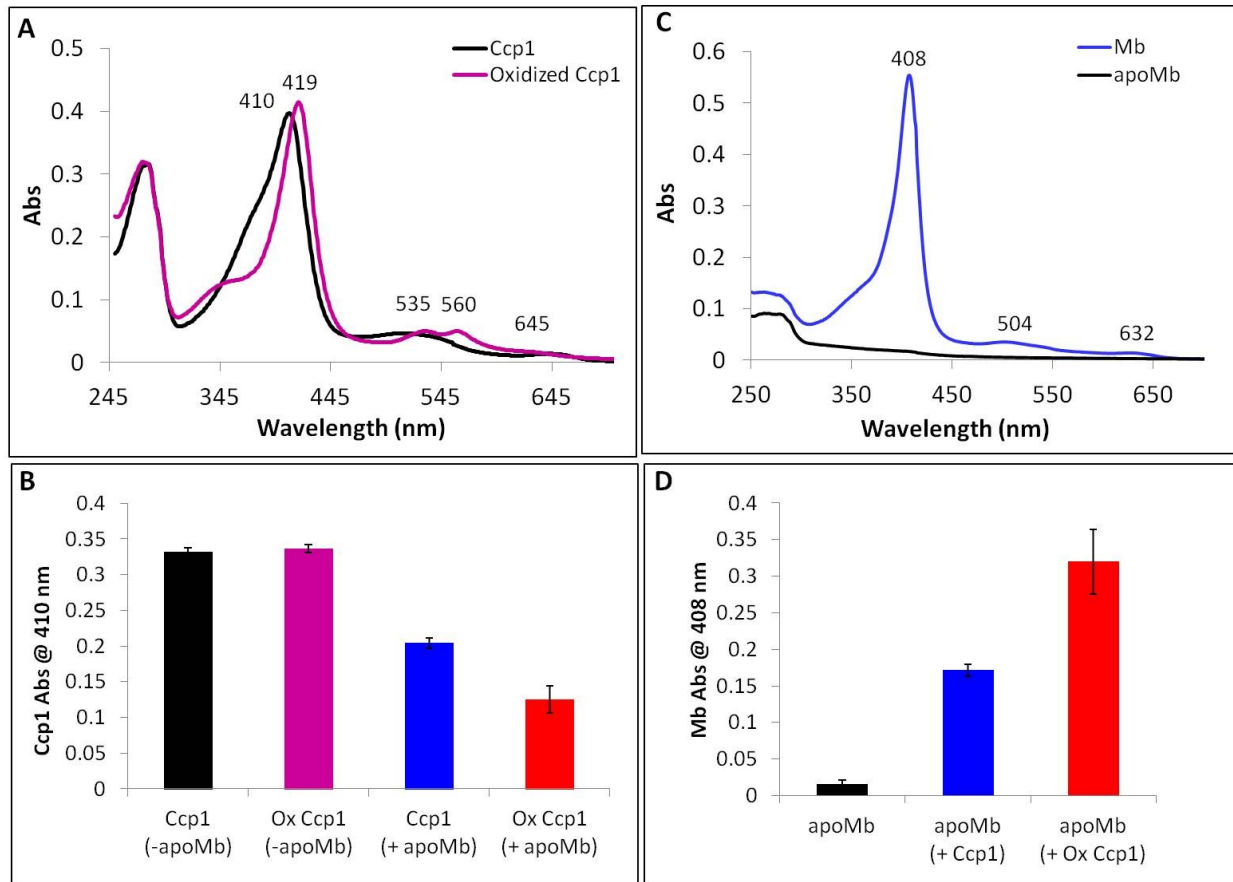


Figure S2.2 Ccp1 hyperoxidation by H₂O₂ increases heme transfer to apoMb. Ccp1 or hyperoxidized Ccp1 (20 μM) was incubated with 60 μM apoMb in 20 mM KPi (pH 7.5) at 30 °C for 60 min. The proteins were separated by anion exchange, diluted to 0.5-3.0 μM and their absorption spectra were recorded in a 1-cm quartz cuvette. Spectrum of (A) Ccp1 and hyperoxidized Ccp1 after 60 min incubation (minus apoMb), and of (B) apoMb and reconstituted Mb. (C) Soret absorbance of Ccp1 and hyperoxidized Ccp1 after 60 min incubation ± apoMb. Note that the Fe^{IV} heme of Ccp1 decayed to Fe^{III} heme during anion-exchange chromatography so the Soret absorbance of the latter ($\epsilon_{410}=98 \text{ cm}^{-1} \text{ mM}^{-1}$) was used to monitor the heme loading of Ccp1. (D) Soret absorbance of Mb ($\epsilon_{408}=188 \text{ cm}^{-1} \text{ mM}^{-1}$) after 60 incubation ± Ccp1 or hyperoxidized Ccp1. The percent heme transfer calculated from the absorbance data in panels C and D is summarized in Table 2.1 of the main text for three independent experiments ($n = 3$).

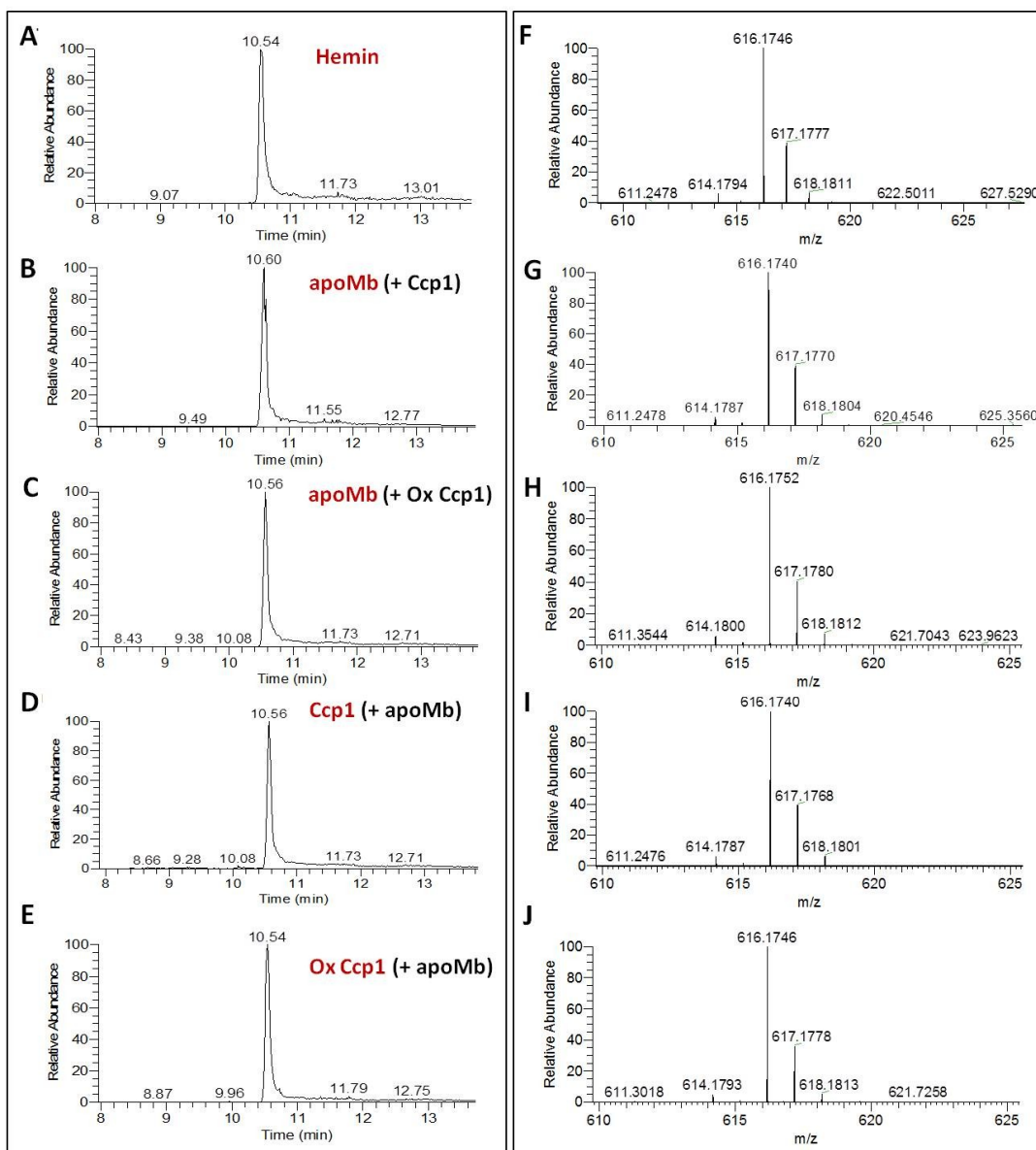


Figure S2.3 Heme from hyperoxidized Ccp1 is not oxidized. Following their separation by anion-exchange chromatography, Ccp1, hyperoxidized Ccp1 (Ox Ccp1) and Mb from the heme-transfer experiments (Figure. S2.2) were diluted 10-fold to 0.5 μM protein with 2% acetonitrile/0.1% formic acid, and 5 μL of each sample was analyzed by LC-MS (SI *Methods and Materials*). **(A-E)** Chromatograms of the hemin that dissociated from the indicated polypeptide (red font) on the LC column at pH 4.0 (the protein partner in the heme-transfer reaction is indicated in brackets). The average hemin retention time on the C4 column is 10.56 ± 0.03 min. **(F-J)** The corresponding hemin mass spectra show the isotopic distribution expected for $\text{FeC}_{34}\text{H}_{22}\text{N}_4\text{O}_4$ (calc monoisotopic mass: 616.1773 u). Ccp1 derived hemin has a mass of 616.1745 ± 0.0005 vs 616.1746 u for authentic hemin (spectrum F), which serves as an external standard.

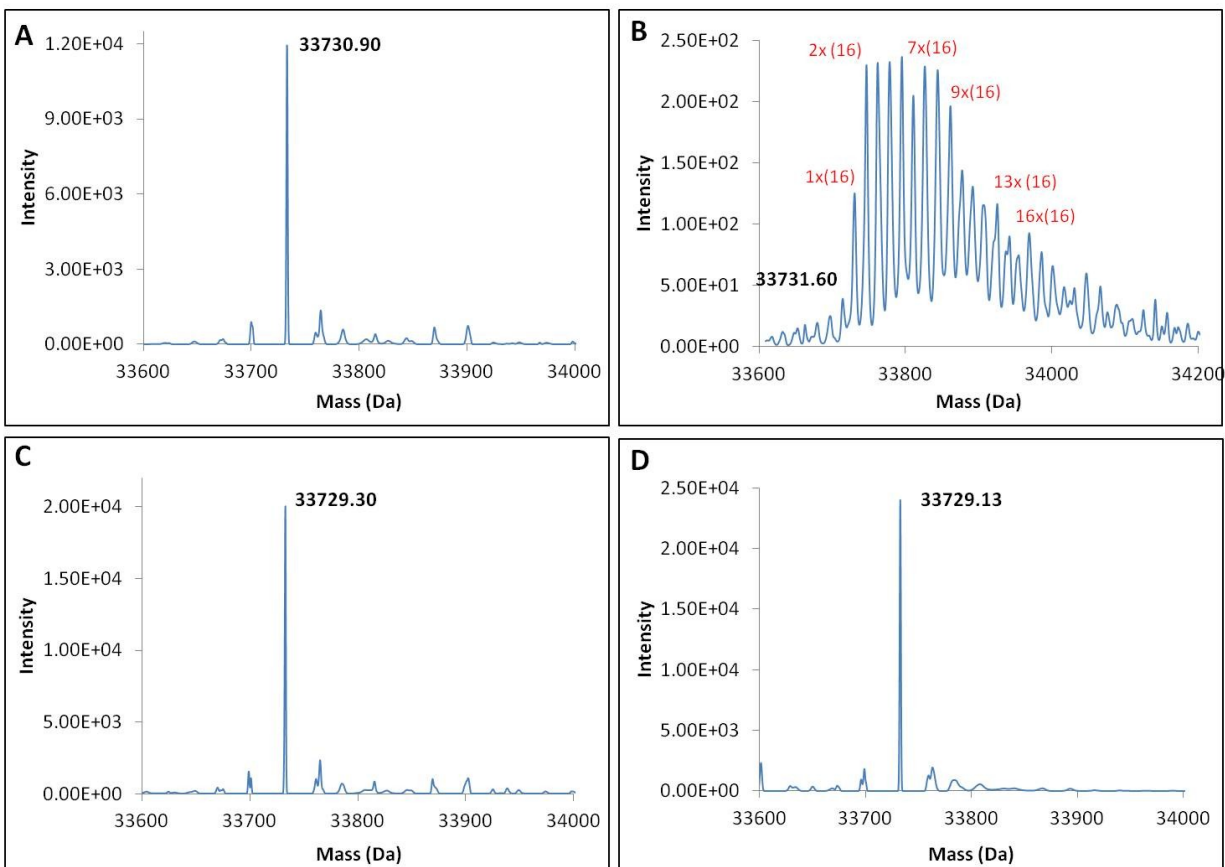


Figure S2.4 H₂O₂ oxidizes holoCcp1 but not apoCcp1. Recombinant holo- or apoCcp1 (5 μ M) was incubated with 50 μ M H₂O₂ in 20 mM KPi (pH 7.5)/100 μ M DTPA at 4 $^{\circ}$ C for 60 min, 0.1 nM catalase was added to remove any remaining H₂O₂ and samples were further incubated at 30 $^{\circ}$ C for 60 min before recording the mass spectra of the intact proteins as described in the SI *Materials and Methods*. Deconvolved mass spectrum of (A) holoCcp1 (control, no H₂O₂ treatment), (B) hyperoxidized Ccp1 with the number of oxygen adducts (+16) indicated in red font, (C) apoCcp1 (control, no H₂O₂ treatment), and (D) H₂O₂-treated apoCcp1. The masses corresponding to the unmodified Ccp1 polypeptide indicated on the peaks in panels A, C and D agree with the calculated mass of 33730.33 u within the accuracy of the QToF3 mass spectrometer, which was mass calibrated using horse heart Mb as a standard (Obs mass 16952.10 u; Calc mass 16951.49 u; 36 ppm error).

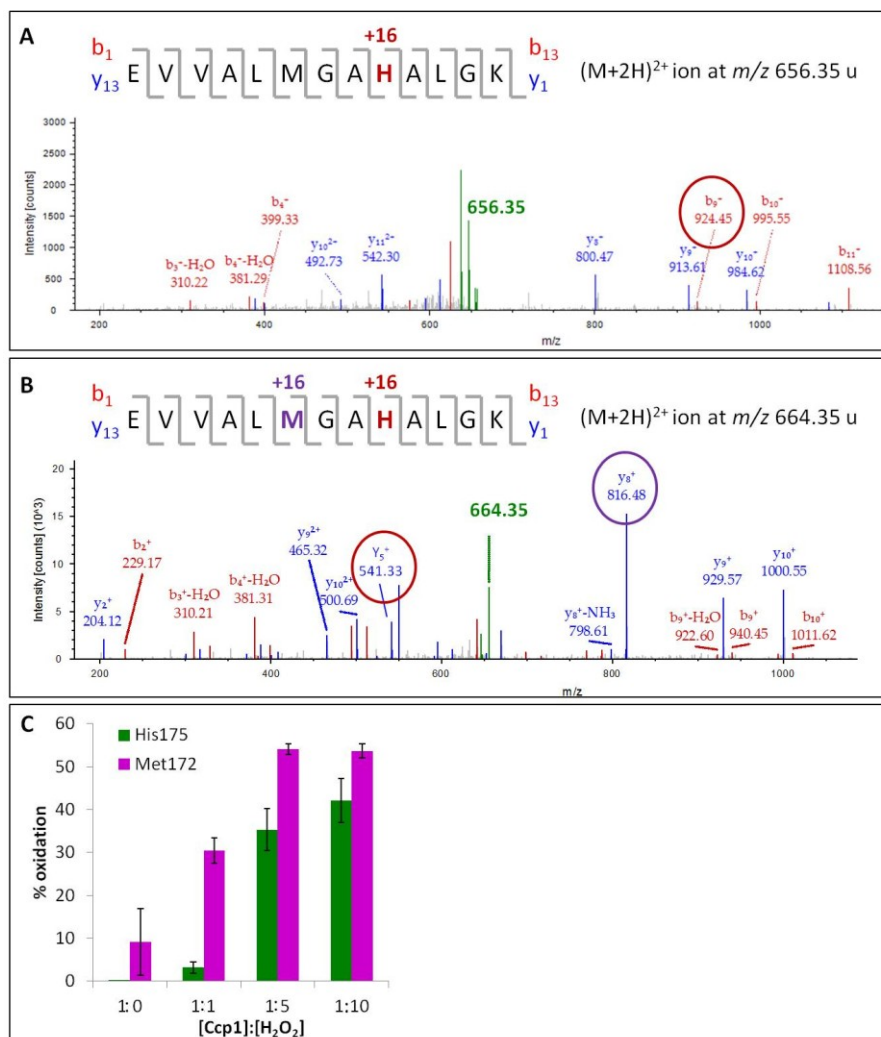


Figure S2.5 H₂O₂ oxidizes His175, the proximal Fe ligand, in recombinant Ccp1. Recombinant Ccp1 (5 μ M) was hyperoxidized with 50 μ M H₂O₂ for 60 min at room temperature, diluted into 50 mM Tris (pH 7.4)/100 μ M DTPA to 1 μ M protein, digested with trypsin and the peptides were analyzed by LC-MS as described in the SI *Materials and Methods*. MS/MS spectrum of the $(M+2H)^{2+}$ precursor ion of the EVVALMG(AH)ALGK peptide oxidized at (A) His175 (+16) and (B) His175 (+16) plus Met172 (+16). The precursor ions at m/z 656.35 and 664.35 (green) were fragmented by CID (30 V) to give b_n (red) and y_n sequence ions (blue). The b_9^+ ion bearing oxo-His175 at its C-terminus, and the y_5^+ and y_8^+ ions bearing oxidized His175 and oxidized Met172 at their N-termini are circled in panels A and B, respectively. (C) Percent oxidized Met172 and His175 increases with amount of H₂O₂ added to Ccp1 (data from Table S2.4). Interestingly, Met172 appears to compete with His175 as an electron donor to H₂O₂ since < 10% of peptide EVVALMG(AH)ALGK is oxidized at both residues (Table S2.4). We speculate that switching between Met172 and His175 as a donor controls heme labilization in Ccp1 *in vivo* but a better understanding of this process requires further detailed examination of hyperoxidized Ccp1.

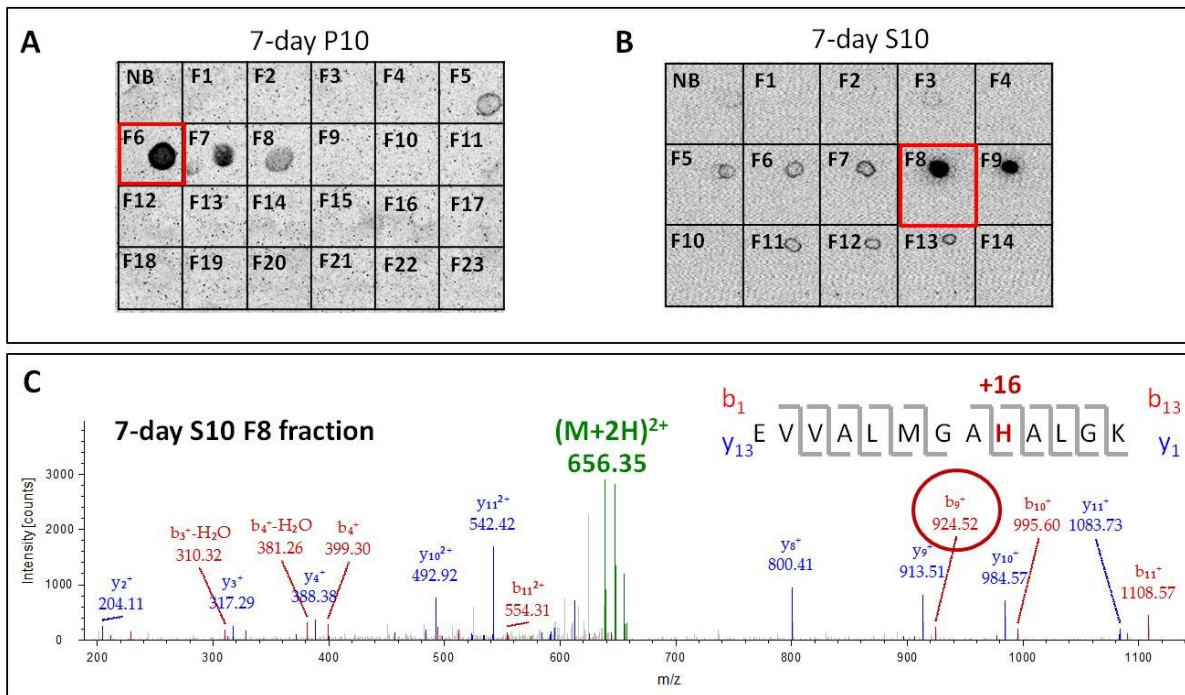


Figure S2.6 LC-MS/MS analysis of extramitochondrial Ccp1 isolated from 7 day cells reveals His175 oxidation. Ccp1 was isolated by anion-exchange chromatography from (A) mitochondrial (P10) and (B) extramitochondrial (S10) subcellular fractions from 7 day cells and the fractions dot blotted onto PVDF membranes and probed with anti-Ccp1. The main Ccp1-containing fractions (red boxes) were analyzed by reducing SDS-PAGE, gel bands were excised, the proteins were digested with trypsin and the peptides were analyzed by LC-MS/MS. (C) The $(M+2H)^{2+}$ precursor ion at m/z 656.35 (green) of the oxidized EVVALMGAAHALGK peptide (+16) from extramitochondrial fraction 8 was fragmented by CID (30 V) to give MS/MS spectrum shown with b_n (red) and y_n sequence ions (blue). The circled b_9^+ ion bears oxo-His175 at its C-terminus, identifying His175 as the site of oxidation. Results are representative of those from three independent cultures ($n=3$) and further experimental details are provided in the SI *Materials and Methods*. The percentages of oxidized His175 in S10 and P10 estimated from peptide peak areas in the LC-MS spectra are plotted in Figure. 2.5B of the main text.

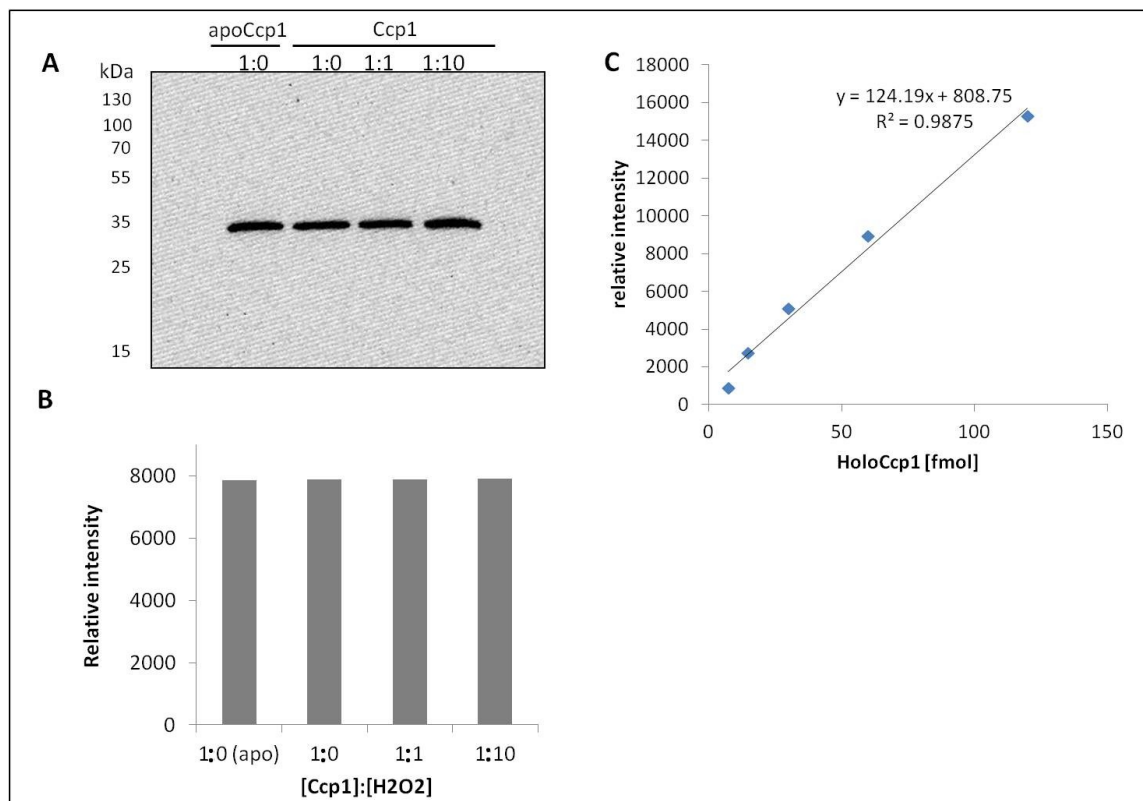


Figure S2.7 The anti-Ccp1 antibody detects the heme free (apo), heme loaded (holoCcp1) and oxidized forms of Ccp1. (A) Immunoblot analysis of 60 fmol of apoCcp1, holoCcp1 (Ccp1), and holoCcp1 treated with 1 (CpdI) and 10 molar equiv (hyperoxidized) of H₂O₂ as indicated by the [Ccp1]:[H₂O₂] ratios. (B) The Ccp1 signals in panel A were quantified and normalized to the sum of the Coomassie bands in the same lane. (C) Standard curve prepared from a representative immunoblot showing the anti-Ccp1 response is linear between 4-120 fmol of recombinant holoCcp1.

Chapter 3: Detailed LC-MS/MS analysis of H₂O₂-treated cytochrome c peroxidase offers insight into heme-based H₂O₂ signaling

3.1) Preface

The work presented in chapter 3 is submitted to: Kathiresan M, and English AM (2015). **Detailed LC-MS/MS analysis of H₂O₂-treated cytochrome c peroxidase offers insight into heme-based H₂O₂ signaling**. JACS. The production and interpretation of the data, writing and revision of the manuscript was performed by me. Dr. English contributed to discussion, data analysis, editing and revisions of the paper.

3.2) Abstract of the manuscript

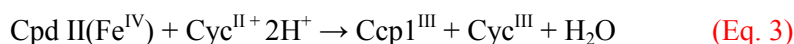
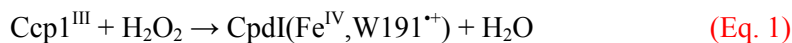
Although long a paradigm in heme peroxidase catalysis, we recently found that cytochrome c peroxidase (Ccp1) primarily functions as a sensor protein when H₂O₂ levels rise in respiring yeast. The availability of its reducing substrate, ferrocyclochrome c (Cyc^{II}), determines whether Ccp1 acts as a H₂O₂ sensor or peroxidase. For H₂O₂ to serve as a signal it must modify its receptor, so we employed high-performance LC-MS/MS to investigate in detail the oxidation of Ccp1 by 1, 5 and 10 M eq of H₂O₂ in the absence of Cyc^{II} to eliminate peroxidase activity. We observed strictly heme-mediated oxidation, implicating sequential binding and reduction of H₂O₂ at Ccp1's heme. This results in the incorporation of ~20 oxygen atoms predominantly at methionine and tryptophan residues. Extensive *intramolecular* dityrosine crosslinking involving Y36/Y39, Y36/Y42 and Y67/Y71 was uncovered by detailed LC-MS/MS analysis. All five methionines as well as W211, W223, Y16, Y229, and Y236 are >5% oxidized in Ccp1 treated with 1 M eq of H₂O₂ and a total of 24 residues are oxidized in Ccp1 treated with 10 M eq of H₂O₂. The proximal heme ligand, H175, is converted to oxo-histidine but remarkably, irreversible heme oxidation is avoided by radical transfer to the polypeptide until oxidation of the

catalytic distal H52 shuts down heterolytic H₂O₂ cleavage. Our analysis points to heme labilization as a key determinant of Ccp1-mediated H₂O₂ sensing and provides new insight into heme-catalyzed protein-based radical transfer as well as exposing the bias of EPR detection toward radicals with low O₂ reactivity.

3.3) Introduction

Until recently H₂O₂ was viewed as an unwanted by-product of aerobic metabolism and associated with many pathologies and biological aging (5, 109–111). However, H₂O₂ signaling is now known to mediate many physiological processes via thiol- and metal-catalyzed protein oxidation (4, 112). There also is an expanding list of enzymes with residues that undergo metal-mediated residue oxidation during their normal catalytic cycle (113). For example, reversible oxidation of tyrosine to a tyrosyl radical (Y[•]) is well documented in the catalytic cycle of ribonucleotide reductase (113, 114) and prostaglandin H synthase (115), and a tryptophanyl radical (W[•]) was first identified in yeast cytochrome c peroxidase (Ccp1) (42, 116).

In vitro, Ccp1 efficiently couples H₂O₂ reduction to ferrocycytochrome c (Cyc^{II}) oxidation (17). The ferric enzyme, Ccp1^{III}, is rapidly oxidized by H₂O₂ to compound I (CpdI) with a ferryl (Fe^{IV}) heme and a cationic W[•] localized on residue W191 (**Eq. 1**). W191^{•+} is reduced by Cyc^{II} to compound II (CpdII) (**Eq. 2**), and a second Cyc^{II} reduces CpdII's Fe^{IV} heme to the resting Ccp1^{III} form (**Eq. 3**):



A critical role in CCP catalysis for W191, which lies in the electron-transfer (ET) pathway between the Ccp1 and Cyc^{II} hemes, is evidenced by the negligible Cyc^{II} activity (**Eqs. 2,3**) of the W191F variant(117).

Ccp1's catalytic cycle (**Eqs. 1-3**) has been examined *in vitro* in exquisite detail over several decades as a model of heme-peroxidase catalysis (17). However, we have recently shown that Ccp1 does not catalytically detoxify H₂O₂ in yeast but rather acts as a mitochondrial H₂O₂ sensor (49, 50). As cells switch from fermentation to respiration, apoCcp1 escapes from the mitochondria (50, 118), with a concomitant increase in the activity of the peroxisomal-mitochondrial catalase (Cta1), suggesting that this antioxidant enzyme is a recipient of Ccp1's heme (118). We detect a 10-fold spike in intracellular H₂O₂ as cells begin to respire (50, 118), and the proximal heme ligand, H175 (Figure 3.1), is extensively oxidized in Ccp1 isolated from respiring yeast (118). Thus, the trigger for heme transfer is likely labilization of Ccp1's heme on H175 oxidation.

To better understand this remarkable and unprecedented mechanism of heme-based H₂O₂ signaling, detailed characterization of Ccp1 oxidation by H₂O₂ was undertaken. It is well-documented *in vitro* that Ccp1 can reduce up to 10 M eq of H₂O₂ by heme-mediated oxidation of residues in its polypeptide in the absence of Cyc^{II} (93). Repeated two-electron reduction of H₂O₂ by Ccp1 requires intramolecular radical transfer from the oxidized heme with the formation of new protein based radicals (93).

Consistent with its ability to endogenously reduce H₂O₂, Ccp1 contains an abundance of oxidizable residues (Figure 3.1) (96). Polypeptide oxidation has been confirmed by the detection of protein-based radicals in CpdI and overoxidized Ccp1 (defined here as Ccp1 oxidized by >1 M eq of H₂O₂) by spectroscopic studies on the wild-type protein and its variants (119–124). A broad

EPR signal at 4 K was unequivocally assigned to W191^{•+} and a narrow EPR signal to Y71[•] and Y236[•] (119–124). Y[•] radicals have been trapped in Ccp1 by 2-methyl-2-nitrosopropane (MNP), and the relatively stable spin adducts (96, 125) were additionally characterized by mass spectrometry (MS) (126–128). MNP mass adducts were localized to tyrosine-containing tryptic peptides T6 (Y36, Y39, Y42) and T26 (Y229, Y236) (96), and to specific residues including Y39, Y236 and Y153 (125). Efficient radical quenching by TEMPO[•] (2,2,6,6-tetramethylpiperidiny-1-oxy) also generates mass adducts amenable to MS analysis and we identified several TEMPO-labeled peptides in overoxidized Ccp1 including T6, T14+T15 (W126), T18+T19 (Y153), T23 (Y187, W191, Y203, W211), T27+28 (Y244, Y251) and T28 (Y251) where the oxidizable residues are in brackets (128).

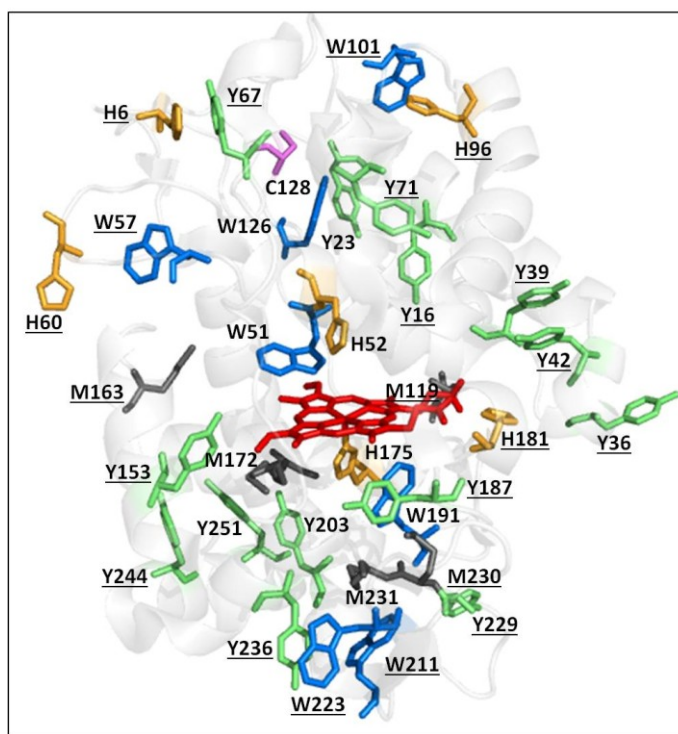


Figure 3.1: Oxidizable residues in Ccp1. PyMOL-generated cartoon of Ccp1 (PDB 1ZBY) showing the protein's 14 tyrosines (Y, green), 7 tryptophans (W, blue), 6 histidines (H, orange), 5 methionines (M, grey) and the single cysteine (C, magenta). Solvent-exposed residues are underlined.

Spectroscopic and spin trapping/scavenging studies have identified a subset of the residues oxidized in Ccp1. We rationalized that high-performance MS, the current method of choice for the qualitative and semiquantitative characterization of oxidative protein modification (129–132), would allow us to identify all residues in Ccp1 that serve as endogenous donors, including those that undergo only small mass changes on oxidation. Indeed, the LC-MS/MS results described here provide a comprehensive map of the residues modified on heme-mediated oxidation of Ccp1 by 1 M eq of H₂O₂, which generates CpdI (**Eq. 1**) (93), and by 5 and 10 M eq of H₂O₂. Multiple cycling of the heme back to its ferric form by radical transfer to the polypeptide enables repeated H₂O₂ activation and reduction at the iron, which increasingly overoxidizes the protein (93, 96, 125, 133–135). The location within Ccp1's polypeptide and the chemical nature of the stable oxidation products are rationalized by considering both the intrinsic reactivity of amino acid radicals combined with their proximity to conserved internal waters and to regions of O₂ density found by molecular dynamics (MD) simulations. Overall, our results reveal how extensive heme-mediated oxidation of Ccp1 promotes its remarkable role as a H₂O₂ signaling and sensing molecule in yeast as well as elucidating how repeated heme-initiated radical transfer is accommodated within a protein matrix.

3.4) Materials and methods

3.4.1) Materials.

Proteins were obtained from the following suppliers: bovine catalase, horse heart cytochrome c (Cyc) type III, myoglobin (Mb) (Sigma), sequencing grade modified trypsin (Promega) and thrombin (EMD Millipore). Recombinant Ccp1 with MI at positions -2 and -1 of the mature protein was overexpressed as the apoprotein in BL21(DE3) cells, purified and reconstituted with

hemin as described previously (118). Suppliers of (bio)chemicals were as follows: Coomassie (MP Biomedicals); hemin chloride, phenylmethylsulfonyl fluoride (PMSF), Benzamidine Sepharose 4 Fast Flow, DEAE Sepharose resins (GE Healthcare); Ni-NTA resin (Qiagen); pET22b(+) vector, C18 Zip Tip pipette tips (EMD Millipore), HPLC grade acetonitrile, diethylenetriamine-pentaacetic acid (DTPA) (Sigma Aldrich); and 30% hydrogen peroxide (Fisher Scientific).

3.4.2) Ccp1 oxidation.

A 5 μ M Ccp1 stock solution was prepared in 20 mM KPi (pH 7.5) with 100 μ M DTPA (Kpi/DTPA) and mixed with a stock H₂O₂ solution in the same buffer to give 1 μ M Ccp1 with the desired H₂O₂ concentration. DTPA was added to all buffers to inhibit catalysis of H₂O₂ or O₂ oxidation of Ccp1's residues by trace metal impurities in the buffers, and catalase (0.1 nM) was routinely added although H₂O₂ was not detected by the HRP/ABTS assay (136) in the samples following incubation at room temperature for 1 h. CCP activity of oxidized Ccp1 was determined by monitoring the oxidation of horse heart Cyc^{II} by H₂O₂ as reported (118).

3.4.3) LC-MS analysis of intact apo- and holoCcp1 \pm H₂O₂ and of Ccp1 derived heme.

Solutions of oxidized apo- and holoCcp1 were diluted into 5% aqueous acetonitrile/0.1% formic acid (MS solvent) and 2 μ L aliquots were loaded onto a reversed-phase Zorbax 300SB-CN (2.1 x 150 mm, 5 μ m) column attached to an Agilent 1200 HPLC and equilibrated with the MS solvent at room temperature. Samples were eluted from the HPLC column at a flow rate of 0.2 mL/min with a 5-95% acetonitrile gradient over 5 min into the Z-Spray source of a QToF3 mass spectrometer (Waters). The acetonitrile concentration was held constant at 95% for 3 min, lowered to 5% over the next 3 min and the column was re-equilibrated with the MS solvent for 8

min prior to the next injection. Mass measurements were performed using the following QToF3 parameters: capillary voltage 3.5 kV, cone voltage 35 V, RF lens 50 V, source temperature 80°C and desolvation temperature 300 °C. Protein envelopes were deconvolved (MaxEnt1 algorithm, Waters) to give intact protein masses.

To monitor its integrity, the exact mass of the heme released at low pH from oxidized Ccp1 was recorded. The oxidized protein in the MS solvent was injected onto a reversed-phase C4 capillary column (100 µm x 4.0 cm) prepared in-house and attached to a NanoLC (EASY-nLC, Thermo Scientific). The column was equilibrated with the same solvent and samples were eluted at 200 nL/min with a 5–95% acetonitrile gradient into the nanoESI source of a LTQ Orbitrap Velos mass spectrometer (Thermo Scientific) and analyzed in full-scan mode (m/z 100–2000) in the Orbitrap high resolution mass analyzer ($R=60,000$ at m/z 400). Other instrument parameters were: electrospray voltage 3 kV, CID collision energy 35 V and heated capillary temperature 200 °C.

3.4.4) LC-MS/MS analysis of tryptic digests of oxidized Ccp1.

Donor residues were identified by sequencing of the oxidized tryptic peptides. Untreated and oxidized Ccp1 were alkylated with 55 mM iodoacetamide for 30 min at room temperature and digested overnight with 12.5 ng/µL (1:20) of trypsin in 50 mM ammonium bicarbonate (pH 8.0)/100 µM DTPA at 37 °C. The digests were desalted on C18 Zip Tips and the tryptic peptides (5 µL/injection) were separated on a homemade reversed-phase C18 capillary column (100 µm x 6.5 cm) equilibrated with 2% aqueous acetonitrile/0.1% formic acid and attached to the NanoLC. Peptides were eluted at a flow rate of 200 nL/min into the nanoESI source of the Orbitrap mass spectrometer using a 2–94% acetonitrile gradient and analyzed in the Orbitrap as described for

heme above. Sequence coverage from the peptide maps was routinely 96-100%, and included all the oxidizable residues shown in Figure 3.1.

Precursor peptide ions were selected in MS1 using a mass exclusion threshold of 10 ppm and fragmented in the Velos linear ion trap at a collision energy of 35 V. MS2 fragments with an intensity count of ≥ 20 were analyzed with a mass tolerance of 0.8 u using Proteome Discoverer 1.3.0 software (Thermo Scientific) and the Sequest search engine with mass filters for the oxidative modifications listed in Table S2.1 in addition to cysteine alkylation by iodoacetamide (+ 57 u). Dynamic exclusion was enabled with a repeat count of 1, a repeat duration of 30 s and an excluded list size of 500. Sequest correlates the MS2 spectra with peptide sequences in the Ccp1 Fasta file downloaded from the NCBI website (<ftp://ftp.ncbi.nlm.nih.gov/>). Also, Sequest's filters, XCorr (>2) and False Discovery Rate (<0.01), were implemented for confident peptide identification (137).

3.4.5) Semiquantitation of residue oxidation.

Label-free quantitation was performed at the MS1-level (138). Peptide ion intensity is expressed as the integrated peak area (PA) extracted within a 10 ppm window from the digest mass chromatogram. Four peptides consistently found unmodified (Table S3.2) were used as internal standards to correct for changes in PA due to variation in instrumental response. The normalized yield of an oxidized form of a residue (X_{ox}) identified by MS/MS is given by:

$$\text{Normalized \% } X_{ox} = \frac{100 \sum PA_{ox}}{\sum PA_{ox} + \sum PA} \quad \text{(Eq. 4)}$$

The numerator sums all normalized PA s of the peptides containing X_{ox} (PA_{ox}) and the denominator sums the normalized PA s of all peptides containing any form of residue X . The

relative standard deviation of the reference peptide *PAs* is ~4% (Table S3.2), which reflects the precision in the percent oxidation of the residues reported here.

3.4.6) Purification and dityrosine fluorescence of monomeric oxidized Ccp1.

Intramolecular dityrosine crosslinking in oxidized Ccp1 was investigated by dityrosine fluorescence. Following its separation from higher molecular weight species by gel filtration chromatography, the fluorescence of monomeric oxidized Ccp1 was monitored at 410 nm, the maximum emission of dityrosine (139), as outlined in the caption to Supplemental Figure S3.2.

3.4.7) Molecular dynamics simulation of O₂ diffusion in Ccp1.

Accessibility of O₂ to internal regions of Ccp1 was examined using MD simulations as outlined in the Supplemental Information.

3.5) Results

3.5.1) Oxidation of Ccp1 by H₂O₂ is heme mediated.

Following oxidation, the mass spectrum of intact holoCcp1 exhibits new peaks with incremental mass shifts of +16 u (Figure 3.2). We assign these peaks to oxidized forms of the protein that have incorporated an oxygen atom at increasing numbers of residues. For example, Ccp1 treated with 10 M eq of H₂O₂ forms up to 20 covalent adducts (Figure 3.2C), signifying extensive overoxidation of its polypeptide by H₂O₂ in the absence of Cyc^{II} (**Eqs. 2,3**), as we and others reported previously (93, 96, 125, 133–135). In sharp contrast, no mass adducts are detected for heme-free, apoCcp1 incubated with 10 M eq of H₂O₂ (Figure 3.2D), demonstrating that oxidation of the holoprotein by H₂O₂ is mediated by its heme.

3.5.2) Localization of the oxygen adducts in oxidized Ccp1.

Using the filters in Table S3.1, the peptides identified in tryptic digests of oxidized Ccp1 based on their monoisotopic m/z values are listed in Table S3.3. Importantly, the <5 ppm error in m/z ensures high confidence in peptide identification.

Four (M119, M163, M172, M231, Figure 3.1) of the five methionine residues in Ccp1 are oxidized to the sulfoxide (MetO; +16 u) above the 5% level in peptides from untreated Ccp1 (Figure 3.3A). With the exception of M163, MetO levels increase to $\sim 40\%$ in CpdI and 50-100% in overoxidized Ccp1 (Figure 3.3A), suggesting that these residues are major donors to the heme. It has been reported that 60 M eq of H_2O_2 extensively oxidizes M119, M230 and M231 in apoCcp1 at pH 4 and that the reconstituted holoenzyme exhibits negligible reaction with H_2O_2 (Eq. 1) (140). However, we detect negligible oxygen incorporation into apoCcp1 treated with 10 M eq of H_2O_2 in KPi/DTPA (Figure 3.2D).

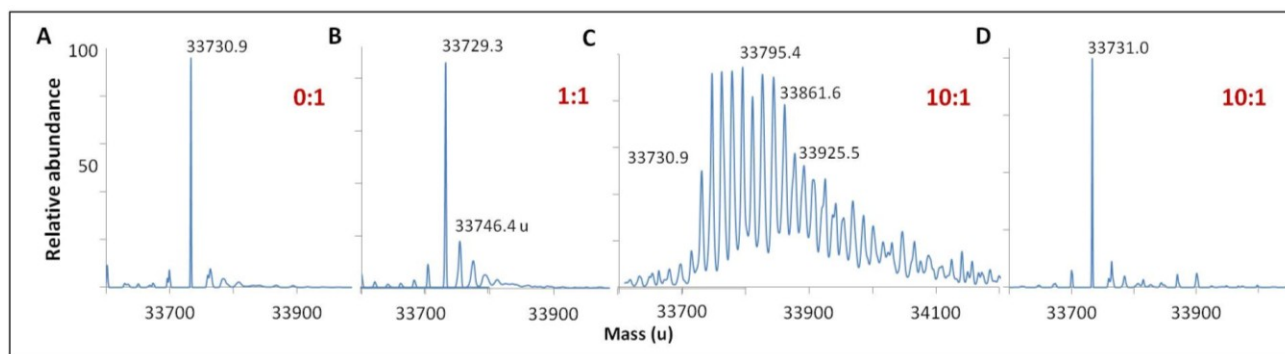


Figure 3.2. Deconvolved mass spectra showing that Ccp1 oxidation by H_2O_2 is mediated by its heme. Oxidized Ccp1 (1 μ M) was diluted 5-fold into the MS solvent and 5 μ L aliquots were analyzed by LC-MS on a Waters QToF3 mass spectrometer (*Materials and Methods*). Mass spectra of (A-C) holoCcp1 oxidized with 0, 1 and 10 M eq of H_2O_2 and (D) apoCcp1 oxidized with 10 M eq of H_2O_2 . The observed mass of the unoxidized polypeptide is 33730.50 ± 1.35 u (calc 33730.33 u) and overoxidation of holoCcp1 but not apoCcp1 gives incremental mass shifts of +16 u (panels B,C vs D).

A single buried cysteine residue (C128) is located >20 Å from the heme in the distal domain. In CcpI $\sim 3\%$ of C128 is oxidized to CysSO₂H/CysSO₃H, and the oxidized forms sum to 60% and 100% on treatment with 5 and 10 M eq of H₂O₂, respectively (Figure 3.3B), revealing that C128 also acts as a donor to the heme.

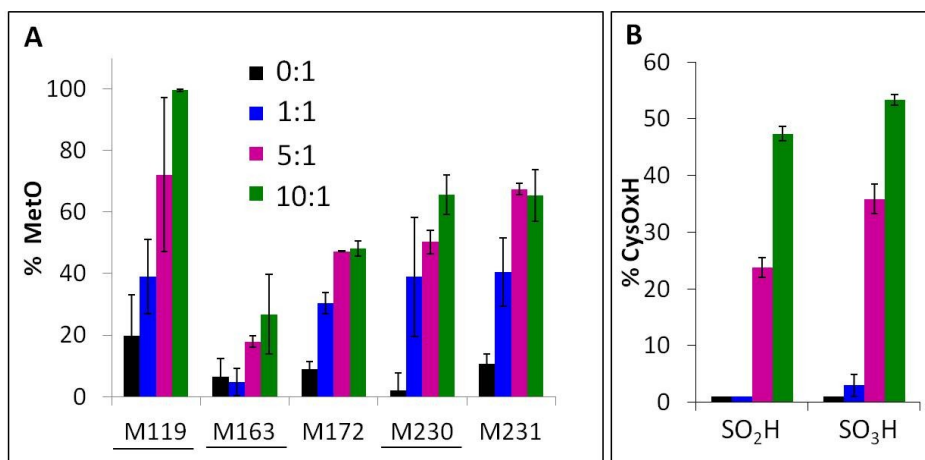


Figure 3.3. Methionine and cysteine oxidation. CcpI (1 μ M) in KPi/DTPA was treated with the indicated molar ratio of H₂O₂ for 1 h at room temperature, digested with trypsin and the peptides were analyzed by LC-MS/MS as described in the *Materials and Methods*. Percent (A) methionine oxidation to MetO (+16 u); (B) C128 oxidation to CysSO₂H (+32 u) and CysSO₃H (+48 u). Yields are based on peptide PAs (Eq. 4) from three independent experiments ($n=3$) and presented as averages \pm SD. Solvent-exposed methionines are underlined in panel A.

CcpI's seven tryptophans undergo extensive H₂O₂-induced hydroxylation and W223 is additionally converted to kynurenine (~ 2 -15%) (Figure 3.4B). Notably, W191, W211, W223 proximal to the heme are ~ 5 -40% oxidized in CcpI, whereas the distal W57 and W126 are extensively oxidized by 5 M eq of H₂O₂ but oxidation of W51 at 3.1 Å from the heme is seen only in protein exposed to 10 M eq of H₂O₂ (Figure 3.4). Furthermore, oxidized W51 and W57 are detected solely as Trp(OH)₂ (dihydroxytryptophan), from which we infer that their TrpOH form is readily oxidized and/or radical transfer to the distal domain becomes more facile in overoxidized CcpI. W101, located on CcpI's distal surface at >25 Å from the heme, undergoes

little oxidation (Figure 3.4) probably because of radical scavenging on residues closer to the heme such as W126 or C128 (Figure 3.1).

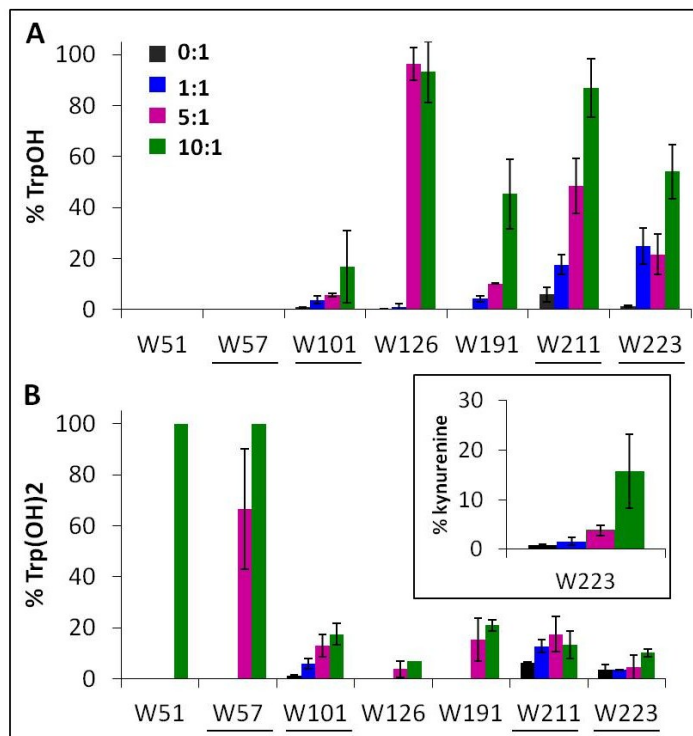


Figure 3.4. Tryptophan residues undergo extensive mono- and dihydroxylation. Percent tryptophan oxidation to (A) TrpOH and (B) Trp(OH)₂ and kynurenine (inset). Experimental details are given in the caption to Figure 3.3, and solvent-exposed tryptophans are underlined.

3.5.3) Tyrosine is oxidized mainly to dityrosine.

Oxygen uptake by tyrosine contributes minimally to the +16 peaks in Figure 3.2C since only Y229 proximal to the heme forms TyrOH (hydroxytyrosine) in high yield. Y16 and Y251 are 10-30% converted to TyrOH (Figure 3.5A) but none of the remaining 11 tyrosines appear to undergo hydroxylation. Peptides T4 (Y23), T18 (Y153) and T27 (Y244) exhibit similar MS1 *PAs* in untreated and oxidized Ccp1 (data not shown), revealing that these tyrosines escape oxidation. In contrast, the *PAs* of T6 (Y36/Y39/Y42) and T8 (Y67/Y71) decrease 100-fold when Ccp1 is overoxidized with 10 M eq of H₂O₂ (Figure S3.2D) so we hypothesized that Y[•] is quenched by

intramolecular dityrosine crosslinking. Dityrosine emits strongly at 410 nm above pH 7 (139), and monomeric oxidized Ccp1 (Figure S3.2B) exhibits increasing 410 nm emission up to a [H₂O₂]:[Ccp1] molar ratio of 10 (Figure S3.2C), which supports H₂O₂-induced *intramolecular* dityrosine formation.

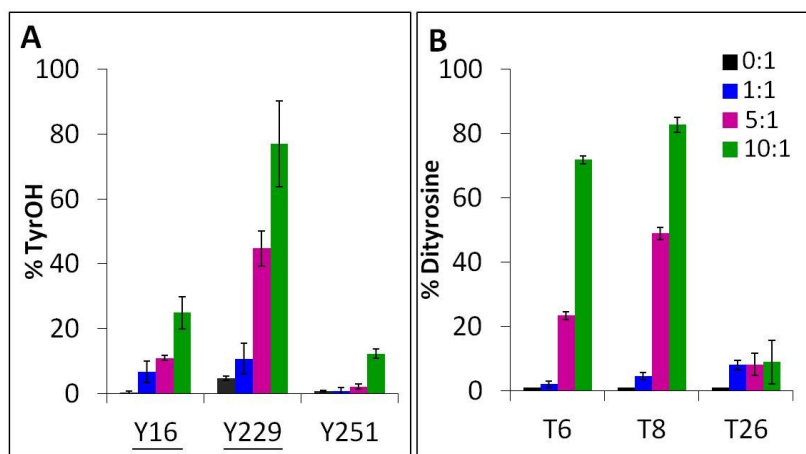


Figure 3.5. Tyrosine oxidation products include TyrOH and dityrosine. Percent tyrosine oxidation to (A) TyrOH (+16 u) and (B) dityrosine (-2 u) in T6 (Y36/Y39/Y42), T8 (Y67/Y71) and T26 (Y229/Y236). Experimental details are given in the caption to Figure 3.3. Solvent-exposed tyrosines are underlined in panel A.

The doubly and triply charged ions of T6 and T8 from untreated Ccp1 show high intensity MS1 signals (data not shown). Overoxidized Ccp1 has peptide ions at two mass units lower which, based on the MS2 spectra in Figures 3.6 and S3.3A,B, are assigned to T6 and T8 that have lost a H atom (-1 u) from two tyrosines. Notably, no b_n or y_n sequence ions arising from peptide-bond fragmentation between the oxidized tyrosines appear in the MS2 spectra (Figures 3.6B and S3B). In fact, the stability of the cyclic peptide region identifies Y36-Y39 and Y36-Y42 as crosslinks in T6 (Table S3.3). The yield of crosslinked T6 and T8 is >70% in overoxidized Ccp1 (Figure 3.5B) and, in addition to M230/M231 oxidation (Figure 3.3A, Table S3.3), T26 also undergoes ~10% Y229-Y236 crosslinking (Figure 3.5B, Figure S3.3D) in competition with Y229 hydroxylation (Figure 3.5A). Intramolecular dityrosine crosslinking has not been reported for

overoxidized Ccp1 previously but *intermolecular* crosslinking involving Y36, Y39, Y42 (125, 134, 135), and Y236 (96) is documented. Presumably, the Ccp1 dimers and trimers separated here (Figure S3.2B) contain such intermolecular crosslinks.

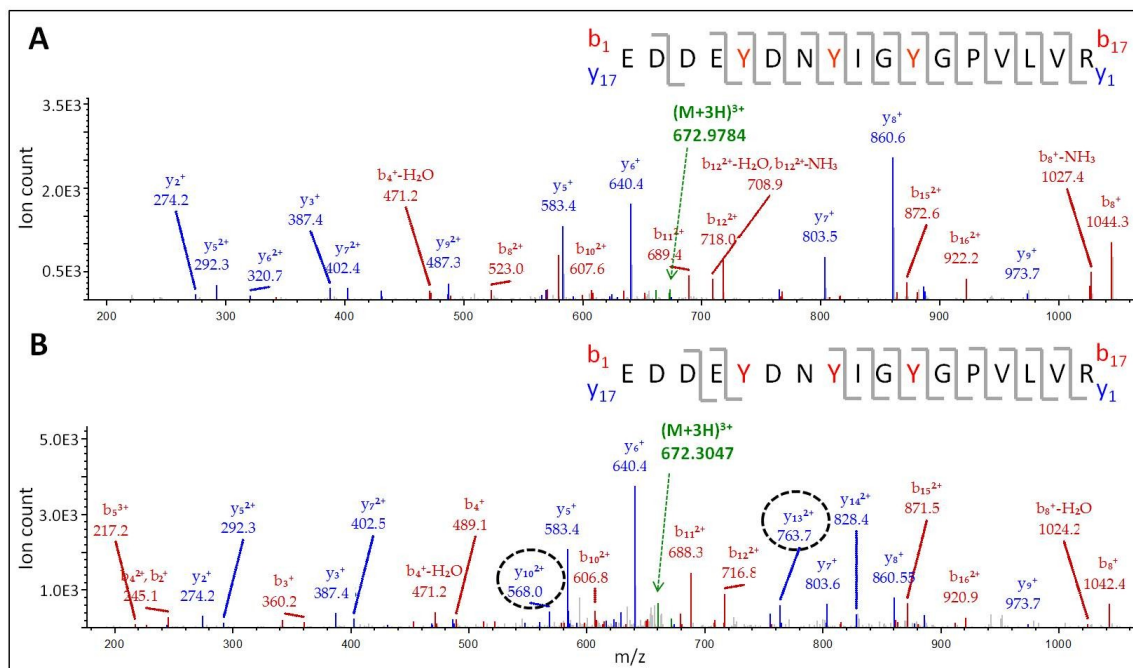


Figure 3.6. LC-MS/MS analysis of dityrosine formation in tryptic peptide T6. MS2 spectrum of the $(M+3H)^{3+}$ ion of: (A) native T6 at m/z 672.9784 and (B) oxidized T6 at m/z 672.3047. The T6 precursor ions (green) were fragmented by CID (30 V) to give b_n (red) and y_n (blue) sequence ions. The y_{10}^{2+} and y_{13}^{+} ions encircled in panel B have masses consistent with loss of an H atom (-1 u) from both Y36 and Y39. The peptide sequence in each panel shows Y36, Y39 and Y42 in red font and the fragmentation sites as vertical lines. Note the absence of fragmentation between crosslinked Y36 and Y39 in panel B.

3.5.4) Oxidation of the proximal iron ligand H175 and of the catalytic distal H52.

Solvent-exposed H6, H60, H96 and H181 are <2% oxidized (+16 u) in overoxidized Ccp1 (data not shown). In contrast, the proximal H175, which coordinates the heme iron, is ~40% oxidized (Figure 3.7A). The absorption spectrum of untreated Ccp1 in KPi/DTPA at pH 8.1 shows a Soret maximum at 410 nm and visible bands at 505 and 645 nm indicative of pentacoordinate high-spin heme (Figure 3.7B) (141). Immediately upon addition of 10 M eq of

H₂O₂, the spectrum converts to that of CpdI with a Soret at 419 nm and 530/560 nm visible bands (Figure 3.7B inset). However, after 1 h the Soret drops in intensity and blue shifts to 414 nm, which we associate with the partial oxidation of H175 to HisO (oxo-histidine). Remarkably, the heme released in the MS solvent at low pH from overoxidized Ccp1 has the same exact mass as that from untreated Ccp1 (616.1745 ± 0.0005 u; Figure S3.4), revealing that it escapes irreversible oxidation by 10 M eq of H₂O₂.

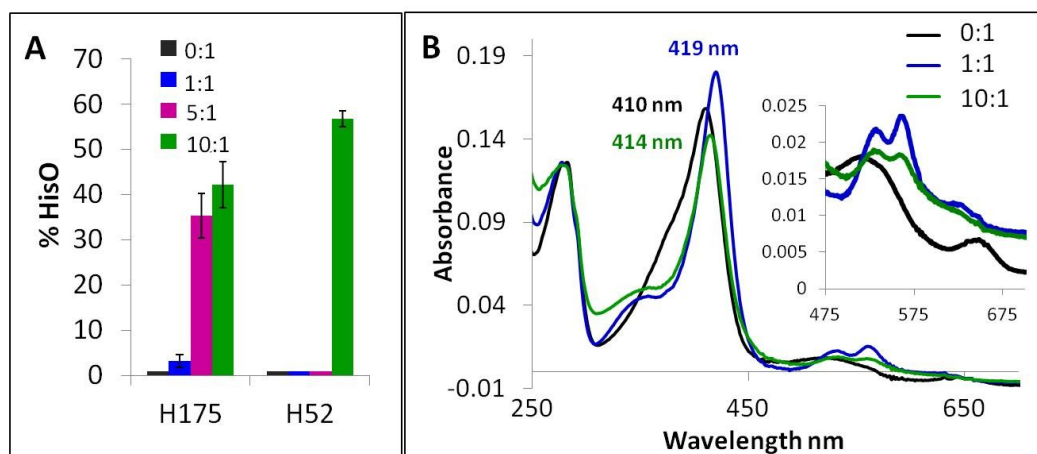


Figure 3.7. The proximal heme ligand H175 and the distal H52 are oxidized to HisO. (A) Yield of HisO formation. Experimental details are given in the caption to Figure 3.3 and Figure S3.5 shows the MS2 spectra of T7 and T21 with oxidized H52 and H175. (B) UV-vis spectrum of 1 μ M untreated Ccp1 (black trace), CpdI (blue trace) and Ccp1 overoxidized with 10 M eq of H₂O₂ (green trace). Spectra were recorded at pH 8.1 in KPi/DTPA 1 h after H₂O₂ addition. Results in panel B are representative of three independent experiments.

Close to 60% of the distal H52 is present as HisO in Ccp1 oxidized with 10 M eq of H₂O₂ (Figure 3.7A). The low CCP activity (11%) of this sample (Table S3.4) reflects the critical function of H52 as an acid-base catalyst in heterolytic cleavage of the peroxy bond of H₂O₂ as evinced by the 10⁵-fold slower H₂O₂ reactivity of the H52L variant (142). Hence, the extensive heme loss in Ccp1 exposed to 100 M eq of H₂O₂ (Figure S3.4C) may initiate from slow homolytic H₂O₂ cleavage at the iron with OH[•] release following H52 oxidation.

3.6) Discussion

This study provides a comprehensive profile of Ccp1 oxidation by 1, 5 and 10 M eq of H₂O₂. Using high performance MS, we identify and semiquantitate stable oxidative modifications of 24 of Ccp1's 294 residues (Figures 3.3, 3.4, 3.5 and 3.7). Key findings include the oxidation of tyrosine to dityrosine, tryptophan to TrpOH and Trp(OH)₂ as well as kynurenine, histidine to HisO, methionine to MetO, and cysteine to CysSO₂H and CysSO₃H. These products result from radical transfer from the heme as Ccp1 endogenously reduces up to ten molecules of H₂O₂. A plausible common mechanism for oxygen incorporation into Ccp1's oxidizable residues is the reaction of their radicals with O₂ to yield peroxy radicals that release superoxide, allowing the hypovalent cations to trap water and deprotonate to give the products detected by MS. Of key interest is how intrinsic radical reactivity is modulated by the local protein environment, which predetermines the preferred donor residues in Ccp1. This question is explored in the following sections before we discuss how overoxidation by H₂O₂, allows Ccp1 to perform its remarkable H₂O₂ sensing and signaling function in the cell.

3.6.1) Intrinsic radical reactivity.

Free methionine and many methionine residues are oxidized to MetO with H₂O₂ as a typical oxidant (143). Nonetheless, MS analysis of H₂O₂-treated intact apoCcp1 provides no evidence for MetO formation (Figure 3.2D), which we attribute in part to inhibition of trace-metal activation of H₂O₂ by the DTPA (100 μM) present in the buffer. Tryptic digestion also was performed in the presence of DTPA but 2-20% MetO is detected in peptides from untreated holoCcp1 (Figure 3.3A), which may be catalyzed by the heme released during proteolysis. Since MetO levels increase significantly in peptides from oxidized Ccp1 (Figure 3.3), the methionines, with the possible exception of M163, appear to be good electron donors to the oxidized heme. The

addition of O₂ to the resultant M[•] (which may be stabilized by a cyclic structure) (144) and elimination of superoxide will generate MetO on water capture (144). These steps must be sufficiently exergonic to drive the thermodynamically unfavorable initial electron transfer step given the E_7 value (~1.5 V) estimated for M^{•+}, which has a pK_a of ~-6 (145).

Radical transfer to cysteine should be more favorable since the reduction potential of C[•] is 0.92 V (146). Also, free C[•] reacts rapidly with O₂ ($8 \times 10^9 \text{ M}^{-1} \text{ s}^{-1}$) (147) to give a peroxy radical (CysSOO[•]) that has been detected by EPR (148, 149). Superoxide release and water capture would give CysOH but C128 conversion to CysO₂H and CysO₃H (Figure 3.3B) may not be all heme-mediated given the instability of sulfenic acids to further oxidation (146).

Neutral W[•], which possesses a reduction potential of +1.01 V (150–152), is also readily converted to the peroxy radical by O₂ (153). Again, superoxide release and water capture by the aryl carbocation lead to TrpOH, with indole-ring hydroxylation at the 2-, 4-, 5-, 6-, or 7-positions. TrpOH can be further oxidized to Trp(OH)₂ (154), and ~30% of W223 in overoxidized Ccp1 is detected as the tryptophan metabolite, kynurenine (Figure 3.4B, inset) (155). Although the pK_a of free W^{•+} is ~4 (150), W191^{•+} is stabilized in CpdI (156) and efficient radical transfer occurs from W191^{•+} to proximal solvent-exposed residues at the protein surface, including W211 and W223 (Figure 3.1). The W^{•+} forms of these residues must rapidly deprotonate and react with nearby O₂ (Table S3.6) as evidenced by their oxidation to TrpOH and Trp(OH)₂ in CpdI (Figure 3.4). Distal W57 is also solvent exposed whereas a number of internal waters are <5 Å from W51 and W126 (Figure 3.8, Table S3.6) to accept a proton from their cation radicals and promote their full conversion to Trp(OH)₂ and TrpOH, respectively, in overoxidized Ccp1 (Figure 3.4).

Neutral Y^\bullet (+0.93 V) possesses a similar reduction potential to W^\bullet (150, 151). However, Y^\bullet reacts with O_2 relatively slowly ($<10^3 M^{-1}s^{-1}$) (157) but rapidly combines with a second Y^\bullet ($5 \times 10^8 M^{-1}s^{-1}$) (158). Hence, dityrosine is the dominant tyrosine oxidation product in overoxidized Ccp1 (Figure 3.5). The side chains of Y36, Y39 and Y42 are separated by 4-8 Å on the same α -helix and Y36/Y39 and Y39/Y42 (Table S3.3) crosslinks are found in T6. The Y67/Y71 pair are 10 Å apart in a large loop region (Figure 3.1) with sufficient flexibility to allow efficient T8 crosslinking (Figure 3.5B, Figure S3.4B). Also, overoxidation may induce structural changes in Ccp1 that enhance crosslinking.

The efficient (~80%) hydroxylation of Y229 is unique among Ccp1's 14 tyrosines (Figure 5A). In fact, half of Ccp1's tyrosines (Y16, Y23, Y153, Y187, Y203, Y244, Y251) undergo little or no oxidation (Figure 3.5). The thermodynamics of Y^\bullet formation requires deprotonation since $Y^{\bullet+}$ has a pK_a of ~-2 (159) but all tyrosines are solvent exposed (Figure 3.1) and/or close to internal waters (Figure S3.6, Table S3.6). This will promote deprotonation and a number are well within crosslinking distance (e.g., Y203-Y251 ~4 Å). Thus, the presence of several unoxidized tyrosines in overoxidized Ccp1 serves to delimit the zones in Figure 3.8 and hence the radical transfer pathways leading from the heme.

H-bonding to D235 imbues H175 with imidazole character, which promotes donation of electron density to the Fe^{IV} heme of CpdI (160). Nonetheless, we detect little radical transfer to H175 in CpdI (Figure 3.7A). Since the pK_a of free $H^{\bullet+}$ is ~5-7 and H^\bullet has an E_7 of 1.17 V (161), radical transfer to histidine residues should be particularly sensitive to their local protein environment. A change in the environment around H175 in overoxidized Ccp1 must switch on radical transfer to this residue as discussed below. The stable HisO product is likely formed from a peroxy radical (162) as proposed for the other oxidizable residues above. HisO generation,

especially at H52 located just above the heme, may additionally arise from slow homolytic H₂O₂ cleavage at the iron in overoxidized Ccp1. Notably, HisO, which is viewed as a marker of protein oxidative damage (163), is produced by free or Cu-bound [•]OH attack on histidine ligands to the metals in CuZn superoxide dismutase (102, 162, 164) following H₂O₂ binding to the catalytic copper. Histidines are also oxidized in the dismutase during cell aging (165, 166).

3.6.2) Radical transfer pathways and electron-donor zones in Ccp1.

The primary donor to the porphyrin π -cation formed on two-electron oxidation of Ccp1's heme is W191 (42, 116). This residue is surrounded by oxidizable residues, and the sulfur atoms of M230 and M231 at ~ 4 Å from the indole ring contribute to stabilizing W191^{•+} (121). Also, our MD simulations find no O₂ docking site within 5 Å of W191 (Figure S3.6, Table S3.6) which, combined with its positive charge, must lower its scavenging by O₂. Hence, radical transfer continues from W191^{•+} to M231 and to residues at the surface of the proximal domain, including M230, W223, W211 and Y229. These residues cluster in a region we label as zone 1 (Figure 3.8) and are all oxidized to detectible levels in CpdI (Figures 3.3, 3.4, 3.5A).

Oxidation of M230 and/or M231 converts W191 into a poorer electron donor as seen on mutation of these residues (120, 121). Thus, radical transfer from the heme to the distal region (zones 2a and 2b, Figure 3.8) opens up. Zone 2a with its numerous oxidizable residues, internal waters (Figure 3.8) and O₂ docking sites (Figure S3.6, Table S3.6) is a rich source of electrons for endogenous H₂O₂ reduction. For example, both W126 and C128 act as major donors in the same molecules of overoxidized Ccp1 (Table S3.5). These neighboring residues are close to 2-3 internal waters and O₂ docking sites (Figure S3.6, Table S3.6), a favorable environment for coupling proton transfer with radical transfer and subsequent O₂ scavenging of neutral radicals. Zone 2b contains solvent-exposed Y36, Y39 and Y42 that undergo efficient crosslinking once

oxidized (Figure 3.5B). The sequence of radical transfer to zones 2a and 2b is not resolved in our study but the clustering of donors in these subzones suggests two distinct routes for radical transfer from the heme with redox-active W51 and M119, respectively, as likely intermediate sites (Figure 3.8).

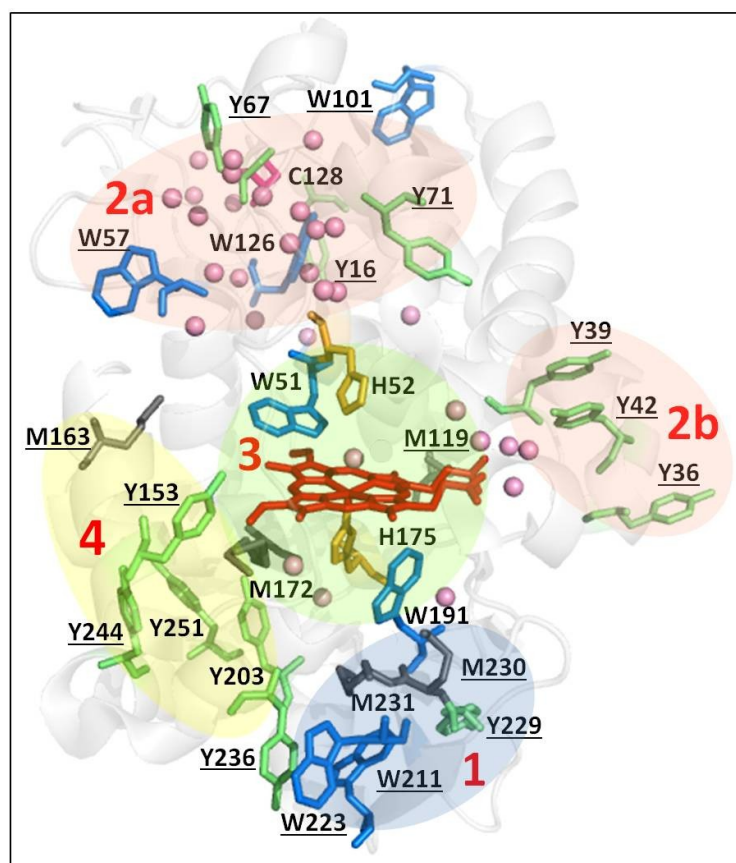


Figure 3.8. Zoning of Ccp1 based on the inferred progression of radical transfer from the heme. PyMOL-generated cartoon of Ccp1 structure (PDB 1ZBY) showing the 24 residues oxidized in heme-mediated H_2O_2 reduction (W, blue; Y, green; H, orange; M, grey; C, magenta). Solvent-exposed residues are underlined and 31 conserved internal water molecules (see SI) are depicted as pink spheres. Radical transfer from the heme via W191 oxidizes residues in **zone 1** (blue). M230/M231 oxidation turns on radical transfer from the heme to **zones 2a** and **2b** (pink) and then to **zone 3** (green) at higher levels of H_2O_2 , when active-site residues are oxidized. Except for ~10% of Y251 (Figure 3.5A), no oxidized residues are found in **zone 4** (yellow), revealing that there is minimal radical transfer from the heme to this zone.

Residues W51, W191 (Figure 3.4) and H52 (Figure 3.7) kick in as major electron donors in Ccp1 treated with 10 M eq of H_2O_2 . We group these active-site residues together with M172 and

H175 into zone 3 (Figure 3.8). Significantly, M172 and H175 approach their maximum oxidation level of ~50% in Ccp1 exposed to 5 M eq of H₂O₂ (Figures 3.3A, 3.7A) and are, for the most part, oxidized in different Ccp1 molecules (Table S3.5). Thus, we hypothesize that radical transfer from the heme to H175 may be controlled by a conformational change in M172. As can be inferred from M230/M231-W191(116, 121, 140) the interaction of the M172 sulfur with the imidazole ring of H175 should lower the reduction potential of the latter and switch on radical transfer from the oxidized heme to its proximal ligand. Subsequent conversion of H175[•] to HisO then will labilize the heme. M172 oxidation, on the other hand, appears to shut down radical transfer to H175 (Table S3.5). The relative orientation of H175 and W191 is fixed by hydrogen bonds to D235, which also modulate the coupling of W191^{•+} to the heme (160). Hence, it appears that the susceptibilities to oxidation of the three proximal residues, M172, H175 and W191, that critically control Ccp1's function, are interdependent.

Interaction with M163 may promote oxidation of W57 (Figure 4.3B), thereby driving radical transfer from the heme over 12 Å into the distal domain. Additionally, proximity to M230 and/or M231 may boost Y229 hydroxylation, the only TyrOH formed in high yield (Figure 5.3A). Recently, methionine-aromatic interactions have been found in 33% of proteins in the PDB and the interaction energy (~1-3 kcal mol⁻¹), which stabilizes protein structure (167), also appears to regulate the redox properties of aromatic residues as documented for W191 (116, 121, 140).

3.6.3) Comparison of MS and EPR studies on Ccp1 oxidation.

Radicals are detected by EPR, which directly confirms their transient presence in proteins during catalysis. For example, catalytic Y[•] that are well-characterized by EPR include those in ribonucleotide reductase, prostaglandin H synthase, photosystem II, and dopamine β

monooxygenase (113, 168). A recent elegant EPR study on H₂O₂-oxidized Ccp1 with multiple mutations identified Y236[•] as a non-catalytic radical and Y71[•] as a catalytic radical in peroxidase turnover with guaiacol as a reducing substrate (124, 169). Our product analysis is consistent with the detection by EPR of Y71[•] and Y236[•] (Figure 3.8) but while Y71 is a major donor in zone 2a (Figure 3.5B), product analysis establishes Y229, not Y236, as a major donor in zone 1 (Figure 3.5). Efficient scavenging of Y229[•] by O₂ (Figure 3.5A) may compete with its detection by EPR. We also find donors in zone 2b (Figure 3.8), where a second molecule of guaiacol is known to bind Ccp1 near residue I40 (169). Furthermore, we demonstrate that Y[•] involved in *intramolecular* dityrosine crosslinking can be readily identified by high-performance MS (Figures 3.6, S3.3) whereas rapid dimerization under high radical flux will compete with the detection by EPR of Y[•] such as those in zone 2.

The assignment of W[•] by EPR can be challenging due to peak broadening (170). Moreover, efficient scavenging of W[•] by O₂ as seen in oxidized Ccp1 (Figure 3.4) will compete with its detection by EPR. In fact, W191^{•+} with low O₂ reactivity is the only indolyl radical reported in EPR studies of CpdI and overoxidized Ccp1 (119–124). Also, MNP trapped Y153[•], Y39[•] and Y236[•] but no W[•] in Ccp1 (96, 171), revealing that spin trapping is also biased toward Y[•] with low O₂ reactivity. Hence, MS and EPR provide complementary information on protein-based radicals. EPR can directly detect relatively long-lived radicals and provide information on their stability and, in some instances, the specific residue(s) oxidized can be selected from EPR spectra (170). MS on the other hand, can characterize the stable end products of all residues oxidized, which reveal mechanisms of radical quenching and also radical transfer pathways when repeated radical translocation occurs from a heme active-site as in Ccp1 or from another type of redox-active metal center.

A recent QM/MM computational analysis confirmed W191^{•+} as the main radical species in CpdI (172) and proposed Y203/Y251 and Y236, along two possible radical transfer pathways from W191^{•+}, as secondary radical sites. Y203/Y251 as well as Y153 and Y244 are clustered in proximal zone 4 (Figure 3.8) and undergo little or no oxidation detectable by MS (Figure 3.5). However, we did detect TEMPO mass adducts in T18 (153), T23 (Y187, Y203, W211), T27+28 (Y244, Y251) and T28 (Y244) (128), and a MNP mass adduct was localized to Y153 (125). Thus, the observed products depend on radical reactivity with the trapping/scavenging agent employed as well as on radical accessibility. We note that O₂ diffuses into the interior of many proteins as seen here for Ccp1 (Figure S3.8) and is present in cells under aerobic conditions so radical scavenging by O₂ is of physiological relevance.

3.6.4) Characterization of overoxidized Ccp1 provides new insights into its physiological function.

We reported that in respiring yeast mitochondria, Ccp1 donates its heme directly or indirectly to catalase A (Cta1) (118). H₂O₂ levels spike ~10-fold when yeast begin to respire (50, 118) causing Ccp1 to become overoxidized (118) since synthesis of its reducing substrate, Cyc1^{II} (Eqs. 2,3), is under O₂/heme control (55), unlike Ccp1 itself (60).

In keeping with its heme-donor function (118), we find that the numerous oxidizable residues in Ccp1 (96) protect the heme from oxidative damage. Heme modification is avoided by diverting oxidizing equivalents from H₂O₂ to zones 1 and 2 (Figure 3.8). W191 plays a critical role in protecting the heme since on reaction with H₂O₂ the W191F variant forms a transient porphyrin π -cation radical that crosslinks to W51[•] (173). Although ascorbate peroxidase (APX) has a very similar active-site structure to Ccp1 (44), heme crosslinking to the residue analogous

to W51 (W41) occurs in the oxidized wild-type enzyme (174). This is associated with the formation of a transient porphyrin π -cation radical in wild-type APX rather than W179^{•+} (44), which occupies the same proximal location as W191 in Ccp1. Notably, a physiological function in plants other than that of a peroxidase has not been defined for APX.

Oxidation of Ccp1's proximal ligand, H175, will labilize the heme as seen in H175 variants with weakened axial ligation (67). On the other hand, conversion of the distal H52 to HisO will greatly slowdown the oxidation of Ccp1 by H₂O₂. H52 is essential for the rapid reaction of Ccp1 with H₂O₂ (142) so its oxidation following radical transfer to zones 1 and 2 (Figure 3.8) will protect the heme.

Intramolecular dityrosine crosslinking is prevalent in Ccp1 overoxidized with 5 and 10 M eq of H₂O₂ (Figure 3.5B). Dityrosine is becoming increasingly identified as a marker of oxidative stress and linked to a number of pathologies including amyloid fibril formation (175). In yeast cells, this crosslinking may prevent apoCcp1 escape from mitochondria (118) and possibly contribute to the triggering of mitophagy, the selective degradation of damaged mitochondria in cells.

3.7) Conclusions

Our detailed analysis reveals that overoxidation of Ccp1 is orchestrated to enable its H₂O₂-sensor function. H₂O₂ serves as a signal by overoxidizing Ccp1 at specific sites including H175, which labilizes the unmodified heme for transfer to apoCta1 in respiring cells (118). Interestingly, iron-catalyzed histidine oxidation previously has been implicated in H₂O₂ sensing by the peroxide resistance protein (PerR) from *B. subtilis* (26). PerR binds H₂O₂ at its non-heme Fe^{II} center, which oxidizes the H37 and H91 ligands, promotes iron release and apoPerR

dissociation from DNA to turn on H₂O₂-inducible genes, including that encoding *kat A*, catalase (26).(26)(26)

Previous studies (93, 96, 125, 128, 133–135) have pinpointed a limited number of residues as sites of radical formation and/or donors to the heme in the endogenous oxidation of Ccp1 by H₂O₂. Here we identify an unprecedented number of donor residues (24) by characterizing their stable end products by LC-MS/MS. The discovery of numerous proximal and distal donors reveals possible radical transfer pathways emanating from Ccp1's heme. All radical transfer routes may not be operative or lead to irreversible residue oxidation in cells because of the efficient repair of protein radicals by glutathione and ascorbate (176) and/or the reversible phosphorylation of tyrosine. Importantly, we have already demonstrated that Ccp1's heme is labilized in mitochondria by H175 oxidation (118), so it remains to be seen if and how Ccp1's oxidation profile in cells differs from that *in vitro*. Finally, we reiterate that applying a universal detection/characterization method such as MS exposes a bias in EPR detection toward protein-based radicals such as Y• with low O₂ reactivity.

3.8) Supplementary information

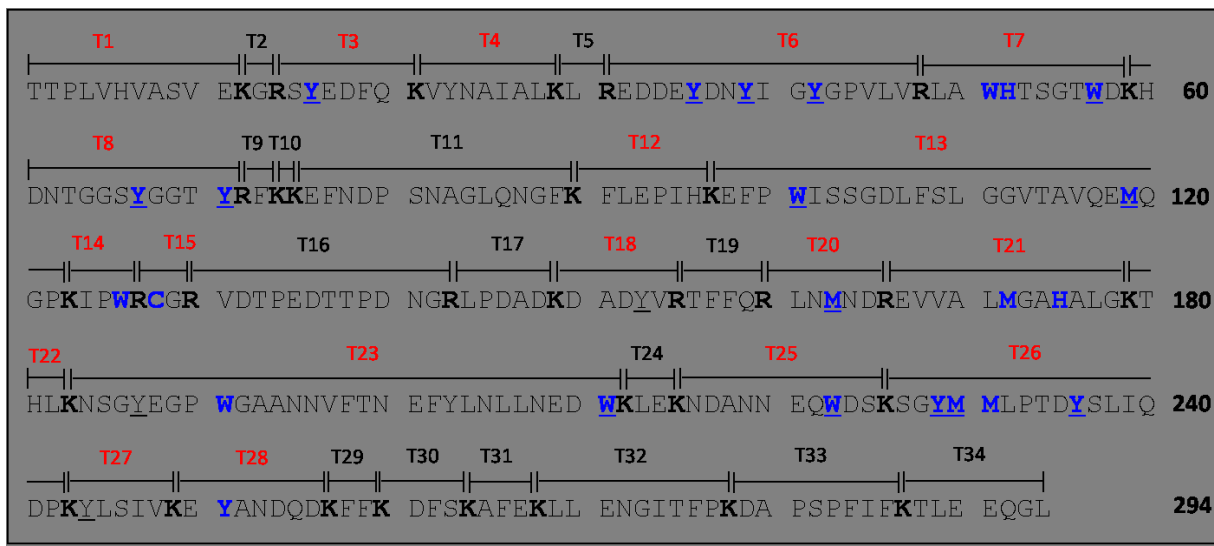


Figure S3.1: Tryptic peptides T1-T34 predicted for Ccp1. The protein's sequence is divided in blocks of 10 residues and the trypsin cleavage sites arginine (**R**) and lysine (**K**) residues are bolded. Peptides that contain oxidizable residues (M, C, Y, W, H) are in labeled in **red font** and the 24 residues found to be >5% oxidized are in **blue font**. Solvent-exposed oxidizable residues are underlined.

Table S3.1: Oxidative modifications considered in database searching

Modification: candidate amino acids ^a	Δm (u) ^b
Monoxidation (ox): K, R, C, M, Y, H, P, W, F, D, N	15.9949
Dioxidation (diox): K, R, C, M, Y, H, P, W, F	31.9898
Trioxidation (triox): C	47.9847
Carbonylation: R, E, Q, I, L, K, V, W	13.9793
Hydroxykynurenine: W	19.9898
Kynurenine (kyn): W	3.9949
Pyrrolidinone: P	30.0105
Pyroglutamic acid: P	13.9792
Asparagine: H	23.0159
Aspartic acid: H	22.0319
Aspartylurea: H	10.0320
Formylasparagine: H	4.9790
Aspartate semialdehyde: M	32.0085
Homocysteic acid: M	33.9691
Dehydro (deH): K, R, C, M, Y, H, P, W, F, D, N ^c	1.00783

^a Reported products of single amino acid oxidation (111, 177).

^b Difference in the monoisotopic mass of the oxidized and native form of the indicated amino acid.

^c Crosslinked residues undergo loss of a hydrogen atom (see main text).

Table S3.2: Peak areas (PA) of the internal reference peptides in the Ccp1 tryptic digests ^a

Peptide sequence	Obs mass (u)	ppm error ^b	PA ^c			
			0:1 [H ₂ O ₂]:[Ccp1]	1:1 [H ₂ O ₂]:[Ccp1]	5:1 [H ₂ O ₂]:[Ccp1]	10:1 [H ₂ O ₂]:[Ccp1]
T4 VYNAIALK	891.5296	0.22	1.59E10 ± 7.12E8 (4.5)	1.50E10 ± 1.77E8 (1.0)	1.56E10 ± 8.57E08 (5.5)	1.66E10 ± 7.28E8 (4.4)
T19 TFFQR	698.3626	0.86	1.76E9 ± 7.80E7 (4.4)	1.78E9 ± 6.87E7 (3.8)	1.69E9 ± 8.50E7 (5.0)	1.76E9 ± 8.50E7 (4.8)
T27 YLSIVK	722.4450	0.41	1.30E9 ± 2.55E7 (2.0)	1.37E9 ± 4.51E7 (3.3)	1.32E9 ± 2.56E7 (1.9)	1.35E9 ± 7.20E7 (5.3)
T34 TLEEQGL	789.3993	0.50	1.59E9 ± 7.03E7 (4.4)	1.68E9 ± 9.67E7 (5.7)	1.66E9 ± 3.75E7 (2.2)	1.72E9 ± 6.79E7 (3.9)
Avg PA of T4, T19, T27 plus T34 ^d			5.14E9	4.96E9	5.07E9	5.36E9

^a No oxidative modifications were detected in these tryptic peptides, which are used as internal reference peptides (178).

^b The error in the observed monoisotopic m/z value in ppm is given by $10^6(\text{Obs } m/z - \text{Calc } m/z)/\text{Calc } m/z$.

^c The intensity of each peptide ion corresponds to its PA in the extracted ion chromatogram (**XIC**) within a 10 ppm exclusion window. Each PA is the average \pm SD of four independent experiments ($n=4$) and the relative standard deviation (% RSD) is given in **red font**.

^d The average PA at each [H₂O₂]:[Ccp1] molar ratio is used as a normalization factor in Eq. 4 of the main text to correct for variation in instrument response and/or ion suppression (178).

Table S3.3: Monoisotopic masses of the tryptic peptides observed in digests of H₂O₂-oxidized Ccp1

Tryptic peptide^a	Residues^a	Residue(s) oxidized^b	Obs MH⁺ (m/z)	Calc MH⁺ (m/z)	ppm error^c
T2+T3	13-21	None Y16 (ox)	1129.5289 1145.5228	1129.5273 1145.5222	1.42 0.52
T3	15-21	None Y16 (ox)	916.4078 932.4005	916.4047 932.3996	3.38 0.97
T4	22-29	None Y23 (ox)	891.5310 907.5249	891.5298 907.5247	1.35 0.22
T5+T6	30-48	None Y42 (ox) Y39 (ox); Y42 (ox) Y36 (deH); Y39 (deH) Y39 (deH); Y42 (deH)	2286.1147 2302.1053 2318.0937 2284.0925 2284.0969	2286.1037 2302.0986 2318.0935 2284.0881 2284.0881	4.81 2.91 0.09 1.93 3.85
T6	32-48	None Y36 (ox) Y39 (ox) Y42 (ox) Y36 (deH); Y39 (deH)	2016.9206 2032.9174 2032.9200 2032.9172 2014.8979	2016.9185 2032.9134 2032.9134 2032.9134 2014.9029	1.04 1.97 3.25 1.87 -2.46
T7	49-59	None W57 (diox) W51 (diox); H52(ox) W51 (diox); W57 (diox) W51 (diox); W57 (diox); H52 (ox)	1301.6290 1333.6188 1349.6158 1365.6086 1384.6035	1301.6273 1333.6171 1349.6121 1365.6069 1384.6018	1.31 1.27 2.74 1.24 1.23
T8	60-72	None Y71 (ox) Y67 (ox); Y71 (ox) Y67 (deH); Y71 (deH)	1384.5857 1400.5811 1416.5842 1382.5776	1384.5876 1400.5825 1416.5775 1382.5720	-1.37 -1.00 4.73 4.05
T13	98-123	None M119 (ox) W101 (ox) W101 (ox); M119 (ox) W101 (diox); M119 (ox)	2780.3697 2796.3589 2796.3635 2812.3628 2828.3554	2780.3600 2796.3549 2796.3549 2812.3498 2828.3447	3.49 1.43 3.08 4.62 3.78
T14	124-127	None W126 (ox)	571.3361 587.3308	571.3351 587.3300	1.75 1.36
T14+T15	124-130	None W126 (ox); C128 (diox) W126 (ox); C128 (triox) W126 (diox); C128 (triox)	887.4668 935.4524 951.4455 967.4446	887.4669 935.4516 951.4465 967.4414	-0.11 0.86 -1.05 3.31
T16+T17+T18	131-155	None	2775.2782	2775.2704	2.81
T17+T18	144-155	None	1377.6588	1377.6645	-4.14
T20	161-166	None M163 (ox)	762.3591 778.3529	762.3563 778.3512	3.67 2.18
T20+T21	161-179	None M163 (ox) M172 (ox); H172 (ox)	2039.0542 2055.0475 2071.0429	2039.0525 2055.0474 2071.0423	0.83 0.05 0.29
T21	167-179	None	1295.7149	1295.7140	0.69

		M172 (ox)	1311.7099	1311.7089	0.76
		H175 (ox)	1311.7060	1311.7089	-2.21
		M172 (ox); H175 (ox)	1327.7065	1327.7038	2.03
T23	184-212	None	3362.5536	3362.5389	4.37
		W191 (ox)	3378.5398	3378.5338	1.78
		W211 (ox)	3378.5353	3378.5338	0.44
		W191 (ox); W211 (diox)	3410.5275	3410.5236	1.14
T23+T24	184-215	None	3732.7527	3732.7605	-2.09
		W211 (ox)	3748.7640	3748.7554	2.30
		W191 (ox); W211 (diox)	3780.7540	3780.7453	2.30
		W191 (diox); W211 (diox)	3796.7544	3796.7401	3.77
T24+T25	213-226	None	1690.7642	1690.7667	-1.48
		W223 (ox)	1706.7592	1706.7616	-1.41
		W223 (diox)	1722.7558	1722.7565	-0.41
		W223 (kyn)	1694.7630	1694.7616	0.83
T25	216-226	None	1320.5460	1320.5451	0.68
		W223 (ox)	1336.5402	1336.5400	0.15
		W223 (diox)	1352.5354	1352.5349	0.37
T25+T26	216-243	None	3260.4611	3260.4511	3.07
		W223 (ox)	3276.4603	3276.4460	4.36
		Y229 (deH); Y236 (deH)	3258.4475	3258.4355	3.68
		Y229 (deH); Y236 (deH); M230 (ox)	3274.4412	3274.4304	3.30
		W223 (ox); M230 (ox); M231 (ox)	3308.4425	3308.4358	2.03
T26	227-243	None	1958.9296	1958.9238	2.96
		Y229 (ox)	1974.9265	1974.9187	3.95
		M230 (ox); M231 (ox)	1990.9207	1990.9136	3.57
		Y229 (ox); M230 (ox)	1990.9192	1990.9136	2.81
		Y229 (deH); Y236 (deH)	1956.9138	1956.9074	3.27
		Y229 (deH); Y236 (deH); M230 (ox)	1972.9081	1972.9031	2.53
T27	244-249	None	722.4450	722.4447	0.42
		Y244 (ox)	738.4380	738.4396	-2.17
		Y244 (diox)	754.4352	754.4345	0.93
T28	250-257	None	982.4110	982.4112	-0.20
		Y251 (ox)	998.4077	998.4061	1.60
T28+T29	250-260	None	1404.6479	1404.6430	3.49
		Y251 (ox)	1420.6410	1420.6379	2.18
T28+T29+T30	250-264	None	1881.8700	1881.8654	2.44
		Y251 (ox)	1897.8605	1897.8603	0.11
		Y251 (diox)	1913.8564	1913.8552	0.63

^a Figure S3.1 gives the tryptic map of CcpI and the sequence of tryptic peptides T1–T34.

^b Observed residue modifications are assigned based on the data in Table S3.1.

^c See Footnote b of Table S3.2.

Table S3.4: CCP activity of H₂O₂-oxidized Ccp1^a

[H ₂ O ₂]:[Ccp1] ^b	CCP activity ^a	Percent activity ^c
0:1	1.70 ± 0.010	100 ± 0.00
0.5:1	1.59 ± 0.021	93.4 ± 0.93
1:1	1.34 ± 0.045	79.0 ± 2.37
3:1	0.92 ± 0.028	54.1 ± 2.16
5:1	0.66 ± 0.036	38.8 ± 3.88
10:1	0.18 ± 0.008	11.0 ± 3.30

^a One unit of CCP activity catalyzes the oxidation by H₂O₂ of 1 μmol of horse heart ferrocycytochrome c per min per mg Ccp1.

^b Stock Ccp1 (5 μM) and H₂O₂ solutions (0.01–1 mM) were prepared in Kpi/DTPA, and mixed to give 1 μM Ccp1 with the desired H₂O₂ concentrations. Samples were incubated at room temperature for 1 h and activities were measured as described previously (118). For the assay, a stock solution of Cyc^{III} was ~90% reduced with sodium dithionite and the Cyc^{II} concentration determined spectrophotometrically ($\epsilon_{550} = 7.6 \text{ mM}^{-1} \text{ cm}^{-1}$) (78).

^c The activity of each fraction was ratioed by the activity of the 0:1 sample to give percent activity. Results are presented as averages ± SD from three independent experiments ($n=3$).

Table S3.5. Peptides T21 (M172, H175) and T14+T15 (W126, C128) are oxidized at two residues ^a

Tryptic peptide	Residue(s) oxidized (X_{ox})	Obs MH^+ (m/z) ^b	Calc MH^+ (m/z) ^c	Error (ppm) ^c	% X_{ox} ^d			
					[H ₂ O ₂]: [Ccp1]			
					0:1	1:1	5:1	10:1
T21	None	1295.7149	1295.7140	0.70	90.9 ± 0.1	66.4 ± 10.2	17.5 ± 1.0	9.2 ± 1.4
T21	M172 +16	1311.7108	1311.7089	1.44	8.8 ± 11.1	30.4 ± 2.9	47.2 ± 5.7	48.2 ± 3.1
T21	H175 +16	1311.7050	1311.7089	-2.97	---	3.2 ± 2.5	28.5 ± 2.0	37.2 ± 3.2
T21	M172 +16, H175 +16	1327.7064	1327.7038	1.95	---	---	6.8 ± 4.0	4.9 ± 0.5
T14+T15	None	887.4668	887.4669	-0.11	100±0.0	96.8±0.6	3.70±2.6	1.86±3.7
T14+T15	W126+16, C128 +32	935.4524	935.4516	0.85	---	---	23.72±5.3	44.95±2.7
T14+T15	W126 +16, C128 +48	951.4455	951.4465	-1.05	---	---	33.59±6.9	48.16±1.4
T14+T15	W126 +32, C128 +48	967.4446	967.4414	3.30	---	---	2.24±0.7	5.12±1.3

^a Ccp1 (1 μM) was reacted with 1, 5 and 10 M eq of H₂O₂ for 1 h at room temperature in KPi/DTPA prior to tryptic digestion and LC-MS/MS analysis (see *Materials and Methods*).

^b The precursor ions selected for MS2 analysis were filtered using a mass exclusion threshold of 10 ppm.

^c The monoisotopic m/z values for the peptide MH^+ ions were calculated using Protein Prospector (<http://prospector.ucsf.edu>), and the errors were calculated as in Footnote b of Table S3.2.

^d The percent oxidation of H175, M172, W126 and C128 was calculated using Eq. 4 of the main text.

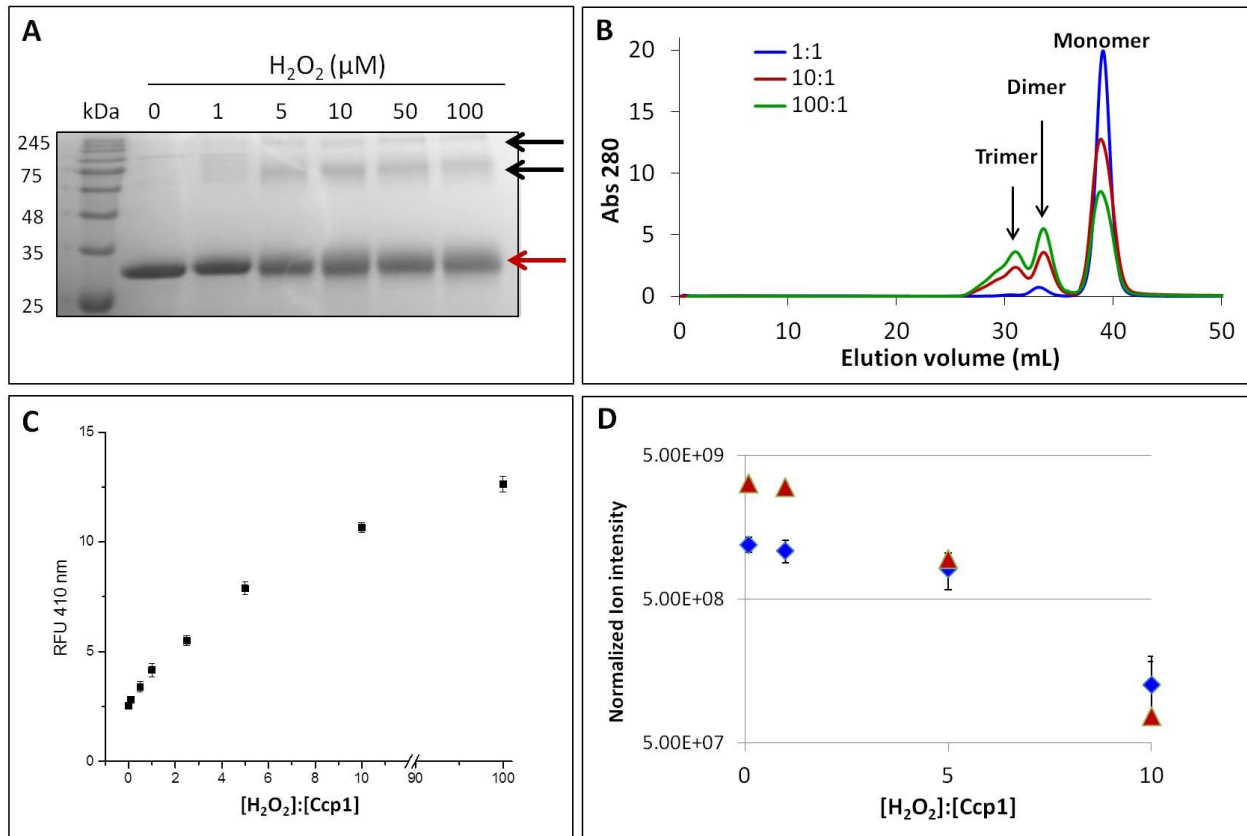


Figure S3.2: Characterization of intramolecular dityrosine crosslinks in H₂O₂-oxidized Ccp1. (A) SDS-PAGE analysis of H₂O₂-oxidized Ccp1 under reducing conditions. Ccp1 (1 μM) was treated with the indicated H₂O₂ concentration in KPi/DTPA for 1 h at room temperature and analyzed by 12% SDS-PAGE followed by Coomassie staining. The red arrow indicates that Ccp1 is predominantly monomeric (~35 kDa) but small quantities of the dimer and trimer (~70 and ~100 kDa) can be detected in the samples treated with 5-100 μM H₂O₂. Notably, the band containing monomeric Ccp1 becomes more diffuse with increasing H₂O₂ indicative of increased protein modification. (B) Gel filtration chromatography of H₂O₂-oxidized Ccp1. Stock solutions in KPi/DTPA were mixed to give 10 μM Ccp1 with 10, 100 and 1000 μM H₂O₂, and incubated for 1 h at room temperature. Aliquots (100 μL) were applied to a 24-mL Superdex 200 HR 10/30 column (fractionation range 10-600 kDa) equilibrated with 20 mM KPi pH 7.5/150 mM NaCl and coupled to an ÄKTApurifier 10 (GE) with 280-nm detection. The protein was eluted in equilibration buffer at a flow rate of 0.5 mL/min and fractions containing monomeric Ccp1 were collected. (C) The monomeric Ccp1 samples were diluted to 1 μM in KPi/DTPA and on excitation at 315 nm, their emission at 410 nm was recorded in a Cary Eclipse fluorometer with 5-nm slits. Relative fluorescence units (RFU) are from three independent experiments ($n=3$) and averages \pm SD are plotted. (D) Normalized ion intensity across three replicates for T6 (Y36, Y39, Y42) [blue diamonds] and T8 (Y67, Y71) [red triangles] plotted vs [H₂O₂]:[Ccp1].

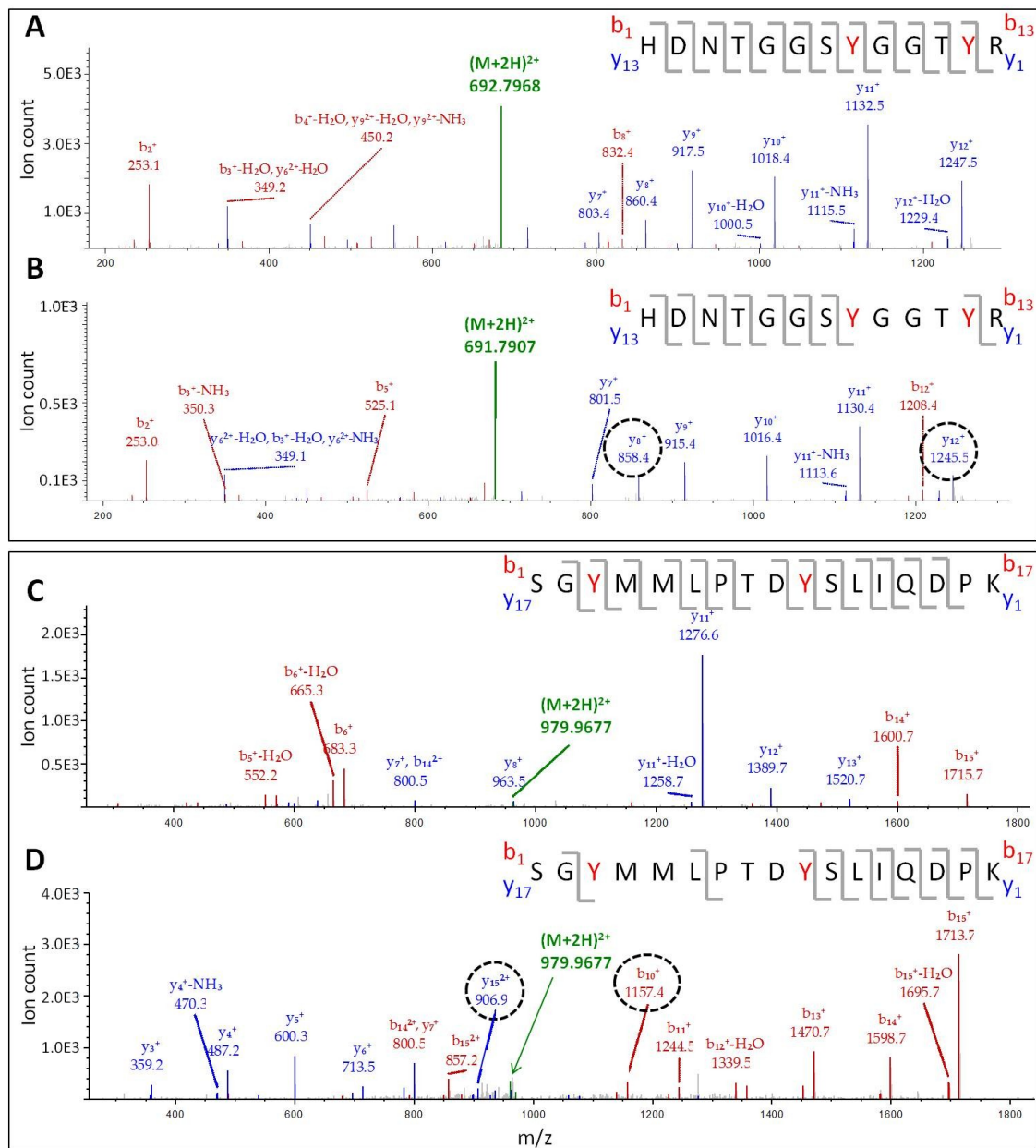


Figure S3.3. LC-MS/MS analysis of dityrosine formation in tryptic peptides T8 and T26. MS2 spectrum of the $(M+2H)^{2+}$ ion of: **(A)** native T8 at m/z 692.7968; **(B)** oxidized T8 at m/z 691.7907; **(C)** native T26 at m/z 979.9677; and **(D)** oxidized T26 at m/z 978.9606. The T8 and T26 precursor ions (green) were fragmented by CID (30 V) to give b_n (red) and y_n (blue) sequence ions. The encircled y_8^{2+}/y_{12}^+ ions in panel B and b_{10}^+/y_{15}^{2+} ions in panel D have masses consistent with loss of an H atom (-1 u) from Y67/Y71 and Y229/Y236, respectively. In panels C,D we selected peaks that do not contain T26 oxidized at M230 or M231 for clarity. The peptide sequence in each panel shows the tyrosines in red font and the fragmentation sites as vertical lines. Note the absence of fragmentation between crosslinked Y67 and Y71 (panel B) and the single fragmentation between crosslinked Y229 and Y236 (panel D).

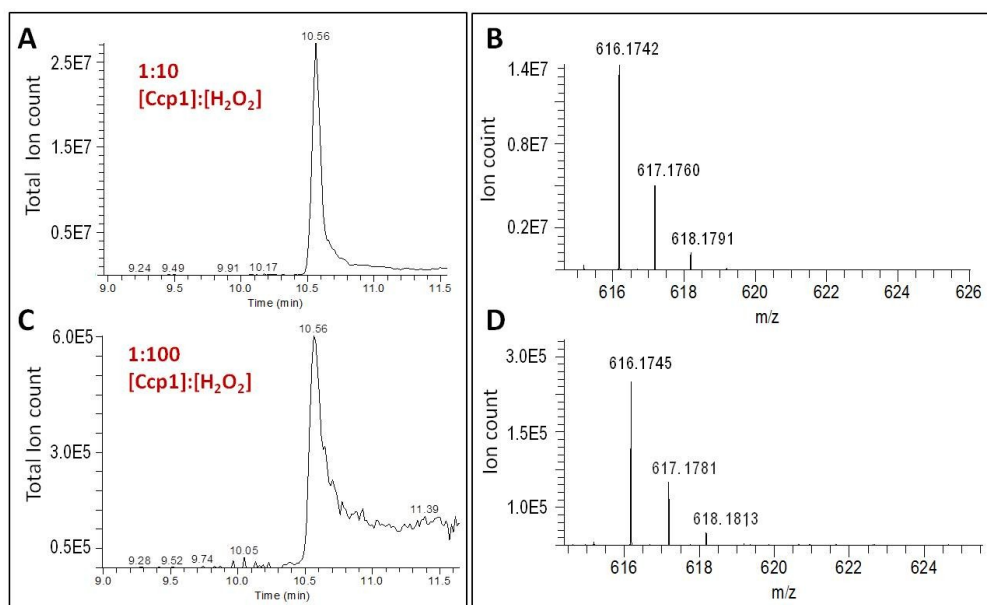


Figure S3.4. LC-MS analysis of hemin released from overoxidized Ccp1. Following oxidation of 1 μM Ccp1 by 10 and 100 μM H_2O_2 in KPi/DTPA for 1 h at room temperature, samples were diluted 10-fold into the MS solvent and 5- μL aliquots were analyzed by LC-MS (See *Methods and Materials* in the main text). **(A,C)** Chromatograms showing the peak at 10.46 ± 0.02 min containing hemin that dissociated from Ccp1 on the C4 column at pH 4.0. **(B,D)** The corresponding hemin mass spectrum showing the isotopic distribution expected for the M^+ ion ($\text{FeC}_{34}\text{H}_{22}\text{N}_4\text{O}_4$; calc mass 616.1773 u). The exact mass of hemin released from Ccp1 is 616.1745 ± 0.0005 u compared to 616.1746 u for authentic hemin, which was used as an external standard. Note the ~ 100 -fold lower total ion count (y-axis) in panels C,D vs panels A,B, which reflects the extensive destruction of Ccp1's heme by 100 M eq of H_2O_2 that is not seen at 10 M eq of H_2O_2 .

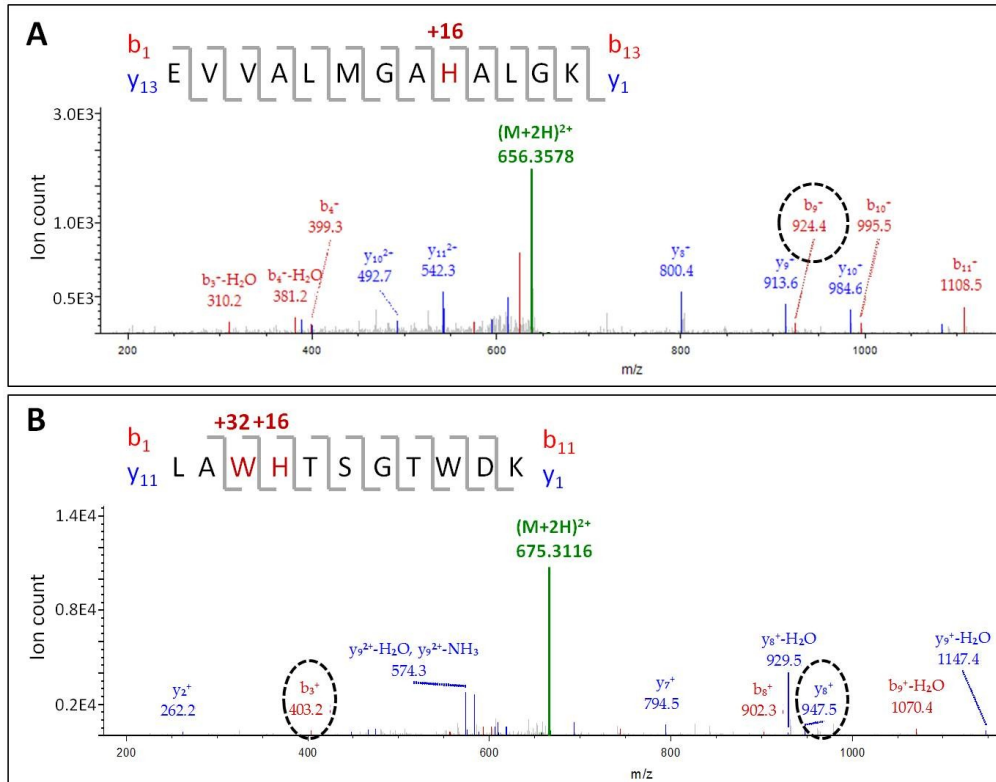


Figure S3.5: LC-MS/MS analysis of H175 and H52 oxidation in tryptic peptides T21 and T7. The MS2 spectrum of the $(M+2H)^{2+}$ ion of: **(A)** T21 with oxidized H175 at m/z 656.3578; and **(B)** T7 with oxidized H52 at m/z 675.3116. The T21 and T7 precursor ions (green) were fragmented by CID (30 V) to give b_n (red) and y_n sequence ions (blue). The encircled b_9^+ and y_8^+ ions have masses consistent with addition of an oxygen atom (+16 u) to both H175 and H52. Also, the mass of the encircled b_3^+ ion in panel B indicates the addition of two oxygen atoms (+32 u) to W51.

Standard MD simulations of Ccp1 in water with O₂ molecules

The crystal structure of CCP 1ZBY (156) was chosen as the initial structure for all-atom MD simulations. The positions of the side-chain O and N atoms in Asn and Gln residues, and the protonation states of His, Asp and Glu residues were established by examining the surrounding protein environment. Note that all the oxidizable residues in Figure S3.6 are in the neutral form except H60 and H181, which are protonated. Conformer A was selected for residues R48, K123, D152, R166, M172, A193, A194, N195, D210, S246, and K287. Conserved internal crystal water 770 was removed to prevent steric clashing with R48. The remaining 836 crystal waters were embedded with Ccp1 into a box of TIP3P water molecules (179) to provide a water layer of >8 Å around the protein. Sodium and chloride ions were added to ensure charge neutrality and to set the NaCl concentration to 0.15 M. Ten or 100 O₂ molecules were added into the box outside the protein, and the resulting system was simulated using periodic boundary conditions.

MD simulations were performed with the NAMD 2.7 program (180) using the CHARMM36 all-atom force field (181) at a constant temperature of 310 K and a constant pressure of 1 atm. The van der Waals parameters for the O atom ($\epsilon = -0.12$ kcal/mol, $R_{\min}/2 = 1.7$ Å) were taken from the CHARMM36 force field and the published experimental O-O bond length ($l = 1.207$ Å) and its vibrational frequency (1580.19 cm⁻¹) (182) were used to calculate the O-O bond force constant ($k = 1693$ kcal/mol/Å²). The particle-mesh Ewald method (183) with a grid size <1 Å was selected for long-range electrostatics, while a cut-off of 12 Å was assumed for all other non-bonded interactions. Van der Waals interactions were truncated at a distance of 8 Å using a switching function, and bonds involving hydrogen atoms were constrained using the SHAKE algorithm (184), permitting the use of a multiple time-step algorithm (185) to compute bonded and short-range non-bonded interactions every 2 fs and long-range electrostatic forces every 6 fs. The

temperature and pressure were controlled using Langevin dynamics with the Langevin piston Nose-Hoover method and a damping coefficient γ of 5 ps^{-1} (186, 187). The system was heated over 0.4 ns and equilibrated over 1.1 ns, gradually removing the initial restraints on the C_α backbone atoms and the O atoms of the internal water molecules. Then, a productive run of ~32 ns was performed and only productive runs were analyzed.

In total, 7 independent 32-ns standard trajectories with 10 or 100 O_2 molecules were obtained. The size of the periodic box was $\sim 76 \times 76 \times 76 \text{ \AA}^3$ after equilibration, giving O_2 concentrations of ~ 38 and $\sim 380 \text{ mM}$ in simulations with 10 and 100 O_2 molecules, respectively, which are $>10^2$ - 10^3 -fold higher than that of O_2 in water at 293 K and 1 atm ($\sim 0.3 \text{ mM}$). These high O_2 concentrations significantly increased sampling of the O_2 docking sites on the surface of Ccp1 and similar results were obtained with 10 or 100 O_2 molecules but the more intense sampling in simulations with 100 O_2 molecules lead to better convergence. Therefore, the results for simulations with 100 O_2 molecules are shown in Figure S3.6, which was produced with the VMD package (188). Notably, the largest O_2 docking sites are present in hydrophobic grooves on the surface of Ccp1 near H96 and M119, and other surface docking sites are found in hydrophobic patches near Y16, Y42, W101, Y153, Y187, W223, Y236 and Y251. Buried O_2 docking sites, such as the cluster around the distal H52 tend to be smaller than the surface sites due to steric constraints.

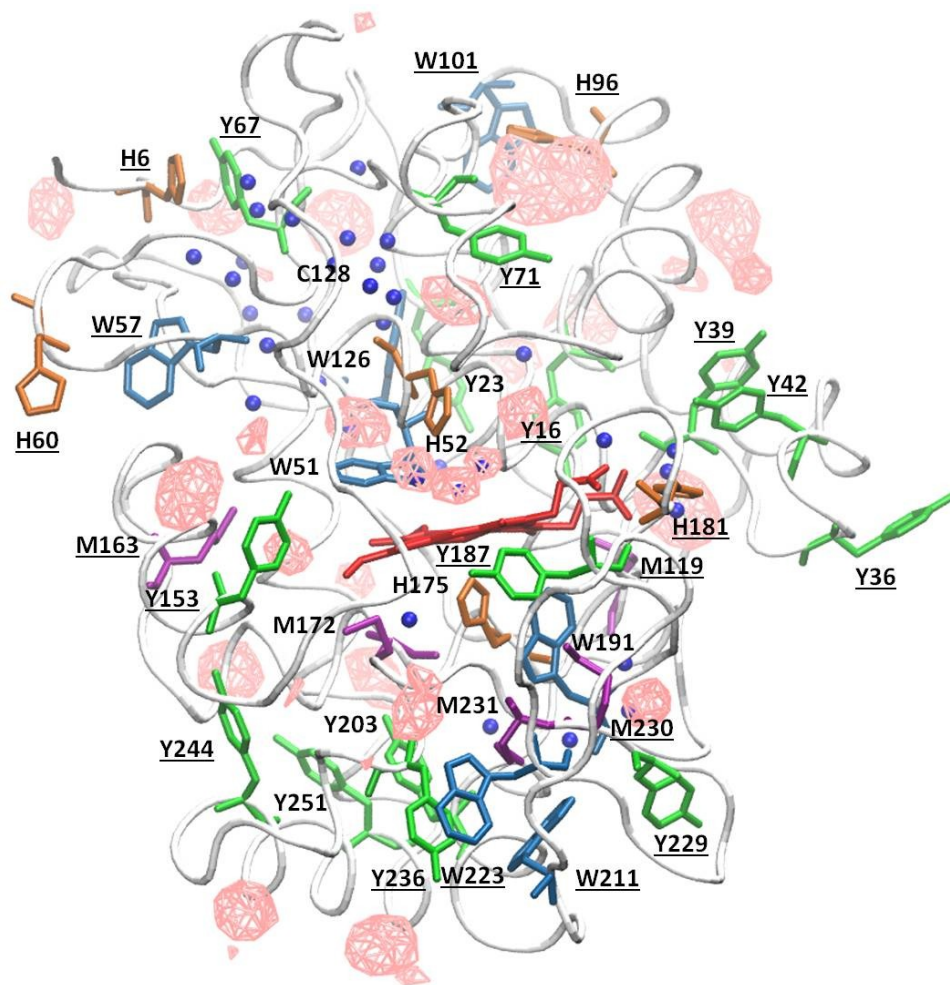


Figure S3.6: MD simulation of Ccp1 in water with 100 added O₂ molecules. VMD-generated (188) cartoon of Ccp1 (PDB 1ZBY) showing all oxidizable residues (W, blue; Y, green; H, orange; M, purple, C, grey) and 31 conserved internal water molecules as blue spheres. Standard MD simulations of Ccp1 with 100 O₂ molecules were run using the NAMD 2.7 program (180). Average O₂ densities from 7 runs of ~32 ns each are shown as pink wire surfaces and represent favorable O₂ docking sites in Ccp1. The number of O₂ docking sites and the internal waters within 5 Å of an oxidizable residue are listed in Table S3.6. The 31 internal water numbers are: 517 518 519 520 525 526 527 528 531 542 543 547 548 549 552 576 578 605 640 644 645 655 656 663 692 693 696 697 698, 895 and 1232.

From Table S3.6, we can see that most (15/24) of the residues found to be oxidized in Ccp1 are within 5 Å of an O₂ docking site, which will promote O₂ trapping of radicals formed on these residues. During the simulations, most of the internal waters remained close to their positions in the crystal structure of Ccp1. Strikingly, 26 of the 31 conserved internal waters are located in the

distal domain and those in the proximal domain (Figure S3.6, Table S3.6) are found mainly in electron-donor zone 1 (Figure 3.8 of the main text). However, all of Ccp1's oxidizable residues are either solvent exposed or within 5 Å of an internal water molecule. The thermodynamics of one-electron oxidation of most residues require proton transfer at physiological pH (with the rare exception of W191). This is facilitated in Ccp1 by water accessibility to its oxidizable residues, which underscores the physiological significance of these residues as donors to the heme when Ccp1's reducing substrate, Cyc^{II} (Eqs. 2,3 of the main text), is unavailable.

Table S3.6: O₂ and water exposure of the oxidizable residues in Ccp1^a

Residue	Oxidation level ^{b,c}	O ₂ docking sites < 5 Å ^d	Conserved internal waters < 5 Å ^d	H-bonding to water ^e	Solvent exposed ^f	Zone ^g
M119	H	1			yes	3
M163	M	0	W520		yes	4
M172	H	1	W605	yes		3
M230	H	0			yes	1
M231	H	0		yes		1
C128	H	3	W549, W656	yes		2
H6	ND	0			yes	NA
H52	H	3	W640, W643, W1232	yes		3
H60	ND	0			yes	NA
H96	ND	1			yes	NA
H175	H	0	W578, W605	yes		3
H181	ND	0			yes	NA
W51	H	2	W640, W1232	yes		3
W57	H	0	W520	no	yes	2a
W101	L	1			yes	2a
W126	H	2	W543, W547, W655	no		2a
W191	H	0	W578	yes		1
W211	H	1			yes	1
W223	H	1			yes	1
Y16	M	1			yes	2a
Y23	ND	0	W543	no		NA
Y36	H (-1)	0	W517, W692	yes	yes	2b
Y39	H (-1)	0			yes	2b
Y42	H (-1)	1	W517	no	yes	2b
Y67	H (-1)	1	W552, W697, W698	yes	yes	2a
Y71	H (-1)	1	W645	yes	yes	2a
Y153	ND	1			yes	4
Y187	ND	1			yes	NA
Y203	ND	0	W576	no		4
Y229	H / L (-1)	0			yes	1
Y236	L (-1)	1			yes	1
Y244	ND	0			partially	4
Y251	L	1			partially	4

^a The 33 oxidizable residues in Ccp1 (see Figure 3.1 of the main text and Figure S3.6)

^b The oxidation level of a given residue is classified as high (H: 40-100%), medium (M: 20-40%), low (L: 5-20%) or not detectable (ND) based on the oxidation yields calculated using Eq. 4 of the main text.

^c Oxidized residues incorporated 1-3 oxygen atoms or lost a hydrogen atom (Table S3.3) where indicated (-1).

^d Number of O₂ docking sites and conserved internal waters within 5 Å of the side chain of the indicated residue (see Figure S3.6).

^e H-bonding is assumed if an internal water oxygen atom and a residue heteroatom are within 3 Å.

^f Solvent exposure based on accessibility of bulk water.

^g See electron donor zones in Figure 3.8 of the main text.

Chapter 4: H₂O₂-induced post-translational modifications convert cytochrome c peroxidase into a H₂O₂ sensor and heme donor in respiring yeast

4.1) Preface

The work presented in Chapter 4 corresponds to the following manuscript in preparation: Kathiresan M, and English AM (2015). **H₂O₂-induced post-translational modifications convert cytochrome c peroxidase into a H₂O₂ sensor and heme donor in respiring yeast.** Target journal: Biochemistry. The production and interpretation of the data, and revision of the manuscript was performed by me. Dr. English contributed to discussion, data analysis, writing, editing and revisions of the paper.

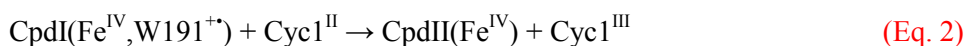
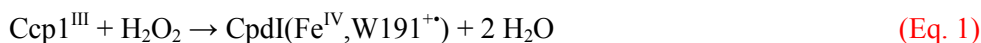
4.2) Abstract of the manuscript

Recently, we reported that yeast cytochrome c peroxidase (Ccp1) functions primarily as a mitochondrial H₂O₂ sensor protein and heme donor. Furthermore, since apoCcp1 exits mitochondria as H₂O₂ levels rise in respiring cells, we questioned its role as a catalytic H₂O₂ scavenger. Our report on recombinant Ccp1 overoxidation by H₂O₂ *in vitro* suggests that heme loss arises from oxidation of critical residues, including the proximal iron ligand (H175). We now report on the oxidative posttranslational modifications (PTMs) detected in Ccp1 enriched from fermenting and respiring cells using a MS-based proteomics approach. Mitochondrial Ccp1 from 16 h and 30 h largely fermenting cells is oxidized mainly at its methionines with average sulfoxide (MetO) yields of ~10% and ~25%, respectively. The dominant PTM after 30 h growth is 85% phosphorylation of Y153 at 6.8 Å from the heme periphery, which may promote heme loss. In contrast, pY153 is not detected in Ccp1 from 7 d mitochondria but the protein is extensively oxidized, exhibiting significant MetO, TrpOH, TyrOH and HisO levels as well as

~8% pY229. Notably, TyrOH formation substitutes for the effective *intracellular* dityrosine crosslinking induced in recombinant Ccp1 by bolus H₂O₂, which indicates less aggressive oxidation in mitochondria as confirmed by adding H₂O₂ stepwise to the recombinant protein. Extramitochondrial Ccp1 from 7 d cells is unphosphorylated and remarkably less modified except for 85% oxidation of H175, which triggers heme loss and mitochondrial export. Residues oxidized in fermenting and respiring cells generally overlap those oxidized *in vitro* by 1 and 10 M eq of H₂O₂, respectively, verifying that Ccp1's oxidative PTMs stem from its heme-mediated overoxidation by H₂O₂, which underlies its main physiological functions

4.3) Introduction

Reactive oxygen species (ROS), including the superoxide radical anion (O₂^{•-}), and its metabolites, hydrogen peroxide (H₂O₂) and the hydroxyl radical (•OH), are continuously produced in cells as by-products of aerobic metabolism (189). These by-products can impair numerous biological processes through alteration of protein conformation (189), disruption of enzymatic function (189) and DNA mutation (189, 190). Because mitochondria are major sites of ROS generation (62), they are highly enriched in antioxidant enzymes that in yeast include the heme enzyme cytochrome c peroxidase (Ccp1) located in the mitochondrial intermembrane space (IMS). Over seven decades of *in vitro* research has defined Ccp1 as an efficient peroxidase that couples the fast two-electron reduction of H₂O₂ using electrons provided by its physiological partner cytochrome c (Cyc1) (17, 42):



Ferric Ccp1^{III} reacts with H₂O₂ (Eq. 1) to form compound I (CpdI) with a ferryl (Fe^{IV}) heme and a cationic indole radical localized on W191⁺. The latter is reduced by Cyc1^{II} to compound II (CpdII) (Eq. 2) and its Fe^{IV} heme is subsequently reduced by a second Cyc1^{II} (Eq. 3).

It has long been known that Ccp1 accumulates as the heme-free, (apo) form in fermenting yeast grown under anaerobic conditions but rapidly converts to the heme-loaded holoform upon oxygen exposure (60, 61). Thus, Ccp1 was viewed as a frontline defense that catalytically removed H₂O₂ in the IMS produced when cells switched to aerobic respiration (48, 191). For Ccp1 to function as a catalytic scavenger of H₂O₂, its reducing substrate, Cyc1^{II}, must be available to supply electrons. However, apoCyc1 synthesis as well as its conversion to the holoprotein is coupled to heme synthesis and is under glucose repression (55, 66, 192). Thus, when heme appears, apoCcp1 must be among the first recipients, but the limited availability of Cyc1 results in holoCcp1 overoxidation by H₂O₂, which converts it into a H₂O₂ sensor protein (50, 118). Notably, Ccp1's H₂O₂ sensing/signaling function is independent of its peroxidase activity (Eqs. 1-3) since genetic studies have shown that fermenting yeast producing Ccp1 or its W191F variant with negligible CCP activity (117) respond to exogenous H₂O₂ challenge by activating the transcriptional regulator, Skn7 (54). Work in our group has further demonstrated that Ccp1 or Ccp1^{W191F} signaling in response to *endogenous* H₂O₂ produced in respiring yeast increases the activity of the peroxisomal/mitochondrial catalase A (Cta1) (50, 118), whereas *exogenous* H₂O₂ challenge of fermenting cells increases peroxiredoxin and cytosolic Ctt1 catalase activity (50, 63) since Cta1 expression is repressed by glucose (55, 192).

Hence, mounting evidence defines Ccp1 as a mitochondrial H₂O₂ sensor and signaling protein. We previously explored how Ccp1 sensing/signaling increases Cta1 activity and found that the spike in H₂O₂ as cells begin to respire overoxidizes Ccp1 as evidenced by conversion of

its proximal Fe ligand (H175) to oxo-histidine (HisO). This weakens the heme-polypeptide interaction and converts Ccp1 into a heme donor that transfers its heme directly or indirectly to mitochondrial apoCta1, which emerges as glucose is consumed (118). To gain further insight at the molecular level into the mechanism of heme labilization and in particular the roles of its numerous oxidizable residues (Figure 4.1A) (193), we characterized overoxidized recombinant Ccp1 in detail using high-performance LC-MS/MS (194). Strikingly, in keeping with Ccp1's role as a heme donor, its heme mediates the oxidation of 24 different residues in the protein by 10 M eq of H₂O₂ without undergoing irreversible oxidation (194).

Based on our characterization of the stable oxidation products generated by repeated H₂O₂-initiated radical transfer (RT) from the heme, we partitioned Ccp1's oxidizable residues into four main zones (Figure 4.1A) (194). Different RT pathways from the heme direct oxidizing equivalents into each zone. For example, the preferred RT pathway via W191 operative in CpdI formation (Eq. 1) (117) results in oxidation of residues in zone 1 including M230/M231 that promote RT to W191. Oxidation of these methionines turns on RT from the heme to zones 2a likely via W52 and 2b via M119 and finally to the active-site residues in zone 3, which shuts down heterolytic cleavage of H₂O₂ at the heme after the reduction of ~10 M eq (194). Interestingly, negligible RT from the heme to zone 4 was observed in recombinant Ccp1(194) despite the abundance of oxidizable residues in this zone (Figure 1A). Following characterization of Ccp1's oxidation profile *in vitro*, we questioned if the overoxidized protein experienced the same modifications in the cell or if a common posttranslational modification (PTM) such as phosphorylation alters RT pathways from the heme and/or if radical repair by intracellular antioxidants such as glutathione (GSH) competes with formation of some of the stable oxidation products seen *in vitro*.

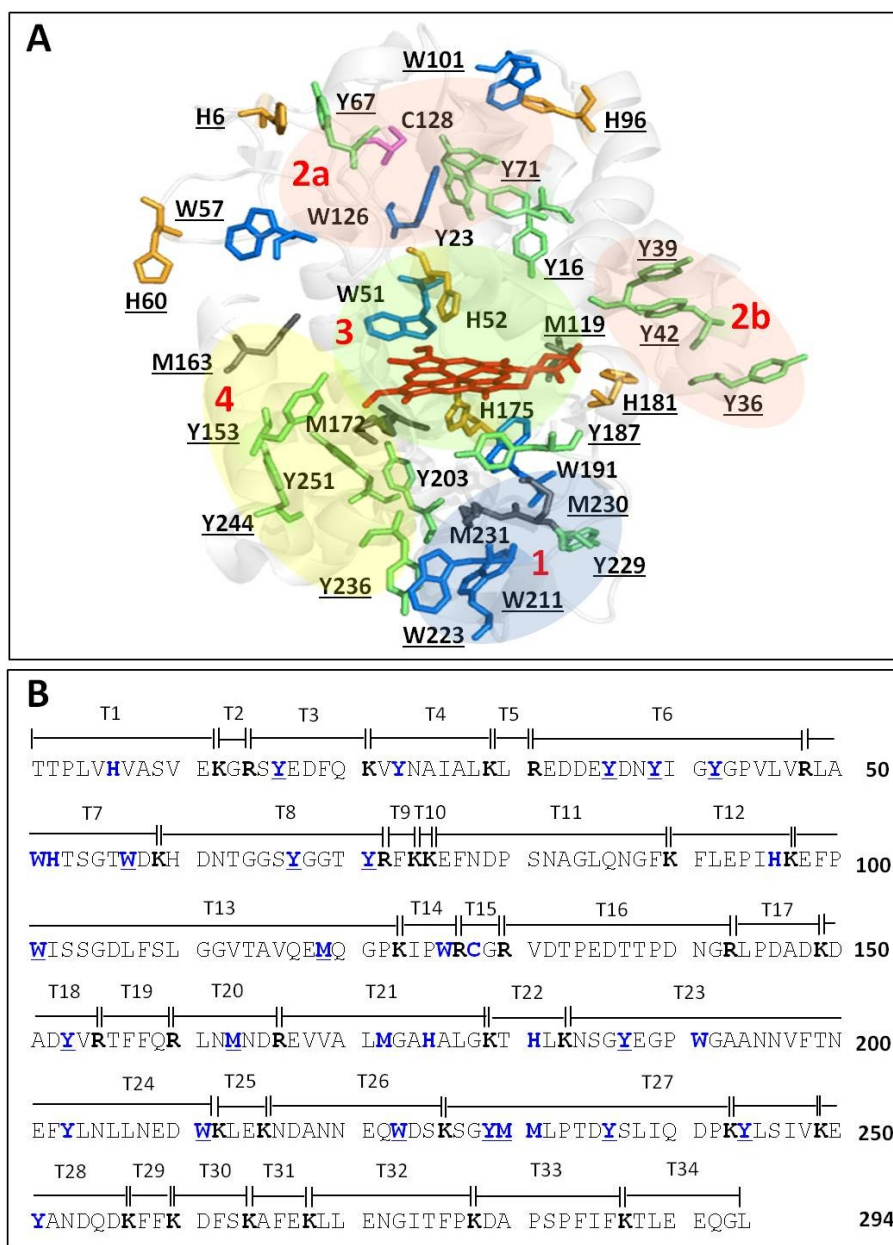


Figure 4.1. Oxidizable residues in Ccp1 and their location in the protein's tryptic peptides (A) PyMOL-generated cartoon of Ccp1 (PDB 1ZBY) showing its 33 oxidizable residues (W, blue; Y, green; H, orange; M, grey; C, magenta). Zones 1-4 identified in H₂O₂-oxidized recombinant Ccp1 (194). Residues in **zone 1** (blue) are oxidized by RT from the heme via W191. M230/M231 oxidation turns on RT from the heme to **zones 2a** and **2b** (pink) and then to **zone 3** (green) at higher levels of H₂O₂, when active-site residues are oxidized. No oxidized residues are found in **zone 4** (yellow) in recombinant Ccp1 treated with H₂O₂ (194). **(B)** Tryptic peptides T1-T34 predicted for Ccp1 in blocks of 10 residues with the cleavage sites (**K, R**) in bold font and the oxidizable residues in **blue font**. Solvent-exposed oxidizable residues are underlined in both panels. Table 1 lists tryptic peptides not covered in MS/MS analysis for Ccp1 isolated from yeast cells.

Hence, in this study we map the oxidative PTMs in Ccp1 from yeast cultures at three different time points. The protein was enriched from 16 h exponentially growing fermenting yeast, 30 h cells entering aerobic respiration, and in 7 d stationary-phase respiring cells. Mitochondria-free as well as mitochondria-enriched extracts were examined from 7 d cells since at this stage a large fraction of Ccp1 has exited the mitochondria (118). Ccp1 exhibits very different PTM profiles, including phosphotyrosine (pY) levels, in fermenting vs stationary-phase yeast and in mitochondrial vs extramitochondrial extracts. Comparing its growth-dependent PTMs with the oxidative modifications induced by bolus and stepwise addition of H₂O₂ confirms that Ccp1 is overoxidized by H₂O₂ in respiring mitochondria. Nonetheless, the comparison highlights the more efficient labilization of heme *in vivo*, which appears to be promoted by strategic pY formation, a PTM known to be redox sensitive (195). Overall, our results reveal that PTMs have a direct bearing on Ccp1's cellular location, heme status, catalytic activity and its H₂O₂ signaling role.

4.4) Materials and Methods

4.4.1) Materials

Proteins were obtained from the following suppliers: bovine catalase (Sigma Aldrich), sequencing grade modified trypsin (Promega) and thrombin (EMD Millipore). Recombinant Ccp1 with MI at positions -2/-1 of the mature protein was prepared as described previously (118). Suppliers of (bio)chemicals were as follows: Coomassie (MP Biomedicals); a 7×25 mm HiTrap Q anion-exchange column (GE Healthcare), C18 Zip tips (EMD Millipore), hydrogen peroxide 30% (Fisher Scientific); acetonitrile (HPLC grade), diethylenetriamine-pentaacetic acid (DTPA) (Sigma Aldrich); yeast extract, peptone, microbiology grade agar, galactose (Bioshop); glucose (Fisher Scientific). The antibodies used for Western blotting were: rabbit anti-Ccp1

serum kindly provided by Professor David Goodin (University of California, Davis); mouse anti-porin (ab110326 Abcam); HRP-conjugated secondary antibodies (goat anti-rabbit, goat anti-mouse, Biorad).

4.4.2) Yeast strain, media and growth conditions.

The *S. cerevisiae* BY4741 strain (Mat a; his3 Δ 1; leu2 Δ 0; met15 Δ 0; ura3 Δ 0), purchased from the European *S. cerevisiae* Archive for Functional Analysis (EUROSCARF), was grown in YPD liquid medium (1% yeast extract, 2% peptone and 2% glucose) at a medium-to-flask ratio of 1:5. The cultures at an initial OD₆₀₀ of 0.01 were incubated at 30°C with shaking at 225 rpm. After 72 h, the spent YPD medium was replaced with 0.85% NaCl solution (w/v) to switch cells to stationary phase (196).

4.4.3) Subcellular fractionation of the yeast lysates.

Denucleated (S2), mitochondria-enriched (P10) and mitochondria-depleted (S10) subcellular fractions were isolated from yeast as described previously (50, 118). Briefly, cells were grown in 500 mL of YPD medium for 1 d and 7 d at 30°C as described above, harvested at 2000xg and washed twice with aqueous 0.85% NaCl. The cell pellets were resuspended in 50 mL of pre-warmed 100 mM Tris-H₂SO₄ (pH 9.4) with 10 mM DTT, incubated for 10 min at 30 °C and 80 rpm, harvested at 2000xg, washed twice with 20 mL of 10 mM KPi (pH 7.4) containing 1.2 M sorbitol, and treated with 12 mg of zymolyase 20T/g of wet cells at 30°C. Spheroplast formation was monitored by light microscopy and was complete after 1-2 h incubation at 30 °C with gentle agitation. The resulting spheroplasts were washed twice with 20 mL of the same buffer and resuspended in 20 mL of 10 mM Tris (pH 7.4) containing 0.6 M sorbitol, 1 mM EDTA, 1 mM PMSF and CompleteTM protease inhibitor cocktail. Spheroplasts at

4°C were disrupted by 15 strokes of a glass-Teflon homogenizer, the homogenates were centrifuged at 2000 x g and the supernatants, which correspond to the denucleated lysates (S2 fractions), were collected. The S2 fractions were further centrifuged at 10000 x g for 15 min at 4°C, and the mitochondria-depleted supernatants (S10 fractions) were separated from the mitochondria-enriched pellets (P10 fractions). Fractions were probed with the anti-porin antibody and the P10 and S10 extracts were found to be highly enriched and depleted in mitochondria, respectively (118).

4.4.4) Enrichment by anion-exchange of Ccp1 from the P10 and S10 extracts and immunodot blotting analysis.

Mitochondria-enriched P10 and mitochondria-free S10 extracts from 500 mL cultures of 16 h, 30 h and 7 d cells were dialyzed against 20 mM KPi/100 µM DTPA (pH 6.1) overnight and centrifuged at 14000xg for 10 min. The supernatants (0.5-1 mg total protein) were applied to a 7×25 mm HiTrap Q anion-exchange column equilibrated with the same buffer and attached to an ÄKTApurifier 10 (GE Healthcare). Proteins were eluted from the column using a linear 0-1 M NaCl gradient over 25 min at a flow rate of 2.0 mL/min, 1 mL fractions were collected and 15 µL of each was dot blotted onto a methanol-soaked PVDF membrane and allowed to dry for 10 min at room temperature. The membrane was blocked for 1 h in TBST (50 mM Tris, 150 mM NaCl and 0.05% Tween 20 v/v, pH 7.6) containing 5% skimmed milk (w/v), and incubated with rabbit anti-Ccp1 antibody (dilution 1:10,000) in 1% milk/TBST overnight at 4° C. After washing with TBST, the membrane was incubated for 1 h with the goat anti-rabbit secondary antibody (dilution 1:10,000) in 1% milk/TBST. Ccp1-containing fractions were detected by chemiluminescence using an ECL kit (Thermo Fisher Scientific) and the membrane was scanned on the AlphaImager (ProteinSimple) with an exposure time of 30 s.

4.4.5) SDS-PAGE of anion-exchange fractions and in-gel Ccp1 digestion.

The anion-exchange fractions containing Ccp1 were further decomplexified by 1D SDS-PAGE under reducing conditions on 6% stacking and 12% resolving 8 cm x 5.8 cm x 1 mm gels. After 1 h electrophoresis at 150 V, the gels were Coomassie stained, slices were excised down the entire length of the gel, destained in a solution of 50% acetonitrile in 25 mM aqueous ammonium bicarbonate (pH 8.0), reduced with 10 mM DTT for 30 min at 50 °C and alkylated with 55 mM iodoacetamide for 30 min in the dark at room temperature. The gel slices were incubated overnight with 12.5 ng/ μ L trypsin at 37°C and the peptides were extracted with 5% formic acid in 50% aqueous acetonitrile.

4.4.6) LC-MS/MS of the PTMs in the tryptic peptides of Ccp1.

The tryptic peptides were desalted on C18 Zip Tips and injected (5 μ L/injection) onto a homemade reversed-phase C18 capillary column (100 μ m x 6.5 cm) equilibrated with 2% aqueous acetonitrile/0.1% formic acid and attached to a NanoLC (Easy-nLC II, Thermo Scientific). Peptides were eluted at a flow rate of 200 nL/min into the nanoESI source of an LTQ Orbitrap Velos mass spectrometer (Thermo Scientific) using a 2–94% acetonitrile gradient and analyzed in full-scan mode (m/z 350–2000) in the Orbitrap high-resolution mass analyzer ($R=60,000$ at m/z 400). Other instrumental parameters were: electrospray voltage 3 kV, CID collision energy 35 V and heated capillary temperature 200 °C. Precursor peptide ions were selected in MS1 using a mass exclusion threshold of 10 ppm and fragmented in the LTQ at a collision energy of 35 V. MS2 fragments with an intensity count of ≥ 20 were analyzed with a mass tolerance of 0.8 u using Proteome Discoverer 1.3.0 software (Thermo Scientific) and the Sequest search engine with mass filters for the oxidative modifications listed in Table S1 plus cysteine alkylation by iodoacetamide (+57 u). Dynamic exclusion was enabled with a repeat

count of 1, a repeat duration of 30 s and an excluded list size of 500. Sequest correlates the MS2 spectra with peptide sequences in the Ccp1 Fasta file downloaded from the NCBI website (<ftp://ftp.ncbi.nlm.nih.gov/>). Also, Sequest's XCorr (>2) and False Discovery Rate (<0.01) filters were implemented for confident peptide identification (137).

4.4.7) Semiquantitation of residue oxidation.

Label-free semiquantitation was performed at the MS1-level as described previously (138). Briefly, peptide ion intensity is expressed as the integrated peak area (PA) extracted within a 10 ppm window from the mass chromatogram of the tryptic digest. The yield of an oxidized form of a residue (X_{ox}) identified by MS/MS is given by:

$$\% X_{ox} = \frac{100 \sum PA_{ox}}{\sum PA_{ox} + \sum PA} \quad \text{Eq. 4}$$

The numerator sums the PA s of all peptides containing X_{ox} (PA_{ox}) and the denominator sums the PA s of all peptides containing any form of residue X .

4.4.8) Stepwise oxidation of recombinant Ccp1 with H₂O₂.

A 5 μ M Ccp1 stock solution was prepared in 20 mM KPi pH 7.5 with 100 μ M DTPA (KPi/DTPA). Aliquots (1 μ M) of H₂O₂ in the same buffer was added every 10 min to Ccp1 at room temperature to give samples with a final Ccp1 concentration of 1 μ M and a H₂O₂ concentration of 1, 5 or 10 μ M. DTPA was present in all samples to inhibit catalysis of H₂O₂ or O₂ oxidation of Ccp1's residues by trace metal impurities in the buffers. Catalase (0.1 nM) was routinely added although H₂O₂ was not detected by the HRP/ABTS assay (136) in the samples following incubation at room temperature for 100 min.

4.5) Results

4.5.1) Ccp1 isolated from 16 h or 30 h cells shows little oxidation.

Immunodot blotting with anti-Ccp1 antibody of P10 extracts from 16 h cells shows that Ccp1 eluted from the anion-exchange column mainly in fractions F8 and F9 (Figure 4.2A,B). No Ccp1 was detected in the S10 extracts (Figure 4.2B), which supports the mitochondrial location of Ccp1 in exponentially growing cells (58, 118). Ccp1-containing fractions were further decomplexified by reducing 1D SDS-PAGE as shown in the representative gel of F4-F9 from the P10 extract (Figure 4.2C). The entire F8 and F9 lanes were cut into 2x2 mm gel slices since PTMs may alter the migration of Ccp1 in the gel. However, following in-gel digestion and LC-MS analysis, Ccp1 was identified with high confidence and $\geq 70\%$ sequence coverage from the MS1 spectra of the tryptic peptides isolated from a single slice that bracketed Ccp1's expected molecular weight of ~34 kDa (Table 4.1, Figure 4.2C). This reveals the absence of any high-mass modification such as covalent dimerization of the protein. Sequence coverage from independent samples was routinely 65-85% (Table 4.1), with the lower values being typically for Ccp1 from 16 h fermenting cells and higher values for 30 h and 7 d respiring cells, which express more Ccp1 (48).

Table 4.1: LC-MS analysis of Ccp1 peptides from 16 h, 30 h and 7 d P10 and S10 extracts ^a

Time point	16 h P10	24 h P10	7 d P10	7 d S10
Score ^b	71.15	91.53	122.55	168.88
% sequence coverage ^c	68.9 ± 8.3	83.0 ± 8.1	75.14 ± 8.2	83.38 ± 8.3
% sequence coverage of oxidizable residues	72.7	84.8	90.9	93.9
Unique peptides ^d	16	20	38	40
Tryptic peptides not covered ^e	T13-T14, T19, T22-T24, T30-T31, T34	T22-T24, T31	T22, T29-T32, T34	T14-T15, T30-T31

^a Ccp1 from mitochondrial (P10) and extramitochondrial (S10) fractions were extracted from three independent cultures at each indicated time point, fractionated by anion exchange chromatography and SDS-PAGE, in-gel digested with trypsin and analyzed by LC-MS/MS. This table provides representative results from three cultures.

^b The score calculated by the Proteome Discoverer software is the probability that the identified protein is a correct match based on a comparison of its experimental and theoretical MS / MS spectra. Scores were in the range of 69–169 for the three independent experiments.

^c The % sequence coverage corresponds to the number of residues in all the Ccp1 peptides detected by MS divided by 293 residues in yeast Ccp1. Sequence coverage was in the range of 68–94% for the three independent experiments.

^d Unique peptides are those present in Ccp1 only and absent from all other proteins in the NCBI yeast database (<ftp://ftp.ncbi.nlm.nih.gov/>).

^e Ccp1 tryptic peptides not covered in LC-MS/MS analysis. Map of Ccp1 tryptic peptides found in Figure 4.1A.

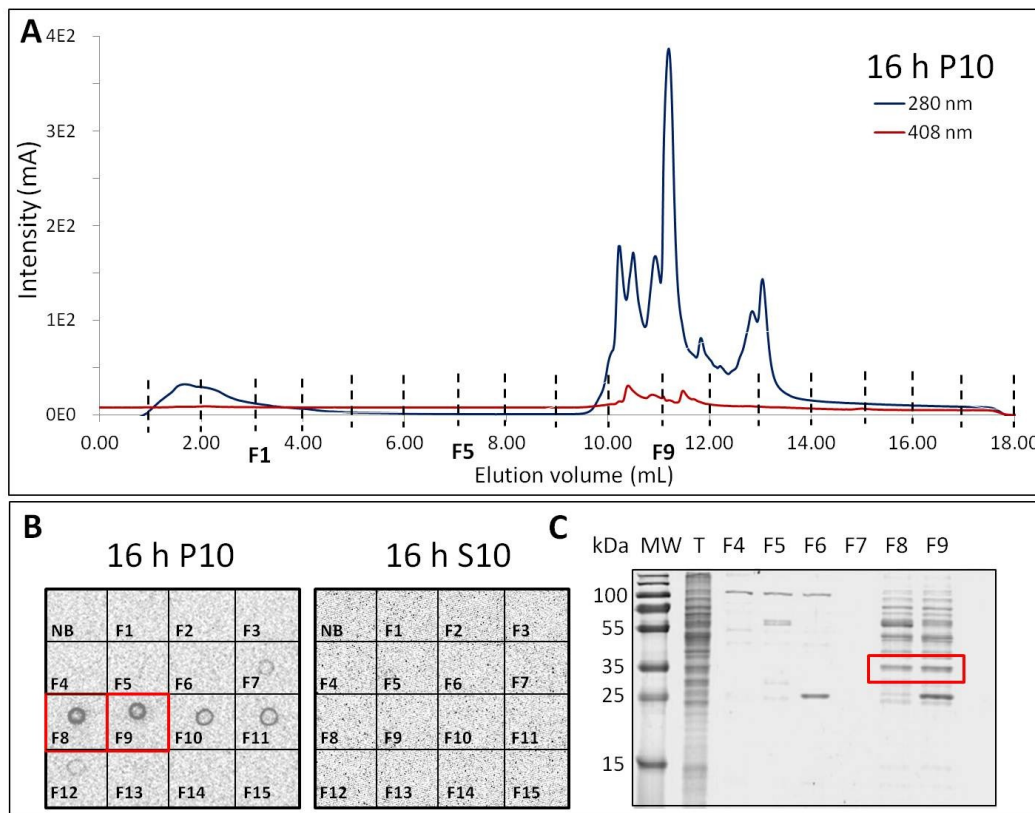


Figure 4.2. Purification of Ccp1 from 16 h yeast cells. (A) Chromatogram of a P10 extract from 16 h mitochondria. Extract (1 mL) in 20 mM KPi/100 μ M DTPA (pH 6.1) containing 0.5 mg of total protein was loaded onto the HighTrap Q anion-exchange column, and eluted with a linear 0-1 M NaCl gradient at a flow rate of 1 mL/min and detected at 280 and 408 nm. (B) Representative anti-Ccp1 immunodot blots of the anion-exchange fractions of P10 mitochondrial and S10 extramitochondrial extracts from 16 h cells. Most of the Ccp1 present in P10 was eluted in fractions F8 and F9 (red boxes) and no Ccp1 was detected in S10. (C) Reducing SDS-PAGE analysis of 25 μ L aliquots of fractions F4-F9 from the P10 extract in panel B. Lanes F8 and F9 were cut into 2x2 mm slices and the proteins subjected to in-gel tryptic digestion and LC-MS analysis. Table 4.1 summarizes the LC-MS results and the bands boxed in red give the highest score and Ccp1 sequence coverage. The gel shown is representative of those obtained for P10 extracts from three independent cultures.

Using the filters in Table S4.1, the peptides from trypsinized Ccp1 identified based on their monoisotopic m/z values are listed in Table S4.2. The frequency of a residue modification identified by MS/MS is based on relative abundance of the peptide(s) bearing the modified residue (Eq. 4). Four of five methionines (M163, M172, M230, M231) in Ccp1 isolated from 16 h mitochondrial P10 extracts are \sim 3-20% oxidized to the sulfoxide (MetO; +16 u) (Figure 4.3).

Methionine residues are readily oxidized during sample preparation since MetO is frequently found in intact proteins and peptides analyzed by LC-MS (197). However, MetO levels increase to ~15-30% in Ccp1 isolated from 30 h mitochondria and M119 is also oxidized (Figure 4.3) which suggests that MetO formation is partially ROS-induced. Additionally, ~5% and up to 20% of Y229 is oxidized to hydroxytyrosine (TyrOH) in Ccp1 from 16- and 30 h cells respectively (Figure 4.3) and W101 and W211 show trace (<5%) oxidation to hydroxytryptophan (TrpOH) in 30 h cells. Overall, however, the relatively low quantity of oxidative PTMs in Ccp1 isolated from 16 and 30 h mitochondria reflects the low ROS levels generated in fermenting cells (YPD medium). Interestingly, Y229 is located in the Cyc1 binding site. We observe similar levels of CCP activity in 1 and 2 d yeast cells suggesting that this level of TyrOH in Y229 does not significantly effect Cyc1 turnover (118).

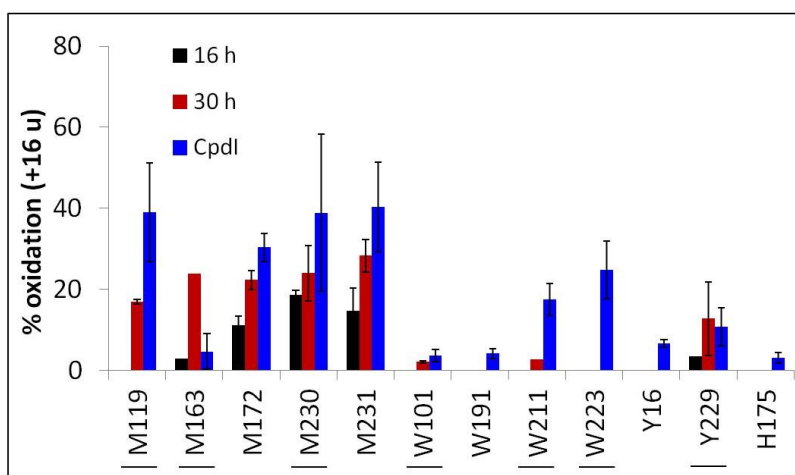


Figure 4.3. Comparison of residue oxidation in Ccp1 from 16- and 30 h mitochondria with that in CpdI generated *in vitro*. Ccp1 present in anion-exchange fractions F8-F9 and F11-F12 (Figures 4.2B and S4.2A, respectively) was isolated by SDS-PAGE, in-gel digested with trypsin and the peptides were analyzed by LC-MS/MS as described in the *Materials and Methods*. Bars show the % oxidation (+16 u) of methionine to MetO, tryptophan to TrpOH, tyrosine to TyrOH and histidine to HisO in Ccp1 isolated from 16 and 30 h mitochondria and from recombinant Ccp1 treated with 1 M eq of H₂O₂ to generate CpdI as described previously.(194) Yields are based on peptide *PAs* (Eq. 4) from three independent experiments (*n*=3) and presented as averages ± SD. Solvent-exposed residues are underlined.

4.5.2) Ccp1 from 7 d mitochondria is heavily oxidized.

Anti-Ccp1 immunodot blotting of the anion-exchange fractions from 7 d P10 and S10 extracts reveal that Ccp1 is present in both (Figure S4.1B,C). Ccp1's dual location in 7 d cells supports our previous finding that apoCcp1 exits the mitochondria of respiring cells (118). LC-MS/MS analysis of Ccp1 from P10 extracts reveals a mass increase of +16 u in several residues (Figure 4.4) including all methionines, which are 30-55% converted to MetO compared to 15-30% oxidation in 30 h mitochondria (Figure 4.3). Also, the one other sulfur-containing residue, C128, is ~45% oxidized to CysSO₂H/CysSO₃H in Ccp1 from 7 d mitochondria (Figure 4.4) but unoxidized in 16 or 30 h mitochondria (Figure 4.3).

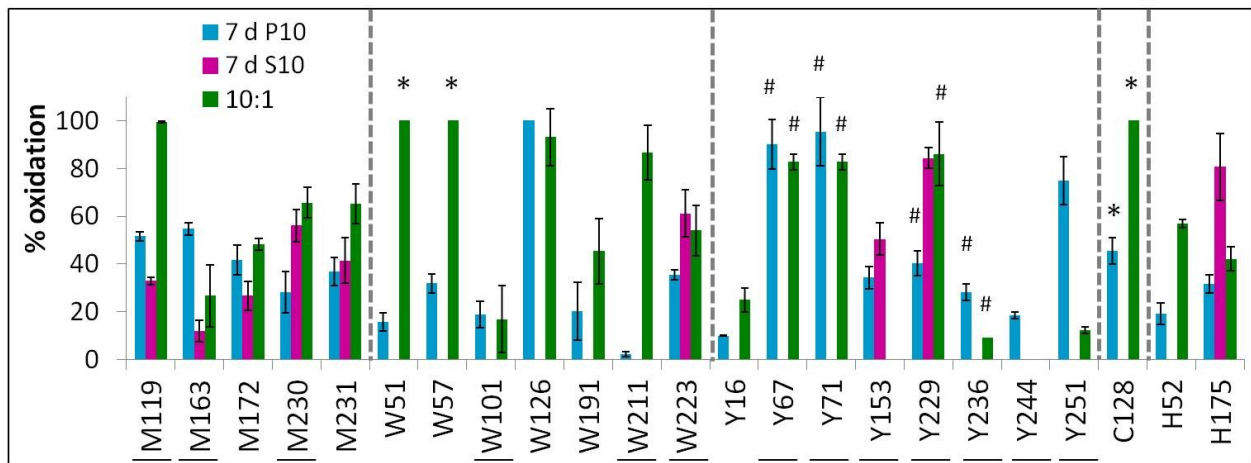


Figure 4.4. Comparison of residue oxidation in Ccp1 isolated from the P10 and S10 extracts from 7 d cells with that in recombinant Ccp1 overoxidized with 10 M eq of H₂O₂. Percent oxidation (+16 u) of methionine to MetO, tryptophan to TrpOH, tyrosine to TyrOH and histidine to HisO in Ccp1 isolated from the 7 d mitochondrial P10 extracts (blue bars, P10) and the 7 d extramitochondrial S10 extract (pink bars) and recombinant Ccp1 treated with 10 M eq of H₂O₂ (green bars) as described previously (194). Asterisks (*) denote tryptophans oxidized to Trp(OH)₂ and cysteine oxidation to SO₂H+SO₃H. Hashes (#) indicate tyrosines oxidized to TyrOH and/or dityrosine (see Figure 4.7). Note tyrosines ≤10% oxidized *in vitro* or *in vivo* (Y23, Y187, Y203) and the tyrosines in T6 (Y36, 39, Y42), which are <5% oxidized *in vivo* but extensively crosslinked *in vitro* (Figure 4.7), are omitted for clarity. Experimental details are given in the caption to Figure 4.3 and solvent-exposed residues are underlined.

All seven of Ccp1's tryptophans are converted to TrpOH (Figure 4.4) and ~3% of W223 is additionally converted to Trp(OH)₂ (data not shown). Notably, W191, a redox cofactor in CCP catalysis (Eqs. 1,2) is ~20% oxidized while W223, proximal to W191, is ~35% oxidized [TrpOH+Trp(OH)₂]. W126 in the distal region of Ccp1 is ~100% oxidized whereas neighboring W57 and W51 are ~30% and ~15%, oxidized, respectively (Figure 4.4). Also, W101, located on Ccp1's distal surface at > 25 Å from the heme, is ~20% oxidized (Figure 4.4).

With the exception of Y187 and Y203, the remaining proximal tyrosines (Y153, Y229, Y236, Y244 and Y251) are oxidized above the 20% level (Figure 4.4). In fact, Y153 and Y251 undergo up to 35 and 80% conversion to TyrOH, respectively (Figure 4.4). In addition, Y67 and Y71 in the distal region exhibit over 80% oxidation to TyrOH but hydroxylation of the remaining tyrosines (Y16, Y23, Y36, Y39, Y42) is <10% (Figure 4.4). However, the MS2 spectra indicate H loss (-1 u) from tyrosines in peptide T5+T6 (Y36, Y39, Y42), T8 (Y67, Y71) and T26 (Y229, Y236) (Figure S4.2). The absence of y_n and b_n sequence ions between oxidized tyrosines supports *intramolecular* dityrosine crosslinking since cyclic peptide regions are resistant to fragmentation as previously observed (194). Yields of crosslinked T6, T8 and T26 are only ~2, 5 and 10% (data not shown), respectively, which in the case of T8 can be attributed to extensive TyrOH formation at Y67 and Y71 (Figure 4.4). However, the lack of tyrosine oxidation to TyrOH or dityrosine in T6 suggests that RT from the heme to zone 2b (Figure 4.1A) is not favored *in vivo* and/or that radicals formed in Y36, Y39 and Y42 are repaired by intracellular GSH. Note that *intermolecular* dityrosine crosslinking involving Y36, Y39, Y42 (125, 134, 135), and Y236 (96) has been documented in H₂O₂-oxidized recombinant Ccp1 but no Ccp1 dimers or trimers were detected by Western blotting with anti-Ccp1 in lysates from 16 h, 30 h or 7 d cells (118).

Of the six histidines in Ccp1, only distal H52 and proximal H175 undergo significant oxidation (Figure 4.4). Around 20% of H52 and 35% of H175 are oxidized to HisO and the drop in CCP activity normalized against Ccp1 protein levels in 7 d mitochondria to $\sim 95 \pm 4\%$ (118). H52 functions as a critical acid-base catalyst in the heterolytic cleavage of the H_2O_2 peroxy bond as evidenced by the 10^5 -fold slower rate of reaction of the H52L variant with H_2O_2 (Eq. 1) than wild-type Ccp1 (142). H175 oxidation will weaken the axial ligation but the effect of HisO formation on H175 and H52 on CCP activity remains to be determined.

4.5.3) H175 is mainly oxidized to HisO in extramitochondrial Ccp1 from 7 d cells.

A large fraction of Ccp1 has exited the mitochondria in 7 d cells (118). This extramitochondrial Ccp1 has no heme and is catalytically inactive (118). LC-MS/MS analysis of Ccp1-containing anion-exchange fractions F8 and F9 from the 7 d S10 extracts (Figure S4.1C) reveals that oxidative modifications (Figure 4.4) are limited to the methionine residues (~ 10 -60% MetO), Y153 (50% TyrOH) at the heme periphery, Y229 ($\sim 85\%$ TyrOH) located in the Cyc1 binding site, W223 ($\sim 60\%$ TrpOH) proximal to the redox cofactor W191, and H175 ($\sim 85\%$ HisO), the proximal iron ligand. Oxidation of this subset of nine residues in extramitochondrial Ccp1 out of the 33 oxidizable residues in the protein (Figure 4.1A) implicates these PTMs in heme release, which is required for Ccp1 exit from mitochondria.

4.5.4) Ccp1 is phosphorylated at Y153 and Y229.

Protein phosphorylation is a reversible PTM that is recognized as a key regulator of mitochondrial function (198). Figure 4.5 summarizes mitochondrial Ccp1 phosphorylation and the MS2 spectra pinpointing the phosphorylation sites are shown in Figure 4.6. Levels of pY153 reach 25% in 16 h mitochondria and 80% at 30 h (Figure 4.5) but oxidized Y153 is not detected

at these time points (Figure 4.3). In contrast, Ccp1 from 7 d mitochondria contains 0% pY153 and 8% pY229 (Figure 4.5) and both are >35% oxidized (Figure 4.4). Collectively, these results suggest possible crosstalk between oxidation and phosphorylation of these two tyrosines in regulating Ccp1 function. We also screened for tyrosine nitration, a modification induced by reactive nitrogen species (RNS) such as the peroxynitrite anion (ONOO^-) and nitrogen dioxide (NO_2) (199). However, nitrotyrosine was not detected in Ccp1 isolated from any of the mitochondrial extracts, which is consistent with our failure to detect this PTM with an anti-nitrotyrosine antibody except in yeast cells stimulated by RNS (unpublished observation).

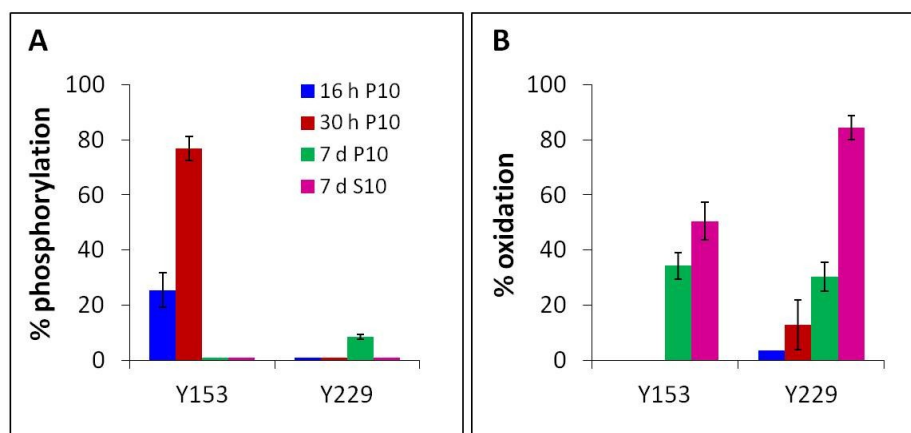


Figure 4.5. Comparison of Ccp1 phosphorylation and oxidation at Y153 and Y229. (A) Percent tyrosine phosphorylation of (B) percent tyrosine (Y153, Y229) oxidation of Ccp1 from mitochondria (P10) and extramitochondrial (S10) extracts of 16-h, 30-h and 7-d cells. The oxidation data are re-plotted from Figures 3, 4. Experimental details are given in the captions to Figures 3 and 6. Both Y153 and Y229 are solvent exposed.

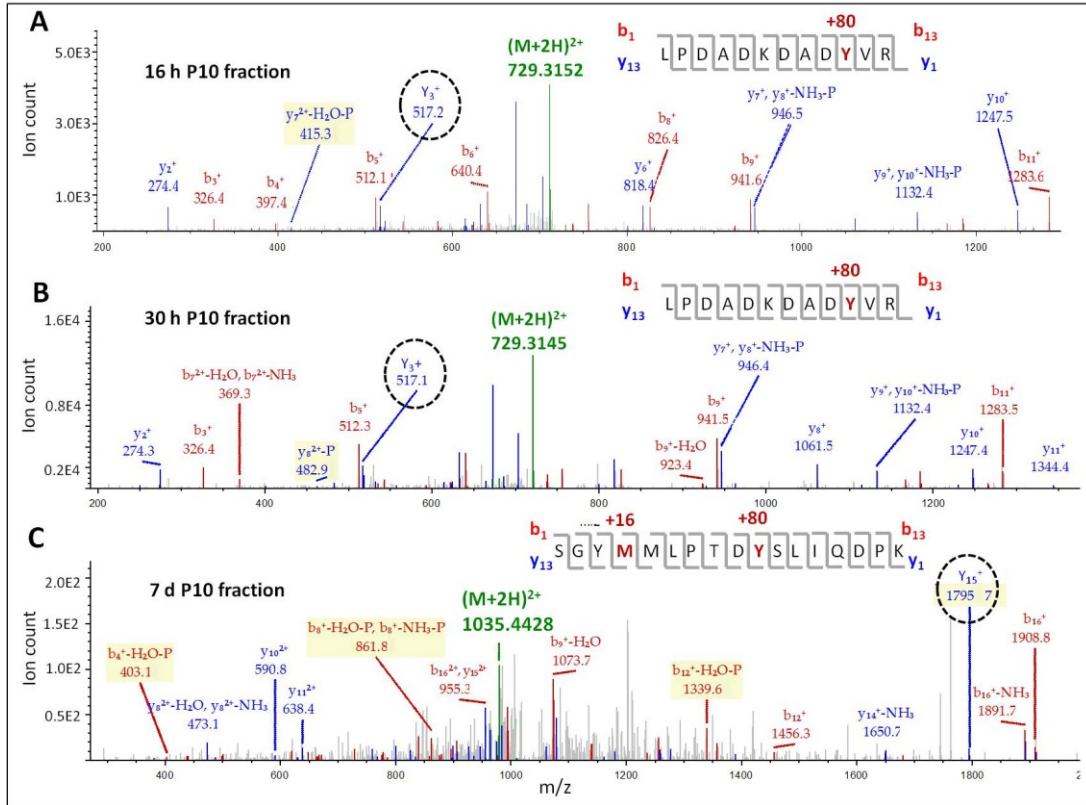


Figure 4.6. LC-MS/MS analysis of Y153 and Y229 phosphorylation in tryptic peptides T17+T18 and T26. MS2 spectrum of the (M+2H)²⁺ ion of phosphorylated T17+T18 at *m/z* 729.3152 from mitochondrial Ccp1 from (A) 16 h and (B) 30 h cells; (C) phosphorylated T26 at *m/z* 1035.4428 of mitochondrial Ccp1 from 7 d cells. The P10 extracts were treated as described in the caption to Figure 3 and the peptide precursor ions (green) were fragmented by CID (30 V) to give *b_n* (red) and *y_n* (blue) sequence ions. The encircled ions have masses indicative of phosphorylation (+80 u) at Y153 in panels A, B and at Y229 in panel C. Spectra are representative of those recorded in 3 independent experiments.

4.5.5) Stepwise vs bolus addition of H₂O₂ to recombinant Ccp1.

Treatment of recombinant 1 μM Ccp1 with a bolus of H₂O₂ containing 10 M eq results in ~80% *intramolecular* dityrosine crosslinking in T6 (Y36/Y39/Y42) and T8 (Y67/Y71) (Figure 4.7B) (194). Since these peptides are only 2-5% crosslinked in Ccp1 isolated from 7 d mitochondria (data not shown), we hypothesized that adding H₂O₂ stepwise would better mimic the situation in respiring mitochondria. Indeed, crosslinked T6 and T8 yields reached only 10-15% when 1 M eq of H₂O₂ was added to Ccp1 at 10 min intervals to a maximum of 10 M eq

(Figure 4.7B). This reveals that the high radical flux from the heme generated by bolus H_2O_2 promotes tyrosyl radical dimerization, which is a rapid reaction ($0.45 \times 10^9 \text{ M}^{-1} \text{ s}^{-1}$) (200). TyrOH increases at the expense of dityrosine in recombinant Ccp1 oxidized stepwise. Distal (Y16, Y23, Y39, Y42, Y67, Y71) and proximal tyrosines (Y153, Y229, Y236, Y251) all undergo >5% hydroxylation (Figure 4.7A) with Y229 (80%), Y67 (50%), Y42 (35%) and Y236 (20%) exhibiting the highest levels of modification on stepwise addition of 10 M eq of H_2O_2 (Figure 4.7A). In contrast, bolus addition of 10 M eq of H_2O_2 hydroxylates Ccp1 only at Y229 (75%), Y16 (25%) and Y251 (10%).

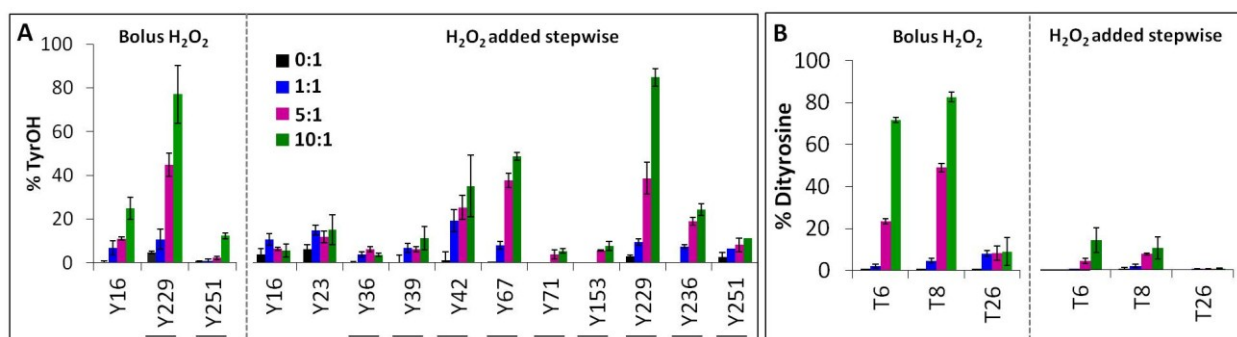


Figure 4.7. Effects of bolus vs stepwise addition of H_2O_2 on the tyrosine oxidation products in recombinant Ccp1. Percentages of (A) TyrOH and (B) dityrosine crosslinking of T6 (Y36/Y39/Y42), T8 (Y67/Y71) and T26 (Y229/Y236) in H_2O_2 -oxidized Ccp1. For bolus oxidation, 1 μM Ccp1 was incubated at room temperature for 60 min in KPi/DTPA with 0 (black), 1 (blue), 5 (magenta) and 10 (green) M eq of H_2O_2 . For stepwise oxidation, 1 M eq of H_2O_2 was added to 1 μM Ccp1 every 10 min over a 0–90 min interval and samples were analyzed after 100 min at room temperature. Yields are based on peptide PAs (Eq. 4) from three independent experiments ($n=3$) and presented as averages \pm SD. Solvent-exposed tyrosines are underlined in panel A. Experimental details are given in the caption to Figure 4.3.

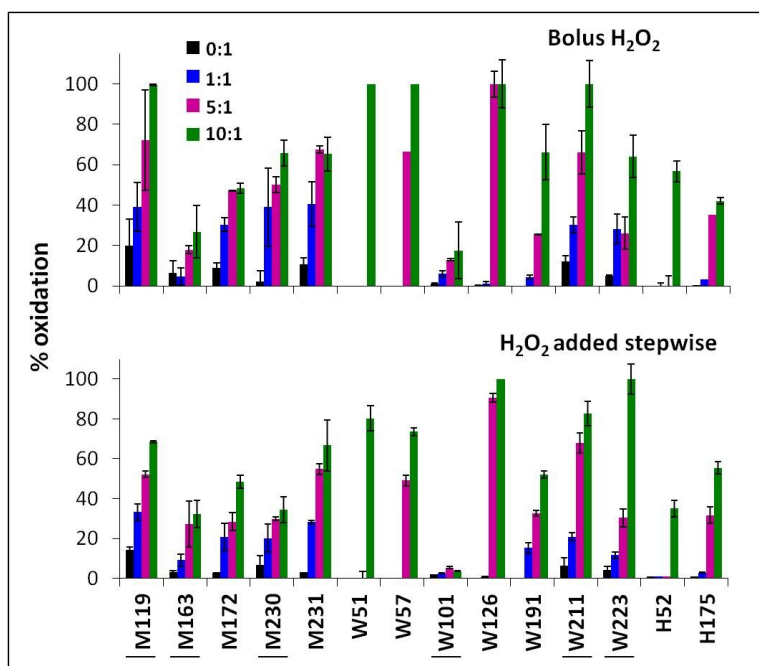


Figure 4.8. Effects of bolus vs stepwise addition of H₂O₂ on methionine, tryptophan and histidine oxidation levels in recombinant Ccp1. MetO, TrpOH+Trp(OH)₂, and HisO percentages in H₂O₂-oxidized Ccp1 are plotted. Experimental details are given in the captions to Figures 4.3 and 4.7. Yields are based on peptide PAs (Eq. 4) from three independent experiments ($n=3$) and presented as averages \pm SD. Solvent-exposed residues are underlined.

In contrast to tyrosine, the oxidation profiles of methionine, tryptophan and histidine are remarkably similar following stepwise vs bolus addition of H₂O₂ to Ccp1 (Figure 4.8). This likely reflects the rapid scavenging by O₂ of their radicals formed on RT from the heme, whereas the slow reaction of tyrosyl radicals with O₂ allows their crosslinking to compete with hydroxylation when the RT flux from the heme is high (194). However, a careful examination of Figure 4.8 reveals that H₂O₂ added stepwise more effectively oxidizes H175 (55%) than bolus H₂O₂ (40%), which is consistent with the high level of H175 oxidation in 7 d extramitochondrial Ccp1 (Figure 4.4) and confirms that HisO formation is not a consequence of exposure to bolus H₂O₂. We also note lower M119 and M230 oxidation on stepwise vs bolus H₂O₂ addition (Figure 4.8), which may influence RT from the heme to zone 2b and zone 3, respectively (Figure 4.1A), since methionines likely play a role in radical formation on aromatic residues (194).

4.6) Discussion

4.6.1) Observed PTMs in Ccp1 confirm that the protein is overoxidized in cells.

We associate overoxidation of Ccp1 with H₂O₂ sensing, loss of heme and cellular relocalization as cells begin to respire and mitochondrial H₂O₂ levels rise (50, 63, 118). This prompted us to investigate PTMs in the protein isolated from yeast cells. After 16 h cell growth mitochondrial Ccp1 exhibits low levels of MetO, which increases after 30 h together with hydroxylation of W101, W211 and Y229 (Figure 4.3). Ccp1 from 7 d mitochondria shows higher levels again of MetO and numerous tryptophan and tyrosine residues are oxidized as well as C128, H52 and H175 (Figure 4.4). Thus, increased oxidation of Ccp1 with cell age confirms that Cyc1^{II} is not always available in the mitochondria to reduce Ccp1 (Eqs. 2,3) following repeated H₂O₂ insults.

A second notable finding is the difference in the PTM profile of mitochondrial vs extramitochondrial Ccp1 from 7 d cells. Only four aromatic residues are modified in the extramitochondrial protein (W223, Y153, Y229, H175) but these have undergone significantly more oxidation (55-85%) than the protein that remained in the mitochondria (~35%) (Figure 4.4). Thus, specific residues must be targeted to promote Ccp1 export, which is obvious in the case of H175 as its conversion to HisO will labilize the heme such that the apoprotein is not retained by the outer mitochondrial membrane (118). Reasons for the high conversion of Y229 to TyrOH in extramitochondrial Ccp1 are not obvious except that this residue is also highly oxidized by H₂O₂ in the recombinant protein (Figures 4.4, 4.7).

Previously, we hypothesized that RT from the heme to H175 may be controlled by a conformational change in M172 (194). Interaction of the M172 sulfur with H175 imidazole ring

should lower the reduction potential of H175 and switch on RT from the oxidized heme to its proximal ligand. The fact that M172 and H175 are oxidized mainly in different molecules of extramitochondrial Ccp1 isolated from 7 d cells (Table S3) and in recombinant Ccp1 (194) supports this hypothesis, which is based on the observation that M230 and/or M231 oxidation convert(s) W191 into a poorer electron donor to the heme (120, 121) due to loss of the stabilizing methionine-aromatic motif (167).

4.6.2) Ccp1 phosphorylation.

Levels of pY found in yeast using 2D electrophoresis and high-resolution LC-MS/MS are <2% compared to ~17% and ~80% found for pS and pT (201, 202). Thus, we detect unprecedented high levels of pY153 in Ccp1 isolated from 16 h (25%) and 30 h (80%) cells (Figure 5). Yeast produce no true protein tyrosine kinases but seven dual-specificity kinases have been predicted based on sequence similarity, including three involved in cell cycle regulation (Rad53, Mps1, Swe1) and four MAPKK proteins (Ste7, Mkk1, Mkk2, Pbs2) (203). Only Ste7 is predicted to localize to the mitochondria (204) so it may be the kinase that phosphorylates Y153. A number of large proteome-scale analyses of whole-cell lysates (202, 205, 206) as well as enriched mitochondrial lysates (207) have attempted to identify all phosphorylation sites in yeast but surprisingly, given its abundance, pY153 was detected in only one study (206).

An examination of Figure 5 reveals that Y153 switches from ~80% pY to 35% TyrOH in mitochondria between 30 h and 7 d. Over the same period, Y229 changes from ~13% TyrOH to ~40% TyrOH plus ~8% pY. High levels of pY are often associated with oxidative stress since protein tyrosine phosphatases become inactivated on oxidation of their active-site cysteines (208). The disappearance of pY153 in 7 d mitochondria was at first surprising but suggests that other factors control the level of this PTM in Ccp1. For example, increased MetO formation in

nearby methionines has been reported to decrease pS/pT/pY levels in a number of proteins (209), including α -synuclein (210), nitrate reductase (211) and mitochondrial pyruvate dehydrogenase (212). Thus, fluctuations in M172 oxidation at ~ 8.5 Å from Y153 may influence pY levels, while M230 and/or M231 at ~ 8 Å may similarly influence Y229, in addition to their role in stabilizing W191^{•+} of CpdI (Eq. 1) (121).

Curiously, as noted previously, Y153 and Y229 are two of the four aromatic residues oxidized in 7 d extramitochondrial Ccp1 (Figure 4.4). Also, they are significantly more oxidized in exported Ccp1, which suggests that oxidation rather than phosphorylation of these residues may facilitate exit of the peroxidase from mitochondria.

4.6.3) Residues in zone 1 are oxidized in Ccp1 from 16- and 30 h mitochondria and in CpdI.

The aromatic residues oxidized in CpdI and Ccp1 from fermenting cells fall largely within zone 1 (Figure 4.1A). Notably, Ccp1 from 30 h mitochondria has undergone $\sim 13\%$ hydroxylation at Y229 and $\sim 3\%$ at W211, while CpdI is additionally oxidized at W223 in zone 1 (Figure 4.3). Following initial H₂O₂ reaction with Ccp1's heme (Eq. 1), RT likely proceeds from W191^{•+} to M231 and on to surface-exposed residues in zone 1 including M230, Y229, W211 and W223. Figure 4.3 provides evidence for minor RT to zone 2a (Y16, W101) as well as oxidation of active-site residues (H175, W191; zone 3) in CpdI, which is more oxidized than mitochondrial Ccp1. This may arise from radical repair in the latter by GSH but overall the results summarized in Figure 4.3 suggest that Ccp1 is exposed to a low H₂O₂ flux in the mitochondria of 16- and 30 h cells.

4.6.4) Comparison of the PTMs in Ccp1 from 7 d mitochondria and Ccp1 overoxidation *in vitro*.

During the shift from fermentation to respiration, H₂O₂ levels rise in mitochondria but Ccp1's reducing partner Cyc1 is likely in limited supply (55). However, it is well-documented *in vitro* that Ccp1 can endogenously reduce up to 10 M eq of H₂O₂ by heme-mediated oxidation of residues in its polypeptide (93). We proposed that oxidation of M230 and/or M231 in H₂O₂-oxidized recombinant Ccp1, which converts W191 into a poorer electron donor (120, 121), switches on RT from the heme to zones 2a and 2b (Figure 4.1A). Zone 2a, in particular, is a rich source of electrons since it contains a large cluster of oxidizable residues (W57, W101, W126, Y16, Y67, Y71, C128; Figure 4.1A). Also, internal waters and O₂ docking sites in this zone (194) provide a favorable environment for coupling RT with proton transfer and subsequent O₂ scavenging of neutral radicals.

Figure 4.4 reveals that the main aromatic donors in zone 2a to the heme of Ccp1 isolated from 7 d mitochondria are W126, Y67 and Y71, which are also major donors in Ccp1 overoxidized with bolus (10 M eq) H₂O₂ (194). In the latter sample, Y67 and Y71 are ~80% crosslinked (Figure 4.7B) which, as discussed above, reflects the high RT flux from the heme on bolus H₂O₂ addition. Bolus H₂O₂ also induces efficient crosslinking of Y36, Y39 and Y42 (Figure 4.7B) in zone 2b (Figure 4.1A) but these tyrosines undergo significantly less oxidation on stepwise H₂O₂ addition to recombinant Ccp1 (Figure 4.7A) and they are <2% crosslinked and <5% hydroxylated in Ccp1 from 7 d cells (Figure 4.7A). This suggests that zone 2b may not act as a major donor to the heme *in vivo* or cells may efficiently repair radicals formed on these tyrosines. Relevant to this point, guaiacol and phenol binding sites have been identified in zones

2a and 2b (173), indicating that RT to these sites may be favored in the presence of alternative Ccp1 reducing substrates.

Active-site residues W51, H52, M172, H175 and W191 (zone 3; Figure 4.1A) are major donors in recombinant Ccp1 treated with 10 M eq of H₂O₂ (Figure 4.4). These residues are 15-40% oxidized in Ccp1 from 7 d mitochondria (Figure 4.4), which confirms its overoxidation by several molecules of H₂O₂. This Ccp1 pool is hydroxylated also at Y153, Y236, Y244 and Y251 in zone 4 (Figures 4.4, 4.1A), residues that are not hydroxylated in recombinant Ccp1 treated with bolus H₂O₂ except for ~10% of Y251 (Figures 4.4, 4.7A). However, stepwise addition of H₂O₂ increases the hydroxylation of zone 4 tyrosines (Figure 4.7A), which suggests that RT from the heme to this zone is turned on in Ccp1 when H₂O₂ is added slowly to the protein or when H₂O₂ is generated in situ as in the mitochondria. On the other hand, rapid production of H₂O₂ should turn on extensive tyrosine crosslinking in zones 2a and 2b as seen on bolus H₂O₂ addition (Figure 4.7B). Such crosslinking may prevent Ccp1 from exiting the mitochondria and possibly contribute to the selective degradation of damaged mitochondria, a process known as mitophagy (90).

4.6.5) The signal for heme labilization in Ccp1.

M172 and H175 are the only active-site residues oxidized in 7 d extramitochondrial Ccp1 (Figure 4.4), which reveals that this pool of Ccp1 has reacted with fewer H₂O₂ molecules than 7 d mitochondrial Ccp1. In fact, the relatively low level of extramitochondrial Ccp1 modification compared to the mitochondrial protein (Figure 4.4) suggests that a pool of unoxidized or weakly oxidized Ccp1 is marked for H175 oxidation and heme labilization. We detect a high level of pY153 in mitochondrial Ccp1 from 30 h cells (Figure 4.5), which may be the signal for H175 oxidation. Phosphorylation is known to disturb the local protein environment, a classic example

being pS313 in pyruvate dehydrogenase, which sterically clashes with a second nearby serine and disrupts a H-bonding network that leads to loss of dehydrogenase activity (213). Y153 is located at 6.8 Å from Ccp1's heme and 8.5 Å from M172. Thus, Y153 phosphorylation likely influences the orientation of M172 and modifies its interaction with H175, which we hypothesize promotes H175 oxidation and heme labilization. Transfer of the labilized heme to Cta1, directly or by unidentified intermediates, allows apoCcp1 to exit the mitochondria. Immunoblotting of the P10 and S10 subcellular fractions with anti-Ccp1 reveals that the main exodus of Ccp1 from mitochondria occurs in 3 to 7 d cells (118). Thus, examination of Ccp1's PTMs over this time period should confirm if pY153 is indeed the signal for heme labilization and apoCcp1 export. Since no pY153 is detected in extramitochondrial Ccp1 (Figure 4.5), this residue must be dephosphorylated and partially hydroxylated (Figure 4.4) before the protein exits the mitochondria or following its relocation.

4.7) Conclusion

This is the first systematic study linking PTMs with the cellular localization and heme loading of a heme protein. Changes in Ccp1's PTMs during growth suggest that reversible non-redox modifications such as phosphorylation and reversible as well as nonreversible redox modifications such as MetO and HisO formation, respectively, regulate Ccp1's physiological functions. Further detailed characterization of Ccp1 variants, including M172S, H175G, W191F and Y153F, will provide important insights into how Ccp1's function as a H₂O₂ sensor and heme donor is driven by oxidative PTMs and phosphorylation in cells.

4.8) Supplementary information

Table S4.1: Oxidative modifications considered in database searching

Modification: candidate amino acids ^a	Δm (u) ^b
Monoxidation (ox): K, R, C, M, Y, H, P, W, F, D, N	15.9949
Dioxidation (diox): K, R, C, M, Y, H, P, W, F	31.9898
Trioxidation (triox): C	47.9847
Carbonylation: R, E, Q, I, L, K, V, W	13.9793
Carbamidomethylation: C ^c	57.02
Hydroxykynurenine: W	19.9898
Kynurenine (kyn): W	3.9949
Pyrrolidinone: P	30.0105
Pyroglutamic acid: P	13.9792
Asparagine: H	23.0159
Aspartic acid: H	22.0319
Aspartylurea: H	10.0320
Formylasparagine: H	4.9790
Aspartate semialdehyde: M	32.0085
Homocysteic acid: M	33.9691
Dehydro (deH): K, R, C, M, Y, H, P, W, F, D, N ^d	1.00783
Phosphorylation : S, T, Y	79.9799
Nitration : Y, W, C, M	44.98

^a Reported products of single amino acid oxidation.(111, 177)

^b Difference in monoisotopic mass of the oxidized and native form of the indicated amino acid.

^c All cysteines were modified with 2-iodoacetamide as outlined in *Materials and Methods*

^d Crosslinked residues undergo loss of a hydrogen atom (see main text).

Table S4.2: Monoisotopic m/z values of the peptide MH^+ ions from trypsinized Ccp1 isolated from yeast

Tryptic peptide^a	Residues^a	Residue(s) oxidized^b	Obs MH^+ (m/z)	Calc MH^+ (m/z)	ppm error^c
T2+T3	13-21	None Y16(ox)	1129.5283 1145.5232	1129.5273 1145.5222	0.88 0.73
T3	15-21	None Y16(ox)	916.4047 932.4005	916.4047 932.3996	0.00 0.96
T4	22-29	None Y23(ox)	891.5290 907.5249	891.5298 907.5247	-0.90 0.22
T5 + T6	30-48	None Y42 (ox) Y36-Y42 (deH) Y36-Y39 (deH) ; Y42 (ox)	2286.1085 2302.1020 2284.0933 2300.0878	2286.1037 2302.0986 2284.0881 2300.0830	2.01 1.47 2.27 2.08
T6	32-48	None Y36-Y39 (deH) Y36 (ox), Y39 (ox)	2016.9213 2014.9103 2048.9111	2016.9185 2014.9029 2048.9083	1.39 3.67 -1.36
T7	49-59	None W57 (Ox) H52 (Ox)	1301.6250 1317.6189 1317.6233	1301.6273 1317.6222 1317.6222	-1.76 -2.50 0.83
T8	60-72	None Y71(Ox) Y67 (Ox) Y67-Y71 (-2Da)	1384.5866 1400.5875 1400.5815 1382.5746	1384.5876 1400.5825 1400.5825 1382.572	-0.72 3.57 -0.71 1.88
T12		None H96 (Ox)	883.5023 899.5007	883.5036 899.4985	-1.47 2.45
T13	98-123	None M119(Ox) W101 (Diox) W101(Ox);M119(Ox) W101(Diox);M119(Ox)	2780.3692 2796.3678 2812.3389 2812.3516 2828.3536	2780.3600 2796.3549 2812.3498 2812.3498 2828.3447	3.30 4.61 -3.87 0.64 3.15
T14+T15		None W126 (Ox) W126 (Ox); C128 (Triox)	----- 903.4606 951.4405	887.4669 903.4618 951.4465	----- -1.32 -4.20
T15+T16		None C128(Diox)	1732.7501 1765.7404	1732.7555 1765.7453	-3.11 -2.77
T16+T17 +T18	131-155	None Y153(Ox) Y153 (P)	2775.2678 ----- 2855.2296	2775.2704 2791.2653 2855.2367	-0.93 ----- -2.48
T17+T18	144-155	None Y153(Ox) Y153(P)	1377.6631 1393.6577 1457.6317	1377.6645 1393.6594 1457.6308	-1.01 -1.22 0.62
T20	161-166	None M163(Ox)	762.3561 778.3512	762.3563 778.3512	-0.26 0.00
T21	167-179	None M172(Ox) H175 (Ox) M172(Ox); H175(Ox)	1295.7134 1311.7090 1311.7049 1327.6989	1295.7140 1311.7089 1311.7089 1327.7038	-0.46 0.08 -3.04 -3.70
T23	184-212	None W211 (Ox) W191(Ox);W211(Diox)	3362.5557 3378.5353 3410.5275	3362.5389 3378.5338 3410.5236	4.99 0.44 1.14 -0.29

T24+T25	213-226	Native W223(ox) W223 (diox)	1690.7662 1706.7652 1722.7607	1690.7667 1706.7616 1722.7565	2.11 2.43 0.07
T25	216-226	Native	1320.5452	1320.5451	0.08
T25+T26	216-243	Native W223(ox)	3260.461 3276.460	3260.4511 3276.4460	3.03 4.27
T26	227-243	Native Y229(ox) M231(ox) M230(ox); M231(ox) Y229 (ox) ; M230 (ox) Y229(ox); M230(ox) ; M231 (ox) Y229 (P) ; M231 (ox) Y229 (deH) ; M230 (ox) ; Y236 (deH)	1958.9241 1974.9265 1974.9280 1990.9131 1990.9129 2006.9088 2054.8985 1972.9034	1958.9230 1974.9187 1974.9187 1990.9136 1990.9136 2006.9077 2054.9077 1972.9023	0.56 3.95 4.71 -0.25 -0.35 0.55 -4.47 0.56
T27	244-249	None Y244(ox) Y244(diox)	722.4442 738.4380 754.4352	722.4447 738.4396 754.4345	-0.69 -2.17 0.92
T28	250-257	None	982.4139	982.4112	2.74
T28+T29	250-260	None Y251(ox)	1404.6418 1420.6401	1404.6430 1420.6379	-0.85 1.55
T28+T29+T30	250-264	None Y251(ox)	1881.8640 1897.8589	1881.8654 1897.8603	-0.74 -0.73

^a Figure 4.1B gives the tryptic map of Ccp1 and the sequence of tryptic peptides T1-T34.

^b Observed residue modifications are assigned based on the data in Table S4.1.

^c The error in the observed monoisotopic m/z value in ppm is given by $10^6(\text{Obs } m/z - \text{Calc } m/z)/\text{Calc } m/z$.

Table S4.3: Peptides T21 (M172, H175) is oxidized at two residues ^a

Tryptic peptide	Residue(s) oxidized (X_{ox})	Obs MH^+ (m/z) ^b	Calc MH^+ (m/z) ^c	Error (ppm) ^c	% X_{ox} ^d	
					7 d cells	
					P10	S10
T21	None	1295.7134	1295.7140	-0.46	29.8 ± 1.0	3.2 ± 1.4
T21	M172 +16	1311.7090	1311.7089	0.08	38.5 ± 5.7	16.6 ± 3.1
T21	H175 +16	1311.7073	1311.7089	-1.22	28.5 ± 2.0	70.4 ± 3.2
T21	M172 +16, H175 +16	1327.6972	1327.7038	-4.97	3.1 ± 4.0	10.3 ± 0.5

^a Ccp1 from 7 d P10 and S10 extracts was trypsinized and analyzed using LC-MS/MS (see *Materials and Methods*).

^b The precursor ions selected for MS2 analysis were filtered using a mass exclusion threshold of 10 ppm.

^c The monoisotopic m/z values for the peptide MH^+ ions were calculated using Protein Prospector (<http://prospector.ucsf.edu>), and the errors were calculated as in Footnote c of Table S4.2.

^d The percent oxidation of H175 and M172 was calculated using Eq. 4 of the main text.

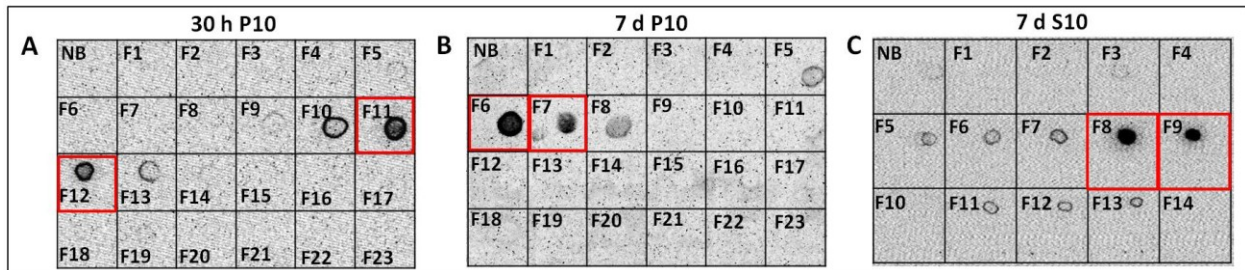


Figure S4.1. Representative anti-Ccp1 immunodot blots of the anion-exchange fractions of (A) the P10 extract from 30 h cells, and of the (B) mitochondria-enriched P10 and (C) extramitochondrial S10 extracts from 7 d cells. Red boxes denote fractions in which most of Ccp1 was eluted. Experimental details are given in the caption to Figure 2 of the main text.

Chapter 5: Cytochrome c peroxidase pull-down assays in yeast reveal numerous novel binding partners including Sod2, Pet9, GAPDH and Tsa1

5.1) Preface

The work presented in Chapter 5 corresponds to the following manuscript in preparation:

Kathiresan M, and English AM (2015). **Cytochrome c peroxidase pull-down assays in yeast reveal numerous novel binding partners including Sod2, Pet9, GAPDH and Tsa1**. Target journal: Proteomics. The production and interpretation of the data, writing and revision of the manuscript were performed by me. Dr. English contributed to discussion, data analysis, writing, editing and revisions of the paper.

5.2) Abstract of the manuscript

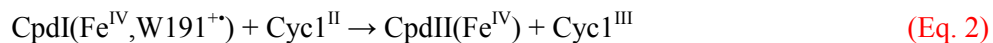
Recently we discovered that cytochrome c peroxidase (Ccp1) functions primarily as a mitochondrial H₂O₂ sensor and heme donor in yeast cells. A large pool of heme-free Ccp1 exits the mitochondria and is targeted to the nucleus and vacuole when cells switch to respiration and mitochondrial H₂O₂ levels rise. During the spike in H₂O₂, Ccp1's heme is labilized by overoxidation of its polypeptide and we identified catalase A (Cta1), the mitochondrial and peroxisomal catalase isoform in yeast, as a recipient of Ccp1's heme. In this study, we examine proteomic interactions involving apo- and holoCcp1 in extracts from 1 d fermenting and 7 d stationary-phase respiring cells to gain insight into Ccp1's H₂O₂-sensing and heme-donor functions. Using glutathione-S-transferase (GST) as an affinity tag in Ccp1 pull-downs, combined with immunoblot analysis, 1D and 2D gel electrophoresis and mass spectrometry, we identified Ccp1's biological partner Cyc1 and novel interactions with mitochondrial superoxide dismutase 2 (Sod2) and cytosolic Sod1, the heme transporter Pet9, the three yeast isoforms of glyceraldehyde-3-phosphate dehydrogenase (Tdh3/2/1), heat shock proteins including Hsp90 and

Hsp70, and the main peroxiredoxin in yeast (Tsa1), and its reducing substrate, thioredoxin (Trx2). These novel protein-protein interactions not only expand our view of Ccp1's role but lead to a more complete understanding of heme trafficking and H₂O₂ cell signaling in the mitochondria and expose several new lines of investigation.

5.3) Introduction

Ccp1 is a nuclear encoded protein that is synthesized as a precursor protein in the cytoplasm and targeted to the mitochondrial inter membrane space. Its 68-residue presequence is threaded through the inner mitochondrial membrane where its cleavage is coordinated by the action of two matrix localized proteases, the ATP-dependent mAAA protease and the rhomboid protease Pcp1 (58). Mature 34-kDa Ccp1 is detected as a soluble protein in the intermembrane space (IMS) (58) with a non-covalently bound b-type heme. The order of proteolytic processing and heme insertion is unknown but apoCcp1 accumulates in yeast under anaerobic conditions, revealing that its synthesis is O₂/heme independent (60, 61).

Extensive biochemical and biophysical studies have characterized Ccp1's peroxidase activity *in vitro* (17). H₂O₂ reacts rapidly with the resting ferric enzyme to give CpdI (compound I) with oxidizing equivalents on the heme and W191 (Eq. 1) that are reduced by Cyc1^{II} (Eqs. 2,3):



Notably, Ccp1 was the first heme enzyme crystallized and structurally characterized (40, 214). The later determination of the structure of the Ccp1-Cyc complex (41) firmly established Ccp1 as a paradigm in studying protein recognition and intermolecular electron transfer reactions (17).

Based on its detection in the IMS, it has long been assumed that Ccp1 protects the electron-transport chain by catalytically consuming the H_2O_2 produced during aerobic respiration (Eqs. 1-3). However, Ccp1 competes with complex IV of the electron transport chain for reducing equivalents from Cyc1^{II} (64). Moreover, yeast cells possess a peroxisomal and mitochondrial catalase A (Cta1) that efficiently disproportionates H_2O_2 to H_2O and O_2 without compromising ATP production (55). Thus, from an energetic perspective, CCP activity (Eqs. 1-3) would appear to be a needlessly expensive way of catalytically detoxifying H_2O_2 , which suggests that Ccp1 has other functions in the cell. In fact, we have reported that Ccp1 functions as a mitochondrial H_2O_2 sensor rather than catalytic H_2O_2 detoxifier in respiring cells (50, 118).

H_2O_2 levels spike during the switch from fermentation to cellular respiration. This is consistent with a lack of Cyc1 for CCP activity (Eqs. 1-3) and for O_2 reduction to H_2O by complex IV. At this point in yeast metabolism, it is likely that Cyc1 and Cta1 are only beginning to accumulate since, unlike Ccp1, synthesis of these proteins is O_2 /heme dependent (55, 101). Thus, Ccp1, which is rapidly heme loaded in the presence of oxygen (60, 61), suffers extensive heme-mediated oxidation by H_2O_2 of its polypeptide, including oxidation of the proximal iron ligand H175, which labilizes its heme. Using biochemical and genetic analysis, we found that apoCta1 is a recipient of heme from oxidized Ccp1 (118). Remarkably, unmodified heme is transferred from Ccp1 either directly or via unidentified intermediate proteins to Cta1 (118), which then catalytically detoxifies mitochondrial H_2O_2 . Heme-free apoCcp1 exits mitochondria and is targeted to the nucleus and possibly the vacuole (118). In the nucleus, Ccp1 conveys an

oxidative stress signal to Skn7, a nuclear transcription factor that upregulates the expression of antioxidant enzymes, including the cytosolic catalase Ctt1, when yeast are challenged with *exogenous* H₂O₂ (108). A role for apoCcp1 in the vacuole has not been proposed.

Large-scale interactome networks built from yeast two-hybrid studies and affinity purification methods (215–217) have identified 22 possible Ccp1 binding partners. Additionally six genetic interactions have been identified for Ccp1 (<http://thebiogrid.org/34197>). However, the published interactomes report on complexes identified from whole-cell lysates of exponentially growing, fermenting yeast (215–217), while we have shown that Ccp1 exhibits different cellular locations and different PTMs in fermenting and respiring cells (118). Thus, its protein binding partners are also likely to change under different metabolic conditions, which we screen for here using mitochondrial and extramitochondrial extracts from 1 d fermenting and 7 d respiring yeast cells as a source of prey proteins. Recombinantly expressed GST-Ccp1 is added to the extracts as a bait protein since this allows us to control Ccp1's heme loading and to manipulate the bait-to-prey ratio for the detection of low-abundance partners and transient interactions. We use GST-apoCcp1 and GST-holoCcp1 as bait in 1 d yeast extracts but just GST-apoCcp1 as bait in 7 d extracts since Ccp1 is largely converted to its apoform in respiring mitochondria (118). Our results confirm the expected mitochondrial Ccp1-Cyc1 interaction and reveal numerous novel Ccp1 interactions. Notable amongst its possible binding partners are Pet9 and GAPDH, implicating a broader role for Ccp1 in intracellular heme transfer/trafficking. Surprisingly, a robust interaction with Sod2 is also detected, which suggests possible H₂O₂ substrate channelling from the dismutase to the peroxidase.

5.4) Materials and Methods

5.4.1) Materials.

(Bio)chemicals were obtained from the following suppliers: Zymolase 20T (Amsbio); sequencing grade modified trypsin (Promega); SuperSignal West Pico enhanced chemiluminescence kit and Tween 20 (Thermo Fisher); Coomassie (MP Biomedicals); hemin chloride, phenylmethylsulfonyl fluoride (PMSF), DEAE Sepharose resins (GE Healthcare); GST resin (Qiagen); pGEX4T and pGEX2T vector (Novagen). The *Saccharomyces cerevisiae* strains in the background BY4741 and the suppliers are listed in Table 5.1. Yeast extract, peptone, microbiology grade agar and galactose (Bioshop); glucose (Fisher Scientific). The following antibodies were used for Western blotting: rabbit anti-Ccp1 serum was kindly provided by Professor David Goodin (University of California, Davis); mouse anti-porin to detect porin as a mitochondrial outer-membrane marker (ab110326 Abcam); goat anti-GST (GE Healthcare); and HRP-conjugated secondary antibodies (goat anti-rabbit, goat anti-mouse, and rabbit-anti goat; Biorad).

Table 5.1. *S. cerevisiae* strains used in this work

Strain	Genotype	Supplier	Ref
BY4741 Wild-type	<i>MATa his3Δ1 leu2Δ0 met15Δ0 ura3Δ0</i>	EUROSCARF	(68)
BY4741 GST-SOD2	<i>BY4741 HIS3MX6GAL1-GST</i>	GE Healthcare	(218)

5.4.2) Construction, expression and purification of GST-Ccp1 from *E. Coli*.

The cDNA for yeast Ccp1 encoding glycine and serine at positions +1 and +2 of the mature protein was subcloned into the BamHI and EcoRI sites of the pGEX-2T GST expression vector (GE Healthcare). *E. coli* BL21(DE3) cells were transformed with pGEX-2T-Ccp1, grown

to OD₆₀₀ 0.6 in LB medium with 100 µg mL⁻¹ ampicillin at 37 °C/250 rpm, induced by 0.5 mM IPTG to express Ccp1 with an N-terminal GST-tag, further incubated at 37 °C/250 rpm for 4 h, and collected at 12000 x g. Following resuspension in lysis buffer (50 mM Tris-HCl pH 7.5, 0.1 mM EDTA, 100 mM NaCl, 100 µg/mL of lysozyme), the cells were lysed by 3 freeze/thaw cycles (liquid nitrogen/37 °C), the lysate was added to 1 X PBS loading buffer (140 mM NaCl, 2.7 mM KCl, 10 mM Na₂HPO₄, 1.8 mM KH₂PO₄, pH 7.5) and sonicated 10 x 10 s. Finally, cell debris were removed by centrifugation at 20000 x g for 20 min.

To purify GST-Ccp1, 1 mL of Glutathione Sepharose 4B resin (GE Healthcare) equilibrated in loading buffer was added to 10 mL of supernatant, incubated at 4 °C for 1 h, and the resin was washed 3X with loading buffer. GST-Ccp1 was eluted from the resin by 10 mM reduced glutathione in 50 mM Tris-HCl (pH 8.0) and dialyzed against 20 mM KPi (pH 7.5) overnight. GST was isolated from cells transformed with the empty pGEX-4T vector following the same procedure, and GST-Ccp1 and the GST control were stored in 20 mM KPi (pH 7.5) at -80 °C until use.

Since GST-Ccp1 is purified from *E. coli* with Ccp1 in the apoform, the sample was incubated with 1.1 M eq of hemin in 20 mM KPi (pH 7.5) for 1 h at 4 °C. Unbound hemin was removed on a 0.8 x 4-cm DEAE Sepharose column equilibrated with the same buffer and GST-Ccp1 was eluted from the column on adding 500 mM NaCl to the equilibration buffer. The CCP activity of GST-Ccp1 was determined by monitoring the oxidation of horse heart Cyc^{II} by H₂O₂ as reported previously (118).

5.4.3) Preparation of soluble protein extracts from the subcellular fractions of 1 and 7 d wild-type cells.

Wild-type BY4741 cells were grown under high aeration in YPD liquid medium (1% yeast extract, 2% peptone, 2% glucose) at a flask-to-medium volume ratio of $\geq 5:1$. Cultures at an initial OD₆₀₀ of 0.01 were incubated at 30 °C with shaking at 225 rpm and the medium was replaced with 0.85% (w/v) NaCl solution after 72 h to extend culture viability. Cells were harvested from 1 and 7 d cultures at 2000 x g, washed twice with 0.85% NaCl, pelleted at 2000 x g, resuspended in lysis buffer (100 mM KPi pH 7.4, CompleteTM protease inhibitor cocktail, Roche). In order to generate soluble whole cell lysates (S2), cell suspensions were mixed with an equal volume of 0.5 mm acid-washed glass beads. Suspensions were vortexed for 4 x 15 s, and the cell debris were removed by centrifugation at 13000 x g for 10 min at 4 °C.

Crude mitochondrial (P10) and extramitochondrial (S10) lysates were separated as described previously (219). Briefly, cells were grown in 500 mL of YPD medium for 1 d and 7 d at 30 °C as described above, harvested at 2000 x g and washed twice with aqueous 0.85% NaCl. The cell pellets were resuspended in 50 mL of pre-warmed 100 mM Tris-H₂SO₄ (pH 9.4) with 10 mM DTT, incubated for 10 min at 30 °C and 80 rpm, harvested at 2000 x g, washed twice with 20 mL of 10 mM KPi (pH 7.4) containing 1.2 M sorbitol, and treated with 12 mg of zymolyase 20T/g of wet cells at 30 °C. Spheroplast formation was monitored by light microscopy and was complete after 1-2 h incubation at 30 °C with gentle agitation. The resulting spheroplasts were washed twice with 20 mL of the same buffer and resuspended in 20 mL of 10 mM Tris (pH 7.4) containing 0.6 M sorbitol, 1 mM EDTA, 1 mM PMSF and CompleteTM protease inhibitor cocktail. Spheroplasts at 4 °C were disrupted by 15 strokes of a glass-Teflon homogenizer, the homogenates were centrifuges at 2000 x g and the supernatants, which

correspond to the denucleated lysates (S2 fractions), were collected. The S2 fractions were further centrifuged at 10000 x g for 15 min at 4°C, and the mitochondria-depleted supernatants (S10 fractions) were separated from the mitochondria-enriched pellets (P10 fractions).

5.4.4) Screening for Ccp1 interacting proteins in subcellular fractions from 1 and 7 d yeast.

Assays were carried out using the MagneGST Pull-Down System kit (Promega). Briefly, 300 µg of purified GST-apoCcp1, GST-holoCcp1 or GST (negative control) in 75 µL of buffer (20 mM KPi pH 7.4, 0.1 mM EDTA, 100 mM NaCl) was mixed with end-over-end rotation for 1 h at 4°C with a 200-µL slurry of the GSH-linked magnetic beads that were prewashed 3X in the binding/wash buffer supplied with the kit (4.2 mM Na₂HPO₄, 2 mM KH₂PO₄, 140 mM NaCl, 10 mM KCl). Following GST-apoCcp1, GST-holoCcp1 or GST immobilization, the beads were again washed 3X in the binding/wash buffer, resuspended in 200 µL of this buffer and stored at 4 °C. The S2, P10 and S10 extracts were pre-cleared by incubation with a 20 µL slurry of fresh beads for 2 h at 4 °C with end-over-end rotation, and 500 µL of the precleared supernatants (2 mg/mL S2, P10 and S10) was added to 20 µL-aliquots of GST-apoCcp1, GST-holoCcp1 and GST-bound magnetic beads. Samples were incubated for 1 h at 4 °C with end-over-end mixing and placed at the magnet separation stand (MagneSphere® Technology). The supernatants were collected, the beads were washed 3X with the binding/wash buffer, and GST-apoCcp1/GST-holoCcp1/GST binding partners were eluted using 25 µL of 50 mM reduced glutathione (GSH) in 50 mM Tris pH 8.0. After elution, the beads were boiled in 25 µL of SDS-PAGE loading buffer to determine if protein elution was complete.

5.4.5) Screening for Ccp1 as an interacting partner of Sod2 using the overexpressed GST-Sod2 fusion protein from 1 d yeast cells.

Yeast cells transformed with the GAL1-10 UAS vector containing GST-Sod2 were grown overnight in 20 mL of synthetic complete medium minus uracil containing 2% raffinose (SR-ura) since this plasmid is URA⁺. Raffinose was used since glucose represses GAL1 expression. Cells were pelleted at 2000 x g for 5 min, washed 2X with sterile water and resuspended in 500 mL of SG-ura (4% galactose) or YPG (1% yeast extract, 2% peptone, 4% galactose) to induce GST-Sod2 expression. After 12 h, cells were pelleted at 2000 x g, snap frozen and stored at -80 °C until the GST-Sod2 pull-down assays were performed as reported (220). Briefly, cells were resuspended in binding buffer (20 mM Tris pH 7.5, 100 mM NaCl, 1 mM EDTA, 10% glycerol, 0.1% NP-40, 10 mM β -mercaptoethanol and 1 mM PMSF) and broken by vortexing for 5 x 15 s with an equal volume of 0.5 mm acid-washed glass beads in the same buffer. Unbroken cells and cell debris were removed by centrifugation at 2000 x g for 5 min and the lysate was cleared by centrifugation at 13000 x g for 10 min. The supernatant, which corresponds to the soluble protein extract, was loaded onto a 1 mL slurry of Glutathione Sepharose 4B resin (GE Healthcare) in batch mode that had been equilibrated 3X with the binding buffer and the sample was rotated for 1 h at 4°C. The beads were washed 3X with binding buffer and GST-Sod2 and interacting proteins were eluted from the beads in 50 mM Tris buffer, pH 8.0 containing 50 mM GSH.

5.4.6) 1D SDS-PAGE and 2D IEF/SDS-PAGE analysis.

Proteins eluted from GSH-linked magnetic beads and/or Glutathione Sepharose 4B resin were decomplexified by 1D SDS-PAGE under reducing conditions on 8 cm x 5.8 cm x 1 mm 6% stacking and 12% resolving gels for 1 h at 120 V. To further resolve the proteins, selected

samples were also separated on 2D SDS-PAGE gels. Briefly, 25-35 μg of protein in 50 mM Tris pH 8.0 was diluted into rehydration buffer (8 M urea, 2% chaps, 50 mM DTT, 0.2% Bio-Lyte, 3/10 ampholyte, 0.001% bromophenol blue) and incubated in a tray with an immobilized pH gradient (IPG) strip (Biorad) (7 cm, pH 3-10) overnight at room temperature. The rehydrated IPG strip was transferred to the focusing tray and electrophoresis was carried out as specified in the power supply manual (Model Protean® IEF Cell, Biorad, catalogue # 1632099) (0-4000 V, 8-10000 V-hr, rapid ramp at 20 °C). The Ready-strips were equilibrated at room temperature with 2% w/v DTT in SDS-PAGE equilibration buffer (6 M urea, 0.375 M Tris-HCl pH 8.8, 2% SDS, 20% glycerol) followed by 2.5% w/v iodoacetamide in the same buffer for a further 10 min, transferred to 12% SDS-PAGE gels and electrophoresed at 150 V for 1 h.

The 1D and 2D gels were Coomassie and/or silver stained as described (221). Protein bands/spots were excised, transferred to clean 1.5 mL microcentrifuge tubes and destained overnight at 4°C with 25 mM ammonium bicarbonate (pH 8.0)/50% acetonitrile (Coomassie stain) or 15 mM potassium ferricyanide/50 mM sodium thiosulfate (silver stain). The gel pieces were dehydrated with 100% acetonitrile, reduced with 10 mM aqueous DTT at 50 °C for 30 min, dehydrated again with 100% acetonitrile before alkylation with 55 mM aqueous iodoacetamide for 30 min in the dark. Following washing with 50 mM NH_4HCO_3 for 15 min with occasional vortexing, the gel pieces were dehydrated with 100% acetonitrile, dried on a Speedvac for 20 min, and in-gel digestion was initiated by adding 10 μL of 12.5 ng/ μL trypsin in 50 mM ammonium bicarbonate, pH 8.0. The tubes were placed on ice for 1 h to rehydrate the gel pieces, 50 μL of 50 mM ammonium bicarbonate pH 8.0 was added to each and the tubes were placed in a 37 °C incubator overnight. Peptides were extracted 2X with 50% acetonitrile/0.1% formic acid

and the combined extracts were dried and resuspended in 2% acetonitrile/0.1% formic acid (MS solvent) for analysis by LC-MS/MS.

5.4.7) LC-MS/MS analysis of Ccp1's interacting partners.

The tryptic peptides were desalted on C18 Zip Tips (5 μ L/injection) and separated on a homemade reversed-phase C18 capillary column (100 μ m x 6.5 cm) equilibrated with 2% aqueous acetonitrile/0.1% formic acid and attached to a NanoLC (Easy-nLC II). Peptides were eluted at a flow rate of 300 nL/min into the nanoESI source of an LTQ Orbitrap Velos mass spectrometer (Thermo Scientific) using a 2–94% acetonitrile gradient and analyzed in full-scan mode (m/z 350–2000) in the Orbitrap high resolution mass analyzer ($R=60,000$ at m/z 400). Other instrumental parameters were: electrospray voltage 3 kV, CID collision energy 35 V and heated capillary temperature 200 °C. Precursor peptide ions were selected in MS1 using a mass exclusion threshold of 10 ppm and fragmented in the LTQ at a collision energy of 35 V. MS2 fragments with an intensity count of ≥ 20 were analyzed with a mass tolerance of 0.8 u using Proteome Discoverer 1.3.0 software (Thermo Scientific) and the Sequest search engine with mass filters for for oxidation (+16, +32, +48 u) of Met, Cys plus cysteine alkylation by iodoacetamide (+57 u). Dynamic exclusion was enabled with a repeat count of 1, a repeat duration of 30 s and an excluded list size of 500. Sequest correlates the MS2 spectra with peptide sequences in the the publicly available NCBI *Saccharomyces cerevisiae* protein database (www.ncbi.nlm.nih.gov). Also, Sequest's XCorr (>2) and False Discovery Rate (<0.01) filters were implemented for confident peptide identification. Peptides having a cross-correlation score of at least 2.0, and 4 unique peptides were considered for positive identification of the peptide sequence.

5.4.8) Western blotting with anti-Ccp1, anti-GST.

1D gels of the extracts were also probed for Ccp1 and GST. The proteins separated by 1D 12% SDS-PAGE were transferred to a methanol soaked polyvinylidene fluoride (PVDF, BioRad) membrane at 100 mA for 3 h at room temperature. After blocking for 1 h at room temperature with 5% (w/v) skim milk in TBST (50 mM Tris, 150 mM NaCl and 0.05% v/v Tween 20, pH 7.6), membranes were incubated with rabbit anti-Ccp1 serum (1:10,000 dilution) or anti-GST antibody (1:1000) for 2 h, washed 3 times with TBST, and incubated with goat anti-rabbit or rabbit anti-goat HRP conjugated secondary antibody (1:20,000, Biorad) for 1.5 h at room temperature. Blots were visualized using the Super Signal West Pico Enhanced Chemiluminescence (ECL) kit from Thermo Fisher in an AlphaImager (ProteinSimple).

5.5) Results

5.5.1) Characterization of the GST-Ccp1 fusion protein.

GST-Ccp1 was overexpressed in *E. coli* transfected with the plasmid pGEX-2T-Ccp1 (Figure S5.1A, lane 1) and eluted by GSH from the Glutathione Sepharose 4B beads with high purity (Figure S5.1A, lane 5). Similarly, GST was purified from cells transfected with the empty pGEX-2T GST expression vector in high purity (Figure S5.1A, lane 6). The yield of highly purified GST-Ccp1 and GST was typically ~50 and ~80 mg/L, respectively. GST-Ccp1 purified from *E. coli* exhibits a 408/280 absorbance ratio of 0.12 (data not shown), indicating that Ccp1 is mainly heme-free but incubation with hemin increases the 408/280 ratio to 0.77 ± 0.03 (Figure S5.1B). Adding the calculated 280 nm absorbance (222) of GST based on its sequence ($\epsilon_{280}=43 \text{ mM}^{-1}\text{cm}^{-1}$), to the published value for apoCcp1 ($\epsilon_{280}=56 \text{ mM}^{-1}\text{cm}^{-1}$) and holoCcp1 ($\epsilon_{280}=77 \text{ mM}^{-1}\text{cm}^{-1}$) (78) gives a ϵ_{280} value of 99 and 120 $\text{mM}^{-1}\text{cm}^{-1}$ for GST-apoCcp1 and GST-holoCcp1,

respectively. Assuming GST-holoCcp1 and holoCcp1 have the same heme absorbance ($\epsilon_{408}=98 \text{ mM}^{-1}\text{cm}^{-1}$) (86), we calculate a 408/280 absorbance ratio of 0.79 for GST-holoCcp1, which is within the range observed for GST-holoCcp1 (0.77 ± 0.03 ; Figure S5.1B). Hence, we assume that after incubation with hemin, GST-Ccp1 is fully heme loaded. Nonetheless, GST-Ccp1 exhibits only ~60% CCP activity of Ccp1 (Table S5.1), suggesting that the GST tag may somehow slowdown reduction of CpdI/II by Cyl^{II} (Eqs. 2, 3), which are the rate-limiting steps in CCP catalysis.(86)

5.5.2) 1D SDS-PAGE is sufficient to resolve Ccp1's interacting partners.

The prey proteins captured by GST-holoCcp1, GST-apoCcp1 and the GST control were separated by 1D and 2D gel electrophoresis to establish sample complexity. The 2D gels did not show an abundance of spots (Figure 5.1, gels 2, 4), indicating that 1D gel electrophoresis is sufficient to resolve the prey proteins eluted from the GSH magnetic beads. Importantly, the GST tag alone (negative control) showed minimal protein binding (Figure 5.1, gels 2, 4), which reveals that the proteins that bind to GST-Ccp1 exhibit a high level of specificity for Ccp1. Representative 1D gels are compared in Figure 5.2 for S2, P10 and S10 extracts from 1 vs 7 d cells and show the relatively low binding of prey proteins to the GST-Ccp1 bait protein and the even lower binding of prey proteins to the GST tag alone. This suggests that proteins found in complex with Ccp1-GST are specific to Ccp1 and not the GST tag.

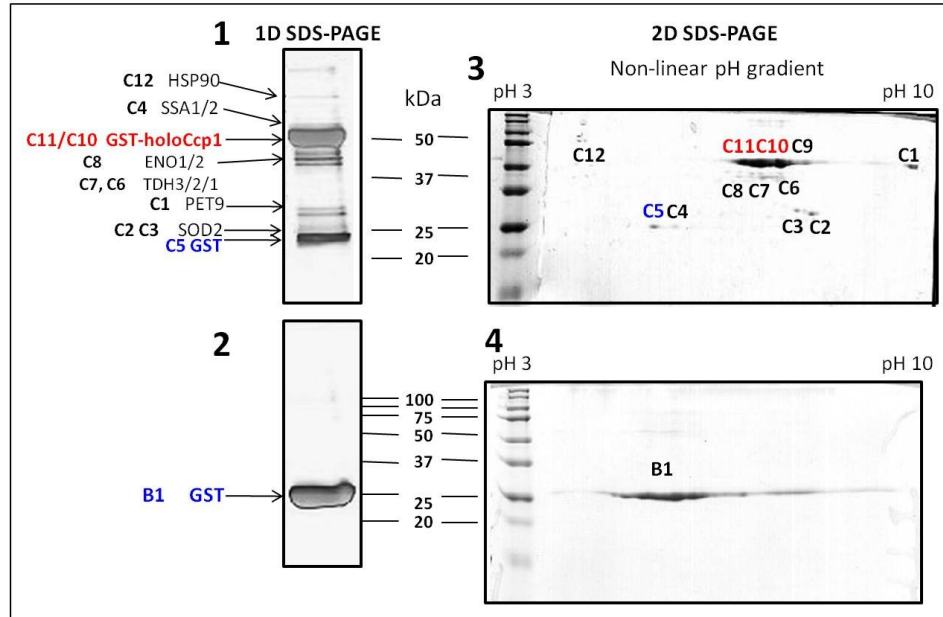


Figure 5.1. 1D SDS-PAGE and 2D IEF/SDS-PAGE analysis of the proteins in GST-holoCcp1 and GST pull down from the S2 extract from 1 d yeast. The extract was probed with (gels 1, 3) GST-holoCcp1 and (gels 2, 4) GST as bait. The silver-stained gels shown were destained, 2 mm bands were excised the length of the 1D gels and the protein spots were excised from the 2D gels. Proteins in the gel pieces were reduced with DTT, alkylated with iodoacetamide and trypsinized for analysis by LC-MS/MS as described in the *Materials and Methods*. Note the presence of endogenous GST (C5) in gel 1.

Proteins in the gel pieces were trypsinized and the tryptic peptides isolated from the gels were analyzed by mass spectrometry as described in the *Materials and Methods*. Four independent experiments ($n=4$) on each of the S2, P10 and S10 extracts from 1 d and 7 d cells show that the added GST-apoCcp1, GST-holoCcp1 or GST bait traps prey proteins in these six different extracts with high reproducibility and that most of the interactions are specific to Ccp1 (Tables S5.2, S5.3, S5.4). The high resolving power and sensitivity of the LTQ-Orbitrap Velos mass spectrometer used for the LC-MS and LC-MS/MS analyses resulted in high sequence coverage (30-85%) and accurate mass measurements (<5 ppm error) of the tryptic peptides isolated from the gels.

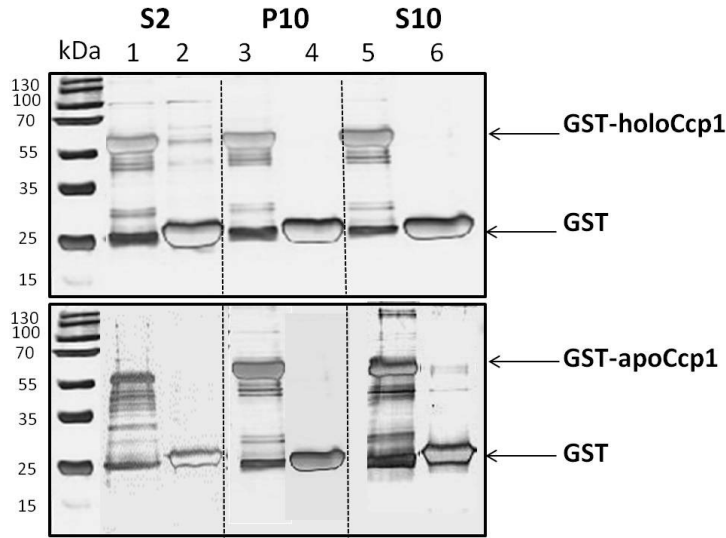


Figure 5.2. Representative 1D gels of the S2, P10 and S10 extracts from 1- and 7 d cells. Proteins pulled down by GST-holoCcp1 in the S2, P10 and S10 extracts from 1 d cells (top panel) and by GST-apoCcp1 from 7 d cells (bottom panel). Molecular weight markers are shown in lane MW. Proteins pulled down by GST-Ccp1 bait are shown in lanes 1, 3, 5 and by the GST control bait in lanes 2, 4, 6. The bait proteins are indicated by the arrows on the left. Proteins were eluted from the GSH beads with 50 mM GSH at pH 8, the silver-stained gels were destained, 2 mm bands were excised from the length of the gels, proteins in the bands were reduced with DTT, alkylated with iodoacetamide and trypsinized for analysis by LC-MS/MS as described in *Materials and Methods*.

Table S5.2 and S5.3 list all of the prey proteins trapped by GST-Ccp1 in 1 d and 7 d cells, respectively, while Table S4 lists those trapped by GST, the negative control. The ~30 prey proteins identified that bind specifically to apo- and holoCcp1 can be classed into four major groups, antioxidant, glycolytic, heat shock and miscellaneous proteins. Here we focus on interacting proteins (Tables 5.2, 5.3) with relevance to Ccp1's antioxidant role as a H₂O₂ sensor/signaling molecule and its possible heme transfer/heme trafficking functions as discussed in the *Introduction*. Future consideration of other interacting partners will likely shed additional light on Ccp1's biological functions.

Table 5.2: GST-apoCcp1 and GST-holoCcp1 interacting proteins detected in 1 d cells

Bait protein ^a	Accession number ^b	Protein ID ^c	% sequence coverage ^d	Unique peptides ^e	Cell location ^f	Extract ^g
apo-, holoCcp1	YJR048W	CYC1^h	56.9 ± 5.8	2 ± 0	M	S2, P10
apo-, holoCcp1	YHR008C	SOD2	65.2 ± 8.7	13 ± 2	M	S2, P10
apo-, holoCcp1	YGR192C	TDH3	67.5 ± 11.4	12 ± 3	C, M, PM	S2, P10, S10
apo-, holoCcp1	YJR009C	TDH2	60.8 ± 9.4	10 ± 4	C, M	S2, P10, S10
apoCcp1	YBL030C	PET9	61.0 ± 10.4	22 ± 2	M	S2, P10
apo-, holoCcp1	YMR186W	HSC82: HSP90	39.7 ± 15.8	4 ± 2	C, M, PM	S2, P10
apo-, holoCcp1	YDL229W	SSB1/SSB2: HSP70^h	35.1 ± 4.6	4 ± 1	PM	S2, P10
apo-, holoCcp1	YAL005C	SSA1:HSP70	60.0 ± 5.8	6 ± 2	C, N, PM	S2, S10
apo-, holoCcp1	YLL024C	SSA2:HSP70	48.4 ± 4.6	4 ± 1	C, V, M	S2, P10, S10

^a Bait proteins: GST-apoCcp1 and GST-holoCcp1

^b The GenBank identifier assigned to each gene sequence

^c 4 letter/number notation for yeast protein

^d The percentage of a protein's residues in its peptides identified by LC-MS.

^e A peptide that exists only in one protein of the proteome of interest, which here is *S. Cerevisiae*

^f Subcellular location: C, cytoplasm/cytosol; M, mitochondria; PM, plasma membrane; V, vacuole; N, nucleus; R, ribosome.

^g Subcellular fraction in which prey proteins were trapped: S2, denucleated cell lysate; P10, crude mitochondria-enriched fraction; S10, mitochondria-depleted fraction

^h Interactions in red font have been previously identified (see Table 5.5)

Table 5.3: GST-apoCcp1 interacting proteins detected in 7 d cells

Bait protein ^a	Accession number ^b	Protein ID ^c	% sequence coverage ^d	Unique peptides ^e	Cell location ^f	Extract ^g
apoCcp1	YJR104C	SOD1	66.2 ± 12.5	6 ± 2	C	S2, S10
apoCcp1	YGR209C	TRX2	37.5 ± 3.2	4 ± 1	C, V	S2, S10
apoCcp1	YML028W	TSA1^h	63.3 ± 5.2	11 ± 2	C	S2, S10
apoCcp1	YGR192C	TDH3	61.7 ± 10.4	7 ± 3	C, M PM	S2, P10, S10
apoCcp1	YJL052W	TDH1	50.9 ± 12.6	12 ± 4	C, M	S2, P10, S10
apoCcp1	YJR009C	TDH2	50.6 ± 6.9	8 ± 3	C, M	S2, P10, S10
apoCcp1	YPL240C	HSP82/HSP90	37.9 ± 4.3	4 ± 1	C	S2, S10
apoCcp1	YDL229W	SSB1/SSB2: HSP70^h	37.4 ± 7.3	4 ± 1	PM	S2, S10
apoCcp1	YAL005C	SSA1:HSP70	60.0 ± 11.8	6 ± 4	C, N, PM	S2, S10
apoCcp1	YLL024C	SSA2:HSP70	48.4 ± 9.5	6 ± 2	C, V, M	S2, P10, S10

^{a-h} See corresponding footnotes to Table 5.2

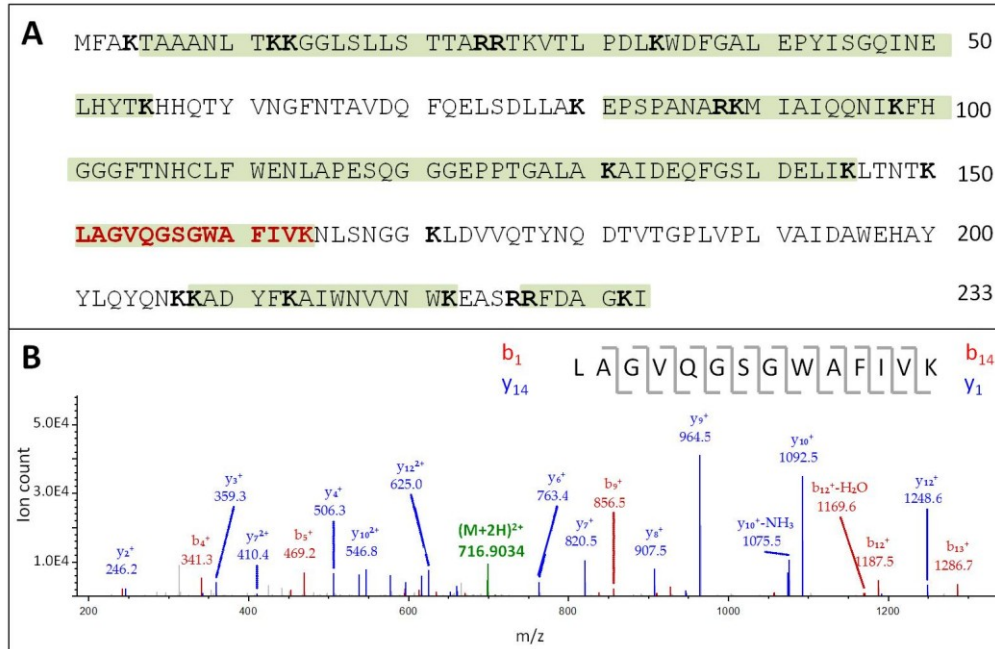


Figure 5.3. Identification of Sod2 in a GST-holoCcp1 pull down from the P10 extract from 1 d yeast. (A) Sod2 sequence with the trypsin cleavage sites (**K**, **R**) bolded and peptides covered by MS/MS highlighted in green. **(B)** MS2 spectrum of the $(M+2H)^{2+}$ ion of peptide **LAGVQGSWAFIVK**. The precursor ion at m/z 716.9034 (green) was fragmented by CID (30 V) to give b_n (red) and y_n sequence ions (blue). High confidence Sod2 identification arises from the peptide confidence parameters including: 3.3 ppm error between the observed and calculated MH^+ ion (1432.8 m/z), Xcorr 4.56 and 21/26 ion match. The results are representative of 2 independent experiments using GST-holoCcp1 and GST-apoCcp1 to probe both S2 and P10 ($n=8$, Table 5.2).

5.5.3) GST-apoCcp1 and GST-holoCcp1 bait Sod2, an antioxidant enzyme, in 1 d yeast.

Mitochondrial Sod2 was reproducibly identified in 16 out of 16 independent experiments as an interacting partner of GST-apoCcp1 and GST-holoCcp1 in 1 d cells (Tables 5.2, S5.2) but not of the negative control, GST (Table S5.4). Sod2 was identified with 65.2 ± 8.7 sequence coverage and 13 ± 2 unique peptides (Table 5.2, S5.2), and Figure 5.3 indicates that the Sod2 peptides were identified with high confidence. To independently confirm Sod2 as an interacting partner of Ccp1, GST-Sod2 pull-downs were examined in a yeast strain (Table 1) overexpressing the fusion protein. Figure S5.2 confirms that these cells do indeed overexpress the GST-Sod2 bait and include Ccp1 as a binding partner. The presence of Ccp1 in the pull-downs from 1 d

yeast was confirmed by LC-MS/MS and Western blotting using the anti-Ccp1 antibody (Figure 5.4A, B). Although Sod2 and Ccp1 are reported to be matrix and IMS localized proteins respectively, our results strongly suggest that these proteins interact in the mitochondria of exponentially growing cells.

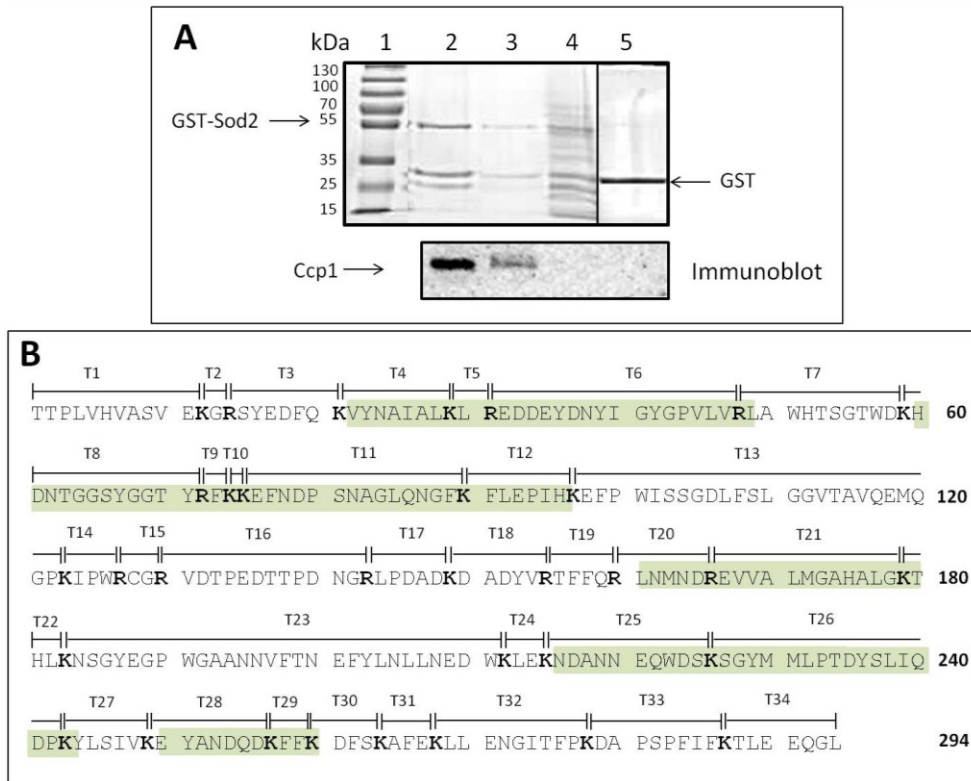


Figure 5.4. Identification of Ccp1 in a GST-Sod2 pull down from a 1 d S2 denucleated extract. (A) Top panel: Coomassie-stained 12% SDS PAGE of GST-Sod2 bait protein and prey proteins in the S2 extract of yeast expressing GST-Sod2. The molecular weight markers (kDa) are in lane 1, proteins pulled down by the GST-Sod1 bait in a two step elution from GSH magnetic beads are shown in lanes 2, 3; and by the GST control bait in lane 5. Lane 4 shows Sod2-GST-GSH magnetic beads boiled in SDS loading buffer. Arrows indicate the bands containing the bait proteins. The experimental conditions are given in the caption to Figure 2. **Bottom panel:** Anti-Ccp1 immunoblot analysis of a region of the gel in the top panel confirming that Ccp1 is present in lane 2 and 3. The experimental details are given in the *Materials and Methods*. **(B)** Ccp1 sequence with the trypsin cleavage sites (**K**, **R**) bolded and peptides covered by MS/MS highlighted in green. We detect ~33% sequence coverage of Ccp1 and 9 ± 1 unique peptides in the GST-Sod2 pull downs. The results are representative of 2 independent experiments ($n=2$).

5.5.4) GST-apoCcp1 baits Sod1, an antioxidant enzyme, in 7 d yeast. Yeast possess two Sod isoforms, the second being a copper- and zinc-containing enzyme, Sod1, which represents 90% of the total cellular SOD activity. Sod1 is located primarily in the cytosol (223), but it was also found in the nucleus (224) and 1-5% accumulates in the mitochondrial IMS along with its metallochaperone, CCS (225). However, Sod1 was identified as a binding partner of GST-apoCcp1 only in 7 d S2 and S10 extracts (Tables 5.3, S5.3) and was not pulled down in any other extracts. Perhaps PTMs in extramitochondrial Sod1 from stationary-phase yeast promote its interaction with Ccp1, which may play a role in the cell's response to H₂O₂ challenge (see *Discussion*).

5.5.5) GST-apoCcp1 baits Tsa1, an antioxidant enzyme, in 7 d yeast.

Thiol-specific thioredoxin peroxidase (Tsa1) and its reducing substrate cytoplasmic thioredoxin (Trx2) were reproducibly pulled down by GST-apoCcp1 in S2 and S10 extracts from 7 d cells (Table 5.3, S5.3). Interestingly, Tsa1 has been previously identified as an interacting partner of Ccp1 through genetic analysis of synthetic fitness or lethality defect (SFL) interactions (Table S5.4) (226). Furthermore, challenge with H₂O₂ of wild-type yeast and yeast expressing the catalytically inactive Ccp1^{W191F} variant (121) (in the CEN.PK2-1C genetic background) resulted in increased Tsa1 mRNA expression (54). Tsa1 and Trx2 are pulled down by GST-apoCcp1 in 7 d yeast, which may be because their expression is regulated by the oxidative-stress-responsive transcription factors, Yap1 (53) and Skn7 (108), and stationary-phase yeast generate high ROS levels (52).

5.5.6 GST-apoCcp1 baits Pet9, a possible heme transporter, in 1 d yeast.

Using the same lysates, Pet9 was reproducibly identified with ~71% sequence coverage and 22 unique peptides (Table 5.2, Figure 5.5) as a potential binding partner of GST-apoCcp1 but not of GST-holoCcp1. This suggests that Ccp1's interacting site for Pet9 may be masked on heme insertion. Pet9 is a member of the gene family encoding adenine nucleotide translocators (ANTs) of the mitochondrial inner membrane (227, 228). The primary role of ANTs is to pump ADP into the mitochondrial matrix and ATP out of the matrix. However, under aerobic conditions, ANTs function in the opposite direction, importing ATP into mitochondria (227, 228). Additionally ANTs have been reported to bind heme and competition experiments suggest that ANTs can import heme precursors into mitochondria (36) (see *Discussion*).

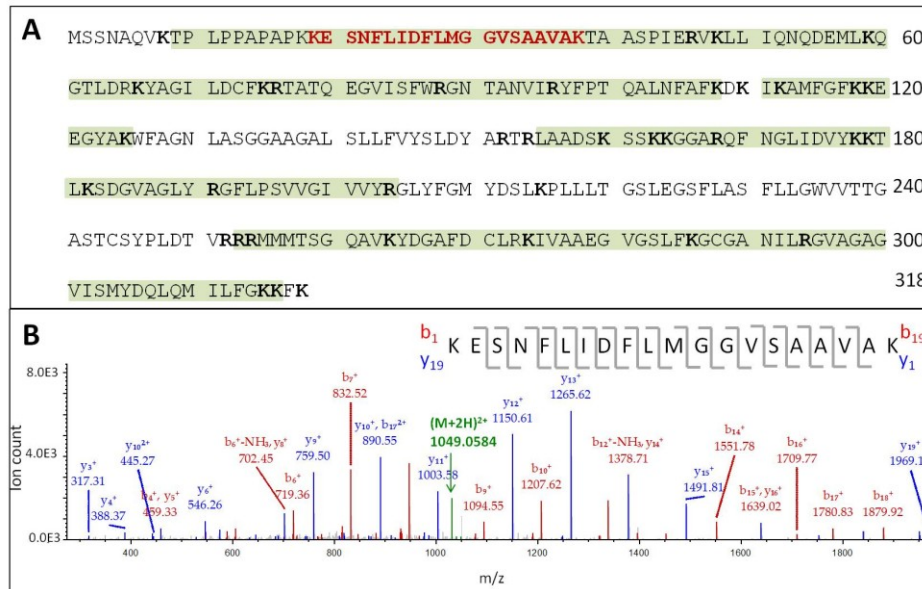


Figure 5.5. Identification of Pet9 in a GST-apoCcp1 pull down from P10 extract from 1 d yeast. (A) Pet9 sequence with the trypsin cleavage sites (**K**, **R**) bolded and peptides covered by MS/MS are highlighted in green. (B) MS2 spectrum of the $(M+2H)^{2+}$ ion at m/z 1049.0584 of peptide **KESNFLIDFLMGGVSAAVAK**. The precursor ion (green) was fragmented by CID (30 V) to give b_n (red) and y_n sequence ions (blue). Peptide confidence parameters include: 2.2 ppm error between the observed and calculated MH^+ ion (m/z 2097.1), Xcorr 6.42 and 31/38 ion match. The results are representative of 4 independent experiments using GST-apoCcp1 to probe both S2, P10 and S10 ($n=8$, Table 5.2).

5.5.7) GST-apoCcp1 and GST-holoCcp1 bait the 3 isoforms of GAPDH (TDH3/2/1) in 1- and 7 d yeast.

Proteins reproducibly pulled down by both GST-apoCcp1 and GST-holoCcp1 include the three isoforms of GAPDH (Tdh3/2/1) found in yeast. Although each isoform is highly abundant ($\sim 1\text{-}2 \times 10^5$ molecules/cell) (229), no isoforms are pulled down by GST, the negative control (Table S5.4) suggesting that Tdh3/2/1 interacts specifically with Ccp1. In contrast, the Eno1/2 isoforms present at $\sim 10^5$ molecules/cell are pulled down by both GST-Ccp1 and GST. We identified Tdh3/2/1 with 50-70% sequence coverage and 8-12 unique peptides (Tables 5.2, 5.3), and Figure 5.6 shows MS2 spectra of peptides unique to each isoform, which were identified with high confidence.

5.5.8) GST-apoCcp1 and GST-holoCcp1 bait Hsp70 and Hsp90 in 1- and 7 d yeast.

A number of heat shock proteins (Hsp) are identified as binding partners of GST-apoCcp1 and GST-holoCcp1 (Tables 2, 3, S2, S3). Reproducible partners include proteins from the Hsp70 and Hsp90 families, which function as molecular chaperones involved in the folding and maturation of a significant fraction of the proteome, including many proteins involved in signal transduction and the stress response. *S. cerevisiae* encodes six cytosolic Hsp70s, Ssa1–4 (heat-shock inducible), and Ssb1-2 (heat-shock repressed) that differ in expression pattern but are together essential for cell viability (230). Specifically, GST-Ccp1 pulls down Ssa1, Ssa2, Ssb1 and Ssb2 in 1 and 7 d yeast extracts (Tables 2, S2, S3) and we note that Ssb2 has been reported as binding partner of Ccp1 in interactome studies (Table S5). *S. cerevisiae* also expresses two Hsp90 isoforms, with Hsc82 constitutively expressed and Hsp82 induced by stress such as heat shock (231). We detect Hsc82 with GST-holoCcp1 in the S2 and P10 1 d extracts (Tables 2, S2) and Hsp82 with GST-apoCcp1 in the 7 d S2 and S10 extracts (Tables 3, S3). The

detection of Ccp1-Hsp interactions with such high reproducibility and our high confidence in Hsp peptide identification (Table 2,3 S2, S3) enticed us to speculate that Hsp proteins may bind to nascent apo-preCcp1 to prevent its misfolding before maturation and/or to prevent nonspecific interactions or aggregation during mature apoCcp1's migration from the mitochondria to its new cellular locations. Hsp90 also has roles in heme trafficking as elaborated in the *Discussion*.

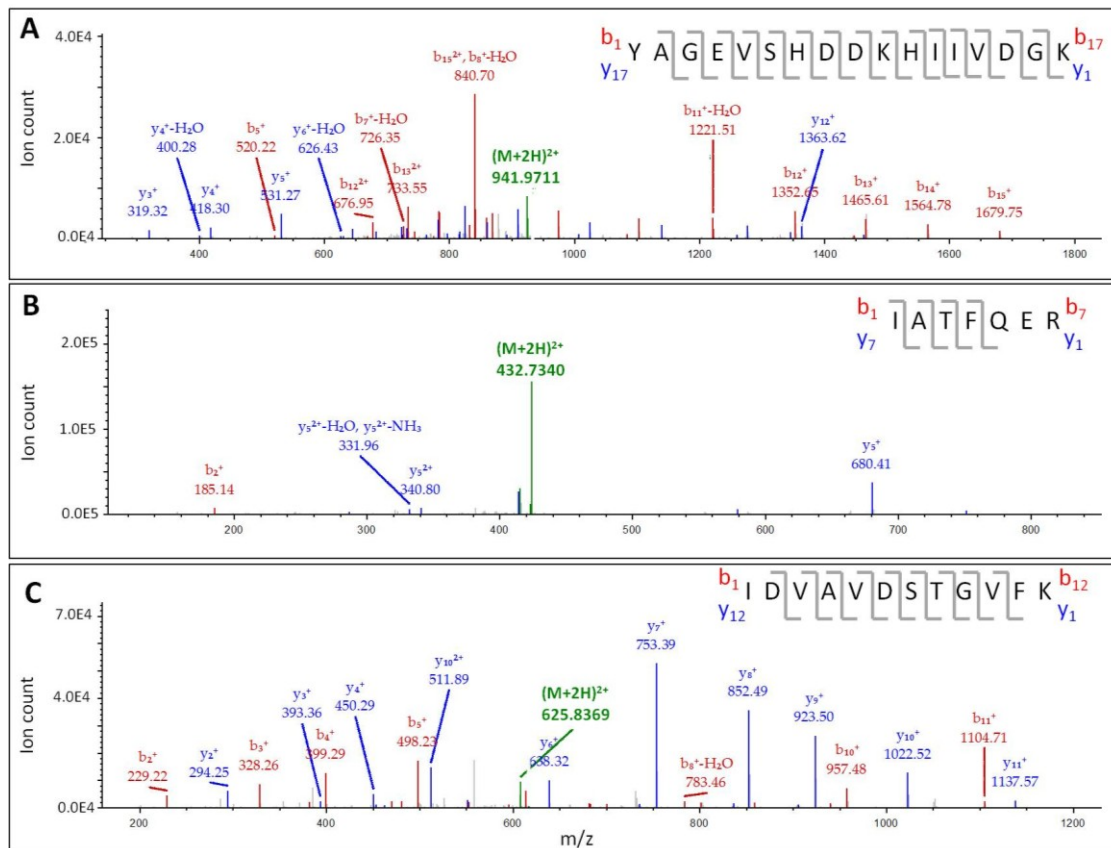


Figure 5.6. Identification of the Tdh3/2/1 isoforms of GAPDH in a GST-apoCcp1 pull down from a S2 extract from 7 d yeast. MS2 spectrum of the $(M+2H)^{2+}$ ion of: (A) Tdh3 tryptic peptide **YAGEVSHDDKHIIVDGK** at m/z 941.9711; (B) Tdh2 tryptic peptide **IATFQER** at m/z 432.7340, (C) Tdh3 tryptic peptide **IDVAVDSTGVFK** at m/z 625.8369. The precursor ions (green) were fragmented by CID (30 V) to give b_n (red) and y_n sequence ions (blue). Peptide confidence parameters include 2.8, 3.0 and 3.9 ppm error between the observed and calculated MH^+ ions; Xcorr values of 4.93, 2.04 and 3.15; and 20/23, 10/12 and 20/22 ion matches for the peptides in panels A, B and C, respectively. These peptides are isoform specific as revealed by the Tdh3/2/1 sequence alignment in Figure S5.3. The results are representative of 4 independent experiments using GST-apoCcp1 to probe S2, S10 and P10 ($n=12$, Table 5.3).

5.6) Discussion

Building on our unexpected discovery that Ccp1 functions as a mitochondrial H₂O₂ sensor and heme donor (50, 118) we sought to investigate its protein binding partners in yeast. Using affinity purification and high-resolution LC-MS/MS we identify 45 unique proteins that are potential Ccp1 binding partners (Tables S5.2, S5.3), only four of which have been identified previously (Table S5.5). Since a subset of these proteins (Tables 5.2, 5.3) have well-characterized antioxidant functions and/or may participate in heme transport/heme trafficking, we discuss below the possible physiological relevance of their interactions with Ccp1, which opens up new avenues of investigation into the role of this peroxidase in its different subcellular locations. This in turn will likely identify new protein-protein interactions critical in coordinating the antioxidant response and heme trafficking in cells, two key interrelated physiological processes.

5.6.1) Ccp1's peroxidase function.

Ccp1 is a highly efficient peroxidase *in vitro* with mitochondrial Cyc^{II} from various sources, including horse heart and yeast, as a reducing substrate (Eqs. 1-3) (232). Cyc1 has been identified by numerous methods, from co-crystallization to affinity purification experiments with tagged Ccp1 as bait (Table S5.5). We detect a Cyc1-Ccp1 interaction in the mitochondria-containing S2 and P10 extracts from 1 d yeast. Both GST-apoCcp1 and GST-holoCcp1 pull down the cytochrome, which is identified with ~57% sequence coverage and two unique peptides (Table 5.2). As expected, no Cyc1 is detected in the mitochondria-free S10 extract from 1 d cells, but surprisingly, GST-apoCcp1 did not pull down Cyc1 from 7 d mitochondrial extracts (Tables 5.3, S5.3). Possible reasons for the loss of this binding interaction could be due to PTMs in Cyc1 or its tighter association with the mitochondrial membrane in 7 d yeast.

5.6.2) Possible H₂O₂ channeling from Sod2 to Ccp1 and possible Ccp1-Sod1/2 crosstalk.

We have biochemical evidence that Ccp1 expression decreases the level of Sod2 activity (50). However, direct interaction between these proteins is surprising since Sod2 has been localized to the mitochondrial matrix (232) whereas mature Ccp1 is found in the IMS of exponentially growing cells (50, 58, 67, 118). The H₂O₂ produced in respiring yeast mitochondria is derived mainly from the dismutation of superoxide (O₂^{•-}) generated by one-electron reduction of O₂ in the electron-transport chain (112). Although O₂^{•-} spontaneously dismutates to H₂O₂ and O₂ ($k \sim 10^5 - 10^6 \text{ M}^{-1}\text{s}^{-1}$), its level in cells is controlled by SODs, which catalyze this reaction ($k \sim 10^9 \text{ M}^{-1}\text{s}^{-1}$) (112). Thus, direct interaction between Ccp1 and Sod2 and close contact of their catalytic sites would allow direct H₂O₂ channeling from the dismutase to the peroxidase and promote Ccp1's role as an H₂O₂ sensor. Our previous work suggests that the spike in H₂O₂ during the diauxic shift as Cyc1 synthesis is ramping up results in Ccp1 overoxidation and labilization of its heme, which is transferred to apoCta1 (118). Direct channeling of H₂O₂ from Sod2 to Ccp1's heme would promote overoxidation of the peroxidase by inhibiting H₂O₂ scavenging by other metal centers such as Cyc1 and Ccp1-Sod1 complexation may slow down electron transfer from Cyc1^{II} to CpdI/II (Eqs. 2, 3). Clearly, this intriguing interaction between Ccp1 and Sod2 warrants further investigation, including careful screening of submitochondrial fractions for the presence of Ccp1 and Sod2 as well as assaying for H₂O₂ channelling between the purified proteins *in vitro*.

Yeast's abundant and largely cytosolic Sod1 also localizes to the IMS (225) and under oxidative stress to the nucleus (224). No Sod1 was pulled down in 1 d extracts but GST-apoCcp1 pulled down Sod1 from the S2 and S10 extracts of 7 d cells (Table 5.3, S5.3). Since S2 extracts are largely depleted of nuclei and S10 extracts are depleted of both nuclei and mitochondria, the

added GST-apoCcp1 must be interacting with cytosolic Sod1. Why this interaction is not detected in 1 d extracts is not obvious at present, but may require age-induced PTMs in Sod1 (165), or other partners may displace Sod1 from Ccp1 in 1 d cells. Interestingly, exogenous H₂O₂ challenge is sufficient to promote Sod1 nuclear localization, where it binds to promoters and regulates the expression of repair and antioxidant genes, including Tsa1 and Prx1 (224). Skn7 together with Yap1 regulates the expression of Ccp1, Tsa1, Trx2, Ctt1, Sod1/2, Ssa1 and Hsp82 (108). As discussed in the next section, Ccp1 may also localize to the nucleus and interact with the nuclear transcription factor Skn7 in response to H₂O₂ challenge (54). Binding partners of Sod1/2 identified in interactome studies include 78 different protein partners which can be viewed at www.yeastgenome.org. Interestingly, Ccp1 is not in the list but Sod1 and Sod2 bind to each other. Thus, these two Sod isoforms may compete for binding to Ccp1, which may be driven by PTMs in the partners.

5.6.3) Interaction with Tsa1 and Hsp70 may target extramitochondrial Ccp1 to the nucleus and vacuole, respectively.

GST-apoCcp1 pulls down Tsa1, a peroxiredoxin (Prx), in the S2 and S10 extracts of 7 d cells (Table 5.3). *S. cerevisiae* produces five Prxs namely, the thiol-specific antioxidant proteins Tsa1 and Tsa2, disrupter of telomere silencing protein 5 (Dot5), alkyl hydroperoxide reductase 1 (Ahp1) and Prx1, which differ in their target substrates and subcellular location (233). Cytosolic Tsa1, the most abundant yeast Prx, is crucial for resistance to exogenously added H₂O₂ (234, 235) as is Ccp1 (50) which conveys an oxidative stress signal to the nuclear transcription factor, Skn7 (54). Previously, we found ~10% of extramitochondrial Ccp1 in the nucleus of 7 d cells (118), and we speculate that interaction with Tsa1 may play a role in targeting Ccp1 to this organelle and in Skn7 activation. Skn7 cooperates with a second transcription factor, Yap1, to

regulate the expression of numerous antioxidant enzymes, including Ccp1 and Tsa1 (108). Since we examine denucleated fractions in this study, we did not find Skn7 in our pull-down assays, but possible coordination between apoCcp1 and Tsa1, and possibly Sod1, in controlling the Skn7/Yap1 regulon (108) merits further investigation.

Previously, using fluorescence microscopy we observed that chromosomally expressed Ccp1-GFP (green fluorescent protein) is largely associated with the vacuole in 7 d cells (118). Hsp70s, which are pulled down by both GST-apoCcp1 and GST-holoCcp1 in S10 and P10 extracts from 1- and 7 d cells (Tables 5.2, 5.3), participate in the transfer of cytosolic proteins to yeast vacuoles (236–238). Intriguingly, Ccp1 possesses the pentapeptide motif (KLEKN) identified as the chaperone-mediated-autophagy (CMA) targeting signal recognized by the cytosolic Hsp70 chaperones that deliver substrates to the lysosomes of higher eukaryotes for degradation (239). However, since we detected full-length mature Ccp1 in 7 d cells by immunoblotting (118), vacuolar localization must not trigger its immediate degradation, which suggests that Ccp1 may have signaling roles associated with this organelle. Cytosolic Hsp70s also are known to assist in the translocation of proteins into the ER (240, 241) and mitochondria (242), and their detection in P10 mitochondria-enriched extracts which also contain ER, Golgi and vacuoles (Tables 5.2, 5.3) suggests that they may play a role in stabilizing apoCcp1, for example.

5.6.4) Does Pet9 play a role in heme insertion into Ccp1?

Processing of immature preCcp1 to the mature form involves insertion of a single noncovalently bound b-type heme (58, 243). Mature Ccp1 is located in the IMS but maturation involves threading of the 68-residue mitochondrial-targeting presequence through the inner membrane such that the N-terminus of the immature protein is located in the matrix (58, 243).

Since mature holoCcp1 but not mature apoCcp1 is retained by the outer mitochondrial membrane (67), we speculate that heme loading occurs while pre-apoCcp1 is anchored in the inner membrane. Significantly, GST-apoCcp1 reproducibly pulls down Pet9, the major ADP/ATP carrier of the inner membrane, from the S2 and P10 extracts of 1 d cells (Table 5.2) while no interaction is detected with GST-holoCcp1. *In vitro* biochemical analysis reveals that the mammalian homologue of Pet9 (ANT) also can function as a heme transporter (36), which implicates Pet9 in heme transfer to pre-apoCcp1 at the inner mitochondrial membrane.

Mitochondria are the sole heme synthesizers in budding yeast since the last two reactions of heme synthesis occur in this organelle (31). The final reaction, the insertion of ferrous iron into protoporphyrin IX (31), is catalyzed by ferrochelatase (FECH), which like Pet9, is located in the mitochondrial inner membrane (33). Thus, it is possible that Pet9 is an intermediate in heme transfer from FECH to pre-apoCcp1. However, this requires further investigation since the extracts were not treated to solubilize membrane proteins, which could have prevented the pull down of FECH by GST-Ccp1. Nonetheless, our screening suggests a possible pathway of heme transfer from FECH to Pet9 to preCcp1, which on maturation and overoxidation transfers heme directly or indirectly to Cta1 (118). The catalase was not detected in our analyses (Tables 5.2, 5.3, S5.2, S5.3) but given its low copy number ($<10^3$ molecules/cell) it might have missed detection. Thus, experiments are currently underway to determine if Ccp1 will be pulled down in yeast overexpressing GST-Cta1 as performed here for GST-Sod2. The interactome results collated in the yeast genome database do not include FECH, Pet9 or Cta1 as binding partners of Ccp1 but detection of transient interactions such as that required for heme transfer may require overexpression of the bait protein as performed in the present study.

5.6.5) Heme transfer may occur between GAPDH and Ccp1.

GAPDH catalyzes the conversion of glyceraldehyde-3-phosphate to 1,3-bisphosphoglycerate, which led to its classification as a glycolytic enzyme. However, it possesses additional roles in several unrelated non-metabolic processes, including control of gene expression and apoptosis (244). Recent studies revealed that GAPDH binds heme reversibly and facilitates heme insertion into inducible nitric oxide synthase (iNOS) (245). Redox PTMs such as S-nitrosation of its catalytic C152 (human enzyme numbering) influence GAPDH's subcellular localization (244) and heme binding (245), which suggests that the dehydrogenase is a possible heme carrier protein, a function that appears to be regulated by oxidative PTMs including S-nitrosation (245).

The three GAPDH isoforms in yeast exhibit 88-96% sequence similarity (Figure S5.3), and constitute ~20% of the yeast proteome. Tdh3 is primarily found in the cytoplasm but also in the nucleus and H₂O₂-induced PTMs drive it into the mitochondria (246, 247). Tdh1/2 localize to the cytoplasm and mitochondria (246, 248), and while Tdh1 is synthesized only in stationary-phase cells, Tdh2/3 are also present during exponential growth (246). GST-apoCcp1 and GST-holoCcp1 reproducibly pulled down Tdh2/3 from 1 d cells (Table 5.2) whereas GST-apoCcp1 pulled down all three isoforms from 7 d extracts (Table 5.3). Given the high sequence similarity between the three isoforms and the ability of GST-apoCcp1 and GST-holoCcp1 to bind all isoforms suggests that Tdh3/2/1 binds to Ccp1 through a common binding site that is clearly not present in the GST tag alone (Table S5.4) and does not seem to depend on the heme-status of Ccp1. The multiplex locations of GAPDH and Ccp1 allow a number of possible interactions to occur in different cellular locations as well as in response to a number of environmental cues. This diversity in cellular location and the lack of discrimination by GAPDH between apo- and

holoCcp1 forms suggests that apoGAPDH could accept heme from holoCcp1 and vice versa, a scenario that warrants further investigation.

5.6.6) Hsp90 may influence Ccp1's heme status.

Interestingly, heat shock proteins have been shown to be important in heme regulation (249, 250). Synthesis of this highly conserved family of proteins is induced by stress and many function as molecular chaperones that shield, fold, or unfold substrates in a context-dependent manner (251). In yeast cells, the transcriptional regulator Hap1, whose activity is stringently controlled by the heme concentration, is a substrate of Hsp90 (249). Biochemical and genetic analyses reveal that Hsp90 may promote heme binding to Hap1 and induce or maintain it in a transcriptionally active conformation (249). Furthermore, Hsp90 was found associated with heme-free iNOS in mouse cytokine cells (250), and heme insertion coincided with Hsp90 dissociation *in vitro* (250), which suggests a potential role for Hsp90 in controlling the heme status of proteins.

We find that a number of heat shock proteins specifically interact with Ccp1 (Tables S5.2, S5.3). Hsp90 is pulled down from 1 d S2, P10 and 7 d S10 lysates by both GST-apoCcp1 and GST-holoCcp1 (Tables 5.2, S5.2, S5.3). Thus, Hsp90 may promote heme binding to apoCcp1 and/or heme transfer from holoCcp1 to acceptors such as Cta1. Interestingly, Hsp90 has been identified as a partner of Tdh3/2/1 while Tdh2/1 (252–254) have been identified as interacting partners of Hsp90 (252, 254) in interactome studies. Whether Hsp90 and/or GAPDH function as heme chaperones will be further addressed in our studies using GST-Cta1 as a bait protein.

5.7) Conclusion

Using recombinantly expressed GST-Ccp1 as bait, we detected numerous novel proteins that interact with Ccp1. Potential binding partners include those of relevance to its role in heme transfer and heme trafficking (Tdh3/2/1, Pet9 and Hsp90) and those that likely regulate its antioxidant roles (Cyc1, Sod1/2, Tsa1, Trx1, Hsp70). Many of these interactions possibly influence Ccp1's subcellular localization as well. Our discovery-driven study opens numerous new opportunities for hypothesis-driven investigations into the coordination of intracellular heme trafficking and cellular antioxidant responses, which are highly interrelated, vital processes in aerobic cells.

Comprehensive surveys of all of the protein complexes detected in yeast (the yeast interactome) are published and collated in the BioGRID (<http://thebiogrid.org/>) and *Sacharromyces* genome database (SGD) (www.yeastgenome.org/). Most of the reported complexes were identified in large-scale interactome networks built from proteomic interactions detected by yeast two-hybrid and affinity-purification methods (215–217). Such global approaches suffer from poor reproducibility with < 9% overlap between datasets (255) and are limited to a single stage of cell growth, which does not reveal the dynamics that govern protein signalling and cellular localization as exposed here in our discovery study targeted to Ccp1's binding partners.

5.8) Supplementary information

Table S5.1: CCP activity of GST-holoCcp1^a

Protein ^b	CCP activity ^a	Percent activity ^c
Wild-type Ccp1	1.70 ± 0.010	100 ± 0.00
GST-apoCcp1	0.96 ± 0.020	56.4 ± 4.86
GST-holoCcp1	0.06 ± 0.008	3.50 ± 0.30

^a One unit of CCP activity catalyzes the oxidation by H₂O₂ of 1 μmol of horse heart ferrocytochrome c per min per mg Ccp1.

^b Recombinant Ccp1, GST-apoCcp1 and GST-holoCcp1 (1 μM) were assayed for CCP activity as described previously. For the assay, a stock solution of Cyc^{III} was ~90% reduced with sodium dithionite and the Cyc^{II} concentration determined spectrophotometrically ($\epsilon_{550} = 7.6 \text{ mM}^{-1} \text{ cm}^{-1}$).⁽⁷⁸⁾

^c The activity of each fraction was ratioed by the activity of wild-type Ccp1 to give percent activity. Results are presented as averages ± SD from three independent experiments ($n=3$).

Table S5.2: Proteins in GST-apoCcp1 and GST-holoCcp1 pull downs from 1 d yeast extracts ($n=2$)^a

Accession ^b number	Protein ID ^c	Protein description ^d	Times detected ^e	% sequence Coverage ^f	Unique peptides ^g	Cellular Location ^h	Subcellular fraction ⁱ	Bait protein ^j
YCR012W	PGK1	Phosphoglycerate kinase	11/12	63.5 ± 13.7	25 ± 6	M, PM, C	S2, P10, S10	apo
YGR192C	TDH3:	Glyceraldehyde-3-phosphate dehydrogenase 3	12/12	67.5 ± 11.4	12 ± 3	C, M PM	S2, P10, S10	apo/holo
YJR009C	TDH2	Glyceraldehyde-3-phosphate dehydrogenase 2	10/12	60.8 ± 9.4	10 ± 4	C, M	S2, P10, S10	apo/holo
YAL005C	SSA1: HSP70	Heat shock protein 70	8/8	60.0 ± 5.8	6 ± 2	C, N, PM	S2, S10	apo/holo
YGR254W	ENO1	Enolase 1	12/12	57.4 ± 12.6	9 ± 1	M, C, PM	S2, P10, S10	apo/holo
YHR174W	ENO2	Enolase 2	12/12	56.1 ± 13.9	9 ± 4	V, M, PM	S2, P10, S10	apo/holo
YOR020C	HSP10	Heat shock protein 10	6/8	53.8 ± 10.4	4 ± 2	M matrix	S2, P10	holo
YOL109W	ZEO1	Protein ZEO1	6/8	52.2 ± 8.4	7 ± 1	M	S2, P10	holo
YKL152C	GMP1	Phosphoglycerate mutase 1	9/12	49.0 ± 7.1	12 ± 3	M	S2, P10, S10	apo
YLL024C	SSA2: HSP70	Heat shock protein 70	12/12	48.4 ± 4.6	4 ± 1	C, V, M	S2, P10, S10	apo/holo
YLR259C	HSP60	Heat shock protein 60	4/8	46.9 ± 3.2	27 ± 3	M	S2, P10	apo/holo
YPR080W	TEF1	Elongation factor 1-alpha	7/12	44.1 ± 4.8	19 ± 2	C, V, M	S2, P10, S10	apo
YDR155C	CPR1	Peptidyl-prolyl cis-trans isomerase	4/8	42.6 ± 4.2	7 ± 4	M, N	S2, P10	holo
YKL085W	MDH1	Malate dehydrogenase	4/8	41.3 ± 5.7	8 ± 3	M	S2, P10	holo
YNL178W	RPS3	40S ribosomal protein	10/12	40.4 ± 3.6	7 ± 1	R	S2, P10, S10	apo/holo
YMR186W	HSC82: HSP90	Heat shock protein 90	8/8	39.7 ± 15.8	4 ± 2	C, M, PM	S2, P10	holo
YHL015W	RPS20	40S ribosomal protein	8/12	38.8 ± 4.4	5 ± 1	R	S2, P10, S10	apo/holo
YLL050C	COF1	Cofilin	5/8	38.4 ± 5.8	4 ± 2	PM	S2, P10	apo/holo
YJR045C	SSC1	Heat shock protein	8/8	37.1 ± 4.9	20 ± 3	M	S2, P10	apo/holo
YBL099W	ATP1	ATP synthase subunit alpha	5/8	36.9 ± 8.4	17 ± 5	M	S2, P10	apo
YPR191W	QCR2	Cytochrome b-c1 complex subunit 2	5/8	36.4 ± 3.1	10 ± 2	M	S2, P10	holo
YNL055C	POR1	Porin	6/8	36.0 ± 9.6	10 ± 2	M	S2, P10	apo/holo
YDL229W	SSB1/ SSB2 – HSP70	Heat shock protein 70	8/8	35.1 ± 4.6	4 ± 1	PM	S2, P10	apo/holo
YDR050C	TPI1	Triosephosphate isomerase	10/12	34.3 ± 8.5	7 ± 2	M, C, PM	S2, P10, S10	apo/holo
YOR374W	ALD4	Potassium-activated	7/8	32.4 ± 7.4	12 ± 3	M	S2, P10	apo/holo

		aldehyde dehydrogenase						
YNL302C	RPS19B	40S ribosomal protein	9/12	31.9 ± 3.2	4 ± 1	R	S2, P10, S10	apo/holo
YDR447C	RSP17B	40S ribosomal protein	9/12	30.9 ± 2.8	4 ± 1	R	S2, P10, S10	apo/holo
YMR143W	RPS16A	40S ribosomal protein	7/12	30.7 ± 6.7	4 ± 1	R	S2, P10, S10	apo/holo
YBL030C	PET9	ADP,ATP carrier protein 2	9/12	61.0 ± 10.4	22 ± 2	M	S2, P10, S10	apo
YJR048W	CYC1	Cytochrome c iso-1	6/8	56.9 ± 5.8	2 ± 0	M	S2, P10	holo
YHR008C	SOD2	Mn Superoxide dismutase	8/8	65.2 ± 8.7	13 ± 2	M	S2, P10	apo/holo

^a Proteins identified with high confidence are listed

^b The GenBank (<http://www.ncbi.nlm.nih.gov/genbank/>) identifier assigned to each gene sequence

^c Four/Five-letter/number yeast notation for protein

^d Protein name/description from given reference(s) and/or SGD website

^e This protein was trapped the indicated number of times in 2 independent experiments using S2, P10 and S10 lysates with GST-apoCcp1 (first number) and GST-holoCcp1 (second number) as bait.

^f The percentage of a protein's residues in its peptides identified by LC-MS.

^g A peptide that exists only in one protein of the proteome of interest, which here is [S. Cerevisiae](#)

^h Subcellular location: C, cytoplasm/cytosol; M, mitochondria; PM, plasma membrane; V, vacuole; N, nucleus; R, ribosome.

ⁱ Subcellular fraction in which prey proteins were trapped: S2, denucleated cell lysate; P10, crude mitochondria-enriched fraction; S10, mitochondria-depleted fraction

^j Bait proteins: GST-apoCcp1 and GST-holoCcp1

Interactions in red font have been previously identified (see Table 5.5)

Table S5.3: Proteins in GST-apoCcp1 pull downs from 7 d yeast extracts (n=4) ^a

Accession ^b number	Protein ID ^c	Protein description ^d	Times detected ^e	% sequence Coverage ^f	Unique peptides ^g	Cellular Location ^h	Subcellular fraction ⁱ
YBR072W	HSP12	Heat shock protein 12	6/12	70.6 ± 4.6	8 ± 2	C, PM, N	S2, P10, S10
YBR072W	HSP26	Heat shock protein 26	5/8	65.4 ± 3.2	18 ± 3	C, N	S2, S10
YCR012W	PGK1	Phosphoglycerate kinase	8/12	63.5 ± 15.9	25 ± 6	M, PM, C	S2, P10, S10
YGR192C	TDH3:	Glyceraldehyde-3-phosphate dehydrogenase 3	12/12	61.7 ± 3.7	7 ± 3	C, M, PM	P10, S10
YJR009C	TDH2	Glyceraldehyde-3-phosphate dehydrogenase 2	12/12	50.6 ± 6.9	8 ± 3	C, M	S2, P10, S10
YJL052W	TDH1	Glyceraldehyde-3-phosphate dehydrogenase 1	12/12	50.9 ± 10.4	12 ± 6	C, M	S2, P10, S10

YAL005C	SSA1:HSP70	Heat shock protein 70	12/12	60.0 ± 11.8	6 ± 4	C, N, PM	S2, P10, S10
YGR254W	ENO1	Enolase 1	12/12	57.4 ± 12.9	9 ± 3	M, C, PM	S2, P10, S10
YHR174W	ENO2	Enolase 2	12/12	56.1 ± 16.3	9 ± 3	V, M, PM	S2, P10, S10
YAL038W	CDC19	Pyruvate kinase 1	5/8	49.4 ± 14.7	29 ± 7	C, PM	S2, S10
YLL024C	SSA2:HSP70	Heat shock protein 70	12/12	48.4 ± 9.5	6 ± 2	C, V, M	S2, P10, S10
YOL086C	ADH1	Alcohol dehydrogenase 1	9/12	48.3 ± 2.4	9 ± 3	C, PM	S2, P10, S10
YPR080W	TEF1	Elongation factor 1-alpha	9/12	44.1 ± 1.9	19 ± 5	C, V, M	S2, P10, S10
YJR104C	SOD1	Cu,Zn Superoxide dismutase	7/8	42.9 ± 10.2	4 ± 1	C, M, N	S2, S10
YDR155C	CPR1	Peptidyl-prolyl cis-trans isomerase	4/8	42.6 ± 6.3	7 ± 2	M, N	S2, P10
YLR044C	PDC1	Pyruvate decarboxylase isozyme 1	9/12	40.7 ± 13.4	14 ± 5	C, N	S2, P10, S10
YNL178W	RPS3	40S ribosomal subunit	10/12	40.4 ± 12.9	7 ± 1	R	S2, P10, S10
YHL015W	RPS20	Uncharacterized protein	10/12	38.8 ± 4.2	5 ± 1	R	S2, P10, S10
YLL050C	COF1	Cofilin	6/8	38.4 ± 9.5	4 ± 2	PM	S2, S10
YPL240C	HSP82:HSP90	Heat shock protein 90	8/8	37.9 ± 4.7	4 ± 2	C	S2, S10
YML028W	TSA1[↓]	Peroxiredoxin	8/8	36.7 ± 10.5	6 ± 2	C	S2, S10
YGR209C	TRX2	Thioredoxin	7/8	37.5 ± 11.9	4 ± 1	C, V	S2, S10
YJR045C	SSC1:HSP70	Heat shock protein 70	7/8	37.1 ± 22.9	20 ± 8	M	S2, P10
YNL055C	POR1	Porin	6/8	36.0 ± 8.4	10 ± 4	M	S2, P10
YDL229W	SSB1/ SSB2[↓]	Heat shock protein	7/8	37.4 ± 7.3	4 ± 2	PM	S2, S10
YDR050C	TPH1	Triosephosphate isomerase	7/12	34.3 ± 4.8	7 ± 2	M, C, PM	S2, P10, S10
YNL302C	RPS19B	40S ribosomal subunit	8/12	31.9 ± 9.4	4 ± 1	R	S2, P10, S10
YDR447C	RSP17B	40S ribosomal subunit	8/12	30.9 ± 8.7	4 ± 0	R	S2, P10, S10
YMR143W	RPS16A	40S ribosomal subunit	9/12	30.7 ± 5.6	4 ± 0	R	S2, P10, S10
YLL039C	UBI4[↓]	Polyubiquitin	8/8	28.9 ± 9.9	4 ± 1	C	S2, S10
YKR097W	PCK1	Phosphoenolpyruvate carboxykinase	8/8	28.4 ± 9.4	11 ± 3	C	S2, S10

^{a-↓} See corresponding footnotes to Table S5.2.

Table S5.4: Protein in the GST pull-downs from 1- and 7 d yeast extracts ($n=6$)^a

Accession ^b number	Protein ID ^c	% sequence Coverage ^e	Protein description ^d	Unique peptides ^f	Cellular Location ^g	Subcellular fraction ^h	Bait protein ⁱ
YNL302C	RPS19B^j	59.7 ± 4.7	40S ribosomal subunit	9 ± 2	R	S2, P10, S10	GST
YLR061W	RPL22A	57.4 ± 9.5	60S ribosomal subunit	15 ± 4	R	S2, P10, S10	GST
YMR143W	RPS16A	55.3 ± 5.4	40S ribosomal subunit	4 ± 7	R	S2, P10, S10	GST
YGR254W	ENO1	57.4 ± 10.6	Enolase 1	9 ± 2	M, C, PM	S2, P10, S10	GST
YHR174W	ENO2	56.1 ± 11.2	Enolase 2	9 ± 7	V, M, PM	S2, P10, S10	GST
YML026C	RPS18B	55.2 ± 9.7	40S ribosomal subunit	9 ± 4	R, M	S2, P10	GST
YBR072W	HSP12	54.1 ± 14.5	Heat shock protein 12	12 ± 8	C, PM, N	S2, P10, S10	GST
YNL178W	RPS3	53.7 ± 3.4	40S ribosomal subunit	9 ± 2	R	S2, P10, S10	GST
YDR012W	RPL4B	53.3 ± 3.4	60S ribosomal subunit	11 ± 6	R	S2, P10, S10	GST
YMR146C	TIF34	52.2 ± 7.8	eukaryotic translation initiation factor 3	8 ± 7	Multi-eIF complex	S2, P10	GST
YCR031C	RPS14A	50.4 ± 16.6	40S ribosomal subunit	12 ± 8	R	S2, P10, S10	GST
YLR150W	STM1	49.6 ± 8.5	Suppressor protein	8 ± 3	C	S2, S10	GST
YAL005C	SSA1: HSP70	49.4 ± 14.4	Heat shock protein 70	11 ± 3	C, N, PM	S2, P10, S10	GST
YPL237W	SUI3	48.6 ± 9.5	Eukaryotic translation initiation factor 2	7 ± 4	Multi-eIF complex	S2, P10	GST
YIL069C	RPS24B	48.4 ± 4.5	40S ribosomal subunit	16 ± 2	R	S2, P10, S10	GST
YDR064W	RPS13	48.1 ± 3.0	40S ribosomal subunit	8 ± 6	R	S2, P10, S10	GST
YJL177W YKL180W	RPL17B/A	47.6 ± 12.6	60S ribosomal subunit	7 ± 2	R	S2, P10, S10	GST
YLL024C	SSA2: HSP70	45.0 ± 7.5	Heat shock protein 70	8 ± 5	C, V, M	S2, P10, S10	GST
YBR009C	HHF1	43.8 ± 4.9	Histone 4	4 ± 2	N	S2, S10	GST
YAL036C	RBG1	42.7 ± 6.7	Ribosome-interacting GTPase 1	4 ± 1	C	S2, S10	GST
YLR197W	NOP56	42.0 ± 14.6	Nucleolar protein 56	11 ± 5	N	S2, S10	GST
YHL015W	RPS20	40.6 ± 14.9	40S ribosomal subunit	18 ± 7	R	S2, P10, S10	GST
YJL131C	AIM23	40.5 ± 5.4	Altered inheritance of mitochondria protein 23	6 ± 2	M	S2, P10	GST
YJR055W	HIT1	40.1 ± 20.6	Protein HIT1	16 ± 7	C, N	S2, S10	GST
YLL039C	UBI4	39.6 ± 3.7	Polyubiquitin	5 ± 1	C	S2, S10	GST
YMR242C	RPL20A	36.9 ± 4.3	60S ribosomal subunit	5 ± 1	R	S2, P10, S10	GST
YDL014W	NOP1	36.6 ± 6.7	rRNA 2'-O-methyltransferase fibrillar	6 ± 2	N	S2, S10	GST

YNL055C	POR1	35.7 ± 22.8	Porin	14 ± 8	M	S2, P10	GST
YDR471W	RPL27B	34.6 ± 6.6	60S ribosomal subunit	5 ± 2	R	S2, P10, S10	GST
YGL030W	RPL30	34.5 ± 8.5	60S ribosomal subunit	5 ± 3	R	S2, P10, S10	GST
YHL001W	RPL14B	34.0 ± 1.2	60S ribosomal subunit	4 ± 0	R	S2, P10, S10	GST
YDL229W	SSB1/SSB2	34.0 ± 4.4	Heat shock protein	5 ± 1	PM	S2, P10	GST
YOL127W	RPL25	33.3 ± 2.3	60S ribosomal subunit	5 ± 0	R	S2, P10, S10	GST
YNL096C	RPS7B	32.8 ± 4.4	40S ribosomal subunit	16 ± 2	R	S2, P10, S10	GST
YER102W	RPS8B	32.6 ± 18.7	40S ribosomal subunit	3 ± 8	R	S2, P10, S10	GST
YDR418W	RPL12B	32.5 ± 4.8	60S ribosomal subunit	5 ± 1	R	S2, P10, S10	GST
YLR074C	BUD20	31.6 ± 14.5	Bud site selection protein 20	14 ± 9	C, N	S2, S10	GST
YDR429C	TIF35	30.7 ± 1.3	Eukaryotic translation initiation factor 3 subunit G	4 ± 0	Multi-eIF complex	S2, P10	GST

^{a-1} See corresponding footnotes to Table S5.2.

^j Proteins in **blue font** were also pulled down by GST-apoCcp1 and/or GST-holoCcp1.

Table S5.5: Reported Ccp1 interactions collated from the yeast genome website ^a

Accession number ^b	Protein ID ^c	Protein description ^d	Interaction type ^e	Assay ^f	Exp format ^g	Refs
YKR066C	CCP1	Cytochrome c peroxidase	Physical	Affinity-capture Co-purification	MC HTS	1,2
YBL009W	ALK2	Protein kinase	Genetic	Negative genetic	HTS	3
YNR001C	CIT1	Citrate synthase	Physical	Co-fractionation	MC	4
YJR048W ^h	CYC1	Cytochrome c	Physical	Co-crystal structure Affinity -capture Co-purification Reconstituted complex	MC	2,5,6
YOR065W	CYT1	Cytochrome c1	Physical	Reconstituted complex	MC	7,8
YDL160C	DHH1	Cytoplasmic DExD/H-box helicase	Physical	Affinity capture	HTS	9
YER019W	ISC1	Inositol phosphosphingolipid phospholipase C	Genetic	Positive genetic	HTS	10
YPL004C	LSP1	Eisosome core component	Physical	Two-hybrid	HTS	11
YKL195W	MIA40	Import and assembly protein in mitochondrial IMS	Physical	Co-purification	MC	12
YKR016W	MIC60	Component of the MICOS complex	Physical	Affinity capture	HTS	13
YCR077C	PAT1	Deadenylation-dependent mRNA-decapping factor	Physical	Affinity capture	HTS	9
YGR101W	PCP1	Rhomboid mitochondrial serine protease	Physical	Biochemical activity	MC	14
YHL034C	SBP1	Protein that binds eIF4G	Physical	Affinity capture	HTS	9
YHR206W	SKN7	Nuclear transcription factor	Genetic	Phenotypic suppression	MC	15
YCL037C	SRO9	Cytoplasmic RNA-binding protein;	Physical	Affinity capture	HTS	16
YNL209W ^h	SSB2	HSP70		Affinity capture	HTS	17
YHR005C-A	TIM10	Forms a complex with tim9p	Physical	Co-purification	MC	12
YNL299W	TRF5	Non-canonical poly(A) polymerase	Physical	Affinity capture	MC	18
YML028W ^h	TSA1	Thioredoxin peroxidase	Genetic	Synthetic growth defect	HTS	19
YLL039C ^h	UBI4	Ubiquitin	Physical	Co-purification	HTS	20
YGR019W	UGA1	Gamma-aminobutyrate (GABA) transaminase	Physical	Negative genetic	HTS	10
YCR007C	-----	Unknown	Genetic	Two-hybrid	HTS	11

^a Ccp1 interacting proteins found at <http://www.yeastgenome.org>.

^b The GenBank (<http://www.ncbi.nlm.nih.gov/genbank/>) identifier assigned to each gene sequence

^c Four or five-letter/number yeast notation for protein

^d Protein name/description from given reference(s) and/or SGD website

^e Interaction type from given reference(s)

^f Type of assay used to probe interactions

^g Experimental format, MC- manually curated; HTS- high through put screen

^h Proteins identified in this study

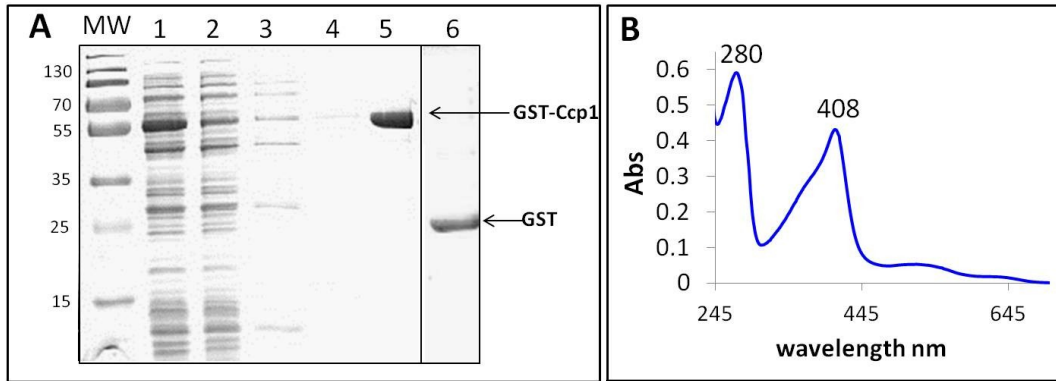


Figure S5.1. SD-PAGE analysis of GST-Ccp1 purification. (A) Coomassie-stained 12% SDS-PAGE gel showing the proteins in: (lane 1) the soluble fraction from *E. coli* BL21(DE3) cells transfected with the pGEX-2T-Ccp1 plasmid, (lane 2) the supernatant (batch-mode) from the Glutathione Sepharose 4B beads (lanes 3, 4) washings from the beads and (lane 5) the GST-Ccp1 fusion protein (MW ~60 kDa) eluted with 50 mM reduced GSH at pH 8.0. Lane 6 shows the GST protein (MW ~26 kDa) eluted from beads added to a lysate of *E. coli* harboring the empty pGEX-4T plasmid. The markers are in lane MW and their molecular weights in kDa are indicated on the left. (B) The room temperature UV-vis spectrum of 4 μ M GST-Ccp1 in 20 mM KPi buffer (pH 7.5) with 500 mM NaCl in a 1 cm pathlength cuvette following reconstitution with heme (see *Materials and Methods* of the main text). The 408/280 absorbance ratio is 0.77 ± 0.03 ($n=3$) which is within 2.5% error of the calculated 0.79 ratio for fully heme-loaded GST-Ccp1.

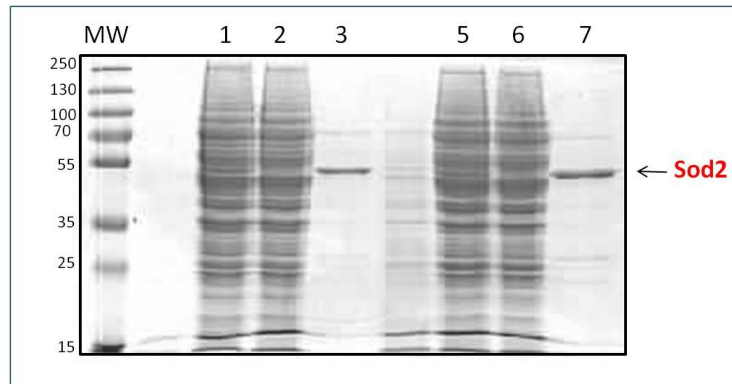


Figure S5.2. Confirmation of GST-Sod2 overexpression in yeast. Coomassie stained 12% SDS-PAGE gel showing the soluble proteins in: (lanes 1, 5) the clarified soluble fraction from yeast cells harboring GAL1-10 UAS GST-Sod2 expressing plasmid, (lanes 2, 6) the supernatant (batch-mode) from the Glutathione Sepharose 4B beads, and (lanes 3, 7) GST-Sod2 fusion protein (MW ~ 52 kDa) eluted with 50 mM reduced GSH at pH 8.0. Proteins from cells induced in SG-ura vs YPG medium are shown in lanes 1-3 and lanes 5-7, respectively (see *Materials and Methods* of the main text). The markers are in lane MW and their molecular weights in kDa are indicated on the left.

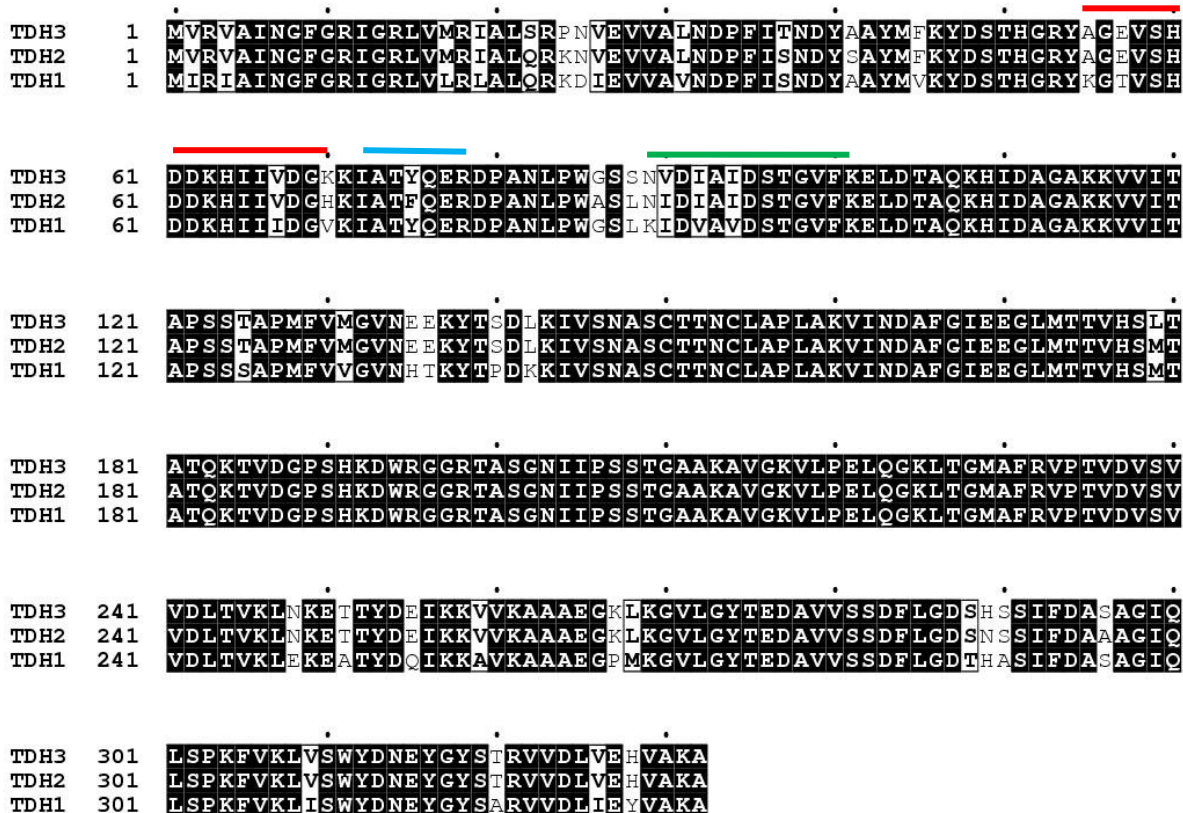


Figure S5.3. Sequence alignment of the Tdh3/2/1 isoforms of yeast GAPDH. Identical, similar and dissimilar residues are indicated by filled-in black boxes, black-outlined boxes and white boxes, respectively. The alignment was carried out using clustalW2 from EMBL (<http://www.ebi.ac.uk/Tools/msa/clustalw2/>) and ESPript was used to generate the alignment image (<http://esprict.ibcp.fr/ESPript/ESPript/>). The red, blue and green line localizes the isoform-specific sequence in panels A, B and C, respectively, of Figure 5 of the main text.

Chapter 6: General conclusions

The culmination of my work requires a paradigm-shift in our view of the function of Ccp1 and possibly other heme peroxidases. Broadly assumed to be a catalytic scavenger of H₂O₂ (17), my results reveal that Ccp1 mainly functions in mitochondrial heme-based H₂O₂ sensing that involves oxidation of its heme ligand (H175) to trigger heme transfer to the mitochondrial catalase A (Cta1) isoform in yeast (118). H₂O₂ sensing mechanisms are of intense current interest and are well-documented for thiol-based cytosolic proteins (21, 256). To our knowledge, Ccp1 is the first heme protein known to act as a mitochondrial H₂O₂ sensor and heme donor. As mentioned in Chapter 2, a prior example of H₂O₂ sensing involving histidine oxidation has been described but this is catalyzed by iron that is not associated with heme (26). A key component of Ccp1's redox regulatory activities is heme donation following oxidation of its proximal H175 ligand (118). Heme labilization from one heme protein as a source of heme for acquisition by a second protein has not been described in the literature. However, this mechanism is attractive from an energetic standpoint since heme biosynthesis is an energetically costly process given that its production requires the work of eight different enzymes (31). Thus, it is energetically less expensive to recycle heme rather than synthesize it.

The relocalization of apoCcp1 to the vacuole and nucleus has major implications in retrograde signalling mechanisms (90). It is well established that the mitochondria and nucleus are semiautonomous organelles in that mitochondria depend on nuclear-encoded proteins for much of their functionality. The role of mitochondrial signaling in promoting changes in nuclear gene expression is of much current interest as are retrograde messengers (90). The relocalization of Ccp1 to the nucleus identifies it as a novel retrograde messenger as well as opening up

unanswered questions pertaining to the Ccp1-Skn7 interaction in controlling the expression of antioxidant genes (54), which will be discussed in future work.

The label-free semiquantitative, targeted proteomics approach implemented in Chapter 3 maps the stable heme-mediated oxidative modifications induced by H₂O₂ in Ccp1 in order to gain mechanistic insights into its unprecedented mode of H₂O₂ sensing. Spectroscopic (EPR, ENDOR, fluorescence (119–124)) and spin trapping/scavenging studies (96, 125–128) have identified small subsets of residues oxidized in Ccp1, but the current LC-MS/MS approach found 24 residues in the protein that serve as endogenous donors, including residues that are buried in the polypeptide and/or undergo only small mass changes on oxidation. This work demonstrates the power of high-performance LC-MS/MS in comprehensively describing, both qualitatively and semiquantitatively, oxidative modifications within a protein matrix. Furthermore, using this LC-MS/MS approach allowed us to readily identify *intramolecular* dityrosine crosslinking, which is a subject of intense interest given its association with pathologies such as eye cataracts, atherosclerosis, acute inflammation, and Alzheimer's disease (257).

Importantly, a view emerges from our detailed product analysis that Ccp1 unlike APX, a structurally similar heme peroxidase, protects its heme from oxidative modification and heme-protein crosslinks by diverting oxidizing radicals to groups of residues that cluster into three or four zones. Although many heme proteins share similar active sites (173, 193), this study speaks to additional levels of polypeptide design that allows heme proteins to perform hitherto unexplored chemistry relevant to novel physiological functions in cells such as we are beginning to uncover for Ccp1.

The same label-free quantitative proteomics approach used in Chapter 3 was further applied to the study in Chapter 4 whereby PTMs in Ccp1 isolated from 16 h, 30 h and 7 d cells

were analyzed in order to link PTMs with Ccp1 cellular function and location. These two studies on oxidative modifications in Ccp1 provide insight into the behavior in a protein environment of a variety of radicals (Met, Cys, His, Trp, Tyr) by elucidating their stable end products and, more importantly for our understanding of oxidative stress, highlight the differences between protein oxidation in a cellular environment vs in a test tube.

On top of uncovering histidine oxidation as a mechanism of Ccp1 H₂O₂ sensing and heme transfer, we also highlighted a strategic role for methionine-aromatic interactions in controlling radical transfer within a protein matrix. Although methionines are the most readily oxidized residues, the biochemical and biophysical roles of methionine remain among the least well understood of the 20 amino acids (167). Our results suggest that methionine residues are critically important in promoting oxidation of aromatic residues (Met230/M231 promote oxidation of W191 and M172 likely promotes oxidation of H175) and that methionine oxidation stabilizes the reduced forms of these residues and shuts down radical transfer to them. This is consistent with recent reports that MetO formation increases the strength of the methionine sulfur-aromatic interaction (167).

The identification of Ccp1 interacting partners in Chapter 5 reveals further insights into its function *in vivo*. Protein partners identified include Sod2, an antioxidant enzyme that catalyzes the dismutation of (O₂^{•-}) to H₂O₂, and proteins putatively involved in heme transfer, GAPDH and Pet9. The interaction between Ccp1 and Sod2 suggests H₂O₂ channelling between these proteins and provides support for Ccp1's role as a primary H₂O₂ sensor. Ccp1's interaction with Pet9 suggests a possible mechanism of heme acquisition by Ccp1. Given that Ccp1 is in contact with the inner mitochondrial membrane during its processing from the immature to the mature form (58, 243), Pet9 located in the inner mitochondrial membrane may facilitate heme

transfer from FECH to Ccp1 (36). The interaction of Ccp1 with GAPDH and Hsp90 also implicates these two proteins in heme transfer in yeast. GAPDH together with Hsp90 may act as heme chaperones and transfer heme to Ccp1 and/or from Ccp1 to another heme acceptor such as Cta1. Notably, Sod2, GAPDH and Pet9 are not identified as binding partners of Ccp1 in the large-scale interactome networks. Published interactomes report on complexes identified from whole cell lysates of exponentially grown yeast. However, following exponential growth, yeast cultures become nutrient limited and generate higher levels of ROS (258) and our study reveals that growth conditions change the proteins that interact with Ccp1.

The link between a protein's location and its interacting protein partners is a key issue that arose in this thesis. Partners necessarily share a common subcellular localization or an interface between two physically adjoining compartments and an increasing number of proteins are being found in multiple subcellular compartments. Ccp1, for example, is located in the IMS, nucleus and vacuole but our overexpressed GST-Ccp1 bait pulled down proteins known to be located in the mitochondrial matrix, the outer mitochondrial membrane and the cytosol in addition to proteins from the IMS, nucleus and vacuole. Although some of these novel interactions may have been detected through loss of cellular or subcellular compartmentalization, a number merit further investigation as outlined in Chapters 5 and 7. In sum, my results are fully aligned with emerging views that environmental stresses such as nutrient limitation and ROS induce protein PTMs and relocalization. Thus, as explored here for Ccp1, the physiological roles a protein can adopt increases in function with its simultaneous presence in and/or migration between different subcellular compartments triggered by its PTMs.

Chapter 7: Future work

The work accomplished in this thesis has opened up several avenues for further investigation. Outlined below are some experimental questions generated from each chapter of my thesis that would be of interest to follow up on.

Future studies inspired by the results in Chapter 2. We previously demonstrated that the H₂O₂ sensing function of Ccp1 leads to increased Cta1 activity, which then attenuates H₂O₂ levels and prevents the activation of the H₂O₂-dependent stress response in yeast cells (50). In Chapter 2 we determined that Ccp1 increased the activity of Cta1 by donating its heme to apoCta1 (118). We observed that when yeast cells switch to respiration, the burst in H₂O₂ overoxidizes Ccp1 which results in heme labilization and apoCcp1 export from the mitochondria to the nucleus and the vacuole (118). Hence, we ask the following questions:

1. **What is the role of extramitochondrial apoCcp1?** Our fluorescence microscopy studies using the Ccp1-GFP fusion protein show that a large portion of apoCcp1-GFP translocates to the vacuole (118). What is the function if any of apoCcp1 in the vacuole? Overoxidized apoCcp1 may be sent to the vacuole simply for degradation as this is the mechanism in yeast for removing or recycling damaged cellular components. Although we do not detect degraded Ccp1 in 7 d cells by Western blotting, it is possible that Ccp1 is degraded later. Thus, it would be of interest to monitor Ccp1 protein levels in older cells by immunoblotting and to enrich Ccp1 from their vacuoles using subcellular fractionation techniques and characterize its oxidative PTM profile. The other possibility is that Ccp1 performs a signaling function in the vacuole as demonstrated for the glycolytic enzyme, enolase (106). As part of a high molecular weight aggregate (HMA), enolase was shown to be important in stimulating vacuole fusion as well as regulating selective protein trafficking to the vacuole. Given that

enolase is pulled down by GST-Ccp1 suggests that Ccp1 may also form part of the HMA. To test whether Ccp1 is an active component of the enolase-HMA, recombinant Ccp1 can be tested for stimulation of the *in vitro* vacuole fusion assay as described in work by Decker and Wickner, *J Biol Chem.* 2006 (106).

A small pool of Ccp1 is also detected in the nucleus. This is in line with previous reports that both Ccp1 and its catalytically inactive variant Ccp1^{W191F} convey an oxidative stress signal to the nuclear transcription factor Skn7, which regulates the expression of a subset of antioxidant enzymes in response to oxidative stress (54). Since only denucleated yeast extracts (S2, S10, P10) were examined in the GST pull-down assays, nuclei could be isolated (as outlined in Chapter 2 *Methods*) from H₂O₂-challenged and unchallenged cells and probed for Ccp1-Skn7 interactions in yeast overexpressing GST-Skn7. PTMs in nuclear Ccp1 could be monitored by MS as could chemical crosslinking of the nuclear extracts. Isolation of crosslinked Ccp1-Skn7 would provide a snapshot of this complex and provide important insight into how Ccp1 executes its role as a retrograde messenger.

2. **Does Ccp1 transfer its heme directly to Cta1?** Our results show that Cta1 is an acceptor of Ccp1 heme. However, we do not know if Ccp1 transfers its heme directly to Cta1. Since Cta1 expression is repressed in fermenting yeast, we could probe for direct Ccp1-Cta1 interactions in respiring cells using GST-Ccp1 and GST-Cta1 as bait. Using green fluorescent protein (GFP) and other fluorescent proteins as probes to follow the heme status of proteins also is a promising strategy since heme is a highly efficient quencher of fluorescence. Moreover, the long-wavelength excitation of GFP (488 nm) avoids spectral overlap with intrinsic protein fluorescence and light scattering from biological samples. Thus, monitoring lifetime

quenching in yeast expressing suitable Ccp1-FP and Cta1-FP' pairs may reveal if these proteins interact and insights on their heme status.

3. Does H175 oxidation modify Ccp1's heme affinity and its biophysical properties?

Histidines are vulnerable to metal-catalyzed oxidation in their ubiquitous role as Fe and Cu ligands (5). To date, there is no known mechanism for HisO repair, which has led to the assumption that this modification is a means of sacrificing the oxidized enzyme and HisO is considered a marker of oxidative stress (26, 163). We detect extensive oxo-H175 formation in Ccp1 so biophysical characterization of recombinant Ccp1 bearing this modification is of interest, including its heme affinity in the presence of acceptors such as apomyoglobin. Since Ccp1 has numerous oxidizable residues, it would be difficult to selectively oxidized H175. However, the Ccp1^{H175G} variant binds free imidazole and the complex exhibits essentially wild-type spectral properties as well as wild-type reaction rates with H₂O₂ (259). Assuming that oxo-H175 corresponds to the commonly observed histidine oxidation product, 2-oxo-histidine (Figure 7.1), Ccp1^{H175G} could be complexed with 2-oxo-imidazole and its CCP activity, spectroscopic properties and heme-transfer propensity compared to wild-type Ccp1.

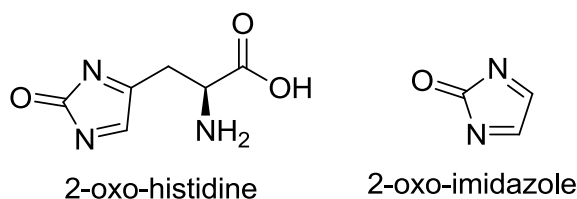


Figure 7.1. Chemical structure of 2-oxo-histidine and 2-oxo-imidazole.

Future studies inspired by the results in Chapter 3. Using high resolution LC-MS/MS, we explored in detail the oxidation of recombinant Ccp1 using 1, 5 and 10 M eq of H₂O₂ and found extensive RT from the heme to zones 1 and 2a. These pathways are turned on by oxidation of

key residues so it would be of interest to characterize variants of Ccp1 that may conformationally gate RT from the heme.

4. **How do methionine-aromatic interactions control Ccp1's function?** Cysteine sulfur- π interactions are prevalent in biochemistry and play an important role in protein folding and stabilization (260). However, interactions between methionine and aromatic residues in proteins are poorly understood. Recently, it has been reported that a third of all proteins in the PDB likely contain stabilizing methionine- π interactions and methionine oxidation may dramatically increase the strength of these interactions (167). We find that M172 and H175 are oxidized in different Ccp1 molecules and speculate that M172 oxidation controls RT to, and hence oxidation of, H175, which could be examined in the Ccp1^{M172S} variant. The M230/M231 residues are believed to control RT to W191 (120, 121), which could be examined in M230S and M231S single and double variants. Furthermore, the relative orientation of H175 and W191 is fixed by H-bonding with D235 (Figure 7.1) so it would appear that susceptibilities to oxidation of M172, H175 and W191, which critically control Ccp1's function, are interdependent. This could be probed by examining overoxidation of the the Ccp1^{H175G} and Ccp1^{W191F} variants. All the proposed variants are reported in the literature and they fold correctly and react with H₂O₂ to form CpdI (42). Also, yeast chromosomally expressing Ccp1^{W191F} has been biochemically characterized by our group.

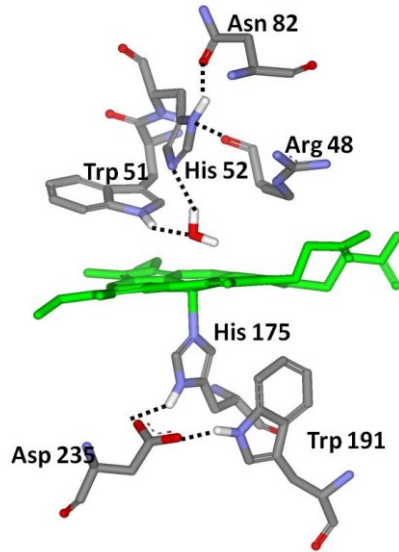


Figure 7.2. Ccp1's active-site residues and H-bonding network. This figure was generated using Pymol software and the coordinates from PDB 1ZBY.

Future studies inspired by the results in Chapter 4. Using LC-MS/MS we explored in detail the overoxidation of Ccp1 isolated from fermenting and respiring yeast cells. Although RT from the heme to zones 1 and 2a is dominant both *in vivo* and *in vitro*, the oxidative profiles of recombinant Ccp1 and Ccp1 isolated from yeast exhibit intriguing differences. Key among these is the extent of intramolecular dityrosine crosslinking. Furthermore, reproducibly high levels of pY153 are detected in Ccp1 from 30 h cells, suggesting that this PTM is linked to Ccp1's H₂O₂ sensing and heme labilization. Questions that arise from this study include:

5. Can dityrosine formation in Ccp1 be used as a probe of mitochondrial oxidative stress?

Dityrosine is associated with high oxidative stress, which is consistent with ~80% intramolecular dityrosine crosslinking of peptides T6 (Y36/Y39/Y42) and T8 (Y67/Y71) from Ccp1 oxidized with bolus (10 M eq) H₂O₂. Approximately, 70-85% crosslinked T6 and T8 is detected in mitochondrial Ccp1 from 7 d cells but none in Ccp1 from fermenting cells, which links dityrosine with the relatively high levels of mitochondrial ROS in stationary-

phase yeast. Mitochondrial ROS could be modulated by altering growth conditions, by knocking out Cta1 (Chapter 2) or by challenging cells with H₂O₂ and monitoring Ccp1's dityrosine levels to see how they vary.

The tyrosines that crosslink in Ccp1 are separated by 2-6 residues and are 3-15 Å apart in the 3D structure of the protein. To further characterize the MS behaviour of this PTM, we have synthesized the T8 peptide (HDNTGGGS**Y**GGT**Y**R) and optimized the crosslinking of free tyrosine (Appendix II). T8 could be crosslinked using the same approach and structurally characterized by proton/carbon NMR. Both crosslinked T8 and dityrosine could be analyzed in detail by MS and MS/MS using fragmentation by CID (collision-induced dissociation), HCD (high-energy dissociation) and possibly ETD (electron-transfer dissociation) for T8.

- 6. Probing pY in Ccp1?** We observe unprecedented levels of pY153 in Ccp1 from 30 h yeast cells using CID, which fragments amide bonds generating b_n and y_n sequence ions (Figure 7.3). In ETD a fluoranthene radical anion transfers an electron to a multiply charged peptide, which results in N-C α bond cleavage, generating c_n and z_n sequence ions (Figure 7.3) (261). ETD works well for large multiply charged peptides and can identify CID-labile PTMs. HCD like CID generates b_n and y_n sequence ions but its higher energy leads to further fragmentation that produces a_n and immonium ions (Figure 7.3) (262). The pY immonium ion (Figure 7.3B; m/z 216.0426) generated by cleavage N- and C-terminally to pY residues is a unique mass-deficient marker which, combined with its high-mass accuracy MS2 spectra, make HCD a promising strategy to confidently detect protein pY ions (262). Hence, phosphorylation of Ccp1 isolated from yeast could be reconfirmed using all three fragmentation modes.

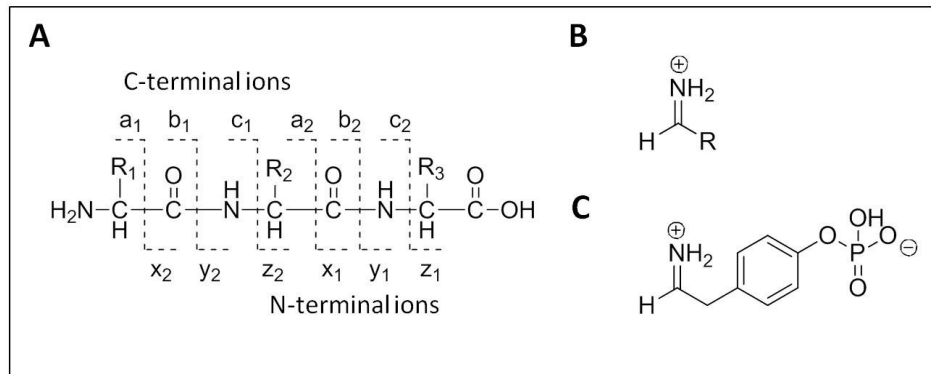


Figure 7.3. Fragmentation along the polypeptide backbone gives sequence ions. (A) fragmentation of the NH-CH, CH-CO and CO-NH bonds along the peptide backbone gives rise to six possible sequence ions for each residue. Ions are labelled a_n , b_n , c_n and x_n , y_n , z_n when the charge is retained on the N- and C-terminal fragments, respectively. Structure (B) of the immonium ion of a residue with side-chain R and (C) of the pY immonium ion.

7. **Can recombinant Ccp1 be selectively phosphorylated at Y153?** It is desirable to test *in vitro* if pY153 formation promotes H175 oxidation in Ccp1. Although it remains unknown which kinase phosphorylates Ccp1 *in vivo*, using crude cellular lysates supplemented with ATP and MgCl₂ may be sufficient to phosphorylate recombinant Ccp1. As an alternative to *in vitro* phosphorylation, Y153D or Y153E variants could be examined. D/E serve as mimics of pS/pT and there are literature examples of glutamic acid being a suitable phosphomimetic for pY (263).
8. **How does the oxidation profile of Ccp1^{W191F} differ from that of wild-type Ccp1?** We previously characterized Ccp1^{W191F} as a hyperactive H₂O₂ sensor and signaling protein and it is capable of hyperactivating the nuclear transcription factor, Skn7 (50, 54). Also, Ccp1^{W191F} cells exhibit higher Cta1 activity than wild-type cells presumably through increased heme transfer (50). Thus, it would be informative to compare oxidation of Ccp1^{W191F} and wild-type Ccp1 *in vitro* and *in vivo* to gain insights at the residue level into why the variant behaves as a hyperactive sensor/signalling molecule.

Future studies inspired by the results in Chapter 5. Several novel binding partners of Ccp1 were identified in Chapter 5, which raises many questions, a few of which are presented here:

9. **Does oxidation of Ccp1 change its binding partners?** Overoxidation of Ccp1 triggers H175 oxidation, heme labilization and subsequent apoCcp1 exit from the mitochondria (118). Thus, it would be interesting to oxidize recombinant GST-holoCcp1 with 1-10 M eq of H₂O₂ and perform GST pull-down assays to determine if Ccp1 oxidation changes its protein interaction partners. Additionally, the heme could be removed from overoxidized GST-holoCcp1. In fact, Cta1 may possibly recognize oxidized Ccp1 with a relatively weakly bound heme.

10. **Does Ccp1 bind to Cta1 in respiring cells?** As mentioned previously, we did not detect Cta1 in the GST-Ccp1 pull-down assays and suggested in (2) above to perform GST-Cta1 pull downs on lysates from respiring cells. Such assays could be compared for cells expressing wild-type Ccp1, Ccp1^{W191F} and in the *CCPI*-null strain as a negative control, and the relative heme-loading of GST-Cta1 from these cells could be compared. Since Cta1 protein levels are elevated in yeast grown on a non-fermentable carbon source such as raffinose, another option would be to probe lysates of these cells with GST-Ccp1 and oxidized GST-Ccp1 as discussed in point 9.

11. **Does Ccp1 acquire heme directly from FECH?** The last step in heme biosynthesis, the insertion of iron into the porphyrin ring, is catalyzed by the inner-membrane protein, FECH. FECH was not identified as a binding partner of GST-Ccp1 but the lysate preparation was not optimized to solubilize membrane proteins. Thus, the addition of detergents such as Tween 80, which is used in the purification of FECH from yeast cells (264), will liberate FECH from the membrane and may allow an interaction with Ccp1. Additional *in vitro*

assays that monitor possible heme transfer from purified FECH to apoCcp1 would shed light on the possible FECH-Ccp1 interaction.

12. **Does Sod2 channel H₂O₂ to Ccp1?** To determine if substrate channeling occurs between these two proteins, a coupled proximity assay that monitors Cyc^{II} oxidation could be implemented. O₂[•] generated by xanthine/xanthine oxidase will be dismutated by Sod2 to H₂O₂ and O₂. If this H₂O₂ is channeled within a Sod2-Ccp1 complex to Ccp1's heme, then CCP activity will be higher in the presence vs absence of Sod2. Notably, it is also possible that H₂O₂-induced RT from Ccp1 to Sod2 may occur in the absence of Cyc^{II}, which can be investigated by adding Sod2 to a Ccp1/H₂O₂ solutions. Catalase should be added before Sod2 to remove any unreacted H₂O₂ ensuring that crosslinking is not due to Sod2 radicals formed by its direct interaction with H₂O₂ (265). Ccp1-Sod2 heteromers can then be analyzed by mass spectrometry.
13. **Does Ccp1 transfer heme to GAPDH?** The interaction between Ccp1 and GAPDH reported in Chapter 5 implicates both proteins in heme trafficking in yeast and supports previous reports of GAPDH has a heme carrier (245). Possible heme transfer between Ccp1 and GAPDH can be monitoring using Ccp1-GFP as a probe as described in (2) above. Also, heme binding to GAPDH can be directly monitored spectroscopically since the Soret band of free hemin changes on binding to a protein.
14. **Will far-Western blotting identify new Ccp1 binding partners?** In far-Western blotting lysates containing the unknown prey proteins are separated by SDS-PAGE or native PAGE and transferred to a nitrocellulose or PVDF membrane (266). After transfer, the membrane is blocked and probed with a known purified bait protein (Ccp1). Following binding of the Ccp1 bait to the prey proteins, the membrane can be probed with anti-Ccp1. Prior separation

of the prey proteins by 1D gel electrophoresis decomplexifies the sample and increases the chance that more prey proteins will be trapped by the Ccp1 bait.

References

1. Stowe DF, Camara AKS (2009) Mitochondrial reactive oxygen species production in excitable cells: modulators of mitochondrial and cell function. *Antioxid Redox Signal* 11:1373–1414.
2. Loschen G, Azzi A, Richter C, Flohé L (1974) Superoxide radicals as precursors of mitochondrial hydrogen peroxide. *FEBS Lett* 42:68–72.
3. Valentine J, et al. (1998) The dark side of dioxygen biochemistry. *Curr Opin Chem Biol* 2:253–262.
4. Veal EA, Day AM, Morgan BA (2007) Hydrogen peroxide sensing and signaling. *Mol Cell* 26:1–14.
5. Berlett BS, Stadtman ER (1997) Protein oxidation in aging, disease, and oxidative stress. *J Biol Chem* 272:20313–20316.
6. Uttara B, Singh A V, Zamboni P, Mahajan RT (2009) Oxidative stress and neurodegenerative diseases: a review of upstream and downstream antioxidant therapeutic options. *Curr Neuropharmacol* 7:65–74.
7. Jamieson DJ (1998) Oxidative stress responses of the yeast *Saccharomyces cerevisiae*. *Yeast* 14:1511–1527.
8. Collinson LP, Dawes IW (1992) Inducibility of the response of yeast cells to peroxide stress. *J Gen Microbiol* 138:329–335.
9. Ristow M, Zarse K (2010) How increased oxidative stress promotes longevity and metabolic health: The concept of mitochondrial hormesis (mitohormesis). *Exp Gerontol* 45:410–418.
10. Galdieri L, Mehrotra S, Yu S, Vancura A (2010) Transcriptional regulation in yeast during diauxic shift and stationary phase. *OMICS* 14:629–638.
11. Fabrizio P, Longo VD (2003) The chronological life span of *saccharomyces cerevisiae*. *Aging Cell* 2:73–81.
12. Moye-rowley WS (2003) Regulation of the transcriptional response to oxidative stress in fungi : similarities and differences. *Eukaryot Cell* 2:381–389.
13. Switala J, Loewen PC (2002) Diversity of properties among catalases. *Arch Biochem Biophys* 401:145–154.
14. Cohen G, Rapatz W, Ruis H (1988) Sequence of the *Saccharomyces cerevisiae* CTA1 gene and amino acid sequence of catalase A derived from it. *Eur J Biochem* 163:159–163.
15. Hartig A, Ruis H (1986) Nucleotide sequence of the *Saccharomyces cerevisiae* CTT1 gene and deduced amino-acid sequence of yeast catalase T. *Eur J Biochem* 160:487–490.
16. Inoue Y, Matsuda T, Sugiyama K, Izawa S, Kimura A (1999) Genetic analysis of glutathione peroxidase in oxidative stress response of *Saccharomyces cerevisiae*. *J Biol Chem* 274:27002–27009.

17. Volkov AN, Nicholls P, Worrall JAR (2011) The complex of cytochrome c and cytochrome c peroxidase: the end of the road? *Biochim Biophys Acta* 1807:1482–1503.
18. Munhoz D., Netto LE. (2006) Cytosolic thioredoxin peroxidase I and II are important defenses of yeast against hydroperoxide insult. *J Biol Chem* 279:35219–35227.
19. Rhee SG (2006) H₂O₂, a necessary evil for cell signaling. *Science (80-)* 312:1882–1883.
20. Rhee SG, Woo HA, Kil IS, Bae SH (2012) Peroxiredoxin functions as a peroxidase and a regulator and sensor of local peroxides. *J Biol Chem* 287:4403–4410.
21. Toledano MB, Delaunay A, Monceau L, Tacnet F (2004) Microbial H₂O₂ sensors as archetypical redox signaling modules. *Trends Biochem Sci* 29:351–357.
22. Gough DR, Cotter TG (2011) Hydrogen peroxide: a jekyll and hyde signalling molecule. *Cell Death Dis* 2:1–8.
23. Chung HS, Wang SB, Venkatraman V, Murray CI, Van Eyk JE (2013) Cysteine oxidative posttranslational modifications: emerging regulation in the cardiovascular system. *Circ Res* 112:382–392.
24. Paulsen CE, Carroll KS (2009) Chemical dissection of an essential redox switch in yeast. *Chem Biol* 16:217–225.
25. Kiley PJ, Storz G (2004) Exploiting thiol modifications. *PLoS Biol* 2:1714–1717.
26. Lee J-W, Helmann JD (2006) The PerR transcription factor senses H₂O₂ by metal-catalysed histidine oxidation. *Nature* 440:363–367.
27. Roeser J, Bischoff R, Bruins AP, Permentier HP (2010) Oxidative protein labeling in mass-spectrometry-based proteomics. *Anal Bioanal Chem* 397:3441–3455.
28. Ponka P (1999) Cell biology of heme. *Am J Med Sci* 318:241–256.
29. Tsiftoglou AS, Tsamadou AI, Papadopoulou LC (2006) Heme as key regulator of major mammalian cellular functions: molecular, cellular, and pharmacological aspects. *Pharmacol Ther* 111:327–345.
30. Mense SM, Zhang L (2006) Heme: a versatile signaling molecule controlling the activities of diverse regulators ranging from transcription factors to MAP kinases. *Cell Res* 16:681–692.
31. Hoffman M, Góra M, Rytka J (2003) Identification of rate-limiting steps in yeast heme biosynthesis. *Biochim Biophys Res Commun* 310:1247–1253.
32. Severance S, Hamza I (2009) Trafficking of heme and porphyrins in metazoa. *Chem Revis* 109:4596–4616.
33. Hamza I, Dailey HA (2012) One ring to rule them all: trafficking of heme and heme synthesis intermediates in the metazoans. *Biochim Biophys Acta* 1823:1617–1632.
34. Sawicki KT, Chang H-C, Ardehali H (2015) Role of Heme in Cardiovascular Physiology and Disease. *J Am Heart Assoc* 4:1–14.

35. Protchenko O, Rodriguez-Suarez R, Androphy R, Bussey H, Philpott CC (2006) A screen for genes of heme uptake identifies the FLC family required for import of FAD into the endoplasmic reticulum. *J Biol Chem* 281:21445–21457.
36. Azuma M, et al. (2008) Adenine nucleotide translocator transports haem precursors into mitochondria. *PLoS One* 3:e3070.
37. Bowman SEJ, Bren KL (2008) The chemistry and biochemistry of heme c: functional bases for covalent attachment. *Nat prod rep* 25:1118–1130.
38. Schneider S, Marles-Wright J, Sharp K, Paoli M (2007) Diversity and conservation of interactions for binding heme in b-type heme proteins. *Nat prod rep* 24:621–630.
39. Paoli M, Marles-Wright J, Smith A (2002) Structure-function relationships in heme-proteins. *DNA cell biol* 21:271–280.
40. Poulos TL, et al. (1980) The crystal structure of cytochrome c peroxidase. *J Biol Chem* 255:575–580.
41. Pelletier H, Kraut J (1992) Crystal structure of a complex between electron transfer partners, cytochrome c peroxidase and cytochrome c. *Science (80-)* 259:1748–1755.
42. Erman JE, Vitello LB (2002) Yeast cytochrome c peroxidase: mechanistic studies via protein engineering. *Biochim Biophys Acta* 1597:193–220.
43. Sharp KH, Mewies M, Moody PCE, Raven EL (2003) Crystal structure of the ascorbate peroxidase–ascorbate complex. *Nat structural Mol Biol* 10:303–307.
44. Barrows TP, Poulos TL (2005) Role of electrostatics and salt bridges in stabilizing the compound I radical in ascorbate peroxidase. *Biochemistry* 44:14062–14068.
45. Meharena Y., Oertel P, Bhasker B, Poulos T. (2008) Engineering ascorbate peroxidase activity into cytochrome c peroxidase. *Biochemistry* 47:10324–10332.
46. Pipirou Z, et al. (2007) Autocatalytic formation of a covalent link between tryptophan 41 and the heme. *Biochemistry* 46:2174–2180.
47. Goodin DB, Davidson MG, Roe JA, Mauk AG, Smiths M (1991) Amino acid substitutions at tryptophan-51 of cytochrome c peroxidase: effects on coordination, species preference for cytochrome c, and electron transfer. *Biochemistry* 30:4953–4962.
48. Kwon M, Chong S, Han S, Kim K (2003) Oxidative stresses elevate the expression of cytochrome c peroxidase in *Saccharomyces cerevisiae*. *Biochim Biophys Acta* 1623:1–5.
49. Jiang H, English A (2006) Phenotypic analysis of the *ccp1Δ* and *ccp1Δ-ccp1W191F* mutant strains of *Saccharomyces cerevisiae* indicates that cytochrome c peroxidase functions in oxidative-stress signaling. *J Inorg Biochem* 100:1996–2008.
50. Martins D, Kathiresan M, English AM (2013) Cytochrome c peroxidase is a mitochondrial heme-based H₂O₂ sensor that modulates antioxidant defense. *Free Radic Biol Med* 65:541–551.
51. Mesquita A, et al. (2010) Caloric restriction or catalase inactivation extends yeast chronological lifespan by inducing H₂O₂ and superoxide dismutase activity. *Proc Natl Acad Sci U S A* 107:15123–15128.

52. Goldberg AA, et al. (2009) Effect of calorie restriction on the metabolic history of chronologically aging yeast. *Exp Gerontol* 44:555–571.
53. Godon C (1998) The H₂O₂ stimulon in *Saccharomyces cerevisiae*. *J Biol Chem* 273:22480–22489.
54. Charizanis C, Juhnke H, Krems B, Entian K (1999) The mitochondrial cytochrome c peroxidase Ccp1 of *Saccharomyces cerevisiae* is involved in conveying an oxidative stress signal to the transcription factor Pos9 (Skn7). *Mol Genet genomics* 262:437–447.
55. Hörtner H, et al. (1982) Regulation of synthesis of catalases and iso-1-cytochrome c in *Saccharomyces cerevisiae* by glucose, oxygen and heme. *Eur J Biochem* 128:179–184.
56. Garcia BA (2010) What does the future hold for top down mass spectrometry? *J Am Soc Mass Spectrom* 21:193–202.
57. Kaput J, Goltz S, Blobel G (1982) Nucleotide sequence of the yeast nuclear gene for cytochrome c peroxidase precursor. *J Biol Chem* 257:15054–15058.
58. Suppanz IE, Wurm CA, Wenzel D, Jakobs S (2009) The m-AAA protease processes cytochrome c peroxidase preferentially at the inner boundary membrane of mitochondria. *Mol Biol Cell* 20:572–580.
59. Michaelis G, et al. (2005) Mitochondrial signal peptidases of yeast: the rhomboid peptidase Pcp1 and its substrate cytochrome c peroxidase. *Gene* 354:58–63.
60. Sels AA, Cocriamont C (1968) Induced conversion of a protein precursor into cytochrome c peroxidase during adaptation of yeast to oxygen. *Biochem Biophys Res Commun* 32:192–198.
61. Djavadi-Ohanian L, Rudin Y, Schatz G (1978) Identification of enzymically inactive apocytochrome c peroxidase in anaerobically grown *Saccharomyces cerevisiae*. *J Biol Chem* 253:4402–4407.
62. Perrone GG, Tan S-X, Dawes IW (2008) Reactive oxygen species and yeast apoptosis. *Biochim Biophys Acta* 1783:1354–1368.
63. Martins D, Titorenko V, English AM (2014) Cells with impaired mitochondrial H₂O₂ sensing generate less •OH radicals and live longer. *Antioxid Redox Signal* 21:1490–1503.
64. Skulachev VP (1998) Cytochrome c in the apoptotic and antioxidant cascades. *FEBS Lett* 423:275–280.
65. Petrova VY, Drescher D, Kujumdzieva A V, Schmitt MJ (2004) Dual targeting of yeast catalase A to peroxisomes and mitochondria. *Biochem J* 380:393–400.
66. Zimniak P, Hartter E, Woloszczuk W, Ruis H (1976) Catalase biosynthesis in yeast: formation of catalase A and catalase T during oxygen adaptation of *Saccharomyces cerevisiae*. *Eur J Biochem* 71:393–398.
67. Kaput J, Brandriss MC, Prussak-Wieckowska T (1989) In vitro import of cytochrome c peroxidase into the intermembrane space: release of the processed form by intact mitochondria. *J Cell Biol* 109:101–112.

68. Brachmann CB, Davies A, Cost GJ, Caputo E (1998) Designer deletion strains derived from *Saccharomyces cerevisiae* S288C: a useful set of strains and plasmids for PCR-mediated gene disruption and other applications. *Yeast* 14:115–132.
69. Winzeler EA (1999) Functional characterization of the *S. cerevisiae* genome by gene deletion and parallel analysis. *Science* (80-) 285:901–906.
70. Huh W-K, et al. (2003) Global analysis of protein localization in budding yeast. *Nature* 425:686–691.
71. Benjamin JJR, et al. (2011) Dysregulated Arl1, a regulator of post-golgi vesicle tethering, can inhibit endosomal transport and cell proliferation in yeast. *Mol Biol Cell* 22:2337–2347.
72. Wang X, et al. (1996) Prenylated isoforms of yeast casein kinase I, including the novel Yck3p, suppress the *gcs1* blockage of cell proliferation from stationary phase. *Mol Cell Biol* 16:5375–5385.
73. Gregg C, Kyryakov P, Titorenko VI (2009) Purification of mitochondria from yeast cells. *J Vis Exp*:15–16.
74. Ide GJ, Saunders CA (1981) Rapid isolation of yeast nuclei. *Curr Genet* 4:85–90.
75. Titorenko VI, Smith JJ, Szilard RK, Rachubinski RA (1998) Pex20p of the yeast *yarrowia lipolytica* is required for the oligomerization of thiolase in the cytosol and for its targeting to the Peroxisome. *J Cell Biol* 142:403–420.
76. Welinder C, Ekblad L (2011) Coomassie staining as loading control in Western blot analysis. *J Proteome Res* 10:1416–1419.
77. Feissner R, Xiang Y, Kranz RG (2003) Chemiluminescent-based methods to detect subpicomole levels of c-type cytochromes. *Anal Biochem* 315:90–94.
78. Yonetani T (1965) Studies on cytochrome c peroxidase*. *J Biol Chem* 240:4509–4514.
79. Velours J, Guerin B, Duvert M (1977) Preparation of an inner membrane-matrix fraction from yeast mitochondria. *Arch Biochem Biophys* 182:295–304.
80. Beers RF, Sizer IW (1952) A spectrophotometric method for measuring the breakdown of hydrogen peroxide by catalase. *J Biol Chem* 195:133–140.
81. Smith ML, Paul J, Ohlsson PI, Hjortsberg K, Paul KG (1991) Heme-protein fission under nondenaturing conditions. *Proc Natl Acad Sci U S A* 88:882–886.
82. Paul J, Chen W, Ohlsson P-I, Smith M (1998) Heme transfer reactions: an important prerequisite for synthetic oxygen carriers. *Turkish J Chem* 22:103–108.
83. Adams PA (1977) The kinetics of the recombination reaction between apomyoglobin and alkaline haematin. *Biochem J* 163:153–158.
84. Berry EA, Trumpower BL (1987) Simultaneous determination of hemes a, b, and c from pyridine hemochrome spectra. *Anal Biochem* 161:1–15.
85. Antonini E, Brunori M (1971) *Hemoglobin and myoglobin in their reactions with ligands* (Elsevier, Amsterdam, The Netherlands, North-Holland).

86. Yonetani T, Anni H (1987) Yeast cytochrome c peroxidase. *J Biol Chem* 262:9547–9554.
87. Yaffe MP (2003) The cutting edge of mitochondrial fusion. *Nat Cell Biol* 5:497–499.
88. Chen S, Brockenbrough JS, Dove JE, Aris J. (1997) Homocitrate synthase is located in the nucleus in the yeast *Saccharomyces cerevisiae*. *J Biol Chem* 272:10839–10846.
89. Dingwall C, Laskey RA (1986) Protein import into the cell nucleus. *Annu Rev Cell Biol* 2:367–390.
90. Whelan SP, Zuckerbraun BS (2013) Mitochondrial signaling: forwards, backwards, and in between. *Oxid Med Cell Longev* 2013:1–10.
91. Burke P V. (1997) Effects of oxygen concentration on the expression of cytochrome c and cytochrome c oxidase genes in yeast. *J Biol Chem* 272:14705–14712.
92. Wright RM, Poyton R (1990) Release of two *Saccharomyces cerevisiae* cytochrome genes, COX6 and CYC1, from glucose repression requires the SNF1 and SSN6 gene products. *Mol Cell Biol* 10:1297–1300.
93. Erman J, Yonetani T (1975) A kinetic study of the endogenous reduction of the oxidized sites in the primary cytochrome c peroxidase-hydrogen peroxide compound. *Biochim Biophys Acta* 393:350–357.
94. Hargrove MS, et al. (1994) Stability of myoglobin: a model for the folding of heme proteins. *Biochemistry* 33:11767–11775.
95. Fox T, Tsaprailis G, English AM (1994) Fluorescence investigation of yeast cytochrome c peroxidase oxidation by H₂O₂ and enzyme activities of the oxidized enzyme. *Biochemistry* 33:186–191.
96. Tsaprailis G, English AM (2003) Different pathways of radical translocation in yeast cytochrome c peroxidase and its W191F mutant on reaction with H₂O₂ suggest an antioxidant role. *J Biol Inorg Chem* 8:248–255.
97. Yogev O, Naamati A, Pines O (2011) Fumarase: a paradigm of dual targeting and dual localized functions. *FEBS J* 278:4230–4242.
98. Tsaprailis G, Chan DW, English AM (1998) Conformational states in denaturants of cytochrome c and horseradish peroxidases examined by fluorescence and circular dichroism. *Biochemistry* 37:2004–2016.
99. Dumont ME, Cardillo TS, Hayes MK, Sherman F (1991) Role of cytochrome c heme lyase in mitochondrial import and accumulation of cytochrome c in *Saccharomyces cerevisiae*. *Mol Cell Biol* 11:5487–5496.
100. Fisher WR, Taniuchi H, Anfinsen CB (1973) On the role of heme in the formation of the structure of cytochrome c. *J Biol Chem* 248:3188–3195.
101. Woloszczuk W, Sprinson DB, Ruis H (1980) The relation of heme to catalase apoprotein synthesis in yeast. *J Biol Chem* 255:2624–2627.
102. Uchida K, Kawakishi S (1994) Identification of oxidized histidine generated at the active site of Cu,Zn-superoxide dismutase exposed to H₂O₂. *J Biol Chem* 269:2405–2410.

103. Traoré DAK, et al. (2009) Structural and functional characterization of 2-oxo-histidine in oxidized PerR protein. *Nat Chem Biol* 5:53–59.
104. Goodrich LE, Paulat F, Praneeth VKK, Lehnert N (2010) Electronic structure of heme-nitrosyls and its significance for nitric oxide reactivity, sensing, transport, and toxicity in biological systems. *Inorg Chem* 49:6293–6316.
105. He C, Neya S, Knipp M (2011) Breaking the proximal Fe(II)-N(His) bond in heme proteins through local structural tension: lessons from the heme b proteins nitrophorin 4, nitrophorin 7, and related site-directed mutant proteins. *Biochemistry* 50:8559–8575.
106. Decker BL, Wickner WT (2006) Enolase activates homotypic vacuole fusion and protein transport to the vacuole in yeast. *J Biol Chem* 281:14523–14528.
107. Martins D, English AM (2014) Catalase activity is stimulated by H₂O₂ in rich culture medium and is required for H₂O₂ resistance and adaptation in yeast. *Redox Biol* 2:308–313.
108. Lee J, et al. (1999) Yap1 and Skn7 control two specialized oxidative stress response regulons in yeast. *J Biol Chem* 274:16040–16046.
109. Beal MF (2002) Serial review: Oxidatively modified proteins in aging and disease. *Free Radic Biol Med* 32:797–803.
110. Levine RL, Stadtman ER (2001) Oxidative modification of proteins during aging. *Exp Gerontol* 36:1495–1502.
111. Møller IM, Rogowska-Wrzesinska A, Rao RSP (2011) Protein carbonylation and metal-catalyzed protein oxidation in a cellular perspective. *J Proteomics* 74:2228–2242.
112. Forman H., Maiorino M, Ursini F (2010) Signaling functions of reactive oxygen species. *Biochemistry* 49:997–1003.
113. Stubbe J, van Der Donk WA (1998) Protein radicals in enzyme catalysis. *Chem Rev* 98:705–762.
114. Minnihan E., Nocera D., Stubbe J (2013) Reversible, long-range radical transfer in E. coli class Ia ribonucleotide reductase. *Acc Chem Res* 46:2524–2535.
115. Tsai A, Kulmacz R, Palmer G (1995) Spectroscopic evidence for reaction of prostaglandin H synthase-1 tyrosyl radical with arachidonic acid. *J Biol Chem* 270:10503–10508.
116. Sivaraja M, Goodin DB, Smith M, Hoffman BM (2014) Identification by ENDOR of Trp191 as the free-radical site in cytochrome c peroxidase compound ES. *Science (80-)* 245:738–740.
117. Miller M, Vitello L, Erman J (1995) Regulation of interprotein electron transfer by Trp 191 of cytochrome c peroxidase. *Biochemistry* 34:12048–12058.
118. Kathiresan M, Martins D, English AM (2014) Respiration triggers heme transfer from cytochrome c peroxidase to catalase in yeast mitochondria. *Proc Natl Acad Sci U S A* 111:17468–17473.
119. Hori H, Yonetani T (1985) Powder and single-crystal electron paramagnetic resonance studies of yeast cytochrome c peroxidase and its peroxide compound, compound ES*. *J Biol Chem* 260:349–355.

120. Goodin DB, Mauk AG, Smith M (1986) Studies of the radical species in compound ES of cytochrome c peroxidase altered by site-directed mutagenesis. *Proc Natl Acad Sci U S A* 83:1295–1299.
121. Fishel, Laurence A Farnum MF, et al. (1991) Compound I radical in site-directed mutants of cytochrome c peroxidase as probed by electron paramagnetic resonance and electron-nuclear double resonance. *Biochemistry* 30:1986–1996.
122. Musah RA, Goodin DB (1997) Introduction of novel substrate oxidation into cytochrome c peroxidase by cavity complementation: oxidation of 2-aminothiazole and covalent modification of the enzyme. *Biochemistry* 36:11665–11674.
123. Ivancich A, Dorlet P, Goodin DB, Un S (2001) Multifrequency high-field EPR study of the tryptophanyl and tyrosyl radical intermediates in wild-type and the W191G mutant of cytochrome c peroxidase. *J Am Chem Soc* 123:5050–5058.
124. Miner KD, et al. (2014) Identifying the elusive sites of tyrosyl radicals in cytochrome c peroxidase: implications for oxidation of substrates bound at a site remote from the heme. *Biochemistry* 53:3781–3789.
125. Zhang H, He S, Mauk AG (2002) Radical formation at Tyr39 and Tyr153 following reaction of yeast cytochrome c peroxidase with hydrogen peroxide. *Biochemistry* 41:13507–13.
126. Fenwick CW, English AM (1996) Trapping and LC–MS Identification of Protein Radicals Formed in the Horse Heart Metmyoglobin–H₂O₂ Reaction. *J Am Chem Soc* 118:12236–12237.
127. Filosa A, English AM (2001) Mass spectral analysis of protein-based radicals using DBNBS. Nonradical adduct formation forriation versus spin trapping. *J Biol Chem* 276:21022–21027.
128. Wright PJ, English AM (2003) Scavenging with TEMPO* to identify peptide- and protein-based radicals by mass spectrometry: advantages of spin scavenging over spin trapping. *J Am Chem Soc* 125:8655–8665.
129. Dalle-Donne I, et al. (2005) Proteins as biomarkers of oxidative/nitrosative stress in diseases: the contribution of redox proteomics. *Mass Spectrom Rev* 24:55–99.
130. Schöneich C, Sharov VS (2006) Mass spectrometry of protein modifications by reactive oxygen and nitrogen species. *Free Radic Biol Med* 41:1507–1520.
131. Charvátová O, et al. (2008) Quantifying protein interface footprinting by hydroxyl radical oxidation and molecular dynamics simulations: application to galectin-1. *J Am Soc Mass Spectrom* 19:1692–1705.
132. Konermann L, Stocks B, Pan Y, Tong X (2010) Mass spectrometry combined with oxidative labeling for exploring protein structure and folding. *Mass Spectrom Rev* 29:651–667.
133. Tsaprailis G, English AM (1996) Redox activity of tryptophan residues in recombinant cytochrome c peroxidase and its W51 F and W191 F mutants. *Can J Chem* 2257:2250–2257.
134. Spangler B, Erman J (1986) Cytochrome c peroxidase compound I: formation of covalent protein crosslinks during the endogenous reduction of the active site. *Biochim Biophys Acta* 872:155–157.

135. Pfister TD, Gengenbach AJ, Syn S, Lu Y (2001) The role of redox-active amino acids on compound I stability, substrate oxidation, and protein cross-linking in yeast cytochrome c peroxidase. *Biochemistry* 40:14942–14951.
136. Childs BRE, Bardsley WG (1975) The steady-state kinetics of peroxidase with 2,2'-Azino-di-(3-ethylbenzthiazoline- 6-sulphonic acid) as chromogen. *Biochem J* 145:93–103.
137. Jones AR, Siepen JA, Hubbard SJ, Paton NW (2009) Improving sensitivity in proteome studies by analysis of false discovery rates for multiple search engines. *Proteomics* 9:1220–1229.
138. Wenhong Z, Smith JW, Huang C-M (2010) Mass spectrometry-based label-free quantitative proteomics. *J Biomed Biotechnol* 2010:1–6.
139. Malencik DA, Anderson SR (1996) Dityrosine formation in calmodulin: cross-linking and polymerization catalyzed by arthromyces peroxidase. *Biochemistry* 35:4375–4386.
140. Kim K, Erman JE (1988) Methionine modification in cytochrome-c peroxidase. *Biochim Biophys Acta* 954:95–107.
141. Yonetani T (1967) Studies on cytochrome c peroxidase: X. crystalline apo- and reconstituted holoenzymes. *J Biol Chem* 242:5008–5013.
142. Erman JE, et al. (1993) Histidine 52 is a critical residue for rapid formation of cytochrome c peroxidase compound I. *Biochemistry* 32:9798–9806.
143. Levine RL, Moskovitz J, Stadtman ER (2000) Oxidation of methionine in proteins : roles in antioxidant defense and cellular regulation. *IUBMB Life* 50:301–307.
144. Schöneich C (2005) Methionine oxidation by reactive oxygen species: reaction mechanisms and relevance to Alzheimer's disease. *BBA* 1703:111–119.
145. Schöneich C (2002) Redox processes of methionine relevant to beta-amyloid oxidation and alzheimer's disease. *Arch Biochem Biophys* 397:370–376.
146. Carballal S, et al. (2007) Sulfenic acid in human serum albumin. *Amino Acids* 32:543–551.
147. Bartona J., Packerb J. (1970) The radiolysis of oxygenated cysteine solutions at neutral pH. The role of RSSR and O₂⁻. *Int J Radiat Phys Chem* 2:159–166.
148. Sevilla MD, Becker D, Yan M (1990) The formation and structure of the sulfoxyl radicals RSO(·), RSOO(·), RSO₂(·), and RSO₂OO(·) from the reaction of cysteine, glutathione and penicillamine thiyl radicals with molecular oxygen. *J Radiat Biol* 57:65–81.
149. Sevilla MD, Yan M, Becker D (1988) Thiyl peroxy radical formation from the reaction of cysteine thiyl radical with molecular oxygen: An ESR investigation. *Biochem Biophys Res Commun* 155:405–410.
150. Harriman A (1987) Further Comments on the Redox Potentials. *Am Chem Soc* 91:6102–6104.
151. DeFelippis MR, Murthy CP, Faraggi M, Klapper MH (1989) Pulse radiolytic measurement of redox potentials: the tyrosine and tryptophan radicals. *Biochemistry* 28:4847–4853.
152. Jovanovic S V, Steenzen S, Simic MG (1991) Kinetics and energetics of one-electron-transfer reactions involving tryptophan neutral and cation radicals. *J Phys Chem* 95:684–687.

153. Svistunenko DA (2005) Reaction of haem containing protein and enzymes with hydroperoxides: the radical view. *BBA* 1707:127–155.
154. Josimović L, Janković I, Jovanović SV (1993) Radiation induced decomposition of tryptophan in the presence of oxygen. *Radiat Phys Chem* 41:835–841.
155. Maskos Z, Rush JD, Koppeno WH (1992) The hydroxylation of phenylalanine and tyrosine : a comparison with salicylate and tryptophan. *Arch Biochem Biophys* 296:521–529.
156. Bonagura CA, et al. (2003) High-resolution crystal structures and spectroscopy of native and compound I cytochrome c peroxidase. *Biochemistry* 42:5600–5608.
157. Hunter EPL, Desrosiers MF, Simic MG (1989) The effect of oxygen, antioxidants and superoxide radical on tyrosine phenoxyl radical dimerization. *Free Radic Biol Med* 6:581–585.
158. Boguta G, Dancewicz A (1981) Radiation-induced dimerization of tyrosine and glycytyrosine in aqueous solutions. *Int J Radiat Biol Relat Stud Phys Chem Med* 39:163–174.
159. Dixon WT, Murphy D (1976) Determination of the acidity constants of some phenol radical cations by means of electron spin resonance. *J Chem Soc, Faraday Trans 2* 72:1221–1230.
160. Goodin D, McRee D (1993) The Asp-His-Fe triad of cytochrome c peroxidase controls the reduction potential, electronic structure, and coupling of the tryptophan free radical to the heme. *Biochemistry* 32:3313–3324.
161. Navaratnam S, Parsons BJ (1998) Reduction potential of histidine free radicals: a pulse radiolysis study. *J Chem Soc Faraday Trans* 94:2577–2581.
162. Gunther MR, Andrew Peters J, Sivaneri MK (2002) Histidinyl radical formation in the self-peroxidation reaction of bovine copper-zinc superoxide dismutase. *J Biol Chem* 277:9160–9166.
163. Uchida K, Kawakishi S (1993) 2-Oxo-histidine as a novel biological marker for oxidatively modified proteins. *FEBS Lett* 322:208–210.
164. Kurahashi T, Miyazaki A, Suwan S, Isobe M (2001) Extensive investigations on oxidized amino acid residues in H₂O₂-treated Cu,Zn-SOD protein with LC-ESI-Q-TOF-MS, MS/MS for the determination of the copper-binding site. *J Am Chem Soc* 123:9268–9278.
165. Martins D, English AM (2014) SOD1 oxidation and formation of soluble aggregates in yeast: Relevance to sporadic ALS development. *Redox Biol* 2:632–639.
166. Maria C, Revilla E, Ayala A, de la Cruz C, Machado A (1995) Changes in the histidine residues of Cu/Zn superoxide dismutase during aging. *FEBS Lett* 374:85–88.
167. Valley CC, et al. (2012) The methionine-aromatic motif plays a unique role in stabilizing protein structure. *J Biol Chem* 287:34979–34991.
168. Pesavento RP, Van Der Donk WA (2001) Tyrosyl radical cofactors. *Adv Protein Chem* 58:317–385.
169. Murphy EJ, Metcalfe CL, Nnamchi C, Moody PCE, Raven EL (2012) Crystal structure of guaiacol and phenol bound to a heme peroxidase. *FEBS J* 279:1632–1639.

170. Jeschke G (2005) EPR techniques for studying radical enzymes. *Biochim Biophys Acta* 1707:91–102.
171. Zhang H, He S, Mauk AG (2002) Radical formation at Tyr39 and Tyr153 following reaction of yeast cytochrome c peroxidase with hydrogen peroxide. *Biochemistry* 41:13507–13513.
172. Bernini C, Arezzini E, Basosi R, Sinicropi A (2014) In silico spectroscopy of tryptophan and tyrosine radicals involved in the long-range electron transfer of cytochrome C peroxidase. *J Phys Chem B* 118:9525–9537.
173. Pipirou Z, et al. (2007) The reactivity of heme in biological systems: autocatalytic formation of both tyrosine-heme and tryptophan-heme covalent links in a single protein architecture. *Biochemistry* 46:13269–13278.
174. Pipirou Z, et al. (2009) Peroxide-Dependent Formation of a Covalent Link between Trp51 and the Heme in Cytochrome c Peroxidase. *Biochemistry* 48:3593–3599.
175. Inoue K, Garner C, Ackermann BL, Oe T, Blair IA (2006) Liquid chromatography/tandem mass spectrometry characterization of oxidized amyloid beta peptides as potential biomarkers of Alzheimer's disease. *Rapid Commun Mass Spectrom* 20:911–918.
176. Gebicki J, et al. (2010) Reduction of protein radicals by GSH and ascorbate: potential biological significance. *Amino Acids* 39:1131–1137.
177. Stadtman ER (1993) Oxidation of Free Amino Acids and Amino Acid Residues in Proteins by Radiolysis and by Metal-Catalyzed Reactions. *Annu Rev Biochem* 62:797–821.
178. Sherrod SD, et al. (2012) Label-free quantitation of protein modifications by pseudo selected reaction monitoring with internal reference peptides. *J Proteome Res* 11:3467–3479.
179. Jorgensen WL, Chandrasekhar J, Madura JD, Impey RW, Klein ML (1983) Comparison of simple potential functions for simulating liquid water. *J Chem Phys* 79:926–935.
180. Phillips JC, et al. (2008) Scalable molecular dynamics with NAMD. *J Comput chem* 26:1781–1802.
181. MacKerell, A. D., Jr. Bashford D, et al. (1998) All-atom empirical potential for molecular modeling and dynamics studies of proteins. *J Phys Chem B* 102:3586–3616.
182. Huber K., Herzberg G (1979) *Molecular spectra and molecular structure* (Van Nostrand Reinhold Company, New York).
183. Essmann U, et al. (1995) A smooth particle mesh Ewald method. *J Chem Phys* 103:31–34.
184. Ryckaert J-P, Ciccotti G, Berendsen HJC (1977) Numerical integration of the Cartesian Equations of Motion of a System with Constraints: Molecular Dynamics of n-Alkanes. *J Comput Phys* 23:337–341.
185. Grubmüller H, Heller H, Windemuth A, Schulten K (1991) Generalized Verlet algorithm for efficient molecular dynamics simulations with long-range interactions. *Mol simulations* 6:121–142.
186. Martyna GJ, Tobias DJ, Klein ML (1994) Constant pressure molecular dynamics algorithms. *J Chem Phys* 101:4177–4189.

187. Feller SE, Zhang YH, Pastor RW, Brooks BR (1995) Constant pressure molecular dynamics simulation: The Langevin piston method. *J Chem Phys* 103:4613–4621.
188. Humphrey W, Dalke A, Schulten K (1996) VMD: Visual molecular dynamics. *J Mol Graph* 14:33–38.
189. Imlay JA (2011) Cellular defenses against superoxide and hydrogen peroxide. *Annu Rev Biochem* 77:755–776.
190. Rowe LA, Degtyareva N, Doetsch PW (2008) DNA damage-induced reactive oxygen species (ROS) stress response in *Saccharomyces cerevisiae*. *Free Radic Biol Med* 45:1167–1177.
191. Boveris A (1976) Mitochondrial production of hydrogen peroxide in *Saccharomyces cerevisiae*. *Acta Physiol Lat Am* 26:303–309.
192. Polakis ES, Bartley W, Meek G a (1965) Changes in the activities of respiratory enzymes during the aerobic growth of yeast on different carbon sources. *Biochem J* 97:298–302.
193. English AM, Tsapraillis G (1995) Catalytic structure–function relationships in heme peroxidases. *Adv Inorg Chem* 43:79–125.
194. Kathiresan M, English A. (2015) Detailed LC-MS/MS analysis of H₂O₂-treated cytochrome c peroxidase offers insight into heme-based H₂O₂ signaling. *J Am Chem Soc* submitted.
195. Monteiro H, Arai R, Travassos L (2008) Protein tyrosine phosphorylation and protein tyrosine nitration in redox signaling. *Antioxid Redox Signal* 10:843–889.
196. Piper P. (2006) Long-lived yeast as a model for ageing research. *Yeast* 23:215–226.
197. Morand K, Talbo G, Mann M (1993) Oxidation of peptides during electrospray ionization. *Rapid Commun Mass Spectrom* 7:738–743.
198. Pagliarini DJ, Dixon JE (2006) Mitochondrial modulation: Reversible phosphorylation takes center stage? *Trends Biochem Sci* 31:26–34.
199. Radi R (2004) Nitric oxide, oxidants, and protein tyrosine nitration. *Proc Natl Acad Sci U S A* 101:4003–4008.
200. Hawkins CL, Davies MJ (2001) Generation and propagation of radical reactions on proteins. *Biochim Biophys Acta* 1504:196–219.
201. Modesti A, et al. (2001) Expression of the small tyrosine phosphatase (Stp1) in *Saccharomyces cerevisiae*: A study on protein tyrosine phosphorylation. *Electrophoresis* 22:576–585.
202. Chi A, et al. (2007) Analysis of phosphorylation sites on proteins from *Saccharomyces cerevisiae* by electron transfer dissociation (ETD) mass spectrometry. *Proc Natl Acad Sci U S A* 104:2193–2198.
203. Tony H, Gregory DP (1997) The protein kinases of budding yeast: six score and more. *Trends Biochem Sci* 22:19–22.
204. Brinkworth RI, Munn AL, Kobe B (2006) Protein kinases associated with the yeast phosphoproteome. *BMC Bioinformatics* 7:47.

205. Li X, et al. (2007) Large-Scale Phosphorylation Analysis of α -Factor-Arrested *Saccharomyces cerevisiae*. *J Proteome Res* 6:1190–1197.
206. Albuquerque CP, et al. (2008) A multidimensional chromatography technology for in-depth phosphoproteome analysis. *Mol Cell Proteomics* 7:1389–1396.
207. Reinders J, et al. (2007) Profiling phosphoproteins of yeast mitochondria reveals a role of phosphorylation in assembly of the ATP synthase. *Mol Cell Proteomics* 6:1896–1906.
208. Chiarugi P, Taddei M, Ramponi G (2005) Oxidation and tyrosine phosphorylation: synergistic or antagonistic cues in protein tyrosine phosphatase. *Cell Mol life Sci* 62:931–936.
209. Rao RS, Xu D, Thelen JJ, Miernyk J a. (2013) Circles within circles: crosstalk between protein Ser/Thr/Tyr-phosphorylation and Met oxidation. *BMC Bioinformatics* 14:S14.
210. Oien DB, Carrasco G a, Moskovitz J (2011) Decreased Phosphorylation and Increased Methionine Oxidation of α -Synuclein in the Methionine Sulfoxide Reductase A Knockout Mouse. *J Amino Acids* 2011:721094.
211. Hardin SC, Larue CT, Oh M-H, Jain V, Huber SC (2009) Coupling oxidative signals to protein phosphorylation via methionine oxidation in Arabidopsis. *Biochem J* 422:305–312.
212. Miernyk JA, et al. (2009) Oxidation of an adjacent methionine residue inhibits regulatory seryl-phosphorylation of pyruvate dehydrogenase. *Proteomics Insights* 2:15–22.
213. Kato M, et al. (2010) Structural Basis for Inactivation of the Human Pyruvate Dehydrogenase Complex by Phosphorylation: Role of Disordered Phosphorylation Loops. *Structure* 9:1–14.
214. Poulos TL, et al. (1978) Crystallographic determination of the heme orientation and location of the cyanide binding site in yeast cytochrome c peroxidase. *J Biol Chem* 253:3730–3735.
215. Gavin A-C, et al. (2002) Functional organization of the yeast proteome by systematic analysis of protein complexes. *Nature* 415:141–147.
216. Goll J, Uetz P (2006) The elusive yeast interactome. *Genome Biol* 7:223.
217. Ho Y, et al. (2002) Systematic identification of protein complexes in *Saccharomyces cerevisiae* by mass spectrometry. *Nature* 415:180–183.
218. Zhu H, et al. (2001) Global analysis of protein activities using proteome chips. *Science* 293:2101–2105.
219. Meisinger C, Pfanner N, Truscott KN (2006) Isolation of yeast mitochondria. *Methods Mol Biol* 313:33–39.
220. Mok J, Im H, Snyder M (2009) Global identification of protein kinase substrates by protein microarray analysis. *Nat Protoc* 4:1820–1827.
221. Chevallet M, Luche S, Rabilloud T (2006) Silver staining of proteins in polyacrylamide gels. *Nat Protoc* 1:1852–1858.
222. Pace CN, Vajdos F, Fee L, Grimsley G, Gray T (1995) How to measure and predict the molar absorption coefficient of a protein. *Protein Sci* 4:2411–2423.

223. Crapo JD, Oury T, Rabouille C, Slot JW, Chang LY (1992) Copper,zinc superoxide dismutase is primarily a cytosolic protein in human cells. *Proc Natl Acad Sci U S A* 89:10405–10409.
224. Tsang CK, Liu Y, Thomas J, Zhang Y, Zheng XFS (2014) Superoxide dismutase 1 acts as a nuclear transcription factor to regulate oxidative stress resistance. *Nat Commun* 5:3446.
225. Sturtz LA, Diekert K, Jensen LT, Lill R, Culotta VC (2001) A fraction of yeast Cu,Zn-superoxide dismutase and its metallochaperone, CCS, localize to the intermembrane space of mitochondria. A physiological role for SOD1 in guarding against mitochondrial oxidative damage. *J Biol Chem* 276:38084–38089.
226. Pan X, et al. (2006) A DNA integrity network in the yeast *Saccharomyces cerevisiae*. *Cell* 124:1069–1081.
227. Kolarov J, Kolarova N, Nelson N (1990) A third ADP/ATP translocator gene in yeast. *J Biol Chem* 265:12711–12716.
228. Lawson JE, Douglas MG (1988) Separate genes encode functionally equivalent ADP/ATP carrier proteins in *Saccharomyces cerevisiae*. Isolation and analysis of AAC2. *J Biol Chem* 263:14812–14818.
229. Ghaemmaghami S, et al. (2003) Global analysis of protein expression in yeast. *Nature* 425:737–741.
230. Hasin N, Cusack S a, Ali SS, Fitzpatrick DA, Jones GW (2014) Global transcript and phenotypic analysis of yeast cells expressing Ssa1, Ssa2, Ssa3 or Ssa4 as sole source of cytosolic Hsp70-Ssa chaperone activity. *BMC Genomics* 15:194.
231. Taipale M, Jarosz D, Lindquist S (2010) HSP90 at the hub of protein homeostasis: emerging mechanistic insights. *Nat Rev Mol Cell Biol* 11:515–528.
232. Ravindranath S., Fridovich I (1978) Isolation and characterization of a manganese-containing superoxide dismutase from rat liver. *J Biol Chem* 250:6107–6112.
233. Park SG, Cha MK, Jeong W, Kim IH (2000) Distinct physiological functions of thiol peroxidase isoenzymes in *Saccharomyces cerevisiae*. *J Biol Chem* 275:5723–5732.
234. Garrido EO, Grant CM (2002) Role of thioredoxins in the response of *Saccharomyces cerevisiae* to oxidative stress induced by hydroperoxides. *Mol Microbiol* 43:993–1003.
235. Wong CM, Siu KL, Jin DY (2004) Peroxiredoxin-null yeast cells are hypersensitive to oxidative stress and are genomically unstable. *J Biol Chem* 279:23207–23213.
236. Horst M, Knecht EC, Schu P V (1999) Import into and degradation of cytosolic proteins by isolated yeast vacuoles. *Mol Biol Cell* 10:2879–2889.
237. Chiang H-L, Schekman R (1991) Regulated import and degradation of a cytosolic protein in the yeast vacuole. *Nature* 350:313–318.
238. Terlecky SR, Chiang HL, Olson TS, Dice JF (1992) Protein and peptide binding and stimulation of in vitro lysosomal proteolysis by the 73-kDa heat shock cognate protein. *J Biol Chem* 267:9202–9209.
239. Bejarano E, Cuervo AM (2010) Chaperone-Mediated Autophagy. *Proc Am Thorac Soc* 7:29–39.

240. Chirico WJ, Waters GM, Blobel G (1988) 70K heat shock related proteins stimulate protein translocation into microsomes. *Nature* 332:805–810.
241. Deshaies RJ, Koch BD, Werner-Washburne M, Craig EA, Schekman R (1988) A subfamily of stress proteins facilitates translocation of secretory and mitochondrial precursor polypeptides. *Nature* 332:801–805.
242. Hachiya N, et al. (1995) Reconstitution of the initial steps of mitochondrial protein import. *Nature* 376:705–709.
243. Tatsuta T, Augustin S, Nolden M, Friedrichs B, Langer T (2007) m-AAA protease-driven membrane dislocation allows intramembrane cleavage by rhomboid in mitochondria. *EMBO J* 26:325–335.
244. Zaffagnini M, Fermani S, Costa A, Lemaire SD, Trost P (2013) Plant cytoplasmic GAPDH: redox post-translational modifications and moonlighting properties. *Front Plant Sci* 4:450.
245. Chakravarti R, Aulak KS, Fox PL, Stuehr DJ (2010) GAPDH regulates cellular heme insertion into inducible nitric oxide synthase. *Proc Natl Acad Sci U S A* 107:18004–18009.
246. Delgado M, et al. (2001) The glyceraldehyde-3-phosphate dehydrogenase polypeptides encoded by the *Saccharomyces cerevisiae* TDH1, TDH2 and TDH3 genes are also cell wall proteins. *Microbiology* 147:411–417.
247. Almeida B, et al. (2007) NO-mediated apoptosis in yeast. *J Cell Sci* 120:3279–88.
248. McAlister L, Holland MJ (1985) Differential expression of the three yeast glyceraldehyde-3-phosphate dehydrogenase genes. *J Biol Chem* 260:15019–15027.
249. Lee HC, Hon T, Zhang L (2002) The molecular chaperone Hsp90 mediates heme activation of the yeast transcriptional activator Hap1. *J Biol Chem* 277:7430–7437.
250. Ghosh A, Chawla-Sarkar M, Stuehr DJ (2011) Hsp90 interacts with inducible NO synthase client protein in its heme-free state and then drives heme insertion by an ATP-dependent process. *FASEB J* 25:2049–2060.
251. Verghese J, Abrams J, Wang Y, Morano K a. (2012) Biology of the Heat Shock Response and Protein Chaperones: Budding Yeast (*Saccharomyces cerevisiae*) as a Model System. *Microbiol Mol Biol Rev* 76:115–158.
252. Krogan NJ, et al. (2006) Global landscape of protein complexes in the yeast *Saccharomyces cerevisiae*. *Nature* 440:637–643.
253. Zhao R, et al. (2005) Navigating the chaperone network: An integrative map of physical and genetic interactions mediated by the hsp90 chaperone. *Cell* 120:715–727.
254. McClellan AJ, et al. (2007) Diverse Cellular Functions of the Hsp90 Molecular Chaperone Uncovered Using Systems Approaches. *Cell* 131:121–135.
255. Cornell M, Paton NW, Oliver SG (2004) A critical and integrated view of the yeast interactome. *Comp Funct Genomics* 5:382–402.
256. Paulsen CE, Carroll KS (2009) Chemical dissection of an essential redox switch in yeast. *Chem Biol* 16:217–25.

257. DiMarco T, Giulivi C (2007) Current analytical methods for the detection of dityrosine, a biomarker of oxidative stress, in biological samples. *Mass Spectrom Rev* 26:108–120.
258. Trancíková A, Weisová P, Kiššová I, Zeman I, Kolarov J (2004) Production of reactive oxygen species and loss of viability in yeast mitochondrial mutants: protective effect of Bcl-x L. *FEMS Yeast Res* 5:149–156.
259. Hirst J, et al. (2001) Replacement of the axial histidine ligand with imidazole in cytochrome c peroxidase. 2. Effects on heme coordination and function. *Biochemistry* 40:1274–1283.
260. Ringer AL, Senenko A, Sherrill CD (2007) Models of S / p interactions in protein structures : Comparison of the H 2 S – benzene complex with PDB data. *Protein Sci* 16:2216–2223.
261. Syka J, Coon J, Schroeder M, Shabanowitz J, Hunt D (2004) Peptide and protein sequence analysis by electron transfer dissociation mass spectrometry. *Proc Natl Acad Sci U S A* 29:9528–9533.
262. Olsen J, et al. (2007) Higher-energy C-trap dissociation for peptide modification analysis. *Nat Methods* 4:709–712.
263. Stateva SR, et al. (2015) Characterization of Phospho-(Tyrosine)-Mimetic Calmodulin Mutants. *PLoS One* 10:e0120798.
264. Camadro J-M, Labbe P (1988) Purification and Properties of Ferrochelatase from the Yeast *Saccharomyces cerevisiae*. *J Biol Chem* 263:11675–11682.
265. Lardinois OM, Ortiz De Montellano PR (2001) H₂O₂-mediated cross-linking between lactoperoxidase and myoglobin. Elucidation of protein-protein radical transfer reactions. *J Biol Chem* 276:23186–23191.
266. Wu Y, Li Q, Chen X (2007) Detecting protein-protein interactions by Far western blotting. *Nat Protoc* 2:3278–3284.
267. Malencik DA, Sprouse JF, Swanson CA, Anderson SR (1996) Dityrosine: preparation, isolation, and analysis. *Anal Biochem* 242:202–213.
268. Tilley M, Benjamin R, Srivarin P, Tilley K (2004) Nonenzymatic preparative-scale synthesis of dityrosine and 3-bromotyrosine. *Anal Biochem* 334:193–195.

Appendix I: First page to published manuscripts

Not described in thesis: Cytochrome c peroxidase is a mitochondrial heme-based H₂O₂ sensor that modulates antioxidant defense

Free Radical Biology and Medicine 65 (2013) 541–551



Contents lists available at ScienceDirect
Free Radical Biology and Medicine

journal homepage: www.elsevier.com/locate/freeradbiomed



Original Contribution

Cytochrome c peroxidase is a mitochondrial heme-based H₂O₂ sensor that modulates antioxidant defense



Dorival Martins, Meena Kathiresan, Ann M. English*

PROTEO and Department of Chemistry and Biochemistry, Concordia University, Montreal, QC, Canada, H3B 1R6

ARTICLE INFO

Article history:
Received 23 April 2013
Received in revised form
17 June 2013
Accepted 20 June 2013
Available online 2 July 2013

Keywords:
H₂O₂ sensing
H₂O₂ signaling
Heme-based sensors
Mitochondrial ROS regulation
Antioxidant enzymes
Free radicals

ABSTRACT

Hydrogen peroxide (H₂O₂) is a key signaling molecule that also induces apoptosis. Thus, cells must rapidly sense and tightly control H₂O₂ levels. Well-characterized cellular responses to exogenous H₂O₂ involve oxidation of specific cytosolic protein-based thiols but sensing of H₂O₂ generated by mitochondrial respiration is less well described. Here we provide substantial biochemical evidence that the heme enzyme Ccp1 (cytochrome c peroxidase), which is targeted to the intermembrane space, functions primarily as a mitochondrial H₂O₂ sensing and signaling protein in *Saccharomyces cerevisiae*. Key evidence for a sensing role for Ccp1 is the significantly higher H₂O₂ accumulation in *ccp1*-null cells (*ccp1Δ*) vs *ccp1*^{W919F} cells producing the catalytically inactive Ccp1^{W919F} variant. In fact, intracellular H₂O₂ levels (*ccp1Δ* > wildtype > *ccp1*^{W919F}) correlate inversely with the activity of the mitochondrial (and peroxisomal) heme catalase, Cta1 (*ccp1Δ* < wildtype < *ccp1*^{W919F}). Mitochondrial Sod2 activity also varies in the three strains (*ccp1Δ* > wildtype > *ccp1*^{W919F}) and *ccp1Δ* cells exhibit low superoxide levels. Notably, Ccp1^{W919F} is a more persistent H₂O₂ signaling protein than wild-type Ccp1, and this enhanced mitochondrial H₂O₂ signaling decreases the mitochondrial fitness of *ccp1*^{W919F} cells. However, these cells are fully protected from a bolus (0.4 mM) of exogenous H₂O₂ added after 12 h of growth, whereas the viability of *ccp1Δ* cells drops below 20%, which additionally associates Ccp1 with Yap1-dependent H₂O₂ signaling. Combined, our results strongly implicate Ccp1, independent of its peroxidase activity, in mitochondrial H₂O₂ sensing and signaling to maintain reactive oxygen species homeostasis.

© 2013 Elsevier Inc. All rights reserved.

Introduction

It is now well established that hydrogen peroxide (H₂O₂) is not just a harmful oxidant but also a key signaling molecule that modulates diverse biological processes from cell differentiation to apoptosis [1]. Consistent with its potentially toxic nature, H₂O₂ signals are transmitted over short distances and cellular responses to H₂O₂ are both site and concentration dependent [1]. The focus on cellular defenses to exogenous H₂O₂ has provided significant insight into thiol-based cytosolic H₂O₂ sensors [2,3]. For example, glutathione peroxidase 3 (Gpx3), a cytosolic thiol peroxidase, senses excess H₂O₂ through oxidation of its active-site cysteine and conveys this redox signal via disulfide exchange to the transcription factor Yap1 on exposure of *Saccharomyces cerevisiae* to nonlethal doses of H₂O₂ [3,4]. Oxidized Yap1 is translocated to the nucleus to regulate the transcription of several antioxidant genes [5]. However, oxidative environments exist within eukaryotic cells but sensing of endogenously generated H₂O₂ or other reactive oxygen species (ROS) within these regions is poorly

documented. For example, mitochondria are the main sites of H₂O₂ production in respiring yeast [6] but to date only a single case of mitochondrial H₂O₂ sensing has been reported [7], although ROS sensing by mitochondria has been extensively discussed in the context of oxygen availability [8,9].

Yeast switch from anaerobic to aerobic metabolism when a fermentable carbon source such as glucose becomes limiting. Because mitochondrial ROS spike during this diauxic shift [10], yeast cells must be prepared for an imminent spike in mitochondrial ROS. Given its chemical properties [11] and known signaling functions [1], H₂O₂ is probably a crucial messenger of changes in mitochondrial ROS. We demonstrated previously that cytochrome c peroxidase (Ccp1), a heme peroxidase targeted to the mitochondrial intermembrane space [12,13], protects yeast from challenge with a bolus of exogenous H₂O₂ [14]. This was not surprising given that in vitro Ccp1 serves as a highly efficient H₂O₂ scavenger in the presence of excess donor ferrocyclochrome c (Cyc1^h; Scheme 1) [15]. Unexpectedly, we also found that *ccp1*^{W919F} cells producing the Ccp1^{W919F} variant with negligible cytochrome c peroxidase activity are less sensitive to H₂O₂ than wild-type cells. The added protective effect of Ccp1^{W919F} cannot be attributed to H₂O₂ scavenging because, unlike the oxidized form of wild-type Ccp1 (Cmpdl, Scheme 1), Cmpdl bearing the W191F mutation [16] is not

* Corresponding author. Fax: +514 848 2868.
E-mail address: ann.english@concordia.ca (A.M. English).

Appendix II: Residue oxidation products

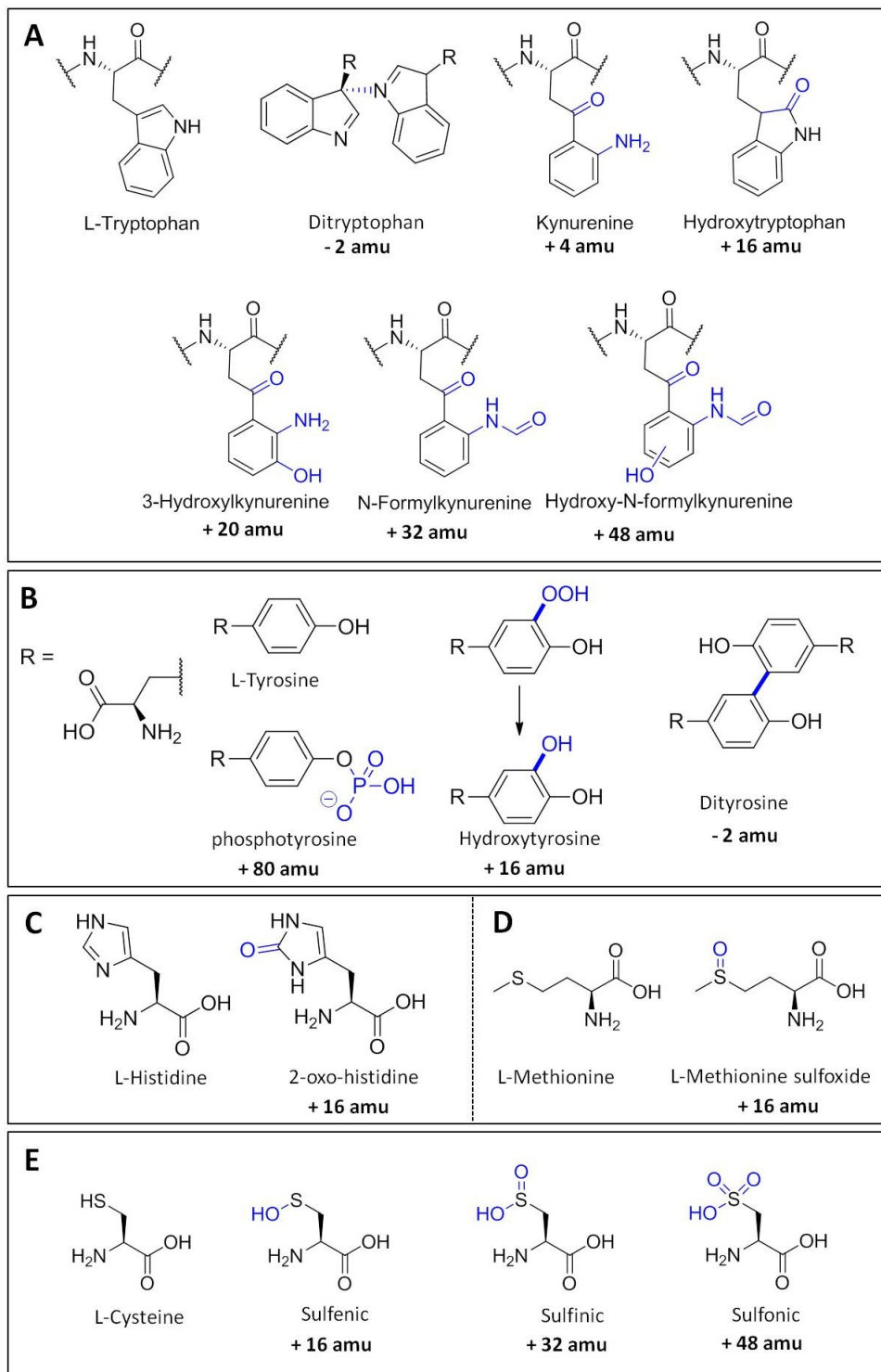


Figure A2.1. Residue modifications revealed by LC-MS/MS analysis in this thesis.

Appendix III: Preparation and synthesis of dityrosine

Dityrosine was prepared using a published method (267), with some modifications. L-tyrosine (45 mg) was dissolved in 40 mL of boiling water and 100 mL of 0.5 M sodium borate buffer (pH 9.0) was added to the solution. Once the solution cooled to 37 °C, lactoperoxidase was added to a final concentration of 0.5 μ M, followed by dropwise addition with stirring of 35% H₂O₂ to a final concentration of 5 mM. The solution turned light brown and was maintained at 37 °C for a further 15 min. The reaction was stopped by addition of 87.5 μ L of β -mercaptoethanol, and the sample was dried on a rotary evaporator. The product was redissolved in 50 mL of water, the pH was adjusted to 8.8 and the solution loaded onto a 3 x 20 cm DEAE-Sepharose column equilibrated with 20 mM NaHCO₃ (pH 8.8). The sample was eluted using 20 mM NaHCO₃ (pH 8.8) and the flow-through fractions were collected, pooled and applied to a centrifugal thin-layer chromatotron (T-squared technology, 7924T-01). Components of the solution were spun off the rotating disk using the elution solvent (butanol:water:acetic acid 4:1:2 v/v/v).

Dityrosine is UV fluorescent and was collected under a UV lamp. The fluorescent fractions were pooled, adjusted to pH 3.0 with formic acid (FA) and loaded onto a preparative-scale HPLC column (Phenomenex C-18, 100 Å pore size, 15 μ m particle size; 2.0 x 25 cm) at a flow rate of 10 mL/min. The column was washed with 0.1% aqueous formic acid for 10 min followed by a 0–8% acetonitrile gradient in 0.1% formic acid over 30 min and the absorbance (280 nm) and emission (ex 325 /em 400 nm) of the eluate were monitored. Unreacted L-tyrosine eluted at 8 min with no fluorescence signal but a major peak at 14 min showed high absorbance and fluorescence (Figure A3.1B). This peak was collected and freeze dried. Purity by LC-MS was >95%, and yield was 6 mg. ESI-MS confirmed the presence of dityrosine with a m/z value

of the MH^+ ion at 361.2 Da (Figure A3.2) and 1D proton NMR (kindly run by Dr. Alexey Denisov) confirmed the structure of 3,3-dityrosine (Figure A3.3).

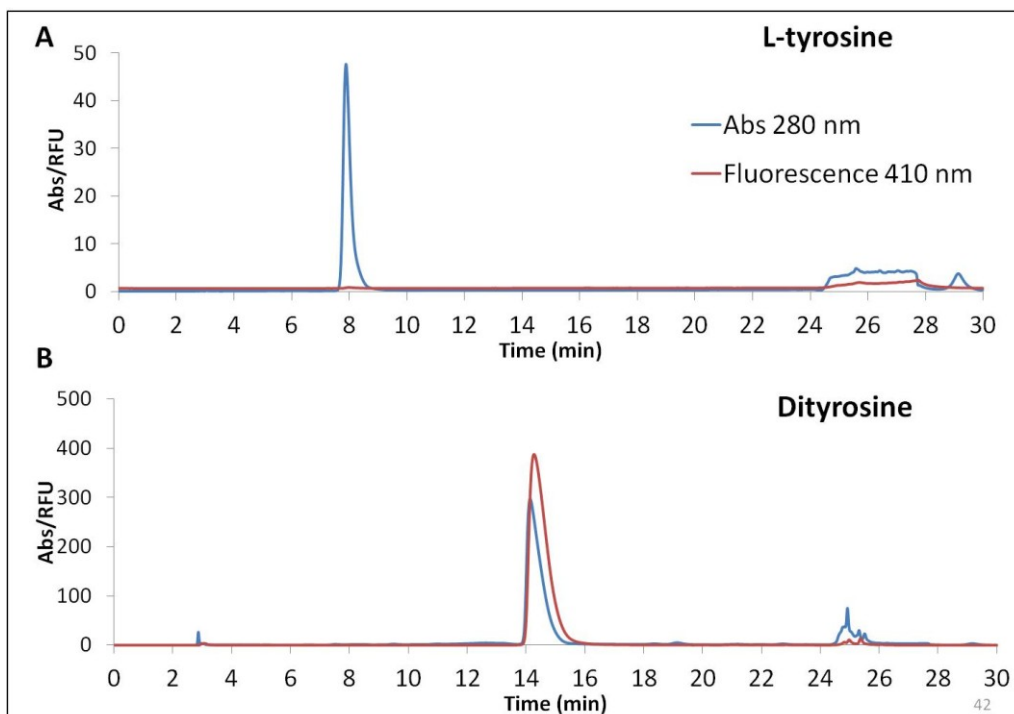


Figure A3.1. HPLC analysis of dityrosine. The fluorescent fractions eluted from centrifugal TLC were adjusted to pH 3.0 with formic acid (FA) and loaded onto a preparative-scale HPLC column (Phenomenex C-18, 100 Å pore size, 15 μm particle size; 2.0 X 25 cm) at a flow rate of 10 mL/min. The column was washed with 0.1% FA in water for 10 min followed by a gradient of 0–8% acetonitrile in 0.1% aqueous FA over 30 min. Absorbance of the eluate was monitored at 280 nm and its fluorescence at 410 nm with 325-nm excitation. Panel A shows the chromatogram of the L-tyrosine reactant and panel B shows the reaction product purified using thin layer chromatography which is dominated by purified dityrosine.

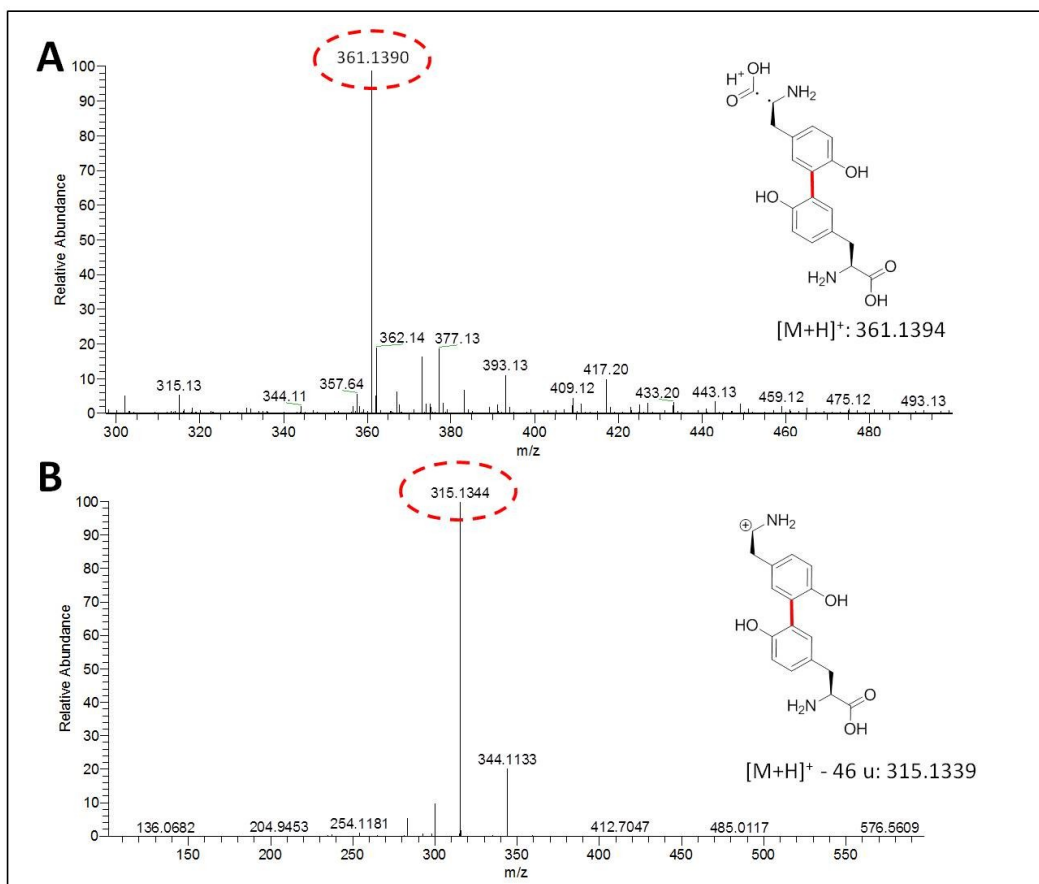


Figure A3.2. Mass spectrometric characterization of dityrosine. The Peak from Figure A3.1B was diluted in 2% aqueous acetonitrile/0.1% FA and loaded onto a homemade reversed-phase C18 capillary column (100 μm x 6.5 cm) equilibrated with 2% acetonitrile/0.1% FA and attached to a NanoLC (Easy-nLC II, Thermo Scientific). The sample was eluted at a flow rate of 200 nL/min into the nanoESI source of an LTQ Orbitrap Velos mass spectrometer using a 2–94% acetonitrile gradient and analyzed in full-scan mode (m/z 350–1000) in the Orbitrap high-resolution mass analyzer ($R=60,000$ at m/z 400). The precursor dipeptide $(M+H)^+$ ion at m/z 361.1390 (Calc m/z 361.1394) was selected in MS1 using a mass exclusion threshold of 10 ppm and fragmented in the LTQ at a collision energy of 35 V. **(A)** The MS spectrum of the $(M+H)^+$ ion of dityrosine at m/z 361.14. **(B)** The MS/MS spectrum of dityrosine showing the neutral loss of 46, resulting in a fragment ion at m/z 315.13

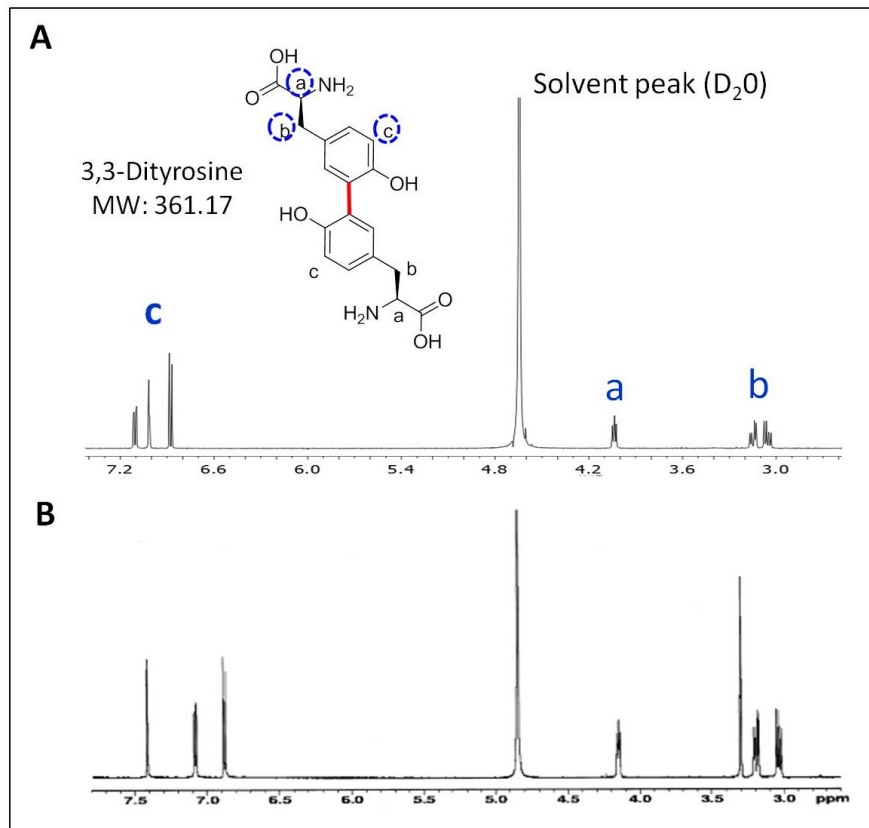


Figure A3.3: (A) Experimental ¹H NMR (500 MHz, D₂O, ppm): 7.11 (dd, 1H, Ar, *J* = 3 & 8 Hz), 7.02 (d, 1H, Ar, *J* = 3 Hz), 6.88 (d, 1H, Ar, *J* = 8 Hz), 4.04 (dd, 1H, J = 5.5 & 7.5 Hz), 3.14 (dd, 1H, J = 5.5 & 15 Hz), 3.06 (dd, 1H, J = 7.5 & 15 Hz). (B) Literature ¹H NMR spectrum of 3',3'-dityrosine (268). Note the impurity at 3.3 ppm.